Modelling the colloidal behaviour of food systems in the presence of fragmented proteins/macromolecules: A Self-Consistent Field approach

Adem Zengin

Submitted in accordance with the requirements for the degree of

Doctor of Philosophy

The University of Leeds

School of Food Science and Nutrition

March 2016

The candidate confirms that the work submitted is his own, except where work which has formed part of jointly-authored publications has been included. The contribution of the candidate and the other authors to this work has been explicitly indicated below. The candidate confirms that appropriate credit has been given within the thesis where reference has been made to the work of others.

The article **Fragmented proteins as food emulsion stabilizers: A theoretical study** by Rammile Ettelaie, Adem Zengin, and Hazel Lee, doi: 10.1002/bip.22487, includes some of the results reported in chapter 4 as the contribution of the candidate. The development of method (i.e. the traditional Self-Consistent Field approach) and implementation of the required numerical programs in this joint article had been undertaken by the other authors.

Acknowledgements

Firstly, I would like to thank my supervisor Dr Rammile Ettlaie for his great support, guidance and encouragement. This Ph.D. could not have been completed without his continuous support. I would like to thank my second supervisor Prof Brent Murray for being part of this success. I express my gratitude to the Ministry of Turkish National Education for funding all the expenses, without which I could not have had the opportunity to undertake this courses. A special thanks must go to Amr Bekhit for his proofreading and for many useful tips for a good thesis structure.

I would like to thank my wife, parents and siblings for their support, patience and encouragement. Finally, I would like to thank my friends and colleagues for their advice and encouragement throughout the entire journey.

Abstract

This thesis presents a theoretical examination of the possibility that the fragments of a protein may provide better colloidal stability than the intact protein itself in the case of α_{s1}-casein. It more generally considers the surface adsorption behaviour of fragmented proteins.

In colloidal systems the polymers are mostly present as polydisperse entities. Polydispersity can either be naturally present or be the result of fragmentation, as happens for food proteins during enzymatic modification. Majority of proteins do not possess the most optimum primary structure expected of an ideal colloidal stabiliser. More desirable surface functionality maybe achieved by hydrolysis of edible proteins. For the theoretical examination of this argument we had to extend and develop a new Self Consistent Field (SCF) approach which also had to be validated first. Although this new approach is an extension of the traditional SCF approach, it is capable of modelling highly polydisperse systems in a manner not currently possible with the more usual technique.

In this preliminary work we present the results of our method for both homopolymers and proteins. In the homopolymer case, we investigate how the preferential adsorption of homopolymer fragments is influenced by various parameters such as solution concentration, degree of hydrolysis (DH), the intact size of the original homopolymer and the strength of affinity of monomers to the surface.

The colloidal stabilising and surface adsorption properties of fragmented proteins were investigated taking the bovine milk protein α_{s1}-casein as an example. The protein was fragmented by selective single bond and also non-selective multiple bond hydrolysis, assumed to be induced by the action of enzyme trypsin. The investigation was carried out at different levels of hydrolysis (DH) and various pH values. We find that the non-selective peptide bond hydrolysis in the case of α_{s1}-casein did not provide a better colloidal stability compared to the intact α_{s1}-casein, at none of the pH values studied here. However, it was shown that a better colloidal stability can be achieved by the selective peptide bond cleavage of particular bonds.

Table of Contents

List of Tables

List of Figures

Chapter 1 Introduction

1.1 Applications of Colloids

Many food products are produced and marketed in the form of one of the many types of food colloids, such as foams, emulsions, gels, and dispersions (e.g. mayonnaise, creams, yogurt drinks). Thermodynamically, colloidal dispersions are metastable or unstable. However, if the rate of change in thermodynamic state is significantly slow over a certain time period (i.e. shelf-life) it can be regarded as colloidally stable (Dickinson, 1992). Colloidal dispersions mostly consist of many otherwise immiscible components dispersed in one another. The components can display creaming or sedimentation under gravity, or aggregation when colloidal domains interact with each other. As a result of this, some of the highly desirable structural, sensory and microbiological stability properties of the food colloid formulations are lost. Thus, surface active materials are needed to prepare food colloids and to keep them in a desired state for a sufficient shelf-life until they are consumed.

Food systems have been structured by using food processing equipment such as spray dryers, mixers, extruders, freeze dryers for many years. In structuring food systems, novel approaches have also been developed which facilitate, for instance, the formation of multilayers, and double emulsions. Multilayers offer delivery of lipophilic bioactive components with encapsulating, protecting and releasing functionalities (McClements, 2010). Similarly, double emulsions are

used to encapsulate hydrophilic healthy compounds and release them at a desired stage of digestion by interaction with an external trigger (Hemar et al., 2010). Additionally, they can be used in manufacturing low-fat food products (Norton and Norton, 2010).

Apart from the food industry, colloidal systems and so the surface active materials (i.e. proteins) as functional components of the colloidal systems are also widely used in other industries such as pharmaceutical, cosmetic, biotechnology, explosives, ink and paint industries. For instance, whey proteins are used as a natural cosmetic ingredients in shampoos providing consistency and foaming ability (Sikora et al., 2007). The emulsifying and stabilising properties of caseins are used in oil and latex paints (Genin, 1958) as well as in adhesives (Smith et al., 2001). Multiple emulsions are used in many biotechnological applications, such as in the controlled delivery of drugs, creating artificial cells, peptide and protein delivery systems (Fanun, 2010). The stability of colloidal systems is highly related to the mediated colloidal interactions that arise due to the layers of adsorbed surface active molecules and their interactions with solvent and surface of colloidal particles. It is useful to explain these interactions at this stage since they will be explored and discussed for predicting the stability of colloidal systems investigated in this study.

1.2 Colloidal Interactions

1.2.1 Van der Waals Interactions

Van der Waals interactions are the attractive interactions between the colloidal particles of the same material. These interactions are ubiquitous and naturally

present and act on colloidal particles largely irrespective of the nature of the adsorbed molecules to the surface of the particles. Once two colloidal particles approach each other closely by the Brownian motion or otherwise (e.g. shear), they stick to each other due to these van der Waals attractive forces. This causes aggregation of the particles and eventually leads to the breakup of the emulsion.

The van der Waals forces arise from dipole-dipole, dipole-induced dipole, or induced dipole-induced dipole interactions. In other words, they arise from asymmetrical distribution of positively and negatively charged regions within a molecule. This kind of distribution can either be induced (e.g. in non-polar molecules) or be inherent (polar molecules). In the approach introduced by Hamaker, the net force between two macroscopic bodies (i.e. colloidal particles) is obtained by summing the van der Waals forces between individual molecules of the two bodies (i.e. interactions are assumed to be pairwise). Also the effect by the molecules of the dispersion medium is considered. These factors are taken into account by a constant A (the composite Hamaker constant) which depends on the nature of the particles and the dispersion medium (Cosgrove, 2010). The van der Waals interactions V_{vw} between two spherical particles of radius R as a function of distance r is then found to be given by Eq. 1.1 (Dickinson and Stainsby, 1982)

$$V_{vw}(r) = -\frac{AR}{12r} \ . \qquad \textbf{1.1}$$

The value of A is dependent both on the material making up the dispersed phase and that from which the dispersion medium is made. However, for oil dispersed in

water the typical value is around 1 k_BT (Dickinson, 2005). The droplet size throughout this study is taken to be 1μm (R=0.5 μm) unless mentioned otherwise. Figure 1.1 shows the van der Waals interactions plotted against the surface separation distance (r) in nm between two oil droplets where A=1 k_BT and R=0.5 μm.

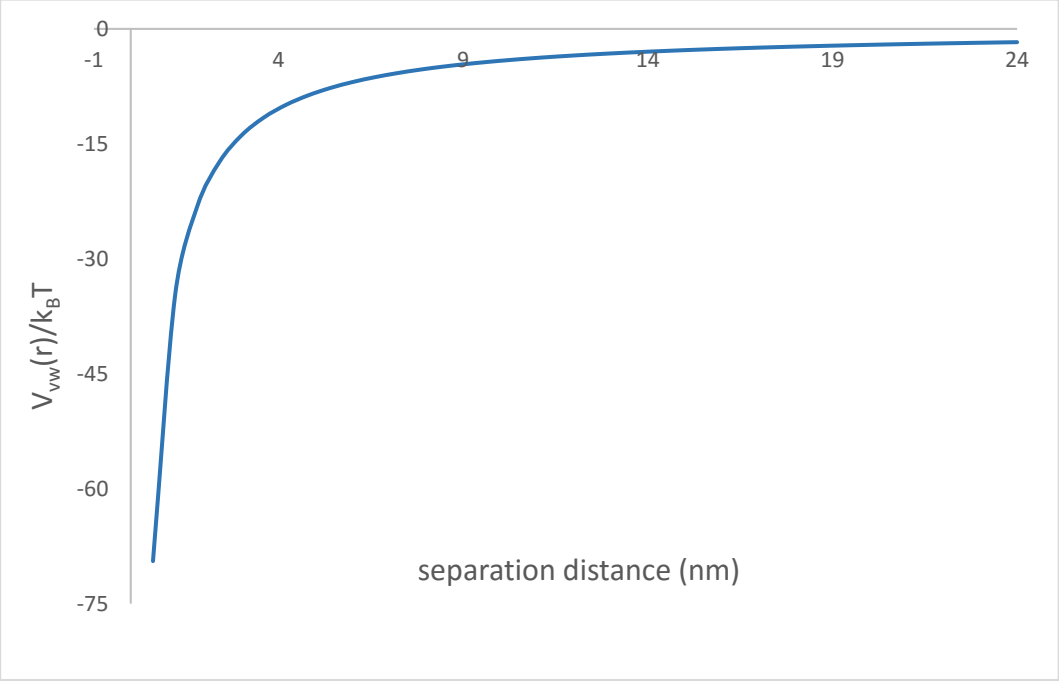

Figure 1.1 Van der Waals interactions $V_{vw}(r)/k_BT$ plotted against the surface separation r/nm. The composite Hamaker constant was taken to be A~1 k_BT and the radius of droplets R=0.5μm.

As seen in the above figure, the van der Waals attractive interactions are stronger at close separations distances. In order to maintain the stability of emulsion, it is required to provide sufficient repulsive forces (e.g. electrostatic and/or steric forces) to keep the droplets sufficiently far apart where the magnitude of the van der Waals attractions are small and therefore easily overcome by thermal Brownian motion of the droplets.

The van der Waals interaction does not involve direct coulombic interactions on a colloidal scale, though of course the nature of these interactions are fundamentally electrostatic in origin.

1.2.2 Electrostatic Interactions

The surface of the particles become charged through adsorption of ionisable charged groups. Positively or negatively charged surface then generates an electric field which attracts the counter-ions (ions of opposite charge to the surface) and repulse the co-ions (ions of the same charge as the surface). The presence of co- and counter-ions drastically alters the nature of the electrostatic interactions from the simpler and more familiar ones seen in vacuum (i.e. in absence of such ions). The electric field is stronger near the surface region and weakens with the distance away from the surface. Thus, the concentration of counter-ions is high near the surface region and gradually decrease to its bulk value with increasing distance. Similarly, the concentration of co-ions is low near the surface region and gradually increase to its bulk value with increasing distance. The concentrated inner region in close proximity with the surface is called *Stern layer* (i.e. compact layer) and the region beyond Stern layer is called *diffuse double layer*. In the former, the electric field falls approximately linearly and in the latter it continues to fall but now approximately exponentially as one moves away from the surface (Hunter, 2001, Dickinson, 1992).

The presence of an electric field also influences the distribution of the polymers that have charged groups. The surfaces repel the polymers carrying the same sign net charge whereas they attract the ones carrying the opposite sign net charge. Besides that, the entropic influences are also in operation for these

polymers (Dickinson and Stainsby, 1982), since the environment near a surface is much more restrictive in terms of the configurations adopted by the polymer chains.

The particle surfaces that become charged with the adsorption of charged polymers repel each other by an electrostatic repulsion. The stability obtained in this way is called the electrostatic stability. However, as mentioned the nature and strength of this repulsion is greatly influenced by the presence of ions in the gap between the particles/surfaces.

The net charge of the polymers is dependent on their ionisation degree which is highly related to pH. This makes the electrostatic stability fragile at pH values near the isoelectric point of such polymers where their net charge is nearly zero. For proteins used in food colloid formulations, the isoelectric point is typically in the range 4-5 pH units. Therefore, the electrostatic stability combined with the steric stabilisation technique is more reliable to maintain the stability of emulsions against such pH changes (Napper, 1983).

1.2.3 Steric Interactions

Consider two oil droplets covered with hydrophilic polymer chains. When these two droplets approach each other by Brownian motion, the adsorbed chains will start to overlap. Then the two droplets will repel each other due to the interactions between the adsorbed chains. This interaction is called the steric interaction and the stability provided in this way is called the steric stability. The steric repulsive interactions originate to some extent from the reduction in the entropy of the adsorbed overlapped polymer chains, but even more significantly

from the increase in the osmotic pressure between the overlapping region and the rest of the solution. This osmotic effect arises from the partial exclusion of the solvent molecules from the gap where the overlap of the adsorbed layers increases the local concentration of the chains.

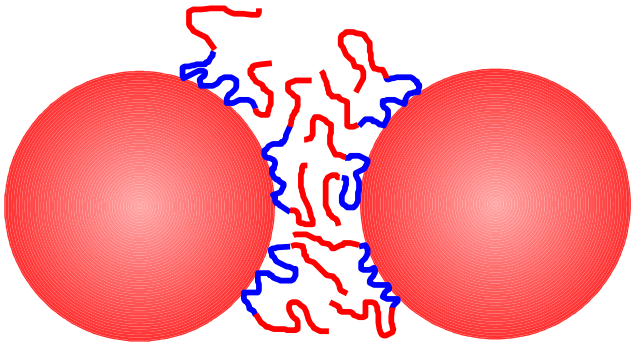

Figure 1.2 Illustration of the steric stability provided by the adsorbed overlapped polymer chains. The overlap of layers increases the local concentration of the polymer in the gap between the particles.

The steric interactions become significant at the overlapping distance of adsorbed polymers for two approaching surfaces (e.g. for an anchored and completely stretched linear polymer, the overlapping distance will be double the length of the polymer.) The magnitude of the steric interaction can be evaluated by monitoring the changes in the free energy against the separation distance of the two approaching surfaces. When the separation distance is decreased, the adsorbed layers become overlapped and the free energy (i.e. the repulsive interaction) is increased.

In order to obtain a steric repulsion, the polymer chains need to be anchored or strongly adsorbed to the surfaces. Otherwise, they can be depleted from the interparticle region, if the entropy loss becomes higher than the adsorption energy keeping the chains near the surface. Furthermore, the surface of the

particles needs to be completely covered. For partly covered particles, it is possible to obtain bridging flocculation which is explained in section 1.2.4 in this chapter. Another requirement for obtaining steric stabilisation is that the thickness of the adsorbed layer must be adequate. The overlap of the adsorbed polymer chains occurs at closer separation distances if the adsorbed layers of polymers are thin. The repulsive force induced by such thin adsorbed layers may prevent further approach of the particles, but by this stage the van der Waals attraction is already strong to prevent particles from separating (see Figure 1.1). Finally, a good solvency condition is also important to obtain a steric repulsion when the adsorbed polymers are overlapped (Timothy and Peter, 1999) since it is important that the polymer is well distributed in the solution and available to be readily adsorbed onto the surface of the emulsion droplets/particles.

The steric stability is more important in colloidal systems where the electrostatic stability is not present, such as non-aqueous systems or in food systems at lower pH values (~4-5 pH units).

1.2.4 Bridging

The bridging effect induces an attraction between two adjacent surfaces at close separation distances through the adsorption of two different sections of a polymer chain onto the surfaces of two nearby droplets. A section of a polymer can desorb from one surface and become attached to another nearby surface. Adsorption to the opposite surface, rather than being in solution, is thermodynamically more favourable for the hydrophobic residues of the adsorbed polymer. Two or more adjacent surfaces can then be linked to each other by this

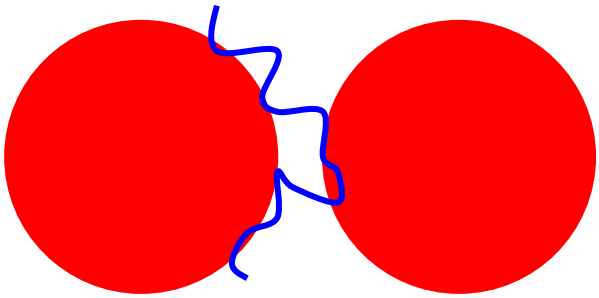

Figure 1.3 Illustration of a bridging conformation of a polymer chain that connects two nearby droplets (not to scale).

bridging effect, which can form flocs of the droplets. This situation is the so-called *bridging flocculation* (Dickinson, 1992).

The bridging conformations occur when the distance between the two opposite particles are sufficiently close where the loops and tails of the adsorbed polymers can contact to the opposite surface without much stretching and loss of entropy that this will entail. The length and the number of loops and tails are the factors that trigger the bridging flocculation. The relatively weak affinity of adsorbed polymers to the surfaces and the incomplete surfaces coverage are the other factors that also increase the number of bridging conformations (Dickinson and Stainsby, 1982). The bridging interactions can occur and become important at distances where the particles are as close as the diameter (i.e. it is the length for linear polymers) of the largest polymer in the system.

1.2.5 Depletion

Interestingly the non-adsorbed polymers (i.e. free polymers in the solution) can also affect the stability of emulsions without the need to form layers at the

surface. When the distance between two approaching particles becomes less than the diameter of the polymers (i.e. it is the length for linear chains), the concentration of the free polymer in the interparticle region can deplete and induce the flocculation of the particles. This occurs because of loss of conformational entropy of the chains when squeezed in the narrow gaps between the particles. If such chains have no affinity for adsorption onto the surfaces, then they leave the gap. Subsequently, the osmotic pressure arises outside of the interparticle region pushes the particles to come even closer. Again the osmotic effect is the result of polymer concentration differences between regions inside and outside the gap.

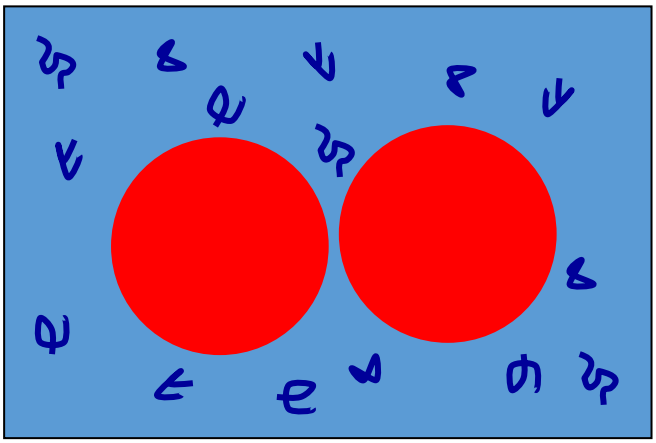

Figure 1.4 Illustration of the depletion flocculation of two oil droplets. The gap between the particles is depleted from polymer giving rise to an osmotic pressure difference inside and outside the gap.

The flocculation induced by the depletion of the free polymers is called *depletion flocculation* (Napper, 1983). It is important to optimise the concentration of the polymers in the solution. This is because the high concentration of polymers leaves a high number of free polymers in the solution once the surfaces are saturated with the adsorbed chains. This causes depletion flocculation, whereas

an insufficient and low concentration of polymers leads to an incomplete surface coverage, causing bridging flocculation, instead. The depletion flocculation can be observed and become important when the distance between two approaching particles are closer than the diameter of the largest free polymer in the system.

1.3 Surface Active Materials

Surface active materials generally have hydrophobic and hydrophilic molecular structures (i.e. amphiphilic). They can be grouped into small sized molecules and macromolecules. Proteins as macromolecules are commonly used as surface active materials in the food industry because of their edible, amphiphilic, and charged structures. The hydrophobic residues of the proteins have affinity for the hydrophobic surfaces, whereas the hydrophilic residues prefer to be away from the surfaces and protrude towards the solution. The stabilisation mechanism of proteins involves steric and electrostatic interactions. Electrostatic interactions become weak when background electrolyte concentration is high, due to the screening of charge, or when pH of the media is near the isoelectric point of the stabilising protein. In such conditions, the stability of emulsions mainly relies on the steric interactions.

Several approaches have been proposed in recent years to obtain superior food colloid stabilisers without deploying high chemical modifications. One approach explores the synergistic effects of proteins and polysaccharides.

Polysaccharides are by and large highly hydrophobic macromolecules and are normally much larger than proteins. If they were to be adsorbed at the surfaces, they could initiate strong steric repulsions between the chains and could also

form much thicker layers compared to proteins. However, their lack of affinity for adsorption to hydrophobic surfaces is the main problem that prevents their utilisation as emulsifiers. In order to benefit from the desirable attributes of both polysaccharides and proteins, they are used together for the formation of protein + polysaccharide multilayers (Ogawa et al., 2003). Proteins are first adsorbed at surfaces then oppositely charged polysaccharides are attracted to the surfaces by the proteins. Polysaccharides are not depleted from the interfacial region when the two droplets approach each other due to this attraction to proteins, driven by the opposite charge of the two molecules. Instead they form a thick layer which provides enhanced stabilisation against the changes in environmental conditions, such as increase in salt concentration (Guzey and McClements, 2007) or thermal treatment (Guzey and McClements, 2006). In a recent theoretical study, it was demonstrated that even thicker layers and stronger repulsions are possible if the charge distribution of the polysaccharides along its backbone is not uniform (Ettelaie and Akinshina, 2014a). However, implementation of the method involves a number of reported challenges, such as finding the appropriate polyelectrolytes or preventing the bridging flocculation occurring in the intermediate stage of the emulsion preparation (McClements, 2006). In the use of an anionic polyelectrolyte at pH values much higher than their isoelectric point as is the case for protein at pH 6 or 7, polysaccharides desorb from the surfaces. This is because at such pH values the charge of protein is now the same sign as the polysaccharides. Thus, instead of attraction, we now have strong electrostatic repulsion between the two sets of biopolymers (Harnsilawat et al., 2006a). At pH=5, similar results were reported but at high salt concentration, where the electrostatic interactions are weak due to screening

(Harnsilawat et al., 2006b). In order to overcome these issues, polysaccharides can be covalently attached to the backbone of proteins. These are the so-called protein-polysaccharide conjugates whose structure and colloidal behaviour will be somewhat similar to a diblock-like polymer. The hydrophobic parts of proteins are adsorbed strongly to the surface and the more soluble polysaccharides protrude into the solution (Dickinson, 2008). A long-range steric repulsion is then provided by the polysaccharides, which force the droplets apart.

Protein-polysaccharide conjugates can occur naturally (e.g. gum Arabic) and can also be synthesized through Maillard reactions. Ovalbumin-dextran (Kato et al., 1990), β-casein-dextran (Semenova et al., 2009), sodium caseinate-maltodextrin (Grigorovich et al., 2012), bovine serum albumin-dextran (Dickinson and Semenova, 1992), β-lactoglobulin-propylene glycol alginate (Dickinson and Galazka, 1991), and whey protein-maltodextrin (Akhtar and Dickinson, 2007) are some examples of the protein-polysaccharide conjugate studies in the literature. Although these conjugates were shown to provide better emulsion stability compared to unmodified proteins, there are still questions regarding the optimal size of polysaccharide relative to protein and the most suitable location on the protein backbone for the attachment. Akinshina et al. (2008) investigated interfacial properties of modified α_{s1}-casein in a theoretical study by using Self Consistent Field (SCF) calculations to address the above questions. In their study, the protein was covalently attached to an uncharged polysaccharide side chain. It was shown that the location of attachment is critical if the length of the side chain is short. When the location was on one of the ends of the protein, the adverse bridging attraction was reduced. However, when the side chain was attached to the central part of the protein, the bridging attraction was increased

and the desired stability was not achieved. Of a more practical consideration, the production of conjugates is often a time consuming process and does require an optimal level of drying that adds to the costs of producing such molecules.

Pickering emulsions are another strategy for stabilising food colloids. This time, rather than using individual molecules to adsorb at a surface, small particles are used instead. The particles require much higher desorption energies to become detached from the surface (Ettelaie and Lishchuk, 2015) compared to the individual molecules. This allows them to keep emulsions stable for longer by preventing coalescence and in particular Ostwald ripening. This is due to their much larger structures. However, in creating submicron emulsions, much smaller particles with appropriate surface chemistries (i.e. nanoparticles) than those currently available are required. Obtaining such small, edible particles with the right surface chemistries for use as Pickering stabilisers, has been a challenge. One approach can be the use of amphiphilic alginate derivatives in the form of nanogels (Oh et al., 2008, Broderick et al., 2006). Another approach can be the use of small, amphiphilic, filamentous fungi protein, hydrophobin, which has a molecular weight less than 10 kDa. It is a natural surfactant and, together its foam-stabilising ability, is a special protein among others. It is also different from, for instance, β-casein and β-lactoglobulin, because it creates an elastic adsorbed layer (Dickinson, 2015). However a recent theoretical study showed that its emulsion stabilising ability may not be as effective as its foam stabilising ability due to the conformational change upon adsorption onto fluid hydrophobic interfaces (Euston, 2014).

The size of a colloidal stabiliser is one of the important parameters in defining its colloidal behaviour. Small molecules (e.g. surfactants) have the advantage over large ones (e.g. proteins) in diffusing to and adsorbing faster at interfaces (Qi et al., 1997). They can rapidly reduce surface tension and provide short lived stability through the so called “Gibbs-Marangoni” effect (Sánchez-Vioque et al., 2004). However, large units diffuse relatively slowly but provide long term stability by creating a thicker film layer at the interfaces (Deleu et al., 1999). An ideal surface active material, depending on the desired properties in a dispersed system, should diffuse rapidly like small molecules and yet also provide long term stability like large macromolecules. However, most proteins, the small particles used as Pickering stabilisers and the biopolymer composites are noticeably too large to diffuse rapidly and by the time they adsorb to the surface of the emulsion droplets or bubbles, the freshly created dispersed system can already lose its stability. Therefore, the third strategy can be the use of smaller molecules, in contrast to the other two approaches discussed above. It has been proposed that peptide chains of suitable length can provide the expected features of an ideal surface active material in order to sufficiently provide both the stability and the rapid diffusion requirement to the surface. In addition, they are also more likely to be in a coil-like disordered conformation which does not require unfolding before adsorption. The main aim of this PhD project is to develop suitable methods and use these to theoretically examine the colloidal stabilising properties of such fragmented peptide chains, produced by hydrolysis of food grade proteins. We note that hydrolysis of protein occurs naturally in the stomach and therefore such fragmented proteins can readily be used as food functional additives.

Polypeptides can be obtained naturally or synthetically. Fragmented proteins obtained from natural sources can be an appropriate alternative for sensitive industries, particularly the food industry, where synthetic materials are not preferred. Therefore, the developments and results of this thesis will be of greater interest to the food industry. Also natural polymers are generally more economical than synthetic ones, depending on the production process, which is another reason to use naturally obtained fragments in food production. However, this preference restricts the degree of control over the type of fragments produced, due to the rather broad degree of peptide bond breaking specificity of most enzymes. Thus, a careful and efficient control and analysis of the characteristics of the peptide fragments is essential if desirable colloidal functionality is to be achieved. For this, we developed a new Self-Consistent Field (SCF) approach based on a significant extension of the usual SCF approach used in previous studies (Ettelaie et al., 2014b, Ettelaie et al., 2014a, Ettelaie and Akinshina, 2014b, Scheutjens and Fleer, 1979, Leermakers et al., 1996). This new approach enables one to model highly polydisperse systems obtained by hydrolysis of a macromolecule, which the usual approach in literature fails to do because of its high computer memory usage and tedious input process. A detailed description of the usual approach, along with a discussion of its limitations, is given in chapter 2.

1.4 Self-Consistent Field Approach: Extensions and Applications

The Self-Consistent Field (SCF) approach has been extended many times to carry out calculations for various colloidal properties in different systems. Some of the key extensions and applications will be given here.

Dolan and Edwards (1975) applied SCF calculations to adsorbed homopolymers. Polymer-solvent interactions were taken into account in their model for the first time and the polymers were assumed to be grafted permanently at one end to the surface. Scheutjens and Fleer (1979) presented a similar theory and introduced size distribution calculations of tails, loops, and trains which were not available in earlier models. The volume fraction of the adsorbed homopolymers particularly at large separation distances was then calculated more accurately since it was given as an exponential decay against the distance in the former theories. The adsorbed polymers found at large distances were determined as long tails and it was highlighted that considering their existence is important for predicting the stability of colloids. Leermakers et al. (1983) modified the Scheutjens and Fleer theory to cover the adsorption of diblock copolymers and they investigated the self-association of surfactants. A further modification was presented by Evers et al. (1990a), where the theory of adsorption of homopolymers from a binary solution was extended to the adsorption of block copolymers from multicomponent mixtures. They theoretically studied the effect of solvent quality and surface affinity on the distribution profiles of block copolymers (Evers et al., 1990a), the effect of the structure of block copolymers on the adsorbed amount and on the adsorbed layer thickness (Evers et al., 1990b), and the interactions

between two adsorbed layers where the free energy interaction was formulated both for full equilibrium and restricted equilibrium (Evers et al., 1991). In the following years, the Scheutjens and Fleer theory was applied to the adsorption of polyelectrolytes by Leermakers et al. (1996). The effects of ionic strength and pH on surface coverage and density profile were studied. For this purpose, β-casein was chosen as a disordered polyelectrolyte and its amino acid sequence was represented in the model by several monomer types for a qualitative analysis. It was reported that the theoretical results were found to be in very good qualitative agreement with the neutron reflectometry and dynamic light scattering experiments (Dickinson et al., 1993, Atkinson et al., 1995). The same authors also carried out the same study for α_{s1}-casein to compare the behaviour of two proteins (Dickinson et al., 1997a, Dickinson et al., 1997b). The adsorbed amount of α_{s1}-casein was found to be more sensitive to ionic strength and pH and significantly lower than β-casein. The repulsive interaction potential induced by β-casein was attributed to steric and electrostatic interaction and long, dangling, charged tails. The attractive interaction potential resulting from α_{s1}-casein layers was attributed to extensive bridging conformations.

The effect of block sizes and the addition of hydrophilic side chains on steric interactions induced by block copolymers was investigated using SCF calculations by Ettelaie et al. (2003). In close separation distances, both the adsorbed amount of hydrophobic blocks and the attractive interactions increased with decreasing block sizes. The corresponding increases were attributed to the possibility of an increase in the number of bridges at such distances. In addition, it was reported that the addition of sufficiently long hydrophilic side chains turned the attractive interactions into repulsive ones.

Parkinson et al. (2005) studied the enhanced steric stabilization by low surface coverage of casein-like polymers in mixed protein layers. For this, β-lactoglobulin was used as the primary emulsifying agent and a few percent of it was replaced with the casein-like polymers. Self-Consistent Field theory is normally not applicable to globular type proteins. However, β-lactoglobulin in this study was simply represented as a short diblock copolymer, composed of hydrophobic and hydrophilic segments, to simulate the adsorption behaviour of this globular protein, leading to a thin but dense interfacial adsorbed layer. Enhanced stability was attributed to large stretching of β-Casein component when a thin dense layer of another protein was already present on the surfaces.

Mixed protein + polysaccharide interfacial layers were modelled in several SCF studies. Ettelaie et al. (2005) investigated the mediated steric interactions by such layers, involving protein + polysaccharide. When all segments of polysaccharide had favourable electrostatic interactions with the primary adsorbed protein layer, the mediated colloidal interactions were predicted to be attractive and the excess presence of polysaccharides at the interfacial area did not contribute much to the thickness of the adsorbed layer. Conversely, strong repulsive interactions and a much thicker adsorbed layer were reported when only some of the polysaccharide segments were charged and therefore had favourable electrostatic interactions with the protein layer.

Akinshina et al. (2008) studied the interactions induced by α_{s1}-casein with covalently attached uncharged polysaccharide side chains as a function of ionic strength and pH. For sufficiently long side chains, steric repulsion was achieved and found to be less sensitive to the attachment location, pH, and ionic strength.

Attachment of the short side chains to one of the ends of the protein also reduced the bridging, found for unmodified α_{s1}-casein, and hence provided enhanced steric stability. However, attachments to the middle part of the protein increased the probability of bridging conformations, compared to the pure protein. The effect of polysaccharide charge distribution on its adsorption behaviour was modelled in another SCF study by Ettelaie et al. (2012). It was shown that the uniform distribution of charges led to formation of a protein + polysaccharide film at the interface and an optimum value of charge was found for the maximum adsorption of uniformly charged polysaccharide. However, in the non-uniform distribution of charges, where only certain short blocks of polysaccharide were highly charged, and the rest were weakly charged, increasing the value of charges on the short block led to the formation of a much thicker adsorbed layer of polysaccharide. The weakly charged long block of polysaccharide extended towards the solution and a distinct protein + polysaccharide multilayer was then observed.

Interactions induced by κ-casein and para-κ-casein between two approaching hydrophobic surfaces were compared using SCF calculations by (Ettelaie et al., 2014a). At close separation distances, the interactions were found to be repulsive with κ-casein, and attractive with para-κ-casein. However, at the larger distances, an energy barrier was observed with para-κ-casein. The origin of the barrier was attributed to electrostatic repulsions, because it was not observed at higher salt concentrations. In the same conditions, interactions mediated by adsorbed κ-casein layers remained repulsive, which indicated the provision of strong steric repulsions by κ-casein. κ-casein is a glycoprotein. The origin of the steric forces

was reported to be the carbohydrate side chains, because the interactions became attractive without them.

The SCF theory has been extended, improved and used for the investigation of many different cases, including in the study of food colloids as seen above. In this study, we present our SCF extension which enables the simulation of highly polydisperse systems obtained by hydrolysis hitherto not attempted before. A few comparisons of experimental and SCF investigations is given in the next section which show the success of the SCF calculations in predicting the experimental behaviour of polymers.

1.5 Homopolymer Adsorption

Polymer adsorption was experimentally and theoretically investigated for the systems involving homopolymers, copolymers, polydisperse polymers, and polyelectrolytes. Some of the theoretical and experimental studies related to the adsorption of polydisperse homopolymers will be reviewed here.

Felter et al. (1969) studied the adsorption of polydisperse polyvinyl chloride (PVC), having a range of molecular weights between 10^3 and 10^6 (number of units of PVC molecules), onto $CaCO_3$ from dilute chlorobenzene by using gel permeation chromatography. They showed that almost all available polymers above a molecular weight 10^5 in the solution were adsorbed. The rest of the polymers were found to be partly adsorbed depending on their molecular weights and availabilities in the solution. In the study by Felter and Ray Jr (1970), they investigated the effect of solution concentration on the preferential adsorption of polymers and found that below the limiting adsorption plateau, there were less

high molecular weight polymers in the residual solution at low concentrations. Furthermore, at high solution concentration, a slight reduction was detected in the adsorbed mass of high molecular weight polymers in the adsorbed layer on the limiting plateau of adsorption isotherm. They concluded that the high solution concentration inhibits the adsorption of high molecular weight polymers.

Furusawa et al. (1982) examined competitive adsorption of polystyrenes in various molecular weights and they suggested that preferential adsorption is not completely dependent on molecular weight and that individual polymer concentrations are also significant. In addition, the level of preference was found to be related to conformations of small polymers at the surfaces. The high number of adsorbed segments influenced the displacement of initially adsorbed small polymers with the large ones. In the study by Furusawa and Yamamoto (1983), they investigated exchangeability in the adsorbed layer and reported that relative size of the displacer and the solution concentration are the important factors for the replacement of initially adsorbed polymers. At low solution concentration, the replacement of small polymers was more difficult compared to the high solution concentration. This was explained by the higher possibility of flat conformations which the small polymers can take at the surfaces in the low concentration solutions.

Janardhan et al. (1990) studied the role of molecular weight and solution concentration on the preferential adsorption and reported similar results as Felter and Ray Jr (1970), which confirms the higher adsorption preference of large polymers at low solution concentrations. Janardhan et al. (1990) suggested that

the loss of entropy for small adsorbed polymers is less at high solution concentrations compared to low solution concentrations.

Preferential adsorption of polymers has also been considered theoretically by several authors. Stuart et al. (1980) plotted their adsorption isotherm for polymers in different molecular weights and distinguished three regions on it. The first region represents the initial stage of the adsorption where all polymers can be adsorbed without any preference. The second region represents the intermediate stage of the adsorption where the surface is almost saturated and the low molecular weight polymers start to be replaced by high molecular weight polymers. The intermediate stage continues until all the small polymers are completely replaced. In the meantime, the adsorbed amount increases with the displacement of small polymers. The third region is a plateau region where the displacement has been completed and the maximum adsorption has been achieved. Hlady et al. (1982) extended the theory of Stuart et al. (1980) and applied it to the adsorption of polydisperse dextran on silver iodide. A satisfactory agreement of the theory and experiment was reported.

Roe (1980) modelled the adsorption of polydisperse polymer chains and suggested that the degree of preference for high molecular weight polymers decreased at high overall solution concentrations. Scheutjens et al. (1982) extended their theory (Scheutjens and Fleer, 1979) for simulation of the preferential adsorption and predicted similar results as Roe (1980). They calculated the contribution of polymers in the total adsorbed amount and confirmed that the high molecular weight polymers had more preference at low concentration solutions.

Another SCF theory on the basis of the Scheutjens and Fleer scheme and Stuart et al. (1980) adsorption theory was presented by Roefs et al. (1994). They predicted the molecular weight distribution in the remaining solution and in the adsorbed layer and found that, down to a certain molecular weight, almost all available large polymers in the solution were adsorbed. The adsorption of the polymers, which had molecular weights below that certain limit, was found to increase with the higher molecular weight. These predictions were compared with the experimental results presented by Linden and Leemput (1978) and found to be in good agreement.

Pattanayek and Juvekar (2003) extended their previous continuum SCF model (Juvekar et al., 1999) to adsorption of polydisperse homopolymers. They also confirmed the preferential adsorption of high molecular weight polymers and again found quantitative agreement with the experimental results of Linden and Leemput (1978).

To sum up briefly, it is obvious from the experimental and theoretical studies given above that the large polymers are preferentially adsorbed. In order to see a preference, of course the surface saturation must be achieved during the adsorption. The displacement of small adsorbed polymers (i.e. the preferential adsorption of large polymers) is related to the solution concentration, the relative size of displacer and the number of contacts of small adsorbed polymers to the surface (high in flat conformations).

1.6 Fragmented Proteins

Emulsifying capacity, activity and emulsion stabilising ability of hydrolysed proteins have been studied in the literature by using a large number of different proteins and enzymes at various degrees of hydrolysis.

Adler-Nissen and Olsen (1979) treated soy protein with alcalase and investigated the relationship between the degree of hydrolysis and the emulsion capacity. They showed that the emulsion capacity of the hydrolysate increased as DH increased up to DH 5%. However further levels of hydrolysis gave lower emulsion capacities. In a later study, Qi et al. (1997) produced soy protein hydrolysates with pancreatin and monitored the emulsion activity and stability against DH. They found that the activity was at its maximum at DH 15% and subsequent hydrolysis resulted in lower activities. However, the emulsion stability was found to decrease as DH increased. Lee et al. (1987) argued that polypeptides having around 20 residues were too short to provide good emulsifying properties. Similarly, Chalamaiah et al. (2010) suggested that the emulsifying properties were lost as a result of extensive hydrolysis and that it is the presence of larger peptides that contributes to the emulsion stability. Sánchez-Vioque et al. (2001) and Chobert et al. (1996) also reported results that confirm this effect on the foaming properties of polypeptides. These experimental results pointed out that limited hydrolysis has the potential to improve the emulsion capacity and emulsion activity of the polypeptides. However, the emulsion stability seems to be negatively affected by extended level of hydrolysis.

The other important parameter in determining the colloidal functionality of polypeptides is the nature of the enzyme used for the hydrolysis. Each enzyme

hydrolyses certain specific peptide bonds which then leads to polypeptides with different sizes, hydrophobicities, and charge densities. The colloidal functionality of the resulting fragments therefore varies with the use of different enzymes. Turgeon et al. (1991) hydrolysed whey protein by using trypsin and chymotrypsin and found that hydrolysates obtained by the tryptic hydrolysis had better emulsifying capacities. It was emphasised that the tryptic hydrolysis gave higher molecular weight fragments and that the hydrolysis may have resulted in polypeptides of a more amphipathic nature. Additionally, the emulsion capacity was increased with the removal of the small peptides and amino acids and it was concluded that good emulsifying properties can best be provided by the peptides that have a certain optimum average size. In another whey protein study, Jost et al. (1982) also reported better results in the emulsion stability achieved by the trypsin hydrolysis of the protein compared to the chymotrypsin hydrolysis.

Davis et al. (2005) treated β-lactoglobulin with three different enzymes (alcalase, trypsin, and pepsin) and compared the foam stability of the hydrolysates. The levels of hydrolysis were 15.6%, 6.7% and 5.2% for the enzymes alcalase, trypsin, and pepsin, respectively. They found that all hydrolysates provided better stability than the untreated protein. In addition to that, pepsin and alcalase hydrolysis produced polypeptides providing better stability than trypsin. It was argued that hydrolysis of the protein enabled a more rapid adsorption at the interface, which was related to the formation of smaller peptides and more exposure of the buried hydrophobic residues upon hydrolysis.

Some of the experimental studies focused on specific fragments to identify the parts of proteins responsible for the stability. These studies involved filtration of

small peptides and amino acids and also purification of the specific fragments. For example, Turgeon et al. (1992) hydrolysed β-lactoglobulin with trypsin and peptide fractions were obtained by ultrafiltration of the hydrolysates. They separated the small peptides and amino acids from the mixture and compared the interfacial properties of the intact protein, total hydrolysate, and permeate (small peptides and amino acids) and retentate (mixture of polypeptides) of the filtration. They found that the retentate displayed the best interfacial properties. They fractionated it further into six groups to determine the structure-function relationship. The results showed that two of the groups had better interfacial properties, which are composed of the peptides 21-40, 25-40, and 41-60. They characterised these peptides by having hydrophobic residues in discrete regions and concluded that poor interfacial properties of a peptide could be related to its uniform distribution of hydrophobic or hydrophilic residues. In another study, Shimizu et al. (1986) reported poor emulsifying activity for the purified α_{s1}-casein N-terminus fragment (f1-23) and positive synergistic effect of the fragment f154-199. Fragments composed of sufficiently large blocks of hydrophobic and hydrophilic residues seem to have better interfacial properties. Caessens et al. (1999) also confirmed this in their experiments where β-casein was hydrolysed with plasmin and peptides were isolated and identified. They showed that the fragment f1-105/107 displayed better emulsion stabilising ability than the fragment f29-105/107. It was concluded that the hydrophilic and highly charged N-terminus side (f1-29) is important to the stabilising ability of these fragments.

1.7 Bitter Taste of Peptides

Taste is a key parameter for foods to be chosen by consumers (Drewnowski, 1997). For instance sweet tasting foods are usually preferred more than bitter tasting ones (Drewnowski, 2001). Bitter compounds either exist naturally or occur chemically and enzymatically during production and storage (Lemieux and Simard, 1991). Polypeptides obtained by enzymatic protein hydrolysis may contribute to bitterness when they are used as emulsifiers in food products. The factors influencing bitter taste formation were investigated in the literature. They can be generalised as the type of amino acids composing the peptide, their locations on the chain, and the chain length. The types of amino acids were reported mostly as hydrophobic (Saha and Hayashi, 2001, Roudot-Algaron, 1996), basic (those that have basic side chains) (Gill et al., 1996), and aromatic (Raksakulthai and Haard, 2003). Solms (1969) analysed the taste properties of pure amino acids and listed the bitter amino acids in descending order as L-Try, L-Phe, L-Tyr, L-Leu. However, no direct correlation was found between bitter amino acids and bitterness in peptides in the analysis. For instance, the bitter taste was not received from a dipeptide containing L-Try. In another study, the contribution of the side chains of amino acids to the bitterness was studied and it was found that the side chains which had at least 3 carbon atoms, led to the bitter taste formation (Ishibashi et al., 1988). The second important factor highlighted in the literature is the location of certain amino acids on the peptide chains. For example, bitter taste was perceived from peptides where the hydrophobic amino acids are located at C-terminal ends and the basic amino acids are located at N-terminal one (Raksakulthai and Haard, 2003). Additionally, in a peptic hydrolysis of soybean proteins, bitter peptides were formed because

of the presence of bitter Leu amino acids at C-terminal ends (Arai et al., 1970). Finally, the chain length or degree of hydrolysis was also found to be important in determining the bitterness. In this regard, Adler-Nissen and Olsen (1979) reported that the bitterness was increased with higher degrees of hydrolysis and it reaches its maximum level at the intermediate degrees. They suggested that at low DH, hydrophobic groups were still masked and not exposed, which made the bitterness less perceivable. At high DH, the hydrophobic amino acids become free or in the terminal positions of the small peptides, which again tends to decrease bitter taste. Matoba and Hata (1972) also confirmed that the bitterness is increased with increased level of hydrolysis.

Many approaches were suggested in the literature to reduce bitterness, such as controlling the degree of hydrolysis (Adler-Nissen, 1984, Heinio et al., 2012), applying a further hydrolysis with exopeptidases (Arai et al., 1970, Umetsu and Ichishima, 1988, Bouchier et al., 1999), filtering and removing the bitter peptides from the hydrolysate (Saha and Hayashi, 2001), and using some additional compounds to mask the bitter taste (Rhyu and Kim, 2011, Sun, 2011). Nevertheless, these methods should be applied with care to the polypeptides and the hydrolysates that are meant to be used as emulsifiers in food colloids. The debittering processes may well lead to loss of emulsifying properties of polypeptides.

Bitterness is a desirable taste in some foods and beverages, such as tea, and coffee. The bitter compounds need to be above threshold amounts to be perceived by consumers and the threshold values vary for different compounds and media (Drewnowski, 2001). For instance, the threshold value of caffeine in

water is measured to be 94 mgL^{-1}, and it is double this in fruit juice. Desirability and perceivable threshold amounts in emulsions should be considered in the control of the bitter taste of food products. While the taste implication of fragmented polypeptides is of some importance in consideration of their use as food emulsifiers, the current project will not address this complex issue. Here we only focus on the physio-chemical aspect of the adsorption of such fragments to interfaces.

1.8 Specificity of Trypsin

Bergmann et al. (1939) used synthetic substrates to determine trypsin specificity. They found that trypsin hydrolysed only an arginine compound among different amino acid compounds containing histidine, lysine, glutamic acid, tyrosine and glycine. Additionally, it was found that the enzyme was sensitive to different arginine compounds. (Bergmann et al., 1939). In their second study they found that lysine compounds can also be hydrolysed by trypsin (Hofmann and Bergmann, 1939). Similarly, it was highlighted in the later studies that trypsin action was restricted to the basic amino acids lysine and arginine (Inagami and Mitsuda, 1964, Perona et al., 1995, Polticelli et al., 1999). This is also confirmed by Olsen et al. (2004) who found that trypsin exclusively hydrolysed the C-terminal to arginine and lysine (Olsen et al., 2004).

Trypsin does not seem to attack different peptide bonds as broadly as some other enzymes and therefore there is less uncertainty about the cleavage sites compared to, for instance, pepsin. Therefore, many research studies have mostly focused on the inhibitors and activators of trypsin.

1.9 Summary and Evaluation on the Literature Review of Fragmented Proteins, Trypsin Specificity and the Bitterness of Peptides

Bitter taste formation in peptides is generally related to the presence of hydrophobic, basic, and aromatic amino acids, especially when they are located at the terminal sides of peptides. Therefore, the bitterness can be reduced by using enzymes which are not specific to these groups of amino acids. The size of the peptide chains is also found to be related to the bitterness. Studies showed that the bitterness rises with increased degree of hydrolysis and it reaches the maximum level at the intermediate degrees.

The interfacial properties of fragmented proteins are widely studied in the literature. While some of them showed that the stability of emulsions was improved by the hydrolysis of the protein, some others reported a deterioration or no considerable difference in the stability. Although the results are rather mixed, there is a general observed trend when one considers all of the results from different studies together. For instance, it is evident that, extensive hydrolysis of proteins is no good for obtaining better interfacial properties relative to unbroken protein. However, some improvements are reported for the cases where the proteins are hydrolysed at low levels. The hydrophobic and hydrophilic character of the resulting peptides are also highlighted to be significant. This is very much related to the enzymes used for the hydrolysis. Peptides having both hydrophobic and hydrophilic residues (amphipathic) were reported to display better interfacial properties. However, a uniform distribution of these residues along the polypeptide backbone is not favourable. Conversely, it was shown that better

interfacial properties are obtained for polypeptides with sufficiently large blocks of hydrophobic and hydrophilic residues in discrete regions on the peptide chain.

Increasing the degree of hydrolysis has a negative effect on both bitterness and interfacial properties. However, we have carried out the investigation both at low and high levels of hydrolysis to help understand the influence of the extent of hydrolysis on interfacial behaviour and colloidal stabilising properties of fragmented proteins.

The bovine milk protein, α_{s1}-casein and its fragmented products are the polypeptides that we investigate here in our theoretical studies. In its intact form, α_{s1}-casein has a roughly triblock-like (hydrophobic-hydrophilic-hydrophobic) structure (Dickinson, 2005) which is thought to allow for derivation of polypeptides with large blocks of hydrophilic and hydrophobic residues, by tryptic hydrolysis.

Trypsin targets the basic (i.e. positively charged at pH=7) amino acids (Lys and Arg). Thus, α_{s1}-casein hydrolysates formed with trypsin will possibly be bitter since these amino acids lead to bitter taste formation when they located at the terminal sides of peptides. Some results were found in the literature (Kodera et al., 2006) that confirm this. When these hydrolysates are used as surface active materials in foods, a suitable debittering process should be considered.

1.10 Aim and Objectives

1.10.1 Aim

The aim of this study is the theoretical examination of the possibility that the fragments of a protein may provide better colloidal stability than the intact protein itself. We are also interested to say under what circumstances and degree of hydrolysis the colloidal stabilising behaviour of such fragments is at its optimum.

1.10.2 Objectives

In order to achieve the above aim, the following objectives are stated:

- Analyse the usual SCF approach to diagnose its shortcoming components that actually require high computer memory to run the calculations.
- Develop a new SCF method based on the more common approach which will provide a more efficient way of handling a polymer and its many different fragments all present in the solution simultaneously.
- Implement a computer program using the new approach and validate it.
- Do a literature review of the experimental studies about the hydrolysed proteins and identify the properties of the hydrolysates or the polypeptide chains that express better interfacial properties.
- Chose an appropriate protein and enzyme to obtain fragments that have possibly good colloidal stabilising properties, for the purpose of the theoretical study.
- Investigate the adsorption behaviour of polydisperse homopolymers under various conditions (e.g. different solution concentrations or adsorption energies) as a simpler case (compared to the polydisperse protein

fragments) to test the new program and also to understand the adsorption phenomena in colloidal systems involving polydisperse polymers obtained by hydrolysis of a macromolecule.

- Investigate the colloidal stabilising properties of protein fragments obtained by the selective single bond and non-selective multiple bond hydrolysis at various pH values.

1.11 Thesis Outline

The thesis is composed of 6 chapters.

Chapter 1 involves industrial applications and benefits of colloids, a brief explanation of colloidal interactions, emulsifying properties of polysaccharides and proteins as one of the main components of food colloid formulations and various strategies in the literature to stabilise colloidal systems. Furthermore, a literature review of the previous extensions and applications of the SCF approach, the adsorption of polydisperse polymers and the experimental studies of surface active properties involving protein fragments, were given in this chapter. We also discussed the specificity of the trypsin (the enzyme considered for the hydrolysis of the protein in our study) and the bitter taste resulting from the formation of fragments, in this introduction chapter.

Chapter 2 presents the detailed description and the limitations of the usual SCF approach as applied to highly fragmented polymer solutions. It also provides the derivations of the new equations underlining our new approach. We also discuss a novel way of calculating the “effective” surface electrostatic potential and finally

the validation of the results obtained by the new computer program which was built based on this novel SCF approach.

Chapter 3 focuses on the preferential adsorption of polydisperse homopolymers obtained by hydrolysis. The chapter starts by introducing the use of polysaccharides as homopolymers in the stabilisation of colloids, the significance of understanding the preferential adsorption and a brief evaluation of the literature review of homopolymer adsorption given in the chapter 1 to differentiate our work. Then the chapter presents the results showing how the preferential adsorption of homopolymer fragments is influenced by various parameters such as bulk solution concentration, degree of hydrolysis, the intact size of the original homopolymer and the strength of the affinity of monomers to the surface.

Chapter 4 investigates the colloidal stabilising properties of hydrolysed α_{s1}-casein. The protein was fragmented into two polypeptides by the tryptic hydrolysis of a single specific peptide bond, each time chosen from the one or other end of the hydrophilic middle section of α_{s1}-casein. The colloidal stabilising properties of the resulting polypeptides and the intact protein was then compared at various pH values.

Chapter 5 again investigates the colloidal stabilising properties of hydrolysed α_{s1}-casein but this time all the susceptible peptide bonds that can be targeted by the enzyme trypsin are hydrolysed at various levels of hydrolysis. The colloidal stabilising and surface adsorption properties of the resulting polypeptides, as well as the intact protein, were investigated and compared at various pH values.

Chapter 6 summarises the results and gives the key findings in this study. In addition, the chapter also involves a discussion of the future work and contributions made by this study.

Chapter 2 Theory and Method

The self-consistent field (SCF) theory based on Scheutjens-Fleer scheme was used in this study. The theory was extended to model the adsorption of fragmented macromolecules onto colloidal particles and to investigate the nature of colloidal interactions that are mediated by such adsorbed layers. In this chapter, first we describe the methodology and examine basic equations appearing in the usual SCF approach as used in a number of previous theoretical studies (Ettelaie et al., 2014b, Ettelaie et al., 2014a, Ettelaie and Akinshina, 2014b, Scheutjens and Fleer, 1979, Leermakers et al., 1996). Then the limitations of the usual approach (i.e. motivation of this study) are highlighted. Finally, the equations of our new approach are given.

2.1 The Usual SCF Approach

Polymer segments, solvent molecules and ions in a solution have interactions (e.g. electrostatic, hydrophobic) with interfaces. In addition, the presence of an interface limits the number of conformations that the polymer chains can take up. Therefore, the concentration profiles at the interfacial area are likely to be significantly different from the uniform concentration profiles in the bulk solution. SCF calculations predict the concentration profiles $\{\phi_i^a(r)\}$ of the solvent, polymers, and ions between two flat parallel surfaces for the profiles that minimise the free energy of a system. $\{\phi_i^a(r)\}$ is predicted for each kind of monomer a that belongs to polymer chains of type i, as a function of distance r

away from the interface. $\phi_i^a(r)$ is the volume fraction of the kind of monomer a that belongs to polymer chains of type i at the distance r away from the surface. The length of the chain i is denoted by N_i from now on and N_i=1 for the solvent molecules and simple ions. The probability of any concentration profile that can arise is given by the corresponding Boltzmann factor for that profile and is proportional to $\sim\exp(-\Delta F(\{\phi_i^a(r)\})/k_BT)$, where $\Delta F(\{\phi_i^a(r)\})$ is the free energy of that profile. Thus the concentration profile with the minimum free energy state is the most probable profile for the system to the extent that the thermodynamic behaviour of the system is predominantly determined by this profile. The fluctuations around this most probable profile are considered negligible due to their low probabilities. This is also known as the SCF approximation which due to this feature can be considered a mean-field type theory. The main goal of the calculations is therefore to find the most probable concentration profile for the solvent, polymers and ions in the interfacial region. The approximation is valid for the dense interfacial layers, which is the case for polymer adsorption (Grosberg and Khokhlov, 1994, Lifshitz et al., 1978, Fleer et al., 1993). This is because there are less fluctuations in the concentration profile for these dense interfacial layers.

The interactions (i.e. steric, electrostatic, hydrophobic etc.) in a system influence the conformation and distribution of polymer chains and other molecules across the gap between opposite surfaces, and this results in a set of concentration profiles $\{\phi_i^a(r)\}$ for each monomer type at a distance r away from the surfaces. In calculating the value of the free energy for any profile, it is often not too difficult to obtain the enthalpy part of the free energy, so long as the interactions between

monomers, monomers and solvent, monomers and interface, etc. are known. The entropy contribution however is much more difficult to obtain. To do so one introduces a set of fields $\psi_a(r)$ that is specific to each type of monomer applied at each distance r away from the surface. This can be considered as an external field that when it is applied solely to a non-interacting system (i.e. monomers that do not affect the conformation and distribution of the neighbouring monomers), the resulting concentration profiles $\{\phi_i^a(r)\}$ would be the same as the desired profile for the equivalent interacting system for the minimum free energy state. By the term “equivalent” we mean that the size and sequence of the polymer chains and the bulk concentrations of the polymer chains and other molecules are all the same in the two systems. The only difference is that in one system monomers only interacting with external field but not with each other, i.e. all internal interactions are switched off. For the purpose of numerical calculations, the distance L between two opposite surfaces is divided into (L/a_0) layers all having an equal thickness of a_0. Here a_0 is taken as ~0.3 nm, and is the nominal size of all the monomeric units (i.e. polymer segments, ions, solvent molecules) in the system which for simplicity are assumed to be equal. A lattice is formed by sub-dividing the layers into identical cubic cells. Figure 2.1 shows the illustration of two oil droplet surfaces and a two dimensional representation of the 3-D lattice between them. Monomers forming a polymer chain and the lattice layers are numbered as n=1,2,3….N_i, and r=1,2,3,….L, respectively. Polymer segments of a chain in the lattice are positioned as Markov chains where the position of

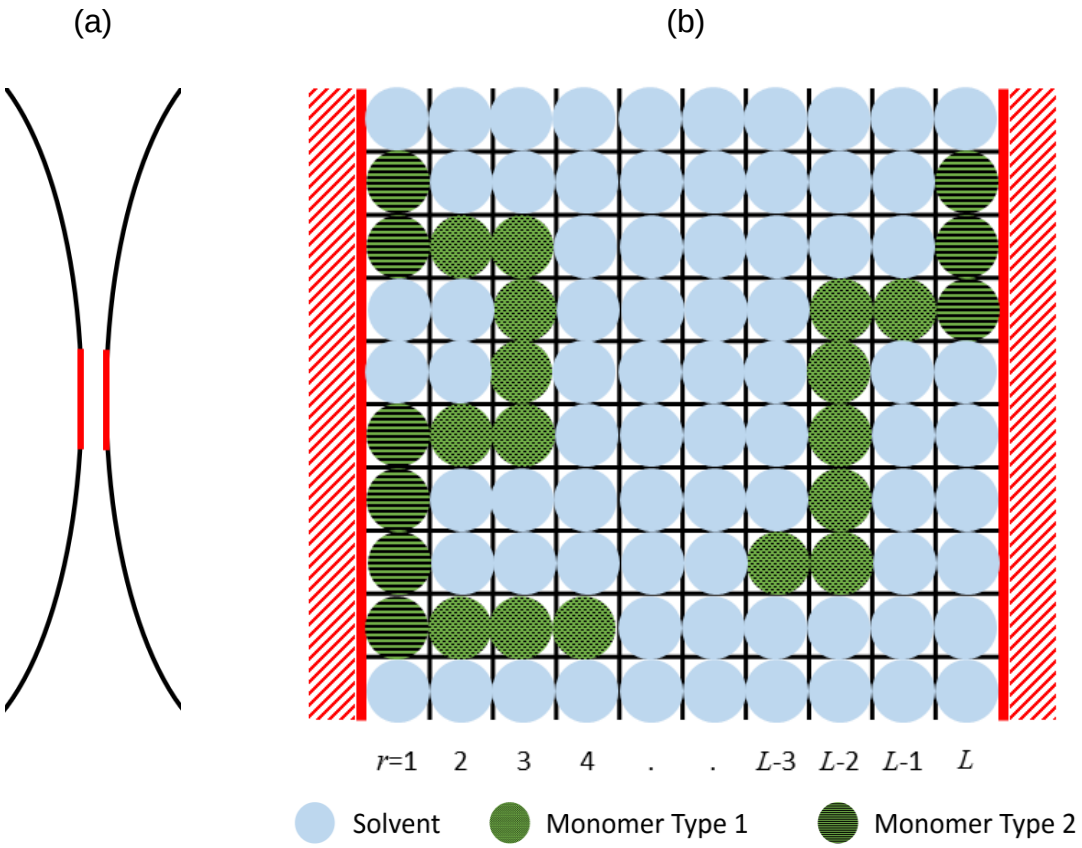

Figure 2.1 Illustration of two flat parallel hydrophobic surfaces (not to scale) (a), and a two dimensional lattice between the surfaces composed of L number of layers r=1 to L (b). All lattice sites are filled with solvent or a monomer and cannot be empty.

monomer n+1 is dependent on the position of monomer n due to the connectivity of monomers in a polymer molecule. In a cubic lattice, if a monomer n is at layer r, n+1 can be at four positions in the same layer r, at one position in layer r+1, and at one position in layer r-1 (Figure 2.2). Thus, the probability of the n+1th segment to be at layers r, r-1, r+1 are statistically (i.e. with no interactions considered) λ_0=4/6, λ_{-1}=1/6, and λ_{+1}=1/6.

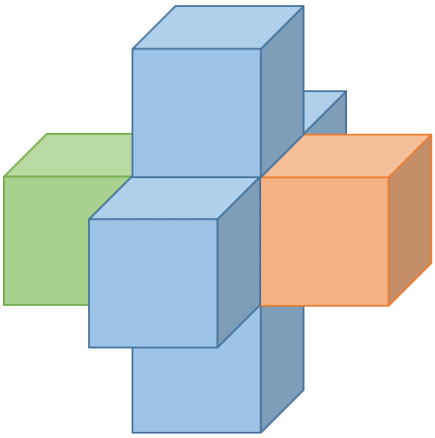

Figure 2.2 Illustration of possible relative positions for a monomer n+1 that is connected to monomer n in a cubic lattice. When the monomer n is placed at the centre (layer r), monomer n+1 can be at four positions in layer r, at one position in layer r-1 and one position in layer r+1.

The solvent molecules, polymer segments, and ions occupy the lattice sites depending on their corresponding mean fields $\psi_a(r)$. Each time there is a monomer of type a at position r, then there is a Boltzmann factor $\exp[-\psi_a(r)]$, where we are expressing $\psi_a(r)$ in units of k_BT (k_B being Boltzmann constant and T temperature). The concentration of the monomer types within a layer is assumed to be uniform. With this assumption, the calculation of the volume fractions $\phi_i^a(r)$ and the mean fields $\psi_a(r)$ for various monomer types between two opposite surfaces can be simplified and proceeded only as a function of the perpendicular distance r away from the surfaces. At distances very far away from the interface (i.e. in bulk solution) $\psi_a(r)$ is equal to 0.

The mean fields $\psi_a(r)$ are expressed in units of k_BT where k_B is the Boltzmann constant and T is the temperature (taken as 298 *K* in this study) and the components of the mean field are shown by

$$\psi_a(r) = \psi_h(r) + \psi_a^{el}(r) + \psi_a^{int}.$$

2.1

$\psi_h(r)$ is the hard core potential arising from the crowding of the monomers in layer r and affects all the monomers equally in this layer. Consider a layer r that is favourable for a monomer type a (a free monomer) to stay in this layer. Monomers of type a in the system start to come to the layer r and the hard core potential in the layer r will increase depending on the abundance of the monomers of type a. The more monomers of type a come to the layer r, the less favourable the layer becomes for monomers of type a. Then monomers of type a go towards other favourable layers that have more empty sites. In this way, the hard core potential ensures the incompressibility of the solution.

$\psi_a^{el}(r)$ represents the contribution of the electrostatic potential again in units of (k_BT) induced by a charged monomer of type a (long-ranged interactions) to the mean field and is calculated by

$$\psi_a^{el}(r) = q_a\psi^{el}(r)\,,$$

2.2

where q_a is the charge of the monomer of type a and $\psi^{el}(r)$ is the electrostatic potential per unit charge expressed in units of (k_BT/e) in layer r. Similar to the

mean fields, the electrostatic potential $\psi^{el}(r)$ also varies only in perpendicular directions to the surfaces and it is determined relative to bulk solution. As such the reference potential is 0 in the bulk solution.

The electrostatic potential $\psi^{el}(r)$ is related to the charge density ρ, through the Poisson equation

$$\nabla^2\psi^{el}(r) = \frac{-\rho(r)}{\varepsilon_0\varepsilon_r},$$

2.3

where ∇^2 is the Laplacian operator, $\rho(r)$ is the charge density in layer r in this study expressed in normalised units (e/a_0^3), ε_0 is the vacuum permittivity and measured in farads per meter (F/m) however, the unit is converted into (e^2/k_BTa_0) in this model for the consistency with the unit of electrostatic potentials (k_BT/e) and charge density (e/a_0^3). ε_r is a dimensionless parameter and represents the relative permittivity of the solvent compared to that of vacuum (taken as 78.5 for water).

The volume charge density $\rho(r)$ can be related to the plane charge density $\sigma(r)$, by the equation $\rho(r) = \sigma(r)/a_0$, for a layer of thickness a_0, and $\sigma(r)$ can be calculated according to

$$\sigma(r) = \sum_a q_a\phi_a(r)\,,$$

2.4

where $\phi_a(r)$ is the volume fraction of monomer type a in layer r. $\sigma(r)$ is expressed in units of e/a_0^2.

The last term ψ_a^{int} in Eq. 2.1 represents the contribution of the potential arising from the short-ranged (nearest neighbour in the lattice model) interactions between a monomer of kind a and all the other monomer types, as well as the surface. ψ_a^{int} is calculated according to

$$\psi_a^{int} = \sum_{\beta}^{w} \chi_{\alpha\beta}\left(\langle\phi_\beta(r)\rangle - \Phi_\beta\right) + \left(\delta_{r,1} + \delta_{r,L}\right)\chi_{as}\,, \qquad \textbf{2.5}$$

where w is the number of types of different monomers that make up the polymer chains, as well as ions and solvent. The set of parameters $\chi_{\alpha\beta}$ are the Flory-Huggins interaction parameter (Fleer et al., 1993) between monomers of type a and β and similarly χ_{as} is the Flory-Huggins interaction parameter between the surface and monomer type a. “The Flory-Huggins interaction parameter χ gives a measure of the interaction of the polymer chains with the solvent molecules as well as the polymer-polymer interaction” (Tadros, 2013). These parameters are calculated by considering the free energy of mixing (i.e. contact) of two pure substances. For instance, experiments show that the free energy change is approximately 12 kJmol^{-1} for pure alkane when it is placed in water ($CH_4 \rightarrow CH_4(aq)$) (Atkins, 2002). This is equal to ~1.0 k_BT for a single molecule and for a single contact in our cubic lattice model. χ parameters are defined for each pair of molecule types in the system including solvent and surface. More details of defining these parameters, for instance for homopolymers and amino acids, are

given in the relevant chapters of the thesis. The Kronecker delta functions $\delta_{r,1} + \delta_{r,L}$ are as usual equal to 1 when r=1 or r=L (the layers that are next to the surfaces), but otherwise are equal to 0. $\langle\phi_\beta(r)\rangle - \Phi_\beta$ gives the excess volume fraction of the monomers of type β that neighbour a monomer type a at position r and interacting with it. $\langle\phi_\beta(r)\rangle$ gives the average volume fraction of the neighbouring monomers and it is calculated according to

$$\langle\phi_\beta(r)\rangle = \lambda_{-1}\phi_\beta(r-1) + \lambda_0\phi_\beta(r) + \lambda_{+1}\phi_\beta(r+1) \qquad \textbf{2.6}$$

to take account of the occupancy number of neighbours that a monomer at position r can have in its own and two other neighbouring layers. As stated before, the total volume fractions of all types of monomers including solvent in each layer must add up to equal 1 as shown by

$$\sum_i \sum_a \phi_i^a(r) = \sum_i \sum_a \Phi_i^a = 1 \qquad \textbf{2.7}$$

for any concentration profile including the most probable one (i.e. the one with the minimum free energy state). The summation of the volume fractions of the polymer chains and monomers in bulk solution (Φ_i^a) is also equal to 1. This incompressibility condition is ensured by the hard core potential $\psi_h(r)$.

Back folding of chains is allowed which means that polymer segment n+1 can be at the same layer as the segment n-1. In other words, a self-avoiding walk is not occurring in this model. However, a real chain segment cannot take up a volume

(i.e. a lattice site) that is already occupied by another chain segment. Besides that, some of the volume around a real chain segment is also inaccessible to other polymer segments due to the steric effect. Therefore, the real polymer chains cannot take up some configurations due to these inaccessible volumes and the effect is called the *excluded volume effect* (Dickinson and Stainsby, 1982).

The excluded volume effect in this model is partly imposed by the hard core potential and Eq. 2.7. It is partly controlled because the hard core potential controls the total volume fractions of monomers for a layer but not for a single lattice site. On the other hand, it was suggested by Flory (1953) that polymer chains behave ideally in a polymer melt where their walk is random and not effected by the presence of the other segments (i.e. the steric effect). This is because the forces arising from the segment-segment interactions around a chain segment in a polymer melt cancel each other. Interfacial layers in polymer adsorption are semi-diluted, which is also the case in our model. Therefore, the behaviour of the polymer chains in the interfacial area is close to the behaviour of ideal chains. In such a system, the chain expansion (swelling) due to the steric effect can be neglected. Thus, the excluded volume effect in semi-diluted layers would not be as significant as it is in diluted layers.

Volume fractions of monomers $\phi_a(r)$ are needed in order to obtain the mean fields $\psi_a(r)$ as seen for instance in Eq. 2.5 . $\phi_a(r)$ can be simply obtained by summing the volume fractions ϕ_a^i of monomers of type a in all chains i that contain this kind of segments in our system which is calculated according to

$$\phi_a(r) = \sum_i \phi_i^a(r)\,.$$

2.8

In order to calculate ϕ_i^a , it is necessary first to obtain the segment weight functions, $G_i(n,r)$. These functions give the probability of a part of the chain i, consisting of the first n monomers of the chain, being found having the n^{th} monomer at layer r. The probability of the first monomer (monomer type a) of a chain or a single free monomer (e.g. solvent molecules and ions) being at layer r, under the influence of a corresponding mean field $\psi_a(r)$, is simply given by

$$G_i^f(1,r) = \exp\big(-\psi_a(r)\big)\,,$$

2.9

where the suffixes "f" and "b" stand for "forward" and "backward". These letters indicate one end or the other of the chain where the numbering starts. The two separate G functions are needed for polymer chains unless the chain is perfectly symmetrical. The probability of the n^{th} monomer (for $N_i \geq n > 1$) ending at layer r is calculated by the recurrence relation

$$G_i(n,r) = \exp\Big(-\psi_{t_i(n)}(r)\Big)\{\lambda_{-1}G_i(n-1,r-1) + \lambda_0 G_i(n-1,r) + \lambda_{+1}G_i(n-1,r+1)\}\,,$$

2.10

where $t_i(n)$ is the type of the n^{th} monomer of the chain of type i. In the above equation, $G_i(n,r)$ is found recursively from a knowledge of $G_i(n-1,r)$ which

means that the position of the n^{th} monomer is dependent on the position of the previous monomer due to the chain connectivity. As mentioned before, λ_{-1}, λ_0, and λ_{+1} are the probability parameters related to the type of lattice determined by the number of possible neighbours a monomer can have in each of the adjacent two layers, r+1 and r-1, or in its own layer r. The connectivity of chains means that two successive monomers have to be either in adjacent layers or within the same layer (Figure 2.2).

The volume fraction of solvent and ions can be calculated according to

$$\phi_i^a(r) = \Phi_i G_i(1,r) \qquad \textbf{2.11}$$

since the solvent molecules and ions are free monomers (i.e. not connected to other monomers through covalent bonds, as part of a polymer chain). In the above equation, Φ_i is the bulk concentration of component i. For the calculation of $\phi_i^a(r)$ of polymer chains, Eq. 2.10 needs to be run for all segments and for all layers, starting from one end, (G_i^f), and then the other, (G_i^b), for all the various polymer types (i). Then the volume fractions of the monomers of type a (the segments of chain i) at layer r $\phi_i^a(r)$, can be calculated by the so called "composition law" (Evers et al., 1990a, Fleer et al., 1993, Ettelaie et al., 2003)

$$\phi_i^a(r) = \frac{\Phi_i}{N_i} \sum_{n=1}^{N_i} \frac{G_i^f(n,r) G_i^b(N_i - n + 1, r) \delta_{a,t_i(n)}}{\exp\left[-\psi_{t_i(n)}(r)\right]}. \qquad \textbf{2.12}$$

In Eq. 2.12, Φ_i/N_i gives the bulk volume fraction of each of the N_i monomers of the chain i. The second term in the equation gives the total probability of

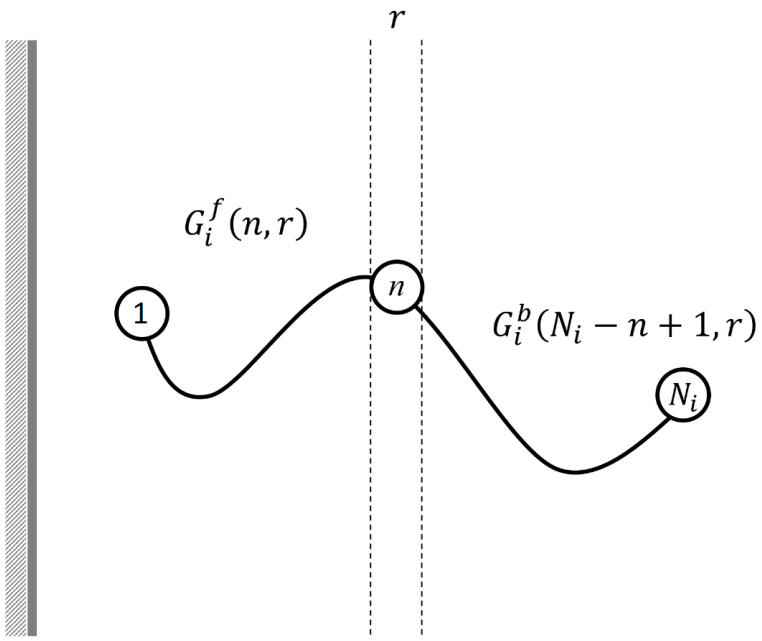

Figure 2.3 Configuration of a chain i, having its n^{th} monomer in layer r.

monomers of type a that belong to chain i being at layer r. $\delta_{a,t_i(n)}$ is the Kronecker delta function and used to calculate such probabilities only for one type of monomer on a chain, so it is equal to 1 if $t_i(n)$ is a, otherwise 0. This ensures that the summation is only over the monomers of type a when calculating $\phi_i^a(r)$. Figure 2.3 shows the configuration of a chain i, having its n^{th} monomer being at layer r. As seen in the figure, $G_i^f(n,r)$ gives the probability of the first n^{th} monomer, counting from the left side of the chain, ending at layer r. The other monomers in the first n-1 monomers can be in any layer (layer r or any other layers) with the restriction of being connected to their neighbouring monomers as dictated by the lattice type used, and of course the mean fields $\psi_a(r)$ acting on them. All these possibilities are taken into account for the

monomers before the n^{th} monomer and combined with the possibility of the n^{th} monomer being at layer r. Similarly, $G_i^b(N_i - n + 1, r)$ gives the probability of $(N_i - n + 1)^{th}$ monomer, now counting from the right side of the chain, ending at layer r. The n^{th} and $(N_i - n + 1)^{th}$ monomers counting from the two ends, respectively, are the same monomer. We note that it is accounted twice, once in the functions G_i^f and once in G_i^b. To correct for this double counting, the multiplied G_i^f and G_i^b functions are divided by $\exp[-\psi_{t_i(n)}(r)]$, which is the probability of a single n^{th} monomer being in layer r. It is useful to point out that G_i^f and G_i^b have the mathematical properties associated with Green's functions (Fleer et al., 1993).

The set of $\phi_i^a(r)$ and $\psi_a(r)$ are central quantities that need to be found in the SCF calculations. Once they are found, it is easy to calculate the volume fractions of individual monomers and chains in any layer r away from the surface. Furthermore, the average distance of each monomer to the surface, electrostatic potentials, adsorbed amounts of monomers and free energy of the system can be calculated and analysed. In order to find these two central quantities, a set of non-linear equations is formed and solved numerically. For this, firstly $\psi_h(r)$ is obtained by subtracting the last three terms in Eq. 2.1 from the mean field $\psi_a(r)$, as given by

$$\psi_h(r) = \psi_a(r) - \psi_a^{el}(r) - \psi_a^{int} \,. \qquad \textbf{2.13}$$

When the free energy of the system is minimum, the above equation should give equal values of $\psi_h(r)$ regardless of the type of monomer (a) used, since $\psi_h(r)$ is

equal for all types of monomers in layer r at the minimum free energy state. Another way of looking at $\psi_h(r)$, from a mathematical point of view, is that it is the Lagrange multiplier associated with the incompressibility conditions, Eq. 2.7, when minimising the free energy. Thus, when the free energy is minimum,

$$\psi_h(r) = \psi_0(r) - \psi_0^{el}(r) - \psi_0^{int}$$

2.14

should give the same value of $\psi_h(r)$ whichever type of monomer a is used.

Subtracting Eq. 2.13 from Eq. 2.14 must result in zero for the function in Eq. 2.15 when the free energy is minimum which leads

$$f_{a,r} = \left[\psi_a(r) - \chi_{as}(r) - q_a\psi^{el}(r) - \sum_{\beta}\chi_{\alpha\beta}\left(\langle\phi_\beta(r)\rangle - \Phi_\beta\right)\right] - \left[\psi_0(r) - \chi_{0s}(r) - q_0\psi^{el}(r) - \sum_{\beta}\chi_{0\beta}\left(\langle\phi_\beta(r)\rangle - \Phi_\beta\right)\right] = 0\,.$$

2.15

In above equation a=1 to w and r=1 to L and w is the total number of types of monomers. The variables in this model are the mean fields for each type of monomer in each layer $\psi_a(r)$, and the electrostatic potentials in each layer, $\psi^{el}(r)$. The number of variables M, is then equal to

$$M = L(w+1)\,.$$

2.16

In here $L(w-1)$ equations are obtained by subtracting the hard core potentials $\psi_h(r)$ (i.e. the Lagrange multiplier enforcing incompressibility) of the $(w-1)$ types of monomers from the one for the solvent (Eq. 2.15).

As mentioned earlier, $\psi_h(r)$ ensures that the total volume fraction of types of any type of monomer must be equal to 1 in any layer r. This requirement is formulated by

$$g_r = \log\left(\sum_i \sum_a \phi_i^a(r)\right) = 0\,,$$

2.17

where a further L equations are created by setting the logarithm of the total volume fraction of all different types of monomers in each of the L layer to zero. We have found that expressing the incompressibility condition in this way help with the convergence of our calculation. An alternative would have been to use Eq. 2.7 directly, but the convergence would be more difficult to achieve then. The number of equations now is Lw, leaving us with a further L equations still needed to solve for the $L(w+1)$ fields (Eq. 2.16). These remaining functions are related to the other variable in the model, which is the electrostatic potential $\psi^{el}(r)$ in each layer. For this, the Poisson equation, Eq. 2.3, can be used as follows

$$h_r = \nabla^2\psi^{el}(r) + \frac{\rho(r)}{\varepsilon_0\varepsilon_r} = 0\,,$$

2.18

where again r=1 to L. The charge density, $\rho(r)$, in Eq. 2.18 is given by Eq. 2.4 and can be replaced with it to yield

$$h_r = \nabla^2\psi^{el}(r) + \sum_a q_a\phi_a(r)/\varepsilon_0\varepsilon_r a_0 = 0\,.$$

2.19

The second derivative of the electrostatic potential in layer r (i.e. the first term of the Eq. 2.19) can now be discretized for the purpose of our numerical calculations as expressed by

$$\nabla^2\psi^{el}(r) = \frac{-\left(\frac{\psi^{el}(r)-\psi^{el}(r-1)}{a_0}\right)+\left(\frac{\psi^{el}(r+1)-\psi^{el}(r)}{a_0}\right)}{a_0}$$

$$= \frac{-2\psi^{el}(r)+\psi^{el}(r-1)+\psi^{el}(r+1)}{(a_0)^2}.$$

2.20

Eq. 2.19 can now be written in the following form of

$$h_r = \frac{\left(2\psi^{el}(r)-\psi^{el}(r-1)-\psi^{el}(r+1)\right)}{(a_0)^2} - \sum_a q_a\phi_a(r)/\varepsilon_0\varepsilon_r a_0 = 0\,.$$

2.21

With L such equations, one for each layer, Eq. 2.21 makes up the required number of $M = L(w+1)$ equations needed to solve for the M field variables, $\psi_a(r)$ and $\psi^{el}(r)$.

Figure 2.4 shows the algorithm of the program for solving these set of M non-linear equations. First, some random values are initially assigned to $\psi_a(r)$ and $\psi^{el}(r)$, before the calculations start. Based on the random values of $\psi_a(r)$, the Green functions (i.e. segment density functions) $G(n,r)$ are calculated in accordance with Eq. 2.9 - 2.10 in the second step. Now the volume fractions of the monomer types are determined in the third step (Eq. 2.6, 2.8, 2.12). In the following step, the values of the functions $f_{a,r}$, g_r and h_r (Eq. 2.15, 2.17, 2.21)

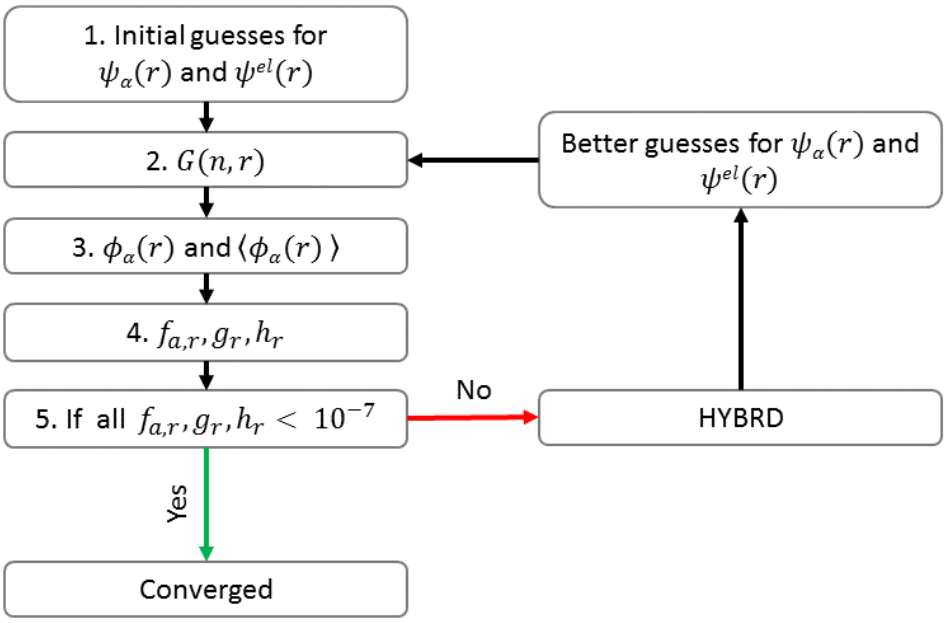

Figure 2.4 Schematic diagram of the steps for our SCF calculations.

are calculated for all monomers a=1 to w and all layers r=1 to L and checked in the fifth step to see whether all the values are sufficiently close to zero. In the current work this implies they being smaller than the accuracy parameter (10^{-7} for this study). If all the values are smaller than the accuracy parameter then convergence is achieved and the other calculations such as the average distance of each monomer away from the surface, and the free energy of the system, can now be performed. If the values of the functions are not smaller than the accuracy parameter, improved values for $\psi_a(r)$ and $\psi^{el}(r)$ which reduce the value of $f_{a,r}$, g_r and h_r functions are suggested. This improved values are achieved through the use of HYBRD algorithm, written by Moré et al. (1984) implemented in FORTRAN, and available as open source. This itself is based on Powell's method of finding minimum of a multi-variable function (Powell, 1964). This cycle continues until the zero functions are minimised to values smaller than

the accuracy parameter. In other words, it continues until the volume fractions of monomer types in each layer $\phi_a(r)$ become consistent with the mean fields $\psi_a(r)$ and the electrostatic fields $\psi^{el}(r)$ in the corresponding layers and with the incompressibility condition in Eq. 2.7. The convergence is usually achieved in a few minutes and the initial guesses do not affect the convergence time significantly.

The accuracy parameter is defined depending on the computer accuracy and the speed of the calculations. At high accuracy levels, the convergence can either be slow or not achieved at all. Thus, it should be defined by considering computational resources such as the speed of the computer, the level of accuracy that is needed, and the complexity of the system (this is related to M) that is modelled. The convergence takes a long time for systems involving many types of monomers and chains, and large surface separations, involving a high number of layers.

The average distance of the n^{th} monomer of chain i away from the surface A_i^n, can be calculated by

$$A_i^n = \sum_{r=1}^{L/2} \left[\phi_i^n(r) r \Big/ \sum_{r=1}^{L/2} \phi_i^n(r) \right], \qquad \textbf{2.22}$$

where $\phi_i^n(r)$ is the volume fraction of the n^{th} monomer of chain i at layer r and $\phi_i^n(r)$ is calculated by using Eq. 2.12.

The Helmholtz free energy equation is given according to the equation below

$$F = E - TS\,,$$

2.23

where E is the internal energy, T is the temperature and S is the entropy of the system. The entropy of the system is related to the concentration profiles of the monomers $\{\phi_i^a(r)\}$ and it is independent from the type of forces that lead to that concentration profile. In other words, it only relates to the number of possible molecular configurations that are consistent with that desired profile. Thus, the entropy of an interacting system (i.e. one where the monomers have steric, electrostatic, hydrophobic interactions with each other) can be calculated by considering the monomers as non-interacting monomers which only interacting and experience a set of external fields $\{\psi_a(r)\}$, leading to the same required concentration profile that is under study in the interacting system (Grosberg and Khokhlov, 1994).

Consider a set of external fields $\{\psi_a(r)\}$ that leads to a set of concentration profiles of the non-interacting monomers $\{\phi_i^a(r)\}$. The free energy of this non-interacting system ΔF is easily obtained and is equal to the excess volume fractions of monomers, which are calculated according to (Fleer et al., 1993)

$$\frac{\Delta F}{k_B T} = \sum_i \frac{1}{N_i} \sum_a (\phi_i^a(r) - \Phi_i^a)\,.$$

2.24

The internal energy E of this system is also simple to calculate and is given by

$$\frac{E}{k_B T} = \sum_a \psi_a(r) \sum_i \phi_i^a(r)$$

2.25

given that each monomer type a only and only interacts with its own corresponding field $\psi_a(r)$. Subtracting Eq. 2.24 and Eq. 2.25 into equation Eq. 2.23 gives the entropy of this non-interacting system for the given set of profiles $\{\phi_i^a(r)\}$. But as we mentioned above, this entropy is also equal to the entropy of an interacting system where the interactions lead to the same concentration profiles of the monomers, $\{\phi_i^a(r)\}$. The free energy per monomer unit area ($a_0{}^2$) in the usual SCF approach is given by

$$\begin{aligned}\frac{\Delta F}{k_B T} = &-\left[\sum_i \frac{1}{N_i} \sum_a (\phi_i^a(r) - \Phi_i^a)\right] - \left[\sum_a \psi_a(r) \sum_i \phi_i^a(r)\right] \\ &+ \frac{1}{2}\left[\sum_i \sum_{a\beta} \chi_{a\beta} (\phi_i^a(r) - \Phi_a)\langle\phi_\beta(r) - \Phi_\beta\rangle\right] \\ &+ \frac{1}{2}\left[\psi^{el}(r) \sum_a q_a \sum_i \phi_i^a(r)\right] + \sum_a \chi_{as} \sum_i [\phi_i^a(1) + \phi_i^a(L)]\end{aligned}$$

2.26

for two parallel flat surfaces separated by a distance of L, immersed in a solution (Grosberg and Khokhlov, 1994, Lifshitz et al., 1978). The first two terms of Eq. 2.26 give the entropy of the interacting system for a given set of profiles $\{\phi_i^a(r)\}$ obtained as discussed above. That is to say by subtracting the free energy of an equivalent non-interacting system (Eq. 2.24) from the enthalpy of that non-interacting system (Eq. 2.25). The interacting and non-interacting systems here are the equivalent systems in the sense that the size and sequence of the

polymers chains and the bulk concentrations of polymer chains and other molecules are all the same. The difference is that it is the set of internal interactions in the interacting system, as oppose to the set of external fields $\{\psi_a(r)\}$ in the non-interacting system, that lead to the same concentration profiles of monomers $\{\phi_i^a(r)\}$ for the two systems.

The summation of the third, fourth and the fifth terms in Eq. 2.26 give the enthalpy component of the interacting system when adopting a set of profiles $\{\phi_i^a(r)\}$. The third and the fifth terms are the short ranged interactions between the monomers, solvent molecules, and the surface, respectively. The fourth term is the long ranged electrostatic interactions. The third and the fourth terms are divided by 2 because of the double summation.

Now the procedure we described in Figure 2.4 essentially minimises the ΔF and obtains the set of values of $\{\psi_a(r)\}$, $\psi^{el}(r)$ and the corresponding profiles $\{\phi_i^a(r)\}$ that achieve this. In this way $\Delta F(L)$ is calculated for different values of surface separation L.

The interaction potentials V arising from the overlap of the adsorbed layers can be obtained by changing the gap size, L, between the two parallel surfaces as shown by

$$V(L) = \Delta F(L) - \Delta F(\infty)\,. \qquad \textbf{2.27}$$

In other words, colloidal interactions between two surfaces, mediated by presence and adsorption of polymers, are given by changes in the free energy of

the system, as the surfaces are moved from an infinite separation to a distance L. For the value of $\Delta F(\infty)$, the free energy for the two parallel surfaces that are sufficiently far away from each other is used. The distance (L) is the distance where the adsorption of polymers on one surface does not influence the adsorption on the other surface. Eq. 2.27 gives the interaction potentials for two flat surfaces and can be manipulated using the Derjaguin approximation (Hunter, 2001) to obtain the interaction potentials for two spherical surfaces of radius R as indicated by

$$V_{sph}(L) = -\pi R \int_{\infty}^{L} V_{flat}(x)dx \,.$$

2.28

2.1.1 Calculation of the Net Charge of Monomers and Polymers at Various pH Values

The charge of monomers is calculated by using pK_a (the negative logarithm of the acid dissociation constant K_a) values which are assumed for each type of charged monomer. The pK_a values for various amino acids used in this study, were taken from the work of Akinshina et al. (2008). For a negatively charged monomer, the fraction of the charge a groups is calculated by

$$q^{-} = \frac{-1}{1 + 10^{pK_a - pH}}$$

2.29

and for a positively charged monomer, the fraction of the charge is calculated by

$$q^{+} = \frac{1}{1 + 10^{pH - pK_a}},$$

2.30

where the equations are derived from the Henderson-Hasselbalch equation for an acid and its conjugate base form in equilibrium with each other,

$AH \leftrightharpoons A^{-} + H^{+}$ (Moore, 1985). The net charge of a polymer is calculated by summing the charge of each monomer that the polymer is composed of.

2.2 Limitations of the Usual SCF Approach

The computer program for the usual SCF approach, when applied to fragmented polymer chains, requires high memory resources to perform the calculations. Therefore, the limitations are related to this issue. For instance, the calculations for a system involving a hydrolysed polymer already become quite time consuming, if the polymer chains are broken from more than two places on their backbone with a finite probability. When a polymer (assuming this is not a homopolymer) is broken from two points with probabilities p $(0 < p < 1)$, there will altogether be 6 different polymer fragments (including the intact chain) present in the system. Indeed, more generally the number of different chains one needs to consider simultaneously is

$$i_{max} = \frac{(x + 2)(x + 1)}{2},$$

2.31

where i_{max} is the total number of different chains when the polymer is potentially cleaved from x different number of places on its backbone. When $x = 3$, i_{max} is

equal to 10 which the computer program with the usual approach finds difficult to handle for such a large number of different chains all present at the same time. Another limitation of the computer program is that it requires a tedious input process. For instance, those 10 different chains are needed to be mapped separately and input into the program.

Amino acid chains of proteins can be targeted from many places by proteolytic enzymes. For instance, trypsin attacks 20 amino acids of α_{s1}-casein. In modelling a system involving this hydrolysis, i_{max} will be equal to 231. Thus, in modelling a system involving protein hydrolysis, the number of resulting fragments can be quite large. It becomes necessary to reformulate the SCF calculations in such a way as to be able to handle this large number of fragments in a single system.

The memory problem arises from the set of non-linear simultaneous equations that involve i parameters. These are the functions that require large amount of computer memory. The segment weight functions (Green's functions) $G_i^f(n,r)$ and $G_i^b(n,r)$ are the central quantities in SCF calculations. The volume fractions of monomers of each type, that are part of a chain i, are calculated by the composition law (Eq. 2.12) which requires these Green functions obtained for each monomer of each chain, at each layer r. These volume fractions are also used in the free energy equation (Eq. 2.26). In order to reduce the high memory usage, one needs to derive a single set of "composite" Green function to replace G functions for every individual fragment type. It is obvious that the new equations should not include i parameter (i.e. no reference to a specific fragment). In this case, a new set of composition law and the free energy

equations are needed to be redefined according to the new “composite” segment weight functions. In the following section, we describe how this extension was achieved by us in this project.

2.3 The New SCF Approach (SCF_N)

Consider a polymer chain composed of N monomers which can either be identical (as in a homopolymer) or of different types (as in a protein). Monomer n represents the n^{th} monomer on the chain counted from one end, as often is labelled in the usual SCF approach. When the polymer is fragmented, the n^{th} monomer will have a different monomer sequence number in a fragment in which it may reside, accordingly to usual SCF approach of Scheutjens and Fleer (Scheutjens and Fleer, 1979). However, in order to simplify labelling the monomers, the meaning of n will be different in SCF_N approach. Monomer n on the intact chain will always continue to be labelled as monomer n, whether it is part of a smaller fragment or that of the intact polymer. Thus, monomer n and the n^{th} monomer may not be the same monomers in the new approach, when we consider a fragment.

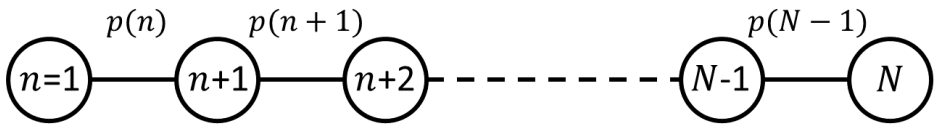

Figure 2.5 A polymer chain composed of N number of monomers. $p(n)$ is the probability of breakage between monomer n and n+1. Once labelled as monomer n on the intact chain, this monomer retains its label even if it resides on a fragment, where it may no longer be the n^{th} monomer along that fragment.

There is a probability of breakage $p(n)$ defined for each bond on the polymer. Figure 2.5 shows the labelling of the monomers of a polymer chain and it shows the probability of breakages $p(n)$ assigned to each bond. $p(0)$ and $p(N)$ are equal to 1 since these bonds are not present (to end terminus of the intact chain). $p(n)$ can be used to determine the degree of hydrolysis and the specificity of the enzyme for each bond. As a result of the many possible bond breakages, many different sizes of fragments can be present in the system at various concentrations. A fragment starting from monomer j (as labelled on the intact chain) and ending at monomer k is denoted as jk. The corresponding segment weight functions will be denoted as $G_{jk}^{f}(n,r)$ and $G_{jk}^{b}(n,r)$ for this fragment jk. These functions give the probability of a monomer n (a monomer that happens to be in fragment jk) being at layer r. The $G_{jn}^{f}(n,r)$ and $G_{jk}^{f}(n,r)$ functions are equal since $j \leq n \leq k$. $G_{jn}^{f}(n,r)$ can be written as

$$G_{jn}(n,r) = \exp\left(-\psi_{t(n)}(r)\right)\Big(\lambda_{-1}G_{jn}(n-1,r-1) + \lambda_{0}G_{jn}(n-1,r) + \lambda_{+1}G_{jn}(n-1,r+1)\Big) \qquad \textbf{2.32}$$

in terms of the same recursive relation we discussed in Eq. 2.10. The probability of monomer n being at layer r only depends on the first part of the fragment (i.e. from monomer j to n) but not the monomers that follow n. The probability of obtaining the fragment jk (P_{jk}) is equal to

$$P_{jk} = p(j-1)p(k)\prod_{l=j}^{k-1} 1 - p(l)\,.$$

2.33

The two terms $p(j-1)$ and $p(k)$ give the probability of breakage at two ends of the fragment and the last term gives the probability of no-breakage occurring for the bonds between monomers j and k, necessary for formation of fragment jk. We now define “composite” segment weight functions $Q_f(n,r)$ and $Q_b(n,r)$ that include all fragments containing monomer n, defined as

$$Q_f(n,r) = \sum_{j=1}^{n}\left(\frac{p(j-1)}{1-p(n)}\prod_{l=j}^{n} 1 - p(l)\right) G_j^f(n,r)$$

2.34

and

$$Q_b(n,r) = \sum_{k=n}^{N}\left(\frac{p(k)}{1-p(n-1)}\prod_{l=n-1}^{k-1} 1 - p(l)\right) G_k^b(n,r)\,.$$

2.35

The forward composite weight function $Q_f(n,r)$ considers only the part of each fragment (jk) that starts from monomer j ($j \leq n$) and ends at monomer n. The monomers after the monomer n (if any are available) on a fragment are not considered since the probability of monomer n being at layer r is not dependent on the chain segments that come after monomer n in the sequence or the backbone of intact chains, as discussed above. Thus for any fragment jk where

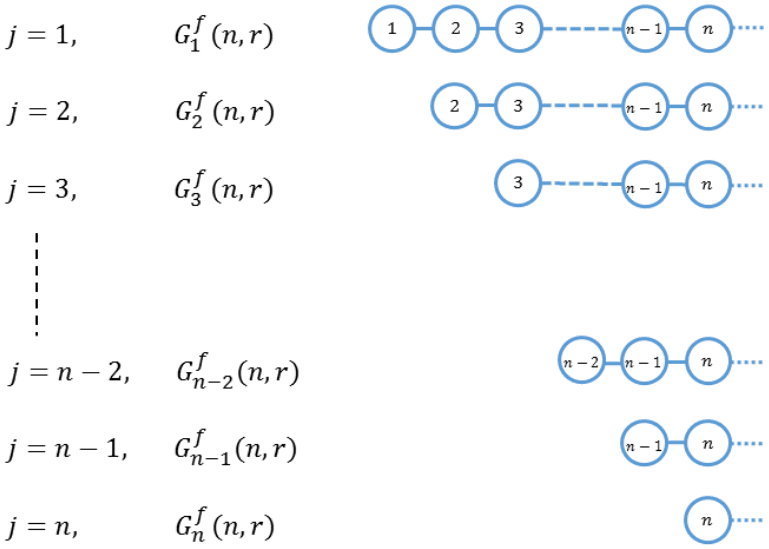

Figure 2.6 Illustration of the parts (jn) of the fragments containing monomer n and considered in the forward composite segment weight function $Q_f(n,r)$. Each $G^f_j(n,r)$ is multiplied by its appropriate weight function and then summed for all j=1 to n to yield $Q_f(n,r)$, (see Eq. 2.34)

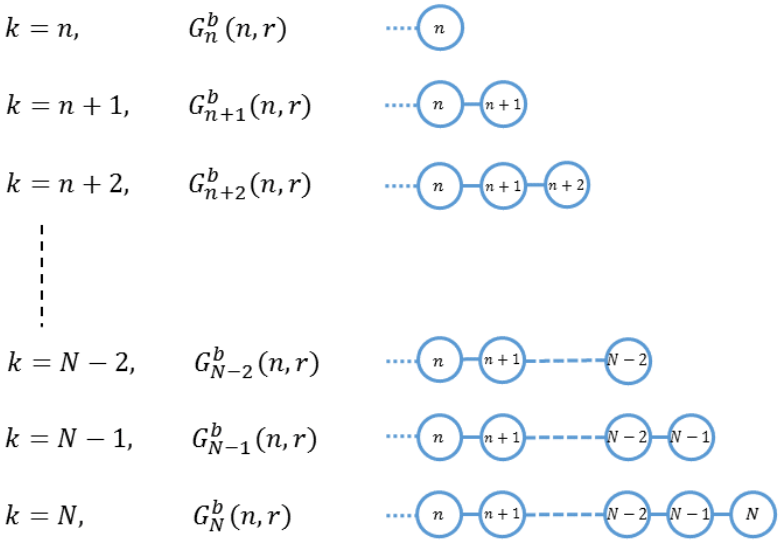

Figure 2.7 Illustration of the parts (kn) of the fragments containing monomer n and considered in the backward composite segment weight function $Q_b(n,r)$. Each $G^f_k(n,r)$ is multiplied by its appropriate weight function and then summed for all k=n to N to yield $Q_b(n,r)$.

$j \leq n \leq k$ we could write $G_{jk}^{f}(n,r) = G_{j}^{f}(n,r)$, irrespective of value of k. Figure 2.6 shows the parts of the fragments and the corresponding $G_{j}^{f}(n,r)$ functions that are considered in the forward composite weight function $Q_f(n,r)$.

Each part of these fragments contributes to the probability of monomer n being at layer r by an amount which is related to two multiplied terms. The first term is the possibility of obtaining this part (jn) of the fragment intact. The second parameter is the usual segment weight $G_{j}^{f}(n,r)$ parameter, which includes the part of all segments starting from monomer j and ending at monomer n. Similarly, the backward composite weight function $Q_b(n,r)$ considers only the part of each fragments that ends monomer k ($k \geq n$) and involves monomer n to k. Figure 2.7 shows the parts (kn) of the fragments containing monomer n and the corresponding $G_{k}^{b}(n,r)$ functions considered in $Q_b(n,r)$. As before for any fragment jk such that $j \leq n \leq k$, we have $G_{jk}^{f}(n,r) = G_{k}^{f}(n,r)$ independent of the first $j \rightarrow n$ of the fragments. j and k are the monomer ranking numbers, which both start from the left side of chains. The question is how to obtain $Q_f(n+1,r)$, now from a knowledge of $Q_f(n,r)$. From Eq. 2.34, $Q_f(n+1,r)$ will be equal to

$$Q_f(n+1,r) = \sum_{j}^{n+1}\left[\frac{p(j-1)}{1-p(n+1)}\prod_{l=j}^{n+1}1-p(l)\right] \times G_{j}^{f}(n+1,r)\,. \qquad \textbf{2.36}$$

Using recursive relations for each fragment (Eq. 2.32), the above equation can be written as

$$Q_f(n+1,r) = \sum_{j}^{n+1}\left[\frac{p(j-1)}{1-p(n+1)}\prod_{l=j}^{n+1}1-p(l)\right]\exp\left(-\psi_{t(n+1)}(r)\right)\left(\lambda_{-1}G_j^f(n,r-1)\right.$$
$$\left.+\lambda_0 G_j^f(n,r)+\lambda_{+1}G_j^f(n,r+1)\right)$$
$$=\left(1-p(n)\right)\left\{\sum_{j}^{n}\left[\frac{p(j-1)}{1-p(n)}\prod_{l=j}^{n}1-p(l)\right]\exp\left(-\psi_{t(n+1)}(r)\right)\left(\lambda_{-1}G_j^f(n,r-1)\right.\right.$$
$$\left.\left.+\lambda_0 G_j^f(n,r)+\lambda_{+1}G_j^f(n,r+1)\right)\right\}+\left(p(n)G_j^f(n+1,r)\right). \qquad \textbf{2.37}$$

Eq. 2.37 can be further simplified to

$$Q_f(n+1,r) = \left[\left(1-p(n)\right)\exp\left(-\psi_{t(n+1)}(r)\right)\left(\lambda_{-1}Q_f(n,r-1)+\lambda_0 Q_f(n,r)\right.\right.$$
$$\left.\left.+\lambda_{+1}Q_f(n,r+1)\right)\right]+\left[p(n)\exp\left(-\psi_{t(n+1)}(r)\right)\right]$$
$$=\left\{\left[\left(1-p(n)\right)\left(\lambda_{-1}Q_f(n,r-1)+\lambda_0 Q_f(n,r)+\lambda_{+1}Q_f(n,r+1)\right)\right]\right.$$
$$\left.+p(n)\right\}\exp\left(-\psi_{t(n+1)}(r)\right), \qquad \textbf{2.38}$$

which gives the recursive relation that will be used to obtain $Q_f(n+1,r)$ from $Q_f(n,r)$. Eq. 2.38 has a term that shows that the bond n is broken with a probability $p(n)$, in which case n+1 is a free end therefore has a probability $\exp\left(-\psi_{t(n+1)}(r)\right)$ of being located at layer r. The probability of bond n not being broken is $\left(1-p(n)\right)$, in which case monomer n+1 is connected to monomer n,

and the segment containing n+1 is a continuation of a segment ending which has to have the monomer n at one of the two neighbouring layers, r+1 or r-1, or in the layer r itself. A similar relation can also be derived for the “backward” composite segment density function $Q_b(n-1,r)$ as given by

$$Q_b(n-1,r) = \{[(1-p(n-1))(\lambda_{-1}Q_b(n,r-1) + \lambda_0 Q_b(n,r) + \lambda_{+1}Q_b(n,r+1)) + p(n)] + p(n-1)\} \exp\left(-\psi_{t(n-1)}(r)\right).$$

2.39

Eq. 2.38 and 2.39 give the iterative relation which can be used to compute our composite segment density function $Q_f(n,r)$ and $Q_b(n,r)$ for any values of n and r starting from $Q_f(1,r) = \exp\left(-\psi_{t(1)}(r)\right)$ and $Q_b(N,r) = \exp\left(-\psi_{t(N)}(r)\right)$ for all r values. The derivation of these new recursive relations, Eq. 2.38 and Eq. 2.39, are one of the key results of this chapter.

The volume fraction of monomer n at layer r, $\phi(n,r)$, is calculated using the composition law in the usual SCF approach (Eq. 2.12). In this new approach, all the fragments jk which contain monomer n need to be considered. The volume fraction of a single monomer of a fragment jk in the bulk solution is

$$\Phi_1^{jk} = \frac{\Phi}{N} P_{jk},$$

2.40

where P_{jk} is given by Eq. 2.33. Thus, the volume fraction of monomer n at layer r, arising from a fragment jk is then

$$\phi(n,r) = \frac{\Phi}{N} p(j-1)p(k) \prod_{l=j}^{k-1} \big(1 - p(l)\big) \frac{G_j^f(n,r) G_k^b(n,r)}{\exp\left(-\psi_{t(n)}(r)\right)}.$$

2.41

Summing Eq. 2.41 over all fragments jk containing monomer n is equal to

$$\phi(n,r) = \frac{\Phi}{N} \sum_{j \le n} \sum_{k \ge n} p(j-1)p(k) \prod_{l=j}^{k-1} \big(1 - p(l)\big) \frac{G_j^f(n,z) G_k^b(n,r)}{\exp\left(-\psi_{t(n)}(r)\right)}$$

$$= \frac{\Phi}{N} \left[\frac{1}{\exp\left(-\psi_{t(n)}(r)\right)} \right] \left[\sum_{j=1}^{n} \left(\frac{p(j-1)}{1-p(n)} \prod_{l=j}^{n} 1 \right. \right.$$

$$\left. \left. - p(l) \right) G_j^f(n,r) \right] \left[\sum_{k=n}^{N} \left(\frac{p(k)}{1-p(n-1)} \prod_{l=n-1}^{k-1} 1 - p(l) \right) G_k^b(n,r) \right].$$

2.42

As an example, the fragments jk containing monomer n for original intact chain of size, N=5 from which the fragments are derived; are shown in Figure 2.8. From definitions of $Q_f(n,r)$ and $Q_b(n,r)$ in Eq. 2.34 and 2.35, Eq. 2.42 can simply be written as

$$\phi(n,r) = \frac{\Phi}{N} \frac{Q_f(n,r) Q_b(n,r)}{\exp\left(-\psi_{t(n)}(r)\right)},$$

2.43

which is the composition law for our ensemble of fragmented chains, now expressed in terms of the composite segment functions.

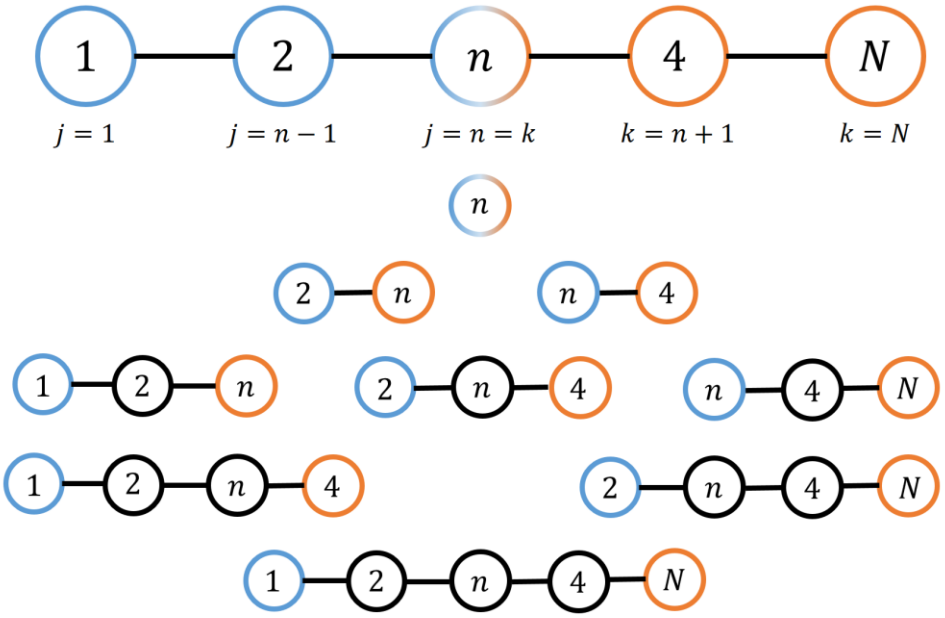

Figure 2.8 Illustration of a polymer N=5 and possible fragments jk ($j \leq n \leq k$) which contain monomer n at various j and k values used in Eq.2.42. j and k are the starting monomers for the calculation of $Q_f(n,r)$ and $Q_b(n,r)$, respectively.

As before, $\psi_{t(n)}(r)$ is the mean field at position r, for the type of monomer to which monomer n belongs. The parts (jn and kn) of the fragments jk (Figure 2.8) that are considered by $Q_f(n,r)$ and $Q_b(n,r)$ are shown in Figure 2.9.

The first step in the algorithm (Figure 2.4) will be assignment of random values to the mean fields $\psi_a(r)$ as we do in the usual SCF approach. In the second step, the calculations of $G_f(n,r)$ and $G_b(n,r)$ are replaced by $Q_f(n,r)$ and $Q_b(n,r)$. In the third step, the total volume fractions of monomers of various types (a) at layer r $\phi_a(r)$ are required in order to calculate the zero functions in Eq. 2.15, 2.17, and 2.21.

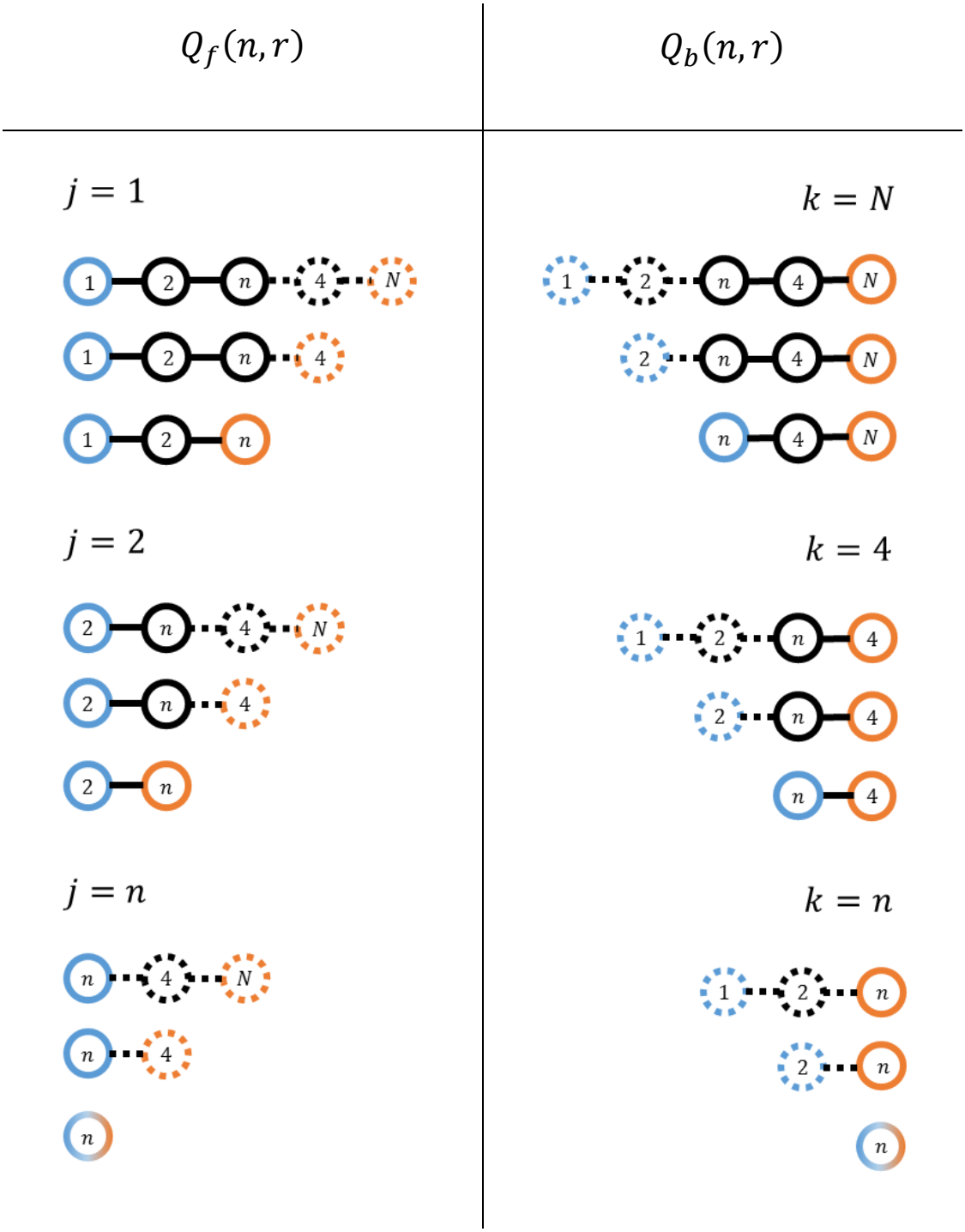

Figure 2.9 The parts (jn and kn) of the fragments (solid lines) jk in Figure 2.8 that are considered by $Q_f(n,r)$ and $Q_b(n,r)$ at various j and k values used in Eq. 2.42. j represents the starting monomer in the left column and ending monomer in the right column which are indicated in blue. k represents the starting monomer in the right column and ending monomer in the left column which are indicated in orange.

$\phi_a(r)$ is obtained by summing Eq. 2.43 over all monomers as shown by

$$\phi_a(r) = \frac{\Phi}{N}\sum_{n=1}^{N}\left(\frac{Q_f(n,r)Q_b(n,r)}{\exp\left(-\psi_{t(n)}(r)\right)}\delta_{a,t(n)}\right), \qquad \textbf{2.44}$$

where as mentioned before, $\delta_{a,t(n)}$ is the Kronecker delta function and is equal to 1 if $t(n) = a$, and otherwise 0. The other steps in the algorithm are the same as the usual SCF approach. Once convergence is achieved, the remaining calculations such as average distance of each monomer, A_n , away from the surface and free energy of the system, ΔF, can then be performed. A_n is calculated by using the same equation (Eq. 2.22) as in the usual SCF approach. However, the equation for ΔF (Eq. 2.26) is not entirely applicable to the new approach as it stands. This is because the volume fraction of monomers type α contributed from a single fragment jk, ϕ_{jk}^{a}, is not available in the new approach which is required for the first term in Eq. 2.26. $Q_f(n,r)$ and $Q_b(n,r)$ consider all fragments containing monomer n as shown in Figure 2.9. Therefore Eq. 2.44 gives the total volume fraction of the monomers of type α, ϕ_a, contributed by all fragments containing such monomers. As can be seen ϕ_a can be used to calculate all the terms in Eq. 2.26 except the first term which is the excess volume fraction of monomers type α from each specific fragment jk. The first term in Eq. 2.26 is handled in a different way in our new approach as follows:

The free energy contribution made by a chain fragment jk (size $m = k - j + 1$) ΔF_{jk} to the free energy of whole system is equal to the excess amount of the

fragment jk when the system is a non-interacting system. From Eq. 2.24, ΔF_{jk} can be written as

$$\Delta F_{jk} = -\frac{1}{m}\sum_{r=1}^{L}\left(\phi_{jk}(r) - \Phi_{jk}\right)$$

$$= -\frac{1}{m}\sum_{r=1}^{L}\phi_{jk}(r) + \frac{1}{m}\sum_{r=1}^{L}\Phi_{jk}\,.$$

2.45

$\phi_{jk}(r)$ in the above equation can be written in the form of Eq. 2.12 as below

$$\Delta F_{jk} = -\frac{1}{m}\sum_{r=1}^{L}\frac{\Phi_{jk}}{m}\sum_{n=\mathrm{j}}^{k}\frac{G_j^f(n,r)\times G_k^b(n,r)}{\exp\left[-\psi_{t(n)}(r)\right]} + \frac{1}{m}\sum_{r=1}^{L}\Phi_{jk}\,,$$

2.46

and involve the “backward” and “forward” segment density functions for that specific fragment $G_{jk}^f(n,r) = G_j^f(n,r)$ and $G_{jk}^b(n,r) = G_k^b(n,r)$. The total segment weight of any given monomer of a chain or fragment in between the two parallel surfaces (i.e. all layers) must be equal to the total segment weight of any other monomer that belong to that same chain or fragment. This is because the monomers on one chain are all connected and cannot be adsorbed individually. That is, if a chain enters the gap between the two plates, then all monomers comprising that chain are in the gap, including the first and the end monomers.

$$\sum_{r=1}^{L}\frac{G_j^f(n,r)\times G_k^b(n,r)}{\exp\left[-\psi_{t(n)}(r)\right]}=\sum_{r=1}^{L}\frac{G_j^f(j,r)\times G_k^b(j,r)}{\exp\left[-\psi_{t(j)}(r)\right]}=\sum_{r=1}^{L}\frac{G_j^f(k,r)\times G_k^b(k,r)}{\exp\left[-\psi_{t(k)}(r)\right]}$$

$$=\sum_{r=1}^{L}G_j^f(k,r)=\sum_{r=1}^{L}G_k^b(j,r)$$

2.47

since $G_j^f(j,r)=\exp\left[-\psi_{t(j)}(r)\right]$ and $G_k^b(k,r)=\exp\left[-\psi_{t(k)}(r)\right]$. This can be used in Eq. 2.46 to yield

$$\Delta F_{jk}=-\frac{1}{m}\sum_{r=1}^{L}\frac{\Phi_{jk}}{m}mG_j^f(k,r)+\frac{1}{m}\sum_{r=1}^{L}\Phi_{jk}$$

$$=-\frac{\Phi_{jk}}{m}\sum_{r=1}^{L}\left(G_j^f(k,r)-1\right).$$

2.48

Φ_{jk}/m in the above equation is the bulk volume fraction of a single monomer of the chain jk. Its value from Eq. 2.40 and Eq. 2.33 can be substituted into Eq. 2.48 to give

$$\Delta F_{jk}=-\frac{\Phi}{N}\left(p(j-1)p(k)\prod_{l=j}^{k-1}1-p(l)\right)\sum_{r=1}^{L}\left(G_j^f(k,r)-1\right)$$

$$=-\frac{\Phi}{N}p(k)\left(\frac{p(j-1)}{1-p(k)}\prod_{l=j}^{k}1-p(l)\right)\sum_{r=1}^{L}\left(G_j^f(k,r)-1\right).$$

2.49

Now for example consider the summation of the contributions to the free energy arising from all chains that start from any j≤N ($j=1\rightarrow N$) but end at N. This is given by

$$\Delta F(N) = \sum_{j=1}^{N} -\frac{\Phi}{N} p(N) \left(\frac{p(j-1)}{1-p(N)} \prod_{l=j}^{N} 1-p(l) \right) \times \sum_{r=1}^{L} \left(G_j^f(N,r) - 1 \right)$$

$$= -\frac{\Phi}{N} \left(\sum_{r=1}^{L} p(N) Q_f(N,r) - L \sum_{j=1}^{N} \frac{p(j-1)p(N)}{1-p(N)} \prod_{l=j}^{N} 1-p(l) \right).$$

2.50

More generally for all fragments starting at any $j \leq k$ ($j = 1 \rightarrow k$) but ending with monomer k, similar consideration gives

$$\Delta F(k) = -\frac{\Phi}{N} \left(\sum_{r=1}^{L} p(k) Q_f(k,r) - L \sum_{j=1}^{k} \frac{p(j-1)p(k)}{1-p(k)} \prod_{l=j}^{k} 1-p(l) \right),$$

2.51

where we have used the definition of composite segment density functions $Q_f(k,r)$ as given by Eq. 2.34 (or its alternative form Eq. 2.36) in Eq. 2.49 and summed this for all fragments ending in k (i.e. over all values of $1 \leq j \leq k$). Now summing over the contribution of all fragments ending at any $k \leq N$ will give the total free energy change

$$\Delta F = -\frac{\Phi}{N} \left(\sum_{r=1}^{L} \sum_{k=1}^{N} p(k) Q_f(k,r) - L \sum_{k=1}^{N} \sum_{j=1}^{k} \frac{p(j-1)p(k)}{1-p(k)} \prod_{l=j}^{k} 1-p(l) \right).$$

2.52

The last term in the above equation is reduced to $L \sum_{k=1}^{N} p(k)$. This is because the summation $\sum_{j=1}^{k} \frac{p(j-1)p(k)}{1-p(k)} \prod_{l=j}^{k} 1-p(l)$ in the last term of Eq. 2.52 is found equal to $p(k)$. This can be proved through proof by induction as given in appendix I.

$(k_n, j_{1\to n})$ is found equal to $p(k_n)$. Eq. 2.52 can now be written as

$$\Delta F = -\frac{\Phi}{N}\left(\sum_{r=1}^{L}\sum_{k=1}^{N} p(k)Q_f(k,r) - L\sum_{k=1}^{N} p(k)\right)$$

$$= -\frac{\Phi}{N}\left(\sum_{r=1}^{L}\sum_{k=1}^{N} p(k)\big[Q_f(k,r) - 1\big]\right)$$

2.53

and the total contribution to the free energy of the whole system made by the fragments of a chain of size N can now be calculated by using composite segment densities only as seen in the above equation. Illustration of fragments jk and their contributions to the free energy $\Delta F(k)$ are demonstrated in Figure 2.10, schematically.

Eq. 2.53 is derived to replace the first term in the free energy equation of the usual SCF approach (Eq. 2.26). As we mentioned before, the first term gives the free energy of non-interacting system which is equal to the total excess amount. The other four terms in the free energy equation of the usual SCF approach (Eq. 2.26) are applicable without modification to the new approach. The free energy for an interacting system in SCF_N approach can now be written as follows

$$\frac{\Delta F}{k_B T} = -\left[\frac{\Phi}{N}\left(\sum_{r=1}^{L}\sum_{k=1}^{N} p(k)\big(Q_f(k,r) - 1\big)\right)\right] - \left[\sum_{a} \psi_a(r)\,\phi_a(r)\right]$$
$$+ \frac{1}{2}\left[\sum_{a\beta} \chi_{a\beta}\big(\phi_a(r) - \Phi_\beta\big)\langle\phi_\beta(r) - \Phi_\beta\rangle\right] + \frac{1}{2}\left[\psi^{el}(r)\sum_{a} q_a\,\phi_a(r)\right]$$
$$+ \sum_{a} \chi_{as}\left[\phi_a(1) + \phi_a(L)\right].$$

2.54

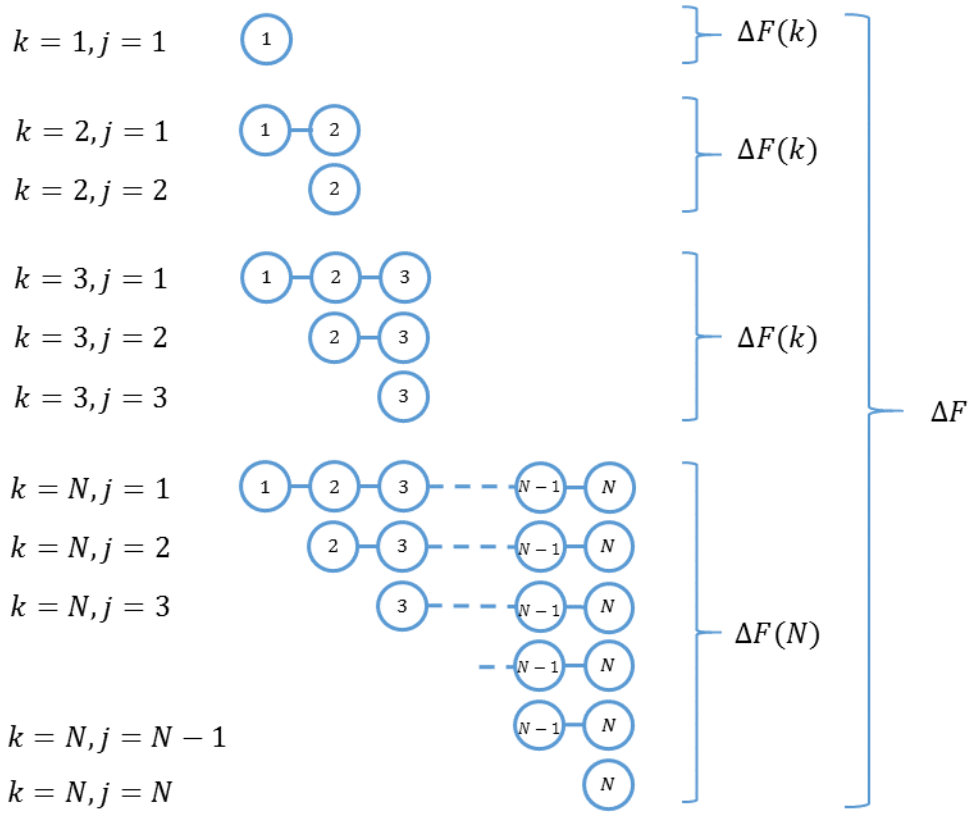

Figure 2.10 Illustration of fragments jk and their contributions to the free energy.

Once convergence is achieved, if the excess volume fraction of a specific fragment jk (i.e. the adsorbed amount) is required then this can be obtained by using the calculated mean fields as follows

$$\phi_{ex}^{jk} = \frac{\Phi}{N}\left(p(j-1)p(k)\prod_{l=j}^{k-1}1-p(l)\right)\sum_{r=1}^{L}\left[\left(\sum_{n=j}^{k}\frac{G_j^f(n,r)G_k^b(n,r)}{\exp(-\psi_{t(n)}(r)}\right)-1\right]$$

$$= \frac{\Phi}{N}P_{jk}(k-j+1)\sum_{r=1}^{L}\left[G_j^f(k,r)-1\right]. \qquad \textbf{2.55}$$

In above equation, n is an index number for the monomers between the starting monomer j and end one k for fragment jk.

G_j^f function in Eq. 2.55 is calculated by using the obtained mean fields, $\psi_a(r)$, that ensure the minimum free energy. The value of G_j^f function is specific to be used only for the fragment jk. Eq. 2.51 also gives the excess volume fraction of the fragment jk. However, in Eq. 2.55, the values of j and k are two constant preferred values $(1 \leq j \leq k \leq N)$ so the excess amount is calculated only for one very specific fragment, jk. As all the fields are already calculated through iterations involving the composite segment density functions, calculating values of G_j^f and G_k^b and hence adsorbed amount of any fragment on the surface (as given by Eq. 2.55) is a relatively quick task and does not need further iterations.

The total adsorbed amount for the fragments of size m is calculated according to

$$\phi_{ex}(m) = \frac{\Phi m}{N} \sum_{j=1}^{N-m+1} \left(p(j-1)p(m+j-1) \prod_{l=j}^{m+j-2} 1 - p(l) \right) \sum_{r=1}^{L} \left[G_j^f(m+j-1, r) - 1 \right].$$

2.56

An example, for a polymer of size $N = 5$ (original intact size) the above equation is illustrated schematically in Figure 2.11, for fragments of size 3.

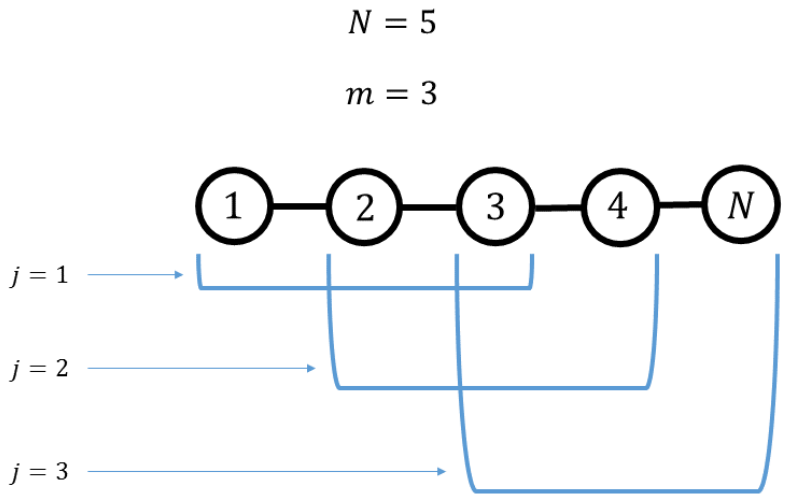

Figure 2.11 Illustration of a polymer with original intact size of N=5 and its potential fragments of size m=3 following hydrolysis for various j values.

2.4 Calculation of Effective Surface Potential

Electrostatic potentials induced by a charged surface drops approximately exponentially in the diffuse layer of ions (Dickinson, 1992). The electrostatic potential ψ^{el}, at a distance of r away from compact layer (see section 1.2.2) is given by Eq. 2.57 (Hunter, 2001)

$$\psi^{el}(r) = \psi_{\delta} \exp(-\kappa r) \,, \tag{2.57}$$

where ψ_{δ} is the electrostatic potential at the inner edge of the diffuse layer and κ is the Debye-Hückel parameter. Eq.2.57 (i.e. Debye-Hückel approximation) is a valid approximation for very small values of ψ_r^{el}(Hunter, 2001).

The Debye-Hückel parameter κ determines the rate of the drop in the electrostatic potential while moving away from the surface. The inverse of this parameter (κ^{-1}) can be used to measure the thickness of the diffuse layer which is known as the *Debye length* (Dickinson, 1992). For a symmetrical $z^+ : z^-$ type salt (e.g. NaCl), κ is defined by

$$\kappa = \sqrt{\frac{2z^2e^2n_0}{\varepsilon_r\varepsilon_0k_BT}}, \qquad \textbf{2.58}$$

where z is the valency of the ions, e is the charge of a proton, n_0 is the salt (electrolyte) concentration in the solution, k_B is the Boltzmann constant, T is the temperature in degree Kelvin, ε_r is the relative permittivity of the solution and ε_0 is the permittivity of free space (F/m) (Dickinson and Stainsby, 1982).

The surfaces in this model are not charged themselves. The presence of the adsorbed layers of charged fragments and ions creates the electrostatic potentials. The electrostatic potentials do not exponentially fall with distance away from the surface inside the adsorbed layers of charged polymers (Figure 2.12a). The layers of polymers, adsorbed at surfaces, are often not compact but extended. Therefore, it is not a priori obvious where the polymer layer ends and where the diffuse double layers of ions begin. The magnitude of these electrostatic potentials in the adsorbed layers varies depending on the distribution of the ions and charged residues of the polymers. On the other hand, the distribution of the ions and charged residues are also affected by the electrostatic

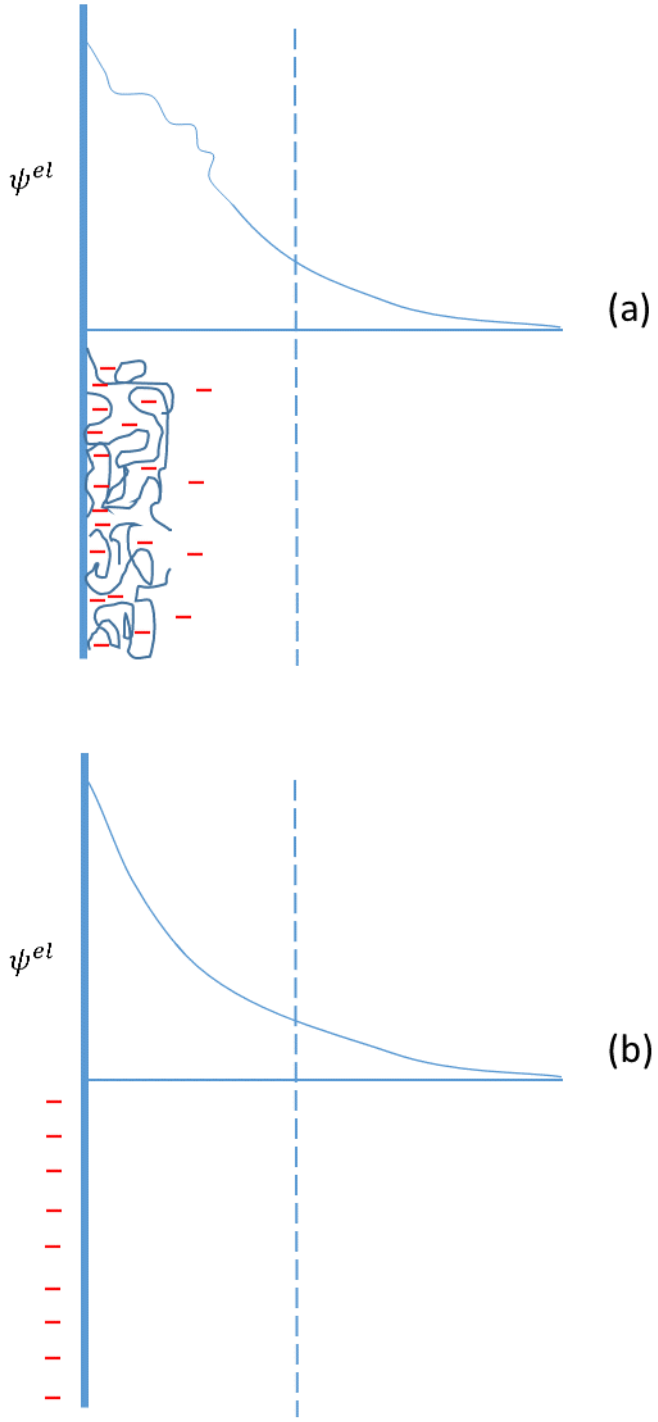

Figure 2.12 Demonstration of the variation of potential against distance away from the surface, between actual calculated ψ^{el} (a) and that from a fictitious charge surface (b), placed at the same position as the plane on which the polymers are adsorbed.

potentials. Therefore, the variation of the electrostatic potentials inside the adsorbed layer does not follow the variation of the electrostatic potentials in the usual diffuse layer theory where one has a well-defined interface on which the potential is ψ_δ and the diffuse double layer begins from this surface, extending into the bulk solution against the distance away from the surface.

Consider an ion in the outer part of the adsorbed layer where the concentration of the charged adsorbed chains is zero or significantly low. This ion is affected by the electrostatic potential induced by all the adsorbed charged monomers present at various distances away from it. The effective surface potential can now be defined as a fictitious surface potential provided by a fictitious charged surface (Figure 2.12b) without any polymer or other species adsorbed to it that would induce an equal electrostatic effect for this ion at the distance away from the surface where the ion resides. We introduce a novel way of calculating the effective surface potentials and its variation against the distance away from the surface based on this concept. Figure 2.13 is an example showing the actual predicted electrostatic potentials induced by the adsorbed layers of hydrolysed α_{s1}-casein at various levels of hydrolysis (a) and the calculated (logarithm of) effective surface potentials obtained in this way for the same corresponding degrees of hydrolysis (b). The variation of the electrostatic potentials is plotted against the distance away from the surface, at pH=3.0. At distances sufficiently far from surface (i.e. outer parts of the adsorbed layer), the electrostatic potentials become small and start to decrease exponentially in accordance with Eq. 2.57. At such distances, we plot the logarithm of the absolute value of the actual predicted electrostatic potentials against the distance away from the

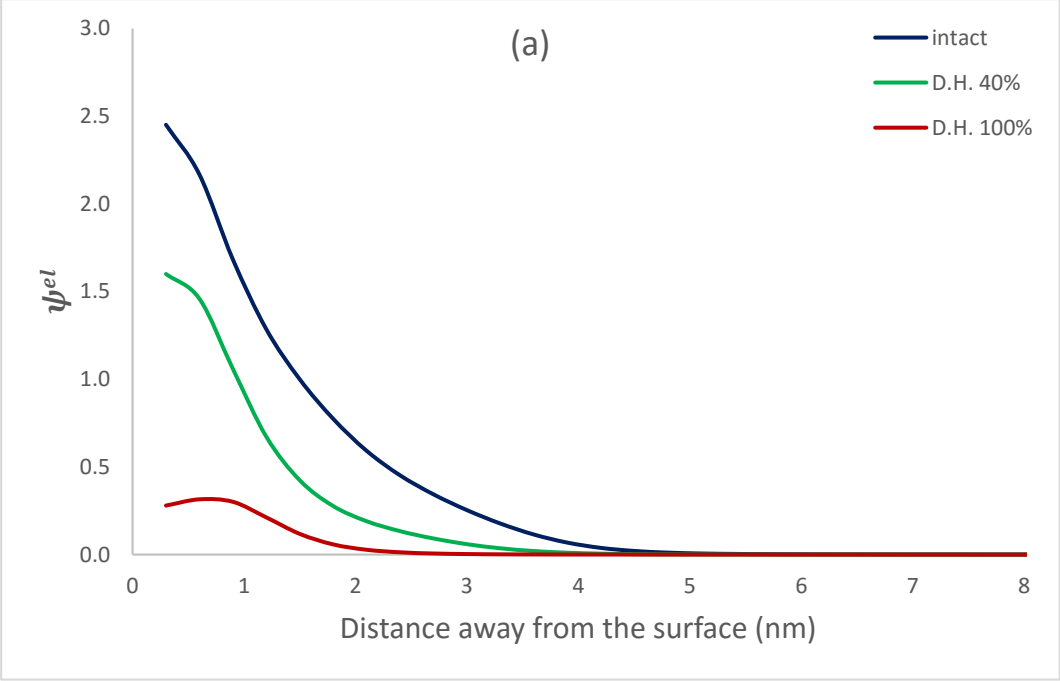

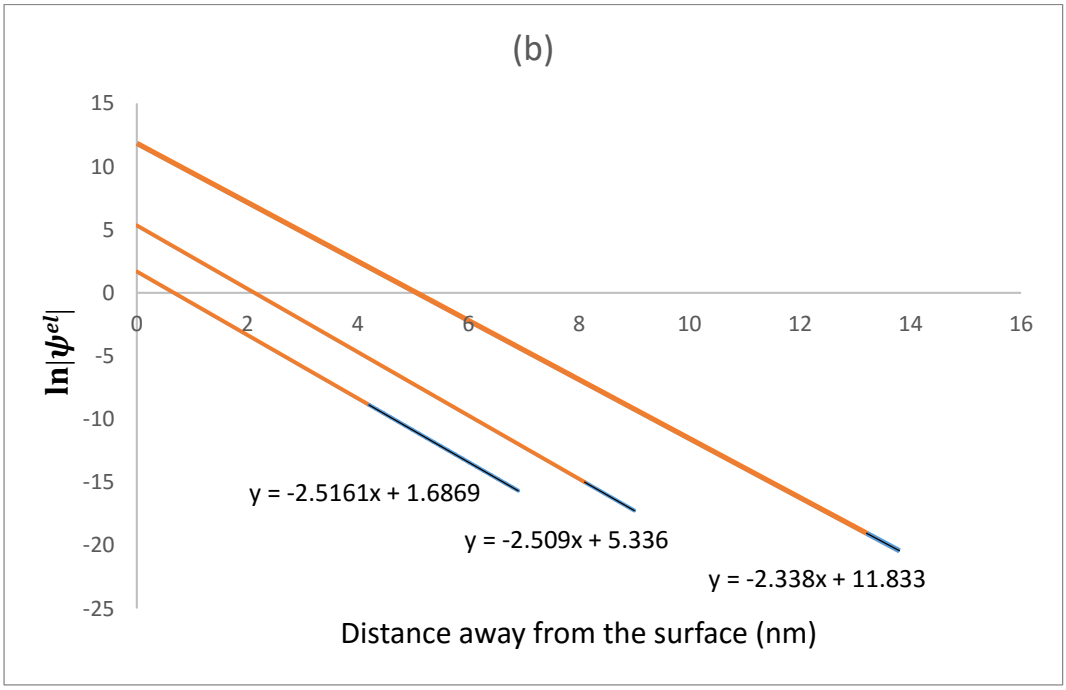

Figure 2.13 The electrostatic potentials $\psi^{el}(k_BTle)$ (a), $\ln(|\psi^{el}(k_BTle)|)$ (b), obtained at various DH values at pH=3.0, plotted against the distance away from the surface (nm). The DH values in Figure 2.13b are 0%, 40%, and 100% from top to bottom. The orange lines in Figure 2.13b are extrapolated results, based on Eq. 2.57, using the blue parts taken from value of $\psi^{el}(r)$ in Figure 2.13a, at distances far from the surface.

surface (blue parts of the lines in Figure 2.13b). Then the linear equations in Figure 2.13b, represented by the blue lines, are obtained by the best linear fit using Microsoft Excel. The linear equations take the form of Eq. 2.59 which is the logarithm of Eq. 2.57:

$$\ln|\psi^{el}(r)| = \ln|\psi_{\delta}| - \kappa r \,. \qquad \textbf{2.59}$$

x and y variables in the equations in Figure 2.13b represent r and $\ln|\psi^{el}(r)|$, respectively. The slopes of the equations provide the value of κ, and the constant values in the equations represent the logarithm of the absolute value of our effective surface potentials, $\ln|\psi_{\delta}|$, defined for a charged surface at $r = 0$. The blue lines are then extrapolated to obtain the complete graphs in Figure 2.13b. As we mentioned, the blue parts of the lines need to be created by using small values of actual electrostatic potentials in the outer parts of the adsorbed layers of polymers, since Eq. 2.57 is a valid approximation only for very small values of $\psi^{el}(r)$. For the small values of $\psi^{el}(r)$, we use the values at distances as far as our model accuracy limit (10^{-7}) allows. At distances very far from the surface, the actual electrostatic potentials become smaller than the accuracy limit of our numerical calculations and hence no longer reliable. For instance, in Figure 2.13a, the accuracy limit is reached at distances of around 12nm, 9nm, and 7nm, for the DH values of 0%, 40%, and 100%, respectively. Therefore, we use the actual electrostatic potentials before the reaching points of DH values of 40% and 100%. However, at 0% hydrolysis, the actual electrostatic potentials before the accuracy limit (~12nm) do not give the correct effective surface potentials because of the presence of the charged tails of intact protein still present at

distance of around 12nm. These tails induce extra local electrostatic potentials that contribute to the overall electrostatic potentials and make it impossible to obtain electrostatic potentials larger than our limit of accuracy at distances where such parts of the adsorbed layers are no longer present. Therefore, we use the actual electrostatic potentials at the distance longer than 13nm although it is beyond the accuracy limit (~12nm) for the non-hydrolyse case, DH=0%. That is why the slope of the line (κ=2.338) for the DH value of 0% is different from the other two slopes (κ=2.509 and κ=2.5161). The values of κ must be equal since the salt concentrations and all other parameters determining κ (Eq. 2.58) are the same at all levels of hydrolysis. Therefore, calculation of the effective surface potential for the intact protein at pH=3.0 seems to be not accurate, with $|\psi^{el}(r)|$ falling below the limit of our accuracy at distances that are still within the extended polymer film.

2.5 Validation of the SCF_N Approach

Validation of the SCF_N approach was carried out by comparing the results of the usual SCF and the SCF_N approaches obtained for an identical system. Of course it is not possible to produce results for a polydisperse system involving high number of breakage of bonds by using the traditional SCF approach of Scheutjens-Fleer (Scheutjens and Fleer, 1979). The computer program of the usual SCF approach can only handle a small number of breakages due to the high computer memory usage and a very large number of different produced fragments that are hard to consider individually. For the comparison of the results that are produced by both approaches, any polymer and any two bonds on that

polymer can be chosen to be broken with two preferred probability of breakages, p_1 and p_2. We choose to hydrolyse α_{s1}-casein as a polyelectrolyte to obtain a relatively complex polydisperse system. The protein consists of amino acids that are different in nature, such as polar, hydrophobic or charged. The two opposite surfaces in the system are attractive only for the hydrophobic amino acids as they are assumed to be hydrophobic themselves (e.g. surface of an oil droplets). The system also includes positive and negative ions that are required for the charge neutrality of the solution and to represent the background electrolyte concentration. By designing such a system, we maximise the types of interactions which helps to validate as many component (i.e. equation, feature, parameter, function) as possible in our new approach. The system parameters used are summarised in Table 2.1.

α_{s1}-casein $(N = 201)$ was hydrolysed by breaking the peptide bonds between the 43rd-44th residues with a probability $p(43) = 0.45$ and 194th-195th residues with probability $p(194) = 0.75$ as an example. The resulting possible polypeptides in this system are monomers 1-201, 1-43, 44-201, 1-194, 44-194, and 195-201. Numbering starts from the N-terminus of the α_{s1}-casein, with first monomer at N-terminus labelled 1. Each amino acid on the backbone of the protein is represented by a monomer type α depending on its nature. There are 6 different categories (i.e. monomer types from 1 to 6 as presented in Table 2.1) into which the amino acids are grouped. The other 3 monomer types specify the solvent molecules (type 0) and positive (type 7) and negative (type 8) ions. The magnitude of short-ranged interaction parameters (Flory-Huggins parameters $\chi_{\alpha\beta}$, for details see sections 3.21.4 and 4.1) between monomer-monomer and monomer-surface are given in Table 2.2. More information about the amino acid

grouping and the magnitude of chosen interaction parameters can be found in section 4.1, later on.

The results are obtained by both of the two approaches are given in the five figures below. Figure 2.14 shows the interaction potentials $V(r)/k_BT$ against the separation distance (nm) between the droplets of size 1μm. The interaction potentials are obtained by Eq. 2.27 for two flat surfaces and manipulated by Eq. 2.28 to yield those for spherical surfaces. The electrostatic potentials $\psi^{el}(r)$ are compared in Figure 2.15. The volume fractions $\phi(r)$ of solvent molecules and total polymer are presented in Figure 2.16. Finally, the volume fractions of the four of the resulting polypeptides obtained due to the hydrolysis are compared in Figure 2.17 and Figure 2.18. The computer program for the normal SCF approach was found to provide volume fractions for only four of the six polypeptide fragments due to the memory limitation we encountered on our computers. In contrast no such problem occurred with the new approach, based on formulation presented in section 2.3. Therefore, the volume fractions of the two of the resulting fragments (1-43 and 195-201) are not compared here. From all the five figures, it is evident that there is a perfect match of the results obtained by both of the approaches which means that the SCF_N approach is a valid approach further supporting proofs we have given in section 2.3. Detail discussion of such results is left to the next few chapters. Here the aim was simply to validate our significantly more efficient approach in dealing with fragmented polymers, as compared to the more usual, but well tested, method found in the literature (Ettelaie et al., 2003, Ettelaie et al., 2008a, Ettelaie et al., 2012, Ettelaie et al., 2014b).

In the next chapters, we use the new approach and present some example results for colloidal systems involving hydrolysed homopolymers and proteins to test our new program and see what benefits it provides us as a research tool.

System Parameters		
$L = 120$ $\quad pH = 3.0$		
Components		
Type (i)	Bulk Volume Fraction (Φ)	
Polymer: α_{s1}-casein (N_1=201) Solvent: water (N_2=1) Positive ion: Na^+(N_3=1) Negative ion: Cl^-(N_4=1)	$\Phi_p = 0.0001$ $\Phi_s = 0.9799$ $\Phi_{Na} = 0.01$ $\Phi_{Cl} = 0.01$	
Probability of Breakages $p(n)$		
$p_1(43) = 0.45$ $p_2(194) = 0.75$		
Monomer Types (a)		
Type	Charges (q) at pH=3.0	pK_a
a_0: Solvent	$q_0 = 0$	-
a_1: Hydrophobic	$q_1 = 0$	-
a_2: Polar	$q_2 = 0$	-
a_3: Positive	$q_3 = +1.0$	10
a_4: Histidine	$q_4 = +0.99982$	6.75
a_5: Negative	$q_5 = -0.03065$	4.5
a_6: Phosphoserine	$q_6 = -0.5001$	3&7
a_7: Ion (+)	$q_7 = +1.0$	-
a_8: Ion (-)	$q_8 = -1.0$	-

Table 2.1 The system parameters used for the calculations carried out by the usual SCF and our SCF_N approach.

Monomer type	0	1	2	3	4	5	6	7	8
0-Solvent	0	2.5	0	0	0	0	0	-1	-1
1-Hydrophobic	2.5	0	2	2.5	2.5	2.5	2.5	2.5	2.5
2-Polar	0	2.0	0	0	0	0	0	0	0
3-Positive	0	2.5	0	0	0	0	0	0	0
4-Histidine	0	2.5	0	0	0	0	0	0	0
5-Negative	0	2.5	0	0	0	0	0	0	0
6-Phosphoserine	0	2.5	0	0	0	0	0	0	0
7-Ion (+)	-1	2.5	0	0	0	0	0	0	0
8-Ion (-)	-1	2.5	0	0	0	0	0	0	0
Surface	0	-2	0	0	0	0	0	0	0

Table 2.2 Flory-Huggins parameters (χ) for the interactions between six amino acid categories, as well as those with solvent, surface and free ions, all in units of k_BT.

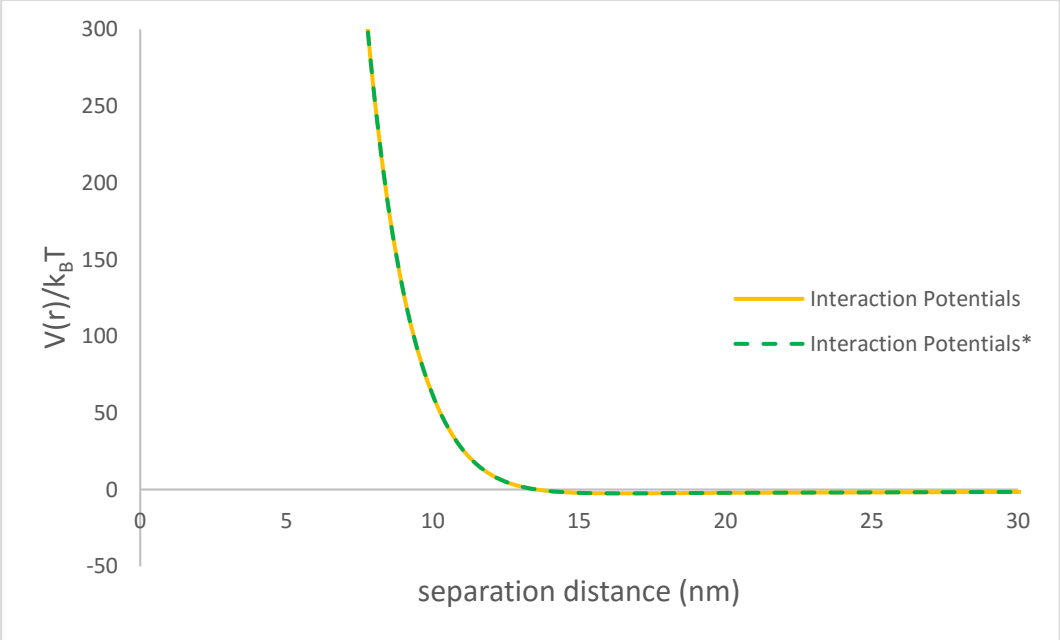

Figure 2.14 The interaction potentials $V(r)/k_BT$ obtained by the usual SCF (orange) and SCF_N (green) approaches, between the droplets of size 1μm, induced by the hydrolysed α_{s1}-casein at pH=3.0, plotted against the separation distance between the droplets (nm). Blue and orange lines are top of each other due to convergence of the solutions.

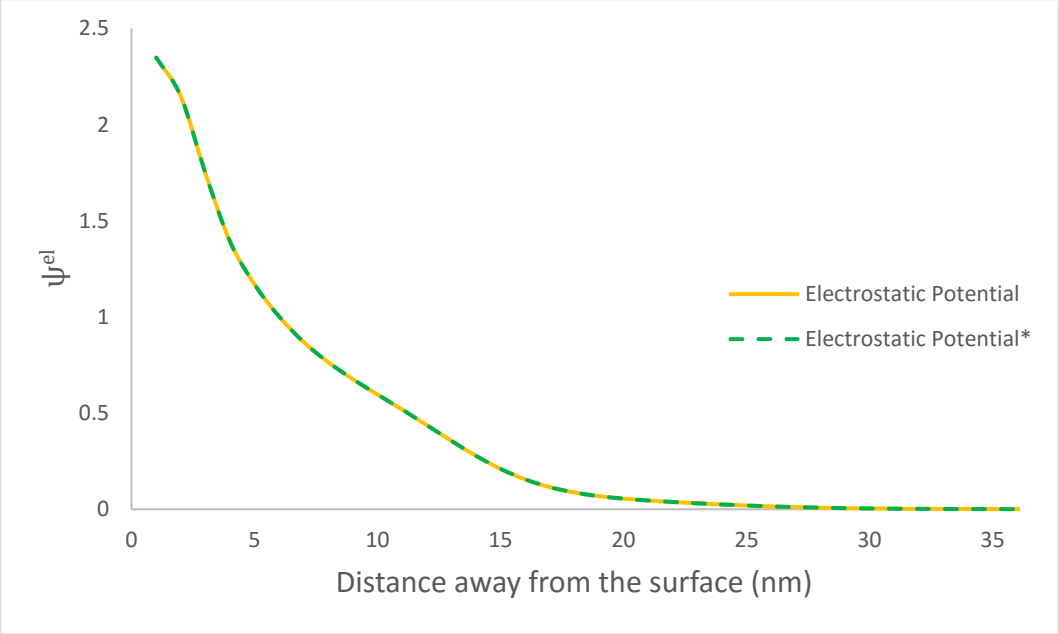

Figure 2.15 The electrostatic potentials $\psi^{el}(k_BT/e)$ obtained by the usual SCF (orange) and SCF$_N$ (green) approaches at pH=3.0, plotted against the distance away from the surface (nm).

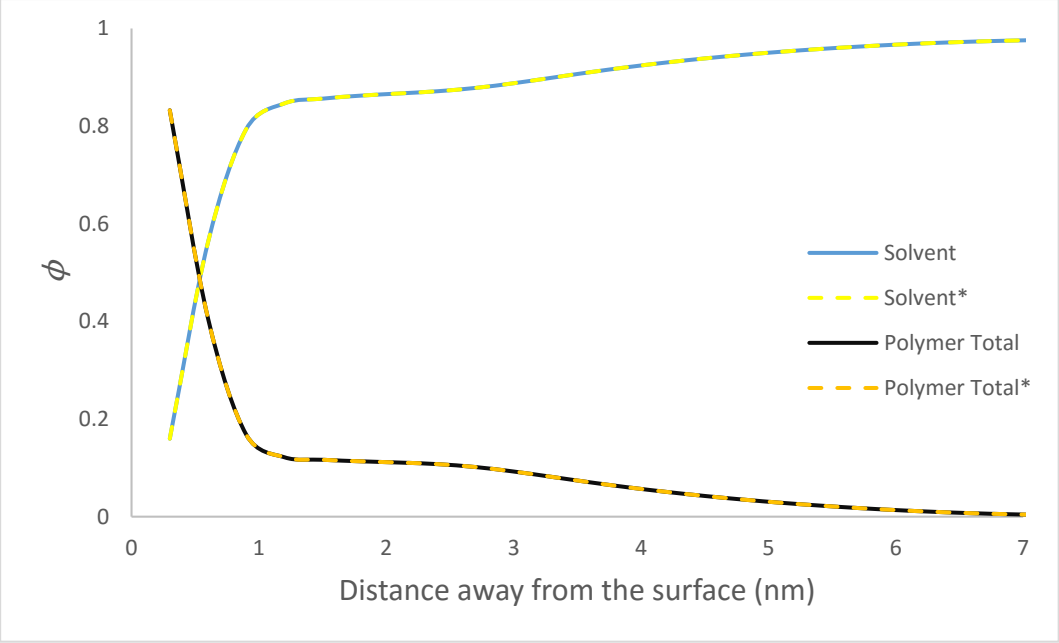

Figure 2.16 The total volume fractions (ϕ) of the polymers (hydrolysed α_{s1}-casein) and solvent molecules obtained by the usual SCF and SCF$_N$ approaches at pH=3.0, plotted against the distance away from the surface (nm). Result indicated by (*) were obtained with the new approach.

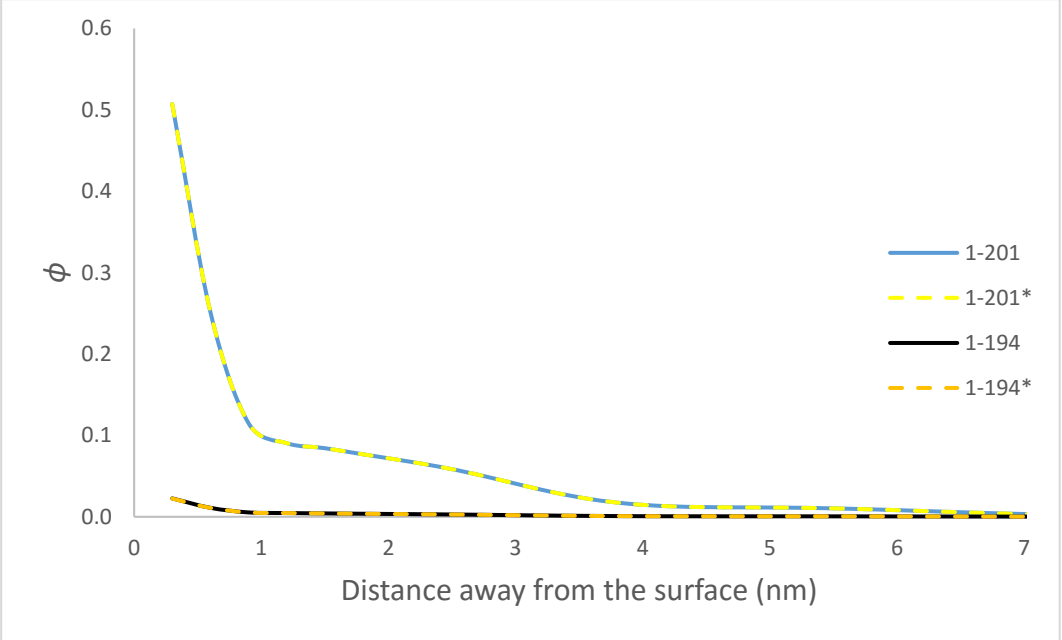

Figure 2.17 The volume fractions (ϕ) of the polypeptides 1-201 and 1-194 obtained by the usual SCF and SCF_N approaches at pH=3.0, plotted against the distance away from the surface (nm). Result indicated by (*) were obtained with the new approach.

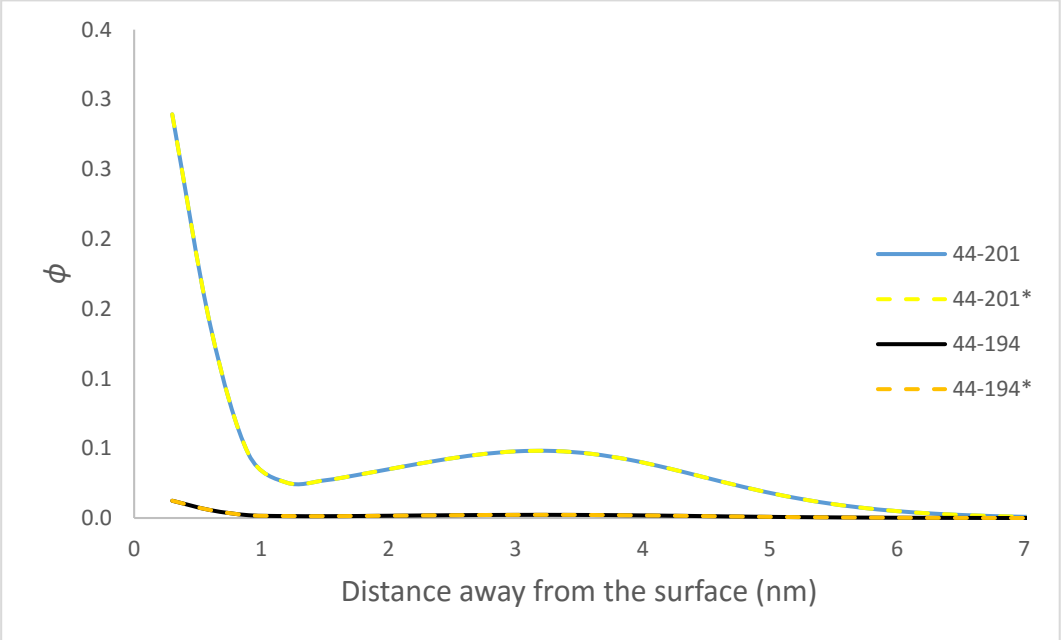

Figure 2.18 The volume fractions (ϕ) of the polypeptides 44-201 and 44-194 obtained by the usual SCF and SCF_N approaches at pH=3.0, plotted against the distance away from the surface (nm). Result indicated by (*) are obtained with the new approach.

Chapter 3 Homopolymers

3.1 Introduction

Polysaccharides are known as homopolymers in food area and are traditionally used in food manufacturing as thickening and stabilising agents. The addition of polysaccharides increases the viscosity of emulsions and reduces gravitational movement of the droplets which is the driving force for creaming and sedimentation. Additionally, the water-holding properties of polysaccharides helps to control microbial activity. These benefits have made polysaccharides highly functional ingredients for the preparation of home-made and industrial foods for many years.

Polysaccharides are the high molecular weight molecules which are mostly of a hydrophilic character. Therefore, they are naturally lacking in emulsifying properties, which confines their usage mainly to colloidal stabilisers. However, polysaccharides can be equipped with emulsifying properties through several approaches. One approach is to chemically attach hydrophobic groups to the backbone of polysaccharide, which was known as modification of starch (Yusoff and Murray, 2011) or cellulose (Murray et al., 2011). Another approach is to form protein-polysaccharide complexes through covalent bonding (Akhtar and Dickinson, 2007) or electrostatic interactions (Guzey and McClements, 2006). The basic principle behind these applications is to create a conjugate having ideal amphiphilic character. The hydrophobic parts ensure strong adsorption of

the conjugate to surfaces and the hydrophilic parts provide strong steric stability. Protein-polysaccharide conjugates can also occur naturally, such as gum arabic, fenugreek, and pectin. Studies showed that they are also capable of forming and stabilising emulsions (Huang et al., 2001).

Homopolymers are also used as stabilisers and dispersants in many other industries. Each industry has its own limitations when it comes to choosing an appropriate polymer for the desired colloidal functionalities. For instance, the polymers used in the food industry for colloidal functionality should be non-toxic and edible biopolymers extracted from natural sources, such as polysaccharides and proteins. For other industries, for instance paint, explosives, and plastics, polymers with the right structures can be designed and synthesised in order to obtain the desired functionalities for the specific/required environmental conditions such as pH and temperature. The only limitation for these industries may be the cost. The polymers are usually obtained non-uniformly, particularly the natural polymers. Producing a synthetic polymer or choosing a natural polymer that possess the right structure for the stability of a colloidal system does not guarantee the stability. This is because those polymers are needed to be adsorbed sufficiently by the surface and not displaced by another competitor present in the dispersion medium. Therefore, a good understanding of polymer adsorption is essential.

Many different aspects of adsorption of polydisperse homopolymers have been extensively studied both theoretically and experimentally in the literature. The polydispersity in these studies was achieved mostly in two ways. The first was by using mixtures of polymers involving a few different molecular weights (Furusawa

et al., 1982, Howard and Woods, 1972, Hlady et al., 1982). The second method was by using polymer samples which were produced in a polydisperse form by condensation polymerisation (Linden and Van Leemput, 1978, Janardhan et al., 1990). In the theoretical studies, the polydispersity formed by polymerisation was modelled using various distribution functions; e.g. Schultz-Flory distribution (Roefs et al., 1994, Pattanayek and Juvekar, 2003). However, the new approach developed in this study enables one to model a polydisperse system formed by hydrolysis of one or many selected chosen bonds. The molecular weight distribution of polymers achieved by hydrolysis and also the concentrations of such polymers in solutions will be different from those which are achieved by polymerisation processes. Figure 3.1 shows the comparison of the molecular weight distributions obtained by hydrolysis of a polymer of size 500 and Schultz-Flory distribution function for polymerisation. There is a significant difference between the molecular weight distributions at the polymerisation degree of 0.99, particularly for the size of 500 as seen in Figure 3.1a. Figure 3.1b shows that the molecular weight distributions become closer at a lower polymerisation degree (0.92). The inset graph in Figure 3.1b shows the differences for the large polymers (450 to 500). The small differences in the inset graph can be negligible for bulk properties. However, these small amounts can be significant in polymer adsorption and can affect the preferential adsorption of large polymers. The molecular weight distribution obtained by hydrolysis is different and giving a spike for unbroken chains because the hydrolysed polymer has a finite size which means that the two bonds on its both ends do not exist. Thus, these bonds are considered to be already broken (see section 3.3.1 for more details).

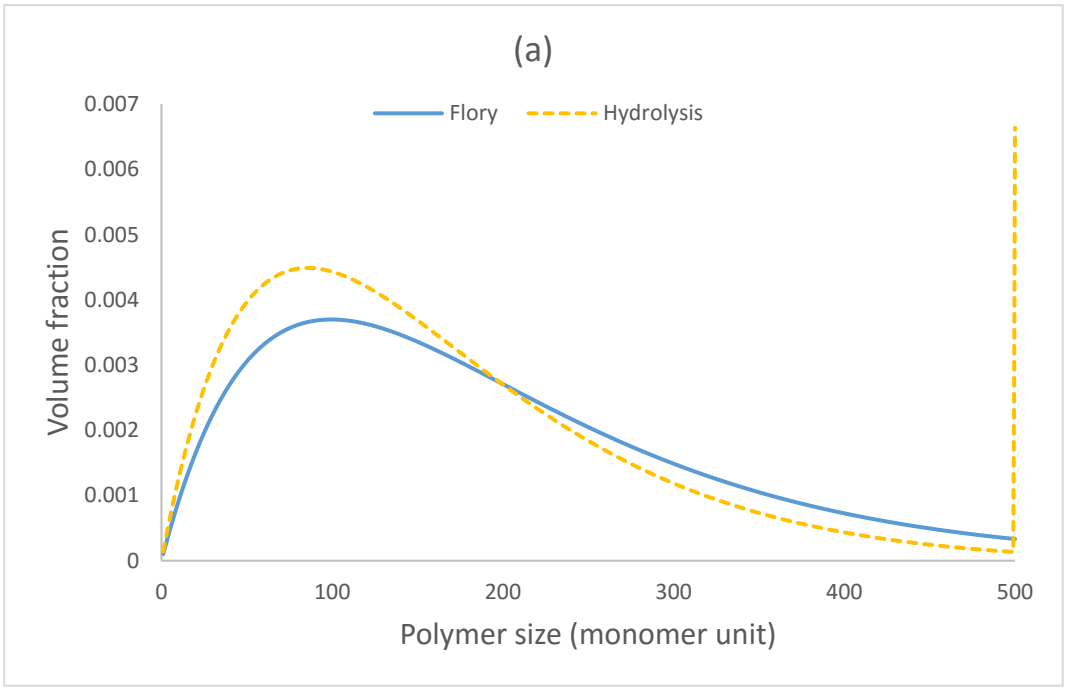

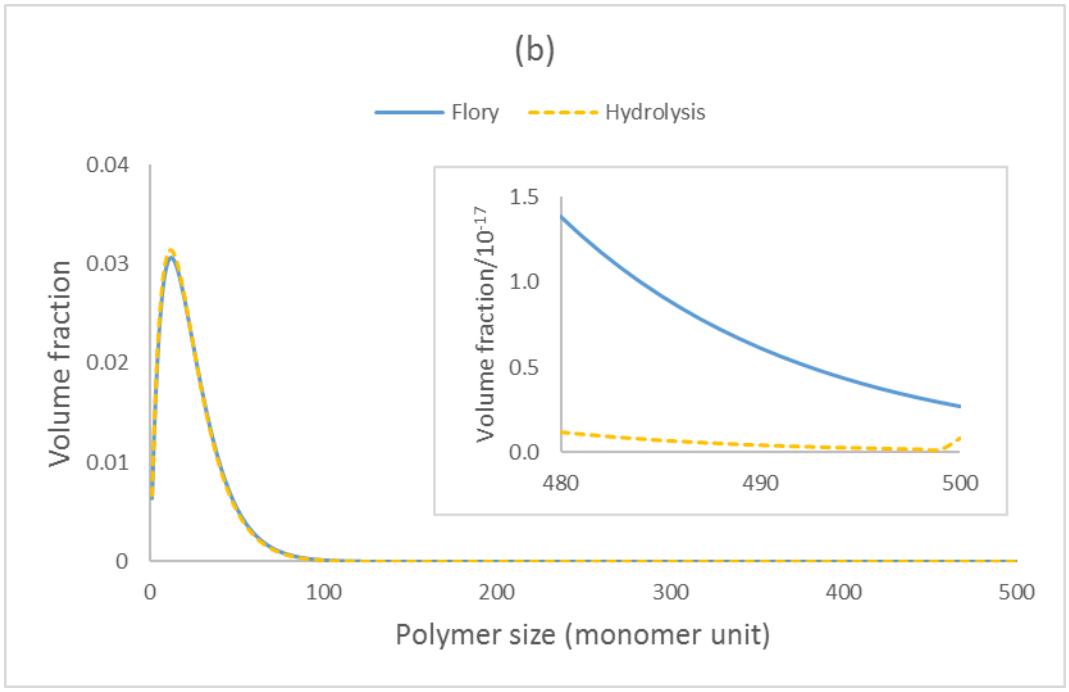

Figure 3.1 Molecular weight distributions of polymers in various sizes (1 to 500) obtained at polymerisation degrees of 0.99 (a) and 0.92 (b) by Schultz-Flory distribution and at equivalent hydrolysation degrees of p=0.01 (a) and p=0.08 (b) by hydrolysing all of the bonds of a polymer that has a finite size of 500. The volume fraction differences in the two distributions for large polymers can only be observed in the magnified inset graph in Figure 3.1b

In this chapter, the effects arising from the molecular weight distribution, variation of bulk solution concentration, degree of hydrolysis (DH), intact (i.e. the initial) polymer size, and the magnitude of monomer-surface interaction on the preferential adsorption will be discussed. Polysaccharides as homopolymers in food colloids are not adsorbed by the hydrophobic surfaces. Therefore, the homopolymers in this model are not considered as polysaccharides. However, there are applications of the homopolymer adsorption in the stabilisation of pigments in paints (Naden et al., 2015) and metal and magnetic nanoparticle suspensions (Hirai and Yakura, 2001, Lim et al., 2009).

3.2 Model Description

A cubic lattice having 100 identical layers (L=100) is used to represent the gap between two parallel surfaces. The bulk conditions were observed (following adsorption of polymers) at distances smaller than L/2=50 a_0 away from each surface which is required to have two opposite isolated surfaces where the adsorption on one surface does not influence the adsorption on the opposite one. Flory-Huggins parameters (χ) were used to define the short ranged interactions between monomers, solvent molecules and the surface. The solvent-surface, and monomer-solvent interactions were set to χ=0 k_BT (no interaction). Monomer-surface interactions were set to χ=-1.0 k_BT (attractive interaction) which is required to explore the adsorption behaviour of the homopolymer chains.

The values for the adsorbed volume fractions represent the total volume fraction of the polymers in that size, but not the number of adsorbed polymers though of

course the two quantities are related. In the all figures that show the adsorbed fractionations, the values of the volume fractions of adsorbed polymers in various sizes were normalised to 1, which the total adsorbed volume fraction of polymers were made equal to 1 throughout this chapter.

The polydispersity was achieved by hydrolysing all the bonds between N identical monomers making up the chains, at various DH. The degree of hydrolysis (DH) was determined by the probability of breakage p which is the same for all the bonds. The value of p can be set for each bond differently depending on enzyme activity and specificity to that bond, as for example to reflect the differences in the susceptibility of bonds to enzyme action towards the two ends of our homopolymer chains. However, in this preliminary study, it was assumed that the enzyme activity and specificity are the same for all the bonds.

3.3 Results and Discussion

3.3.1 The Effect of Bulk Solution Concentration (Φ)

Bulk solution concentration was defined as the bulk volume fraction of the homopolymers prior to hydrolysation. The value does not change as the chains are increasingly fragmented. Homopolymers with polymerisation degree N=500 were hydrolysed at DH 8% and used to form a denser (Φ=0.001) and a more diluted (Φ=0.0001) solutions. The volume fractions of hydrolysed polymers in the bulk solution and adsorbed at the surfaces were plotted against polymer size post hydrolysation in Figure 3.2a for the dense solution, and in Figure 3.2b for the

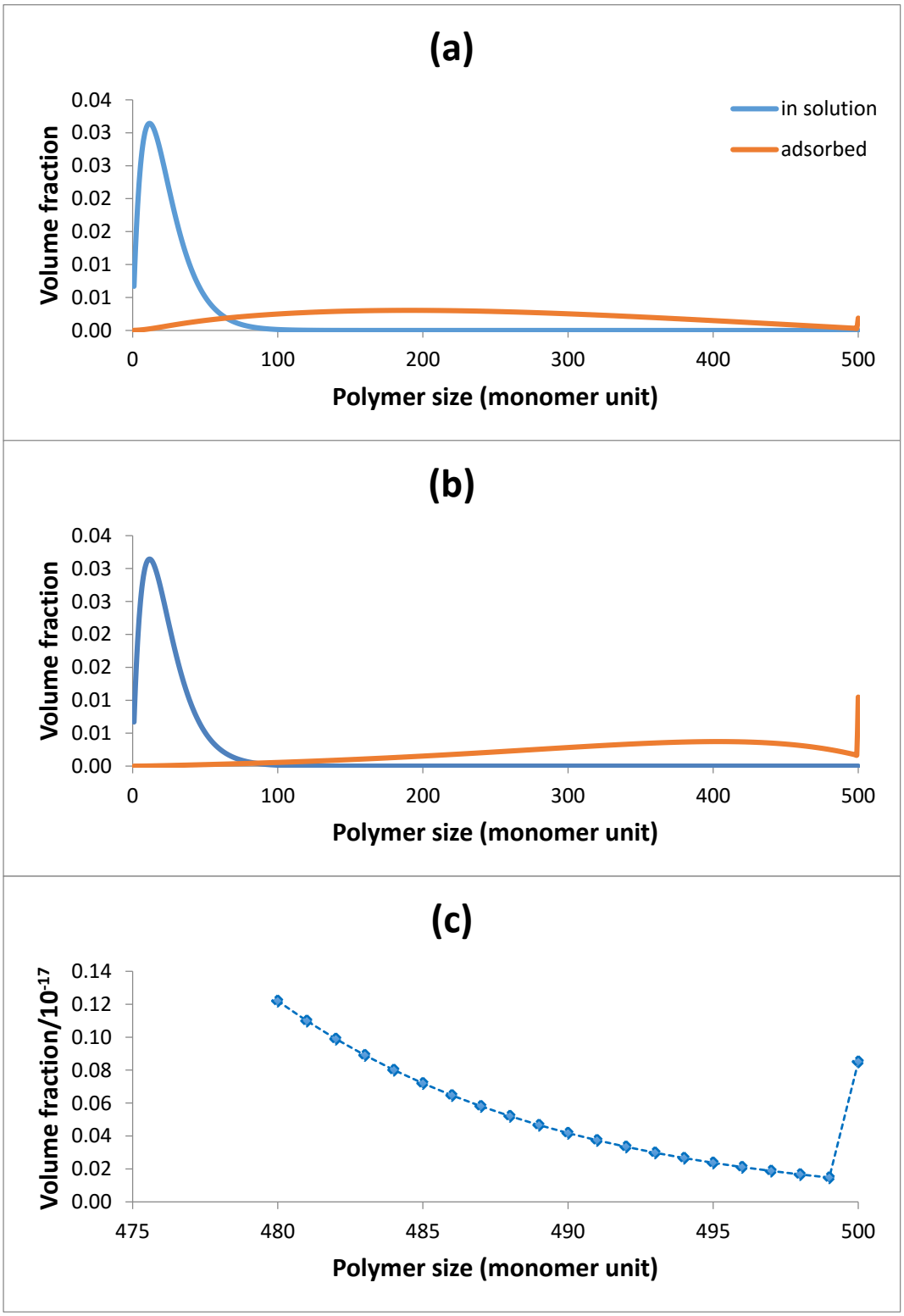

Figure 3.2 Volume fractions of homopolymers in the denser (a), and more diluted (b) solutions plotted against polymer size in monomer units. The volume fractions of polymers, Φ are shown in blue in the bulk solution and in orange for the adsorbed polymers. Φ for large polymers in the size range of 480-500 are shown again in the scaled graph (c).

diluted solution. It can be seen that the size distributions of the homopolymers in both the bulk solutions were the same as expected. The most commonly available fragments in the bulk solutions have a size around 16 monomers. Even a small degree of hydrolysis significantly reduces the availability of large fragments, as well as the intact polymers itself. However, it was clear that the most commonly adsorbed fragment sizes were not the ones most commonly available in the bulk solution. This confirms that the polymer size is a very significant parameter in competitive adsorption. In the denser solution (Figure 3.2a), the surfaces were covered predominantly by the fragments of sizes around 200 and also of exactly size 500 (i.e. the intact chains). In the diluted solution (Figure 3.2b), the size of most strongly adsorbed fragments shifted towards 400 but still also included exactly 500. The reason for the high adsorption of the intact polymer was its greater availability in the bulk solution when compared to other fragments of similar size. This can be seen in Figure 3.2c. The probability of having an unbroken polymer is found to be higher than the probability of having a large fragment whose size is close to the size of the intact polymer. This situation can occur when equation

$$(1-p)^{N-1} > p(1-p)^{N-2} = p < 0.5 \qquad \textbf{3.1}$$

is valid. In other words, it happens when the probability of having all the bonds ($N-1$ bonds) unbroken $(1-p)^{N-1}$ is greater than the probability of having only one bond broken and having the rest unbroken $p \times (1-p)^{N-2}$. The higher availability of the intact polymer is also shown in Figure 3.1 where the probabilities of the breakages were less than 0.5. This is clearly due to the effect

of the finite size of intact chains in hydrolysis. We do not see this effect in previous models, since they use polydisperse polymers obtained by condensation polymerisation where there is no cut off size (Figure 3.1). Figure 3.2c shows that a very small difference in the bulk concentration of the intact polymer leads to a great preferential adsorption of this polymer size. The peak for the adsorbed intact polymers became more prominent in the diluted solution as seen on Figure 3.2b, where the behaviour of the polymers was more dependent on their individual properties rather than their interaction with other nearby chains. The entropy loss upon adsorption became less dependent on chain length, but more controlled by the solution concentration when the concentration is increased. This is also indicated in the theory by De Gennes (1979), who introduced scaling concepts in polymer adsorption. In this theory the behaviour of the chains is dominated by a size scale ξ, called the mesh size. For diluted solutions the value of ξ will be much larger than the radius of gyration of chains. Therefore, behaviour of polymers is governed by their size (radius of gyration, R_g). However, when concentration of polymers in the solution is increased then ξ decreases. When $\xi < R_g$ then the size of chains is no longer relevant to their behaviour. The stronger effect of chain length on the degree of preferential adsorption can also be seen for the other large polymers which were more preferentially adsorbed in the diluted solution. These results confirm that the preferential adsorption of large polymers over small ones is affected by the solution concentration and their individual concentrations in the bulk solution. In addition, the effect of the finite size of the intact chains should be considered in the adsorbed fractionation of polydispersed polymers.

3.3.2 The Effect of DH (p)

A homopolymer of size N=500 was hydrolysed at 1%, 2%, 3%, 4%, 5%, 6%, 7%, 8%, 9%, and 10% (p= 0.01 to 0.1). Calculations were performed at polymer volume fractions of Φ = 0.001 and Φ = 0.0001. With the results from these calculations, it will be possible to see the size distribution of the adsorbed polymer fragments for various degrees of hydrolysis and changes in such adsorption in the denser and more diluted solutions.

Figure 3.3a and Figure 3.3b show the adsorption of polymer fragments of size n=1 to 499 at Φ = 0.001 and Φ = 0.0001 respectively. Figure 3.4 shows the percentage of the intact polymer (i.e. n=500) in the interfacial region. The results for n=500 were excluded in the graphs of Figure 3.3 due to the strong dominant adsorption of the intact chains, which are indicated separately in Figure 3.4. The adsorption fractionation became more clear with this exclusion.

The availability of large polymers in the solution drops with their sizes, excluding the intact polymer as mentioned in the previous section. The preferential adsorption of the polymers seems to be dependent on the balance between the two opposing parameters, i.e. size and availability. If the availability of a large polymer in the bulk solution is significantly low, the preferential adsorption shifts towards the smaller fragments which are more available compared to the larger polymers. For instance, at DH 1% the availability of large fragments was small but not critically low, therefore the largest fragment was dominant on the surface due to their stronger preferential adsorption. However, from DH 3% upwards, a

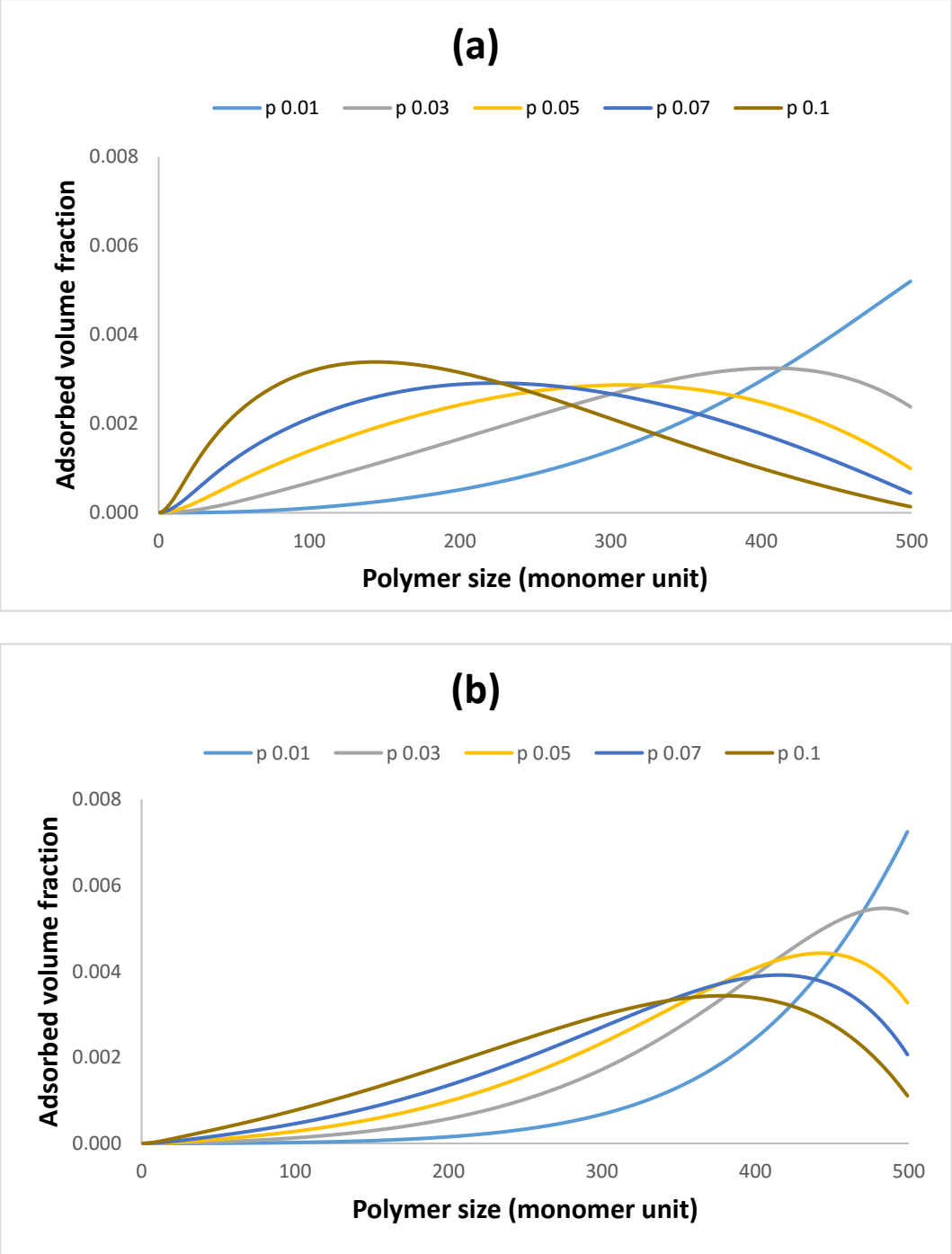

Figure 3.3 Adsorbed volume fractions for each of the size fragments of the hydrolysed polymers in the size range n=1 to 499, at Φ= 0.001 (a) and Φ= 0.0001 (b) different graphs in each case show various degrees of hydrolysis. All the bonds have equal probability of breakage p= 0.01, 0.03, 0.05, 0.07, 0.1. In each case the intact chains (n=500) was excluded here from the graphs due to the very high adsorption peaks for the unbroken chains, as seen in Figure 3.2a and Figure 3.2b.

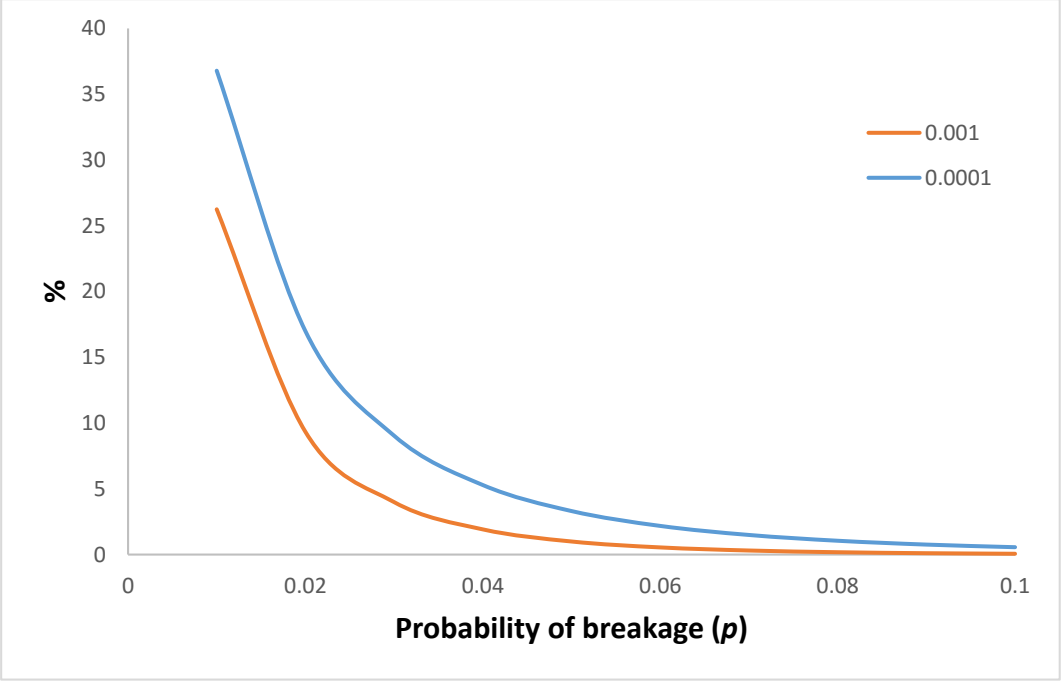

Figure 3.4 Percentage of the total volume fraction of the access polymer in the interfacial region that belongs to the intact polymer chains, at bulk volume fractions of Φ=0.001 and Φ=0.0001.

shift started to appear, which indicated that the availability of the largest fragments became critically low. The shift in the size of adsorbed chains moved towards the smaller fragments with increasing DH and was found to occur earlier on at lower DH values in the dense solution, as expected. As a result of this, the average molecular weight of the adsorbed polymers at the interfacial area was found to be higher in the diluted solution for all levels of hydrolysis as compared to the more concentrated solution. This can clearly be seen in Figure 3.3a and Figure 3.3b.

The percentage of the intact polymer as a fraction of total adsorbed amount at the interfacial region was found to decrease with the increase in DH, as seen in Figure 3.4. The availability of intact polymers similarly became critically low in the bulk solution at higher DH and this significantly reduced the adsorption of these

polymers at the surface when competing with smaller fragments, despite the stronger affinity of the intact chains for the interface. Figure 3.4 also confirms the effect of solution concentration on the preferential adsorption of higher molecular weight polymers. For instance, at DH 1%, the percentage of intact polymers at the interfacial region was found to be 36.79% in the diluted solution, while it was only 26.25% in the more concentrated solution.

In summary, the preferential adsorption of high molecular weight polymers was found to be dependent on their availability in the bulk solution, which was reduced significantly by increasing DH. This dependency was also reported in the experimental study of Furusawa et al. (1982).

3.3.3 The Effect of the Intact (Initial) Polymer Size (N)

In the last section we considered intact polymers of size N=500 monomers. It is useful to investigate how the original size of the intact chains, prior to any hydrolysis, may alter the results reported above. Homopolymers N=500 and N=1000 at Φ= 0.0001 were hydrolysed at DH values from 1% to 10% (p=0.01-0.1). Separate calculations were performed for each of the two polymers. The adsorbed size distributions at the interfacial region were compared and are shown in Figure 3.5. The results for the intact polymers were excluded due to the resulting high adsorption peaks of these, particularly at low DH. The contributions of the intact polymers to the total adsorbed amounts are given separately in Figure 3.7 expressed as a percentage value of the total adsorbed amount, plotted against the degree of hydrolysis. The availability of the fragments in the bulk solutions are shown in Figure 3.6. At DH 1%, the adsorption of polymers was

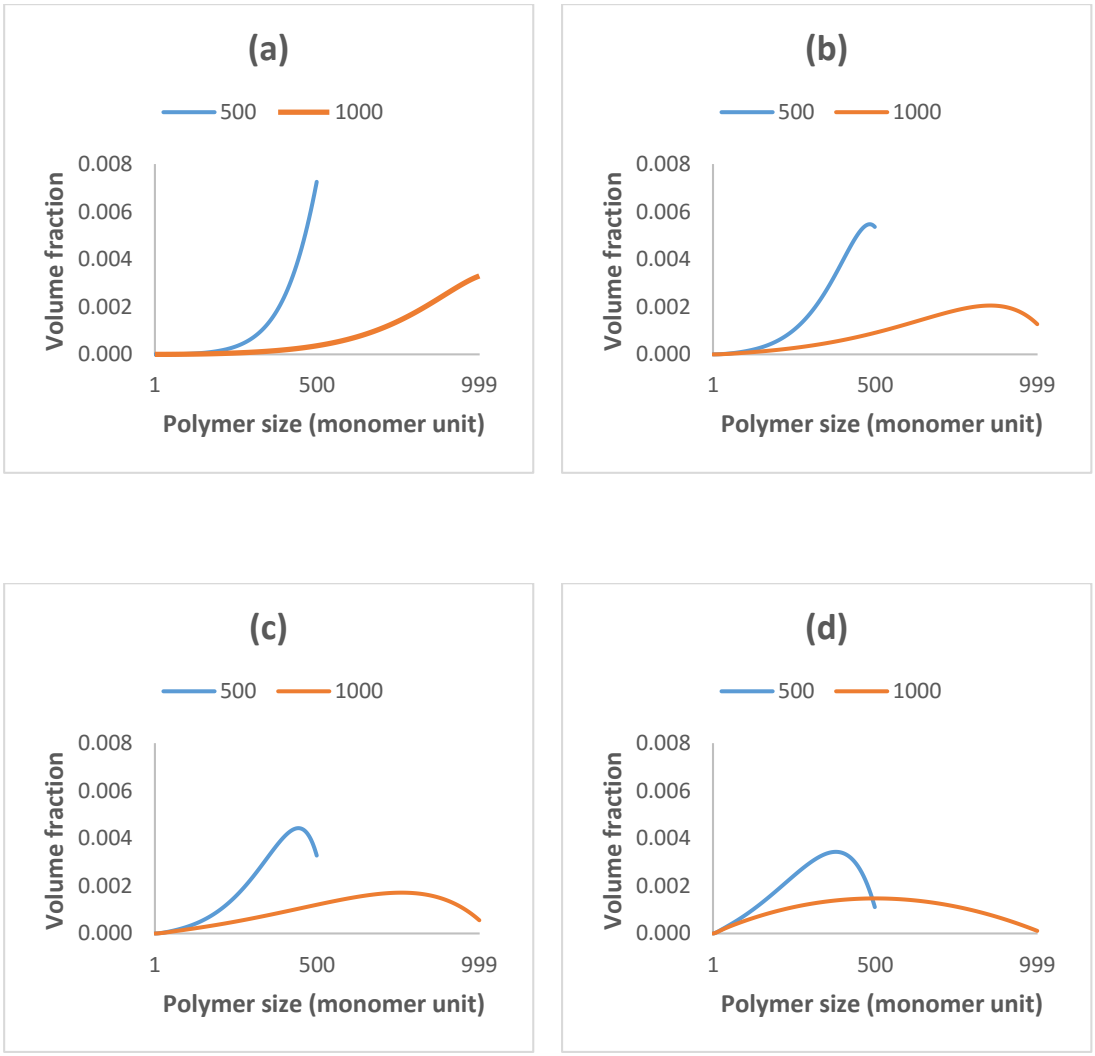

Figure 3.5 Adsorbed volume fractions of hydrolysed polymers at DH 1% (a), 3% (b), 5% (c), 10% (d). The adsorption fractionation of polymers N=500 and N=1000 were compared and results shown for the size of n=1-499 and n=1-999. The adsorbed intact chains have been excluded.

found to increase with the fragment size for both of the two initial polymer sizes (Figure 3.5a). This shows that the availability of large fragments was not limited at these lower DH values to the extent of offsetting their preferential adsorption. However, the competitiveness of the same size fragments obtained by the hydrolysis of N=500 and N=1000 were found to be different for the two systems with different intact original sizes. For instance, the fragment n=400 of N=500

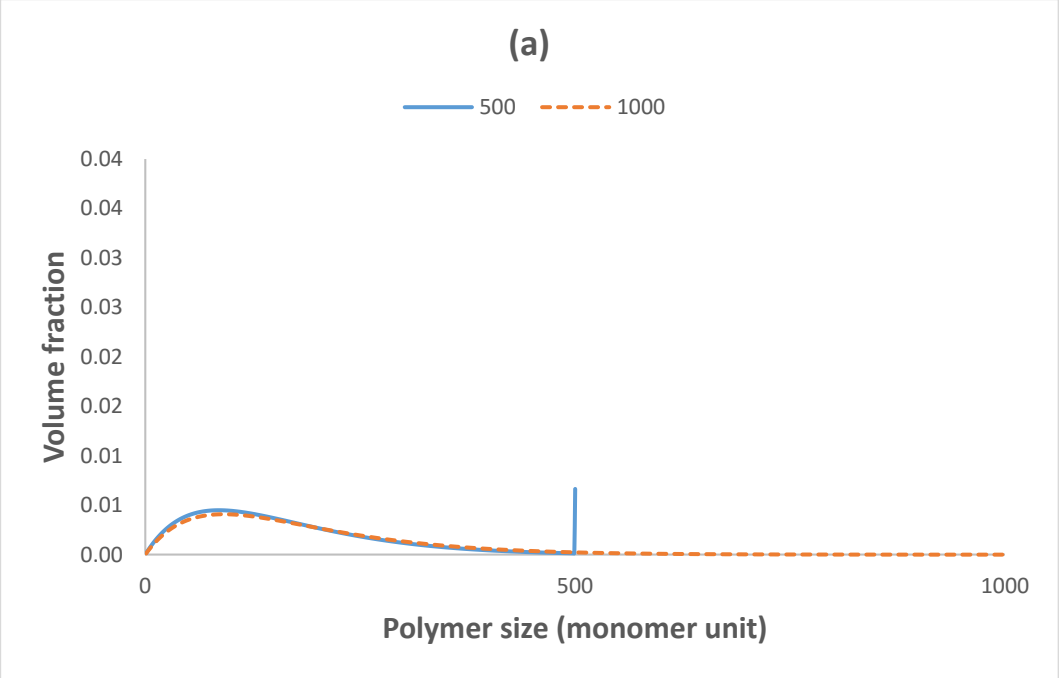
(a)
500
1000
0.04
0.04
0.03
0.03
0.02
0.02
0.01
0.01
0.00
Volume fraction
0
500
1000
Polymer size (monomer unit)

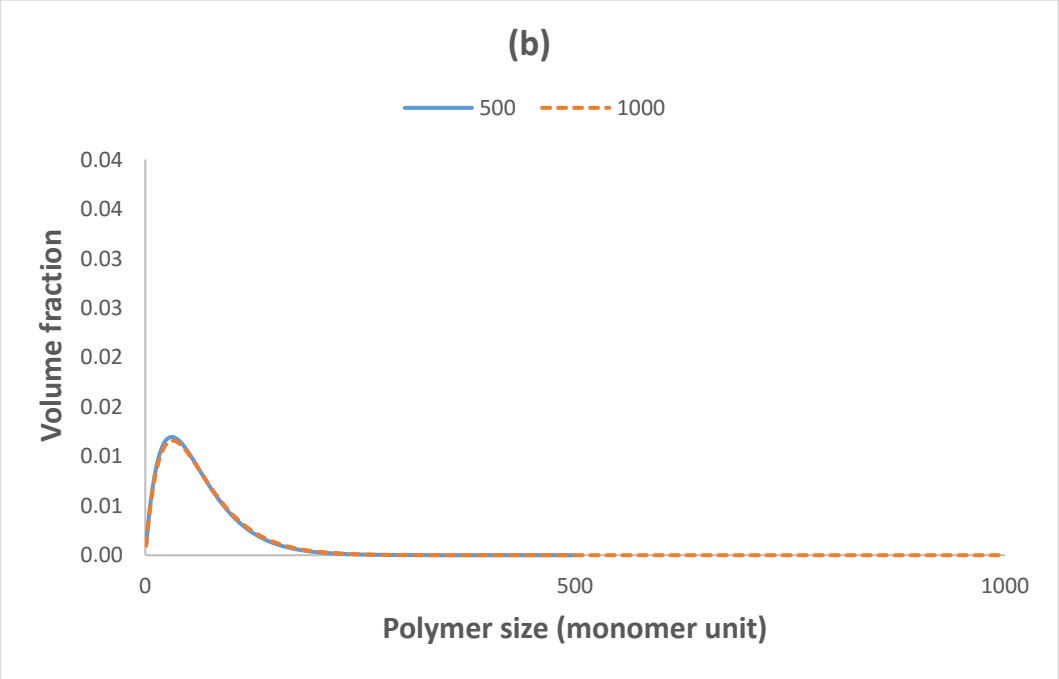
(b)
500
1000
0.04
0.04
0.03
0.03
0.02
0.02
0.01
0.01
0.00
Volume fraction
0
500
1000
Polymer size (monomer unit)

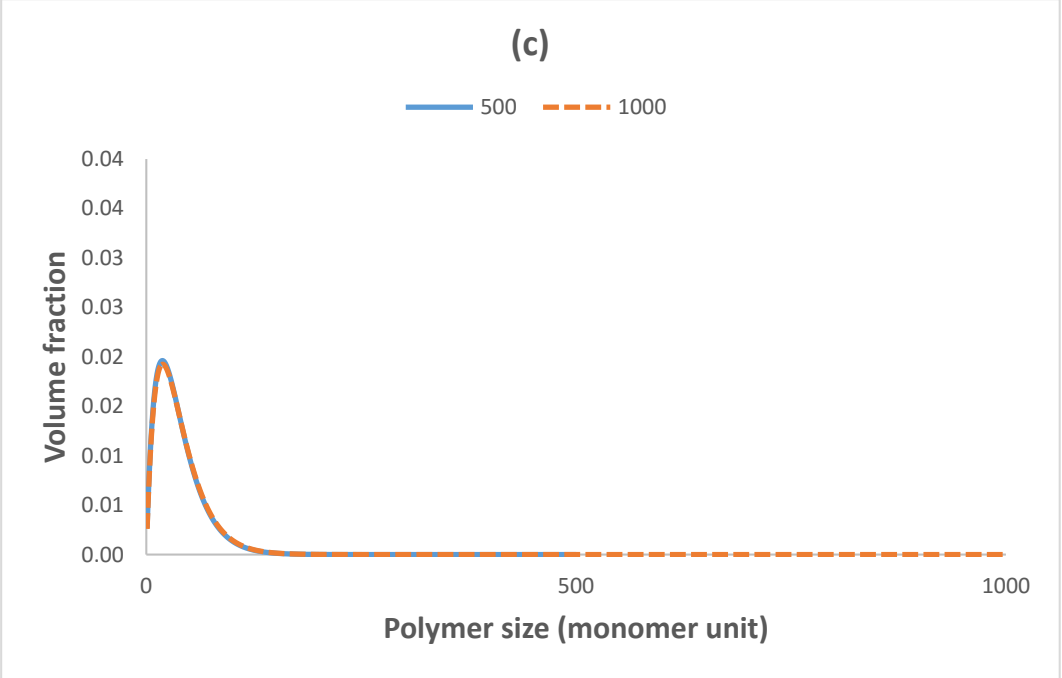

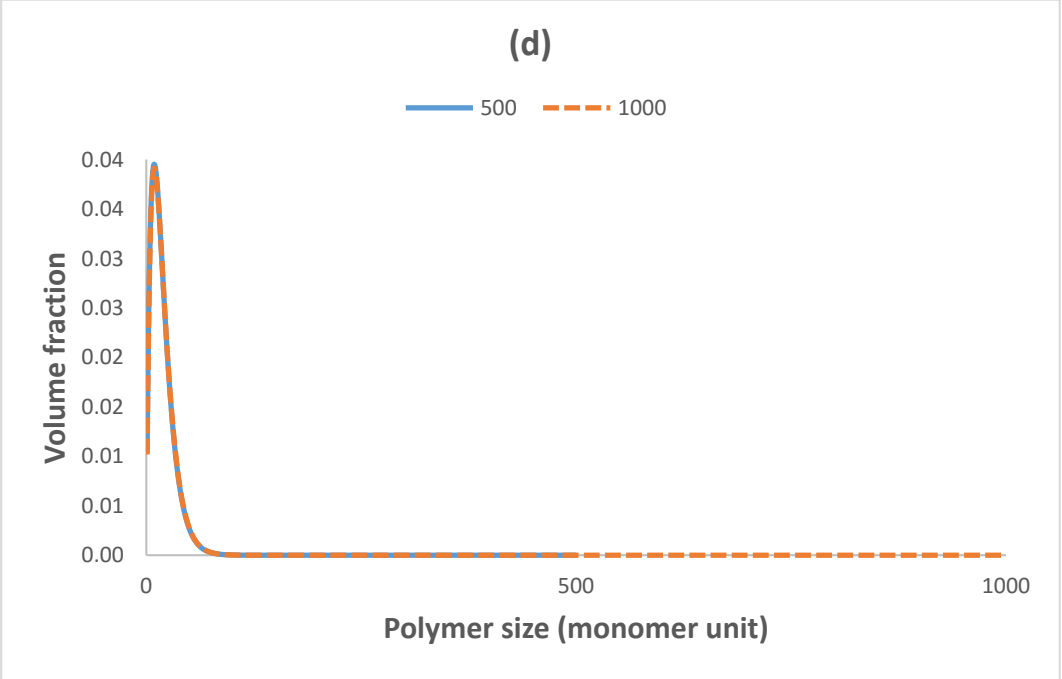

Figure 3.6 The volume fractions of hydrolysed polymers in the bulk solution at DH 1% (a), 3% (b), 5% (c), 10% (d) plotted against the polymer size. Calculations were performed separately for the two polymers of sizes N=500 and N=1000.

was seen to be more competitive than the fragment n=400 of N=1000 among their own set of competitors, although the relative availability of the former was actually less than the latter in the bulk solutions. This shows another factor for preferential adsorption, which is the relative size of a fragment in the solution, strongly favouring larger sizes. At 3%, 5%, and 10% hydrolysis, there was a maximum where the effect of the critically low availability on the preferential adsorption of large polymers manifested itself. The maximum point shifted towards the smaller size fragments with the increasing DH.

The effect of finite size of intact chains on the adsorption of fragments can be seen clearly in Figure 3.6a where there is a jump in the availability of the intact polymer in the bulk solution. It also exists in the other graphs in Figure 3.6, but is not visible due to the smaller relative magnitude. The size distributions of the fragments of both N=500 and N=1000 in the bulk solutions were found to be similar up to n=499 with graphs so closely overlapping that they are hard to distinguish. The graphs in Figure 3.6 also show that the availability of large fragments significantly decreased even at low DH.

The contribution to the total adsorbed amount by the intact chains (n=500 and n=1000) was found to be more for the chains of original size N=500 compared to the ones with size N=1000. But this difference between the two systems narrowed with a higher degree of hydrolysis, as is seen in Figure 3.7. At DH 1%, the intact polymer n=500 was the most available polymer in the bulk solution as displayed in Figure 3.6a. The contribution was 36.79% of the adsorbed polymer for the N=500 system. However, in the other system with original intact polymer

N=1000, the contribution of n=1000 was 16.58% of the total adsorbed polymer. Although the relative size of n=1000 was larger than n=500, the competitiveness (i.e. percentage) of n=500 outperformed n=1000 at all degrees of hydrolysis. This is due to the higher relative availability of n=500 in the bulk solutions, which indicates that the end effect (i.e. finite size of intact chains from which all fragments are derived) of the fragmentation is more significant for shorter chains.

In conclusion, the relative size of polymers was found to be important in preferential adsorption of large polymers and the effect of the finite size of intact chains was observed more clearly and significantly then for the polymers that initially have smaller size.

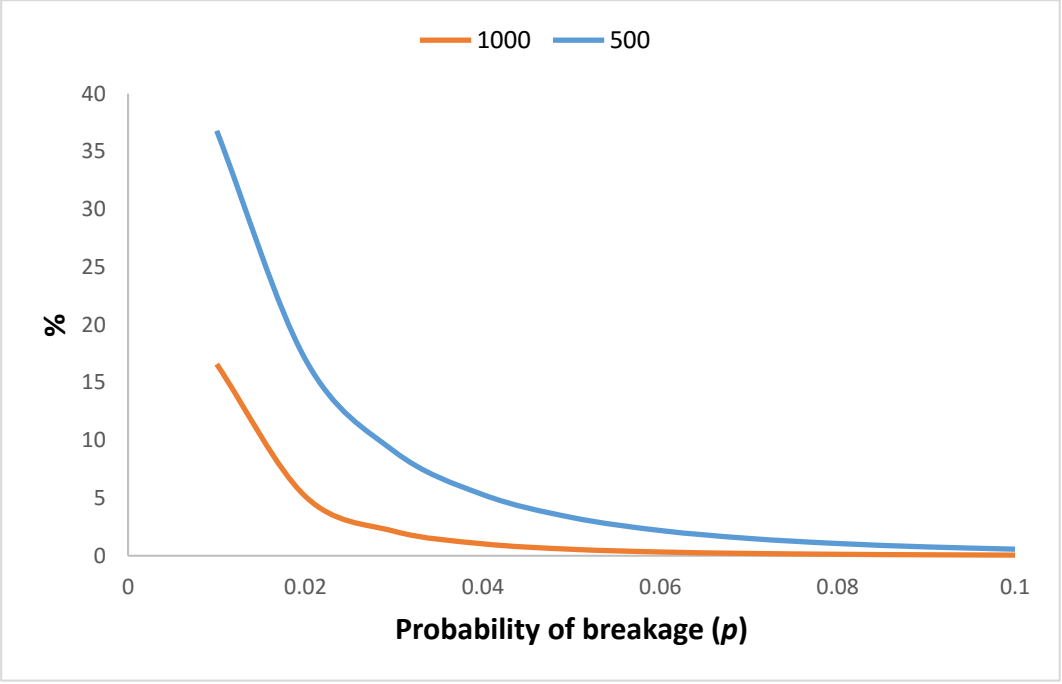

Figure 3.7 Percentage of intact polymer volume fractions adsorbed at the interfacial region given as a percentage of the total volume fractions of adsorbed polymers, for the intact polymer sizes n=500 and n=1000 plotted against the degree of hydrolysis.

3.3.4 The Effect of the Strength of the Interactions Between Surface and Polymer Segments (χ)

As mentioned in the description of the model, we had set χ=-1.0 k_BT for the interaction energy between surfaces and monomers, and χ=0 k_BT for the monomer-solvent and surface-solvent interactions throughout this chapter so far. In this section we consider the influence of the strength of interaction between the surface and monomers on the overall adsorption behaviour of the fragments. We do this by setting the surface-monomer interactions in this section to χ=-1.0 k_BT and χ=-0.5 k_BT and investigating the effect of the adsorption energy on the preferential adsorption of larger polymer fragments. The graphs in Figure 3.8 show a comparison of the adsorbed volume fractions for n=1-499 at high (Figure 3.8a) and low (Figure 3.8b) adsorption energies (i.e. degree of affinities of monomers for the surface).

At low levels of hydrolysis, the preferential adsorption of large chains was not affected as much as that at high DH. For instance, at DH 1% and 3%, the graphs for the corresponding p values in Figure 3.8a and Figure 3.8b are similar. However, the size distribution of adsorbed polymers at low adsorption energy was found to shift towards the smaller fragments with increasing extent of hydrolysis. The total adsorption energy of a polymer is related to the total number of monomers on that polymer chain. Therefore, changing the χ parameter affects large polymers more extensively than smaller polymers. The non-adsorbed large polymers (due to the low availability in the bulk solution) at low adsorption

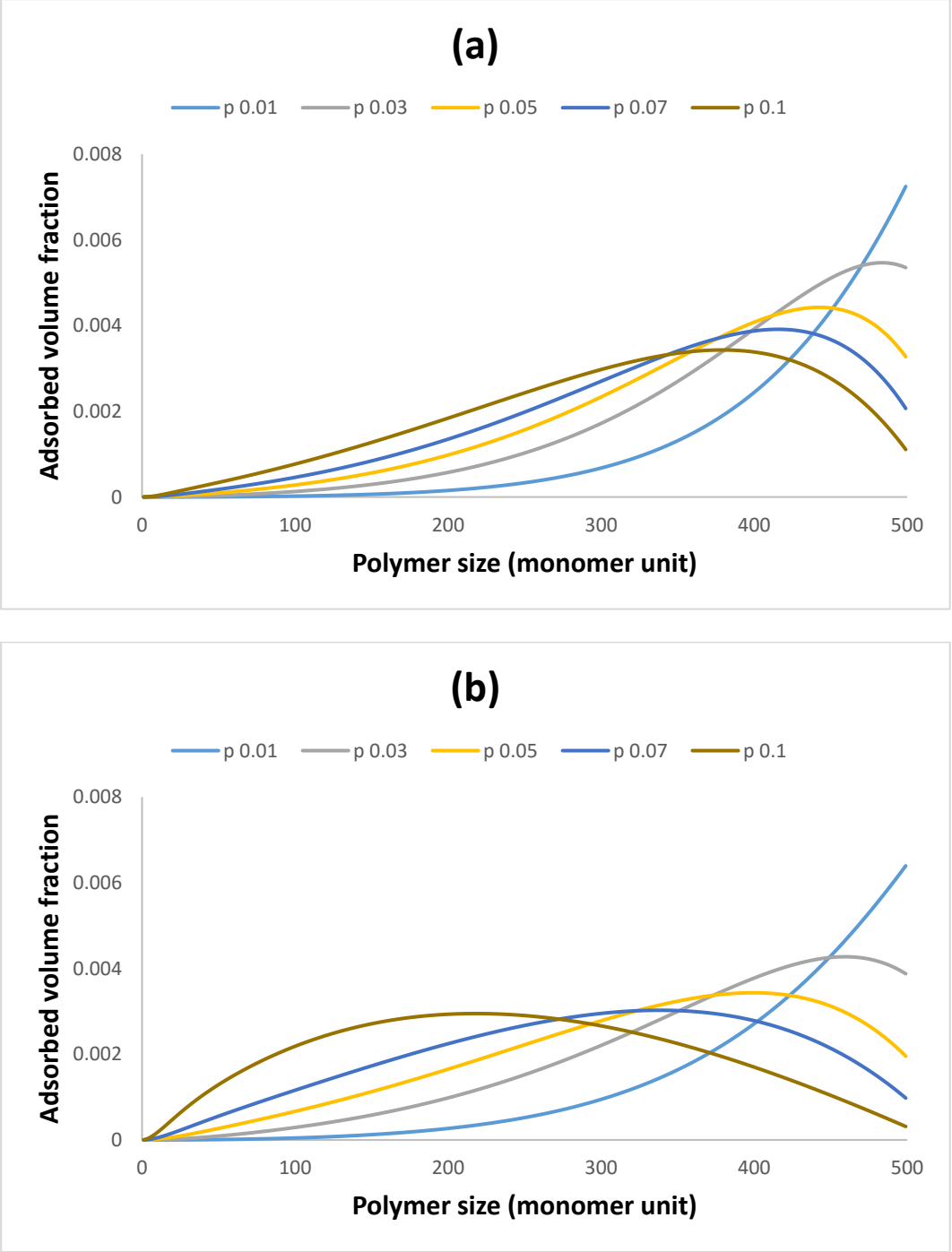

Figure 3.8 Size distribution of adsorbed fragmented polymer chains in the interfacial region at χ= -1.0 (a) and χ= -0.5 (b) at various levels of hydrolysis 1%, 3%, 5%, and 7%. All the bonds had an equal probability of breakage p= 0.01, 0.03, 0.05, 0.07, and 0.1. The high adsorption peak observed for the intact chains (N=500) was not included in the graphs for clarity.

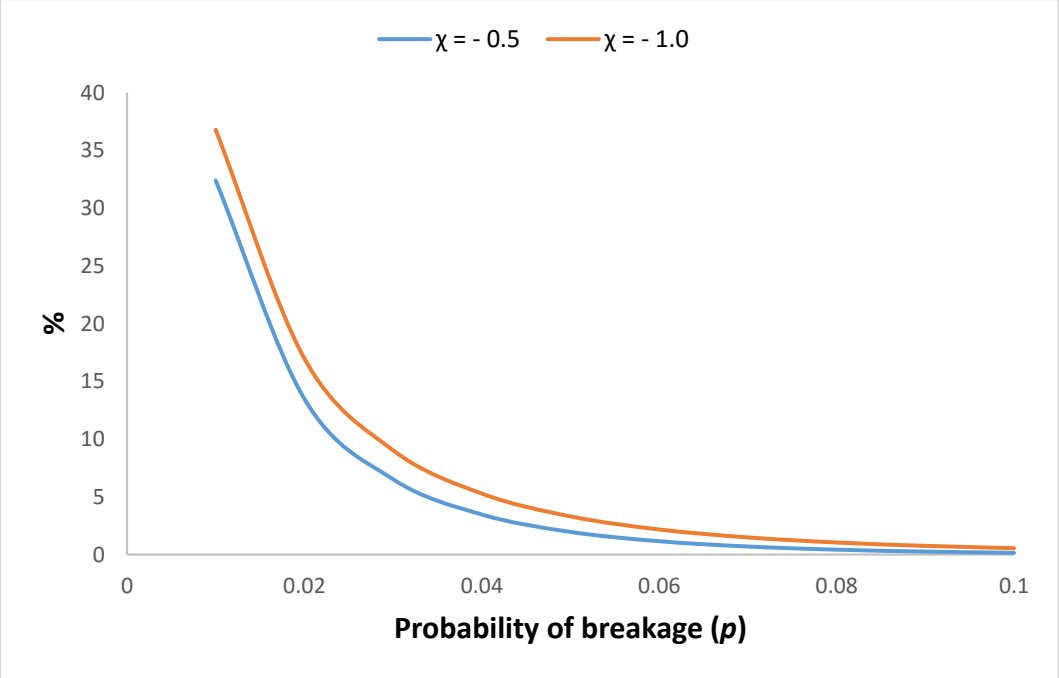

Figure 3.9 Percentage of the volume fractions of the adsorbed intact polymer as a percentage of the total volume fractions of adsorbed polymers plotted against DH for systems with χ=-1.0 and χ=-0.5.

energy, can nonetheless be adsorbed at higher adsorption energy as their much larger adsorption energy now compensates for their low availability in the system.

Figure 3.9 shows the contribution of the intact polymers, at χ=-1.0 and χ=-0.5, to the total adsorbed amount. The degree of preferential adsorption of intact polymers is increased with the higher adsorption energy. At a DH of 6%, the contribution of intact polymer at high adsorption energy was found to be twice as much as that at lower adsorption energy. This was found to be three times as much at a DH of 9%. Once again, the end effect of the fragmentation can be more significant at high adsorption energy, particularly at high DH.

It was concluded in this section that the high adsorption energy increases the influence of the finite size of the intact chains. The number of intact chains in the

system are very small and whether one considers the distribution of fragments as one derived from infinite size chains makes little difference to bulk properties. However, due to much high affinity of large polymer for adsorption the same is not true when one considers the distribution of adsorbed chains. Stronger adsorption energy per monomer makes this effect even more pronounced on the preferential adsorption of large polymers.

3.4 Conclusions

The preferential adsorption of polydisperse homopolymers was investigated theoretically by using SCF calculations. The polydispersity was achieved by the hydrolysis of all bonds between N monomers, making up original intact chains, with equal probability of breakages. The interactions between the surface, solvent, and monomers were specified by a set of Flory-Huggins interaction parameters (χ). The effect of the solution concentration, degree of hydrolysis, intact (initial) size of the homopolymer, and magnitude of the strength of the adsorption χ parameter between surface and monomers, on the preferential adsorption of large polymers were explored.

At p<0.5, the concentration of the remaining intact polymers in the bulk solution upon hydrolysis becomes higher than the large fragments. Although the concentration difference is very small, the effect on the adsorbent profile of the surface is significant, particularly at low p and N values. The amount of large polymers, whether one assumes a finite intact size or ones arising from infinite size chains (often assumed in the literature) is very small in both cases. When dealing with bulk properties of the system (e.g. rheology) it is of

no consequence which distribution is used. However, the relative number of large chains (close to the intact size) are very different between these two cases, due to the finite size of the intact chains, from which the distribution is derived through hydrolysis. Unlike bulk properties, surface adsorption behaviour is much more sensitive to the size and is indeed dominated by these larger chains. Thus differences between the tail end of the two size distribution cause profound impact on the size distribution of adsorbed polymers. In particular, the intact polymers are adsorbed dominantly at the surface due to this end effect of the fragmentation, for more than otherwise will be the case for a distribution arising from infinite chains (no end effects). Clearly the end effect becomes more significant for the shorter intact chains.

The individual concentrations of large polymers in the bulk solution affect their preferential adsorption. At higher levels of hydrolysis, the smaller fragments have a higher probability of getting adsorbed. The mostly adsorbed polymer sizes will be the larger polymers whose concentrations has not dropped to a critically low value.

The adsorption behaviours of the polymers differ depending on their concentration in the solution. The level of adsorption of large polymers is higher at low solution concentrations. The polymer size becomes less significant in denser solutions, which can be explained by the scaling theory and the fact that the adsorption behaviour is governed by the mesh size, ξ, rather than the radius of gyration of polymers if the latter is larger than the former (De Gennes, 1979).

The relative size of a polymer in a polydisperse system is another important

factor for the competitive adsorption.

A higher attraction between surface and monomers that make up the chains favours the preferential adsorption of larger polymers. The favourable adsorption energy becomes multiplied by the number of monomers for a polymer chain, which makes the adsorption of large polymers more favourable than the smaller fragments. The effect is very strong and can make larger chains dominate the adsorption despite their very small number in the solution.

In summary, the end effect of the fragmentation gives a unique size distribution profile in polydisperse systems produced by the hydrolysis. The preferential adsorption of large polymers depends on the balance of the more favoured adsorption of polymers with larger sizes as opposed to their availability in the system. The availability of the large polymers is controlled by the level of hydrolysis. At low solution concentrations and high surface-monomer interactions, the preferential adsorption of the large polymers can be less affected by their lower availability in the solution, arising from hydrolysis. As such larger chains continue to dominate the surface adsorbed chains to a high levels of hydrolysis.

Chapter 4 Colloidal Behaviour of Hydrolysed α_{s1}-casein: Selective Single Bond Breakage

Surface behaviour properties of α_{s1}-casein fragments produced by breaking of only one peptide bond at different locations along the chain, have been investigated. Trypsin is assumed to have been used for the fragmentation. In this chapter, the colloidal stabilising properties of the intact protein and the resulted fragments were investigated and compared to each. One of the reasons for choosing α_{s1}-casein is that it is a highly disordered protein, so it has no tertiary structure and has an insignificant amount of secondary structure which is thought not to have a significant effect on its adsorption characteristics. SCF theory is more applicable to this type of polymer structure. Another reason for this choice is that α_{s1}-casein has weak stabilising ability at high salt concentrations or near its isoelectric point in comparison for instance to β-casein. The aim is to investigate how well the α_{s1}-casein fragments provide colloidal stability relative to the intact protein under these conditions and to understand the mechanism of stability or otherwise provided by these polymer chains. For this purpose, the interaction potentials between two surfaces, electrostatic potentials, the size of the adsorbed protein layers and their volume fractions in the interfacial area will be calculated and analysed.

4.1 Specifying Interactions Between Amino Acid Residues, the Solvent, Free Ions and the Surface in the Model

Interactions between amino acids, the solvent, free ions and the surface were defined by Flory-Huggins parameters (χ) as stated in the chapter 2. Each amino acid type has an interaction parameter with all other types in the system including the surface, solvent and free ions. Leermakers et al. (1996) suggested that a satisfactory model does not need the specification of all the interactions between all the different types of amino acids. Thus there is no need for the full representation of all the amino acid interactions. Instead, they presented a reasonable approximation for the representation of amino acids by grouping them into 6 distinct categories to make the model simpler but yet adequately representative of real disordered protein chains. These six categories are hydrophobic, polar uncharged, positively charged, negatively charged monomers and the last two categories are specific to histidine and phosphoserine. Positively charged histidine has a noticeably different pK_a value than other positively charged amino acids and negatively charged phosphoserine has two pK_a values which necessitates a category of its own. Figure 4.1 illustrates the six categories on the linear polymer structure of α_{s1}-casein. Table 4.2 shows the amino acids in these categories and the number of residues belonging to each group in the case of α_{s1}-casein. The amino acid sequence of α_{s1}-casein was taken from the work of Swaisgood (1992).

A positive (type 3) and a negative (type 5) charge were added to the N-terminus and C-terminus of the α_{s1}-casein. These charges were also added to the both sides of the peptide bond where the breaking take places, for cases where only

one bond was broken. This is done so to represent the ability of a free C-terminus end to carry a negative and an N-terminus to carry a positive charge. Since the ability of C-terminus or N-terminus to carry charge is modelled here by addition of two extra residues at each side of a broken bond, this slightly increases the length of chains. However, for long chains this does not introduce a significant change. However, this was not adopted in systems where the protein was fully hydrolysed by trypsin. Because, now the high number of additional charges (residues) would change the chain length of the protein significantly and the mapped polymer in the model will not represent α_{s1}-casein. The results for the calculated colloidal interaction potentials, induced by this addition of extra residues were compared with cases when this was not adopted to see whether the addition of charges make a significant change in the colloidal stabilising behaviour of those fragments or not. According to the calculations, no significant difference was found between the two conditions. An example of such comparison is presented in section 4.2.1.

The categorisation of the amino acids was used to minimise the number of unknowns which are the mean fields $\psi_a(r)$ for each type of monomer (a) in each layer (r). Keeping these numbers minimum helps the computer solve the free energy equation. The other parameter is the separation distance (L), which while unfeasible for very large surface separations, has to be nonetheless large enough to insure two parallel surfaces can be considered as isolated from each other. At such a distance, the adsorption on one surface should not affect the adsorption on the other surface. The largest separation distance between the two

Monomer type	0	1	2	3	4	5	6	7	8
0-Solvent	0	2.5	0	0	0	0	0	-1	-1
1-Hydrophobic	2.5	0	2	2.5	2.5	2.5	2.5	2.5	2.5
2-Polar	0	2.0	0	0	0	0	0	0	0
3-Positive	0	2.5	0	0	0	0	0	0	0
4-Histidine	0	2.5	0	0	0	0	0	0	0
5-Negative	0	2.5	0	0	0	0	0	0	0
6-Phosphoserine	0	2.5	0	0	0	0	0	0	0
7-Ion(+)	-1	2.5	0	0	0	0	0	0	0
8-Ion(-)	-1	2.5	0	0	0	0	0	0	0
Surface	0	-2	0	0	0	0	0	0	0
pK_a value (s)	-	-	-	10	6.75	4.5	3&7	-	-

Table 4.1 pK_a values of the charged amino acid categories and Flory-Huggins parameters (χ) for the interactions between six amino acid categories, as well as those with solvent, surface and free ions in units of k_BT.

surfaces was taken as 120 in monomer units (a_0) in this study. The bulk solution conditions were already observed at a distance of 40 a_0 away from each surface which proves that L/2=60 a_0 would adequately fulfil the requirement of having two isolated surfaces.

Table 4.1 shows the set of χ parameters used in this model. These parameters were arrived at following a large number of trial runs with different values in a previous SCF study by Leermakers et al. (1996). Positive, negative and 0 values

in the table indicate unfavourable, favourable, and no interaction respectively between monomers belonging to the two corresponding categories.

For instance, the hydrophobic group (group 1) has a favourable (-2 k_BT) interaction with the oil surface which favours the adsorption of such residues to the hydrophobic surfaces. However, the same group has an unfavourable interaction of 2.5 k_BT with the other seven types and a relatively less unfavourable interaction of 2 k_BT with the polar uncharged group (group 2). The ion-solvent interaction parameter was set to -1 k_BT to ensure the contact is promoted between ions and water solvent representing the tendency of ions for hydration. These parameters have also been used in some previous SCF studies (Ettelaie et al., 2008b, Rammile et al., 2009, Akinshina et al., 2008).

Ionisable groups on the polymer carry electric charges which vary depending on the pH of the media. In this study, the surface adsorption and colloidal stabilising behaviour of the fragments will be investigated in pH values 3.0, 4.5, 5.0, and 7.0. This is to see the behaviour of the fragments in systems where the total net charge of chains is positive, nearly zero, slightly negative, and negative, respectively. To this end, the charges of the groups were calculated by using the provided pK_a values in Table 4.1 for each pH and are shown in Table 4.3. It is important that the charge neutrality of the bulk solution is ensured in any model, since there are also ions in the solution. For this purpose, the positive and negative ions (type 7 and 8) were used as background electrolytes and the bulk volume fraction of the ions were set to 0.01, which correspond to approximately 0.3 $molL^{-1}$. These ions were assumed to be monovalent such as Na^+ and Cl^-.

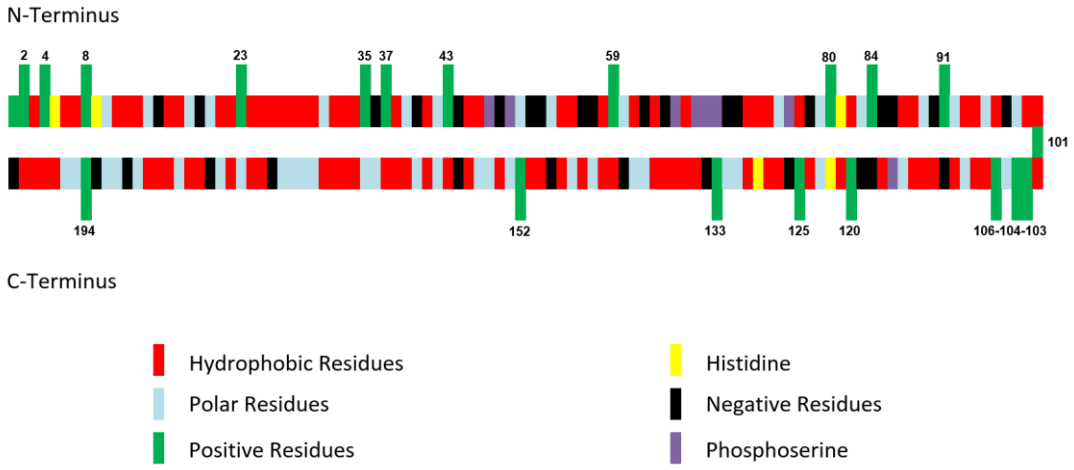

Figure 4.1 Representation of bovine α_{s1}-casein linear polymer structure. Amino acids are divided into 6 groups and each group indicated with a different colour as shown in the legend. Numbers and green bars show the positions of Lys and Arg amino acids.

Monomer Type	Amino acids in the group	Number of residues on α_{s1}-casein
1-Hydrophobic	Pro,Ile,Gly,Leu,Val,Phe,Met,Ala,Trp	89
2-Polar	Gln,Asn,Ser,Thr,Tyr	46
3-Positive	Arg,Lys	20
4-Histidine	His	5
5-Negative	Glu,Asp	31
6-Phosphoserine	Pser	8
Total		199

Table 4.2 Monomer categories and amino acid residue types in each category. The numbers show the number of monomers belonging to each class, as found on α_{s1}-casein.

Monomer Type	pH 3.0	pH 4.5	pH 5.0	pH 7.0
0-Solvent	0	0	0	0
1-Hydrophobic	0	0	0	0
2-Polar	0	0	0	0
3-Positive	1	1	1	0.999
4-Histidine	0.99982	0.99441	0.982528	0.359935
5-Negative	-0.03065	-0.5	-0.75975	-0.99685
6-Phosphoserine	-0.5001	-0.9725	-1	-1.4999
7-Ion(+)	1	1	1	1
8-Ion(-)	-1	-1	-1	-1

Table 4.3 Charge values of the ionisable groups calculated for the given pK_a values for each type monomer as given in Table 4.1, obtained for different solution pH's expressed in the units of *e*.

The total net charge of the intact protein is zero at the isoelectric point. At the pH values other than the isoelectric point, the charge neutrality of the solution is assumed to be satisfied because of the high volume fraction of background electrolytes and the very low volume fraction of protein not adsorbing and remaining in the bulk solution. This remaining volume fraction is set to be 10^{-11} here.

Colloidal stability is not entirely dependent on the adsorbed polymers at the interfaces. Free polymers in solution also affect the stability of emulsion systems, for instance by depleting from the interfacial region. This occurs when the two droplets approach each other closer than the diameter of the polymer chains

which is in turn is dependent on the size of the chain for linear polymers, as given by the number of monomer units comprising the chain (Hunter, 2001). In order to make the depletion effect negligible, a very low remaining protein bulk volume fraction is preferred in real practical cases, following the adsorption of most of the protein to the surface of the droplets. However, we stress that this does not mean that the adsorbed amount of polymers and therefore the total amount of protein in our system is also small. According to the calculations in this study, the minimum surface coverage was found to be around 1mg/m^2 which is the minimum approximate amount to make stable emulsions with caseins as suggested by Fang and Dalgleish (1993).

4.2 Results and Discussion

4.2.1 The Significance of Adding Charges to the C-terminus and N-terminus Ends of Polypeptides

The representation of the charges at the C-terminus and N-terminus ends of intact protein and resulting fragments in our model presented in section 4.1 in this chapter. The significance of adding charges to the both ends of the polypeptides is investigated by comparing two systems which the charges are added in one system and not added in the other system. For this, α_{s1}-casein is fragmented by breaking the 35th peptide bond and the interaction potentials induced by the adsorbed layers of the resulting polypeptides are plotted against the separation distance between two opposite surfaces at pH values 3.0, 4.5, 5.0, and 7.0. The blue lines in Figure 4.2 show the results for the system which the charges are added to the both ends of the polypeptides and the orange lines show

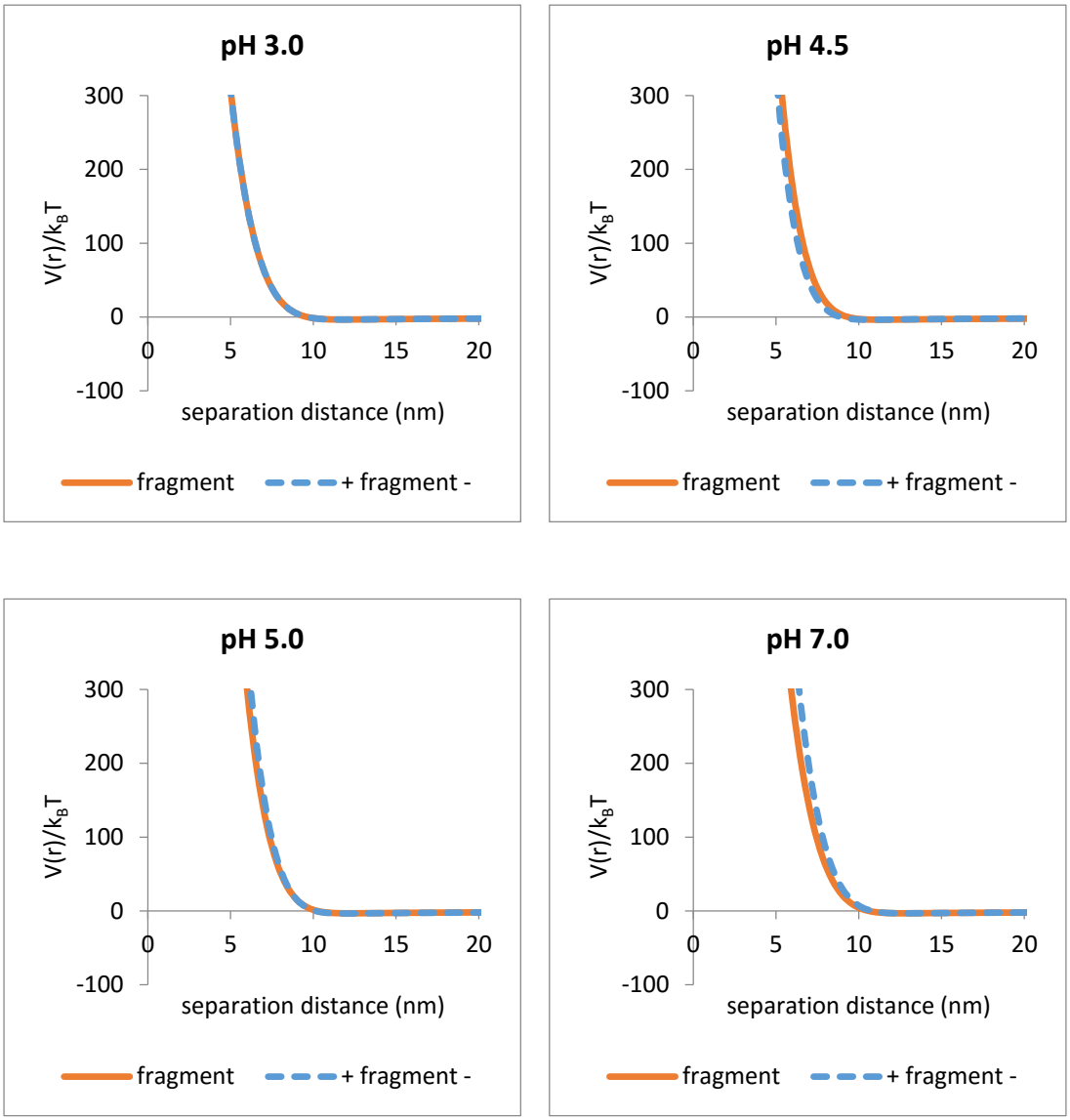

Figure 4.2 The interaction potentials $V(r)/k_BT$ of fragments with (blue) and without (orange) the addition of charged residues to the both ends, plotted against the separation distance.

the results for the other case. According to the graphs in Figure 4.2, there is no significant difference between the cases at all pH values. There are only small quantitative differences which do not change the colloidal behaviour of the polypeptides and the colloidal state of the emulsion systems.

4.2.2 Intact α_{s1}-casein

The hydrophobic amino acids on the backbone of α_{s1}-casein outnumber the other types near the C-terminus and N-Terminus ends of the chain. However, the middle part of α_{s1}-casein consists of the mixture of all 6 types of amino acids as was shown in Figure 4.1. This is the well-known “triblock-like” structure of α_{s1}-casein, where the two ends are more hydrophobic and the middle part is more hydrophilic (Dickinson, 2005). This can also be seen by looking at the average distance of each monomer in the α_{s1}-casein chain away from a planar interface. It is possible to calculate such distances by using the SCF model. The distances were calculated at pH=3.0, pH=4.5, pH=5.0, and pH=7.0 and plotted against monomer sequence number as presented in Figure 4.3a, Figure 4.3b, Figure 4.3c and Figure 4.3d, respectively. The two hydrophobic ends formed the trains of adsorbed monomers, conversely the hydrophilic middle section protruded from the surface and preferred to be more in the bulk solution. As a result, the more hydrophilic middle part creates a loop on the surface which is essential for the colloidal stabilising characteristics of α_{s1}-casein. When the two surfaces belonging to two separate droplets are brought closer, these loops start to overlap and induce strong steric repulsion between the surfaces which forces them apart, preventing closer approach of the two droplets.

The overlapping distance (i.e. the thickness of the adsorption layer), is an important parameter for an adsorbed polymer in defining its stabilising ability.

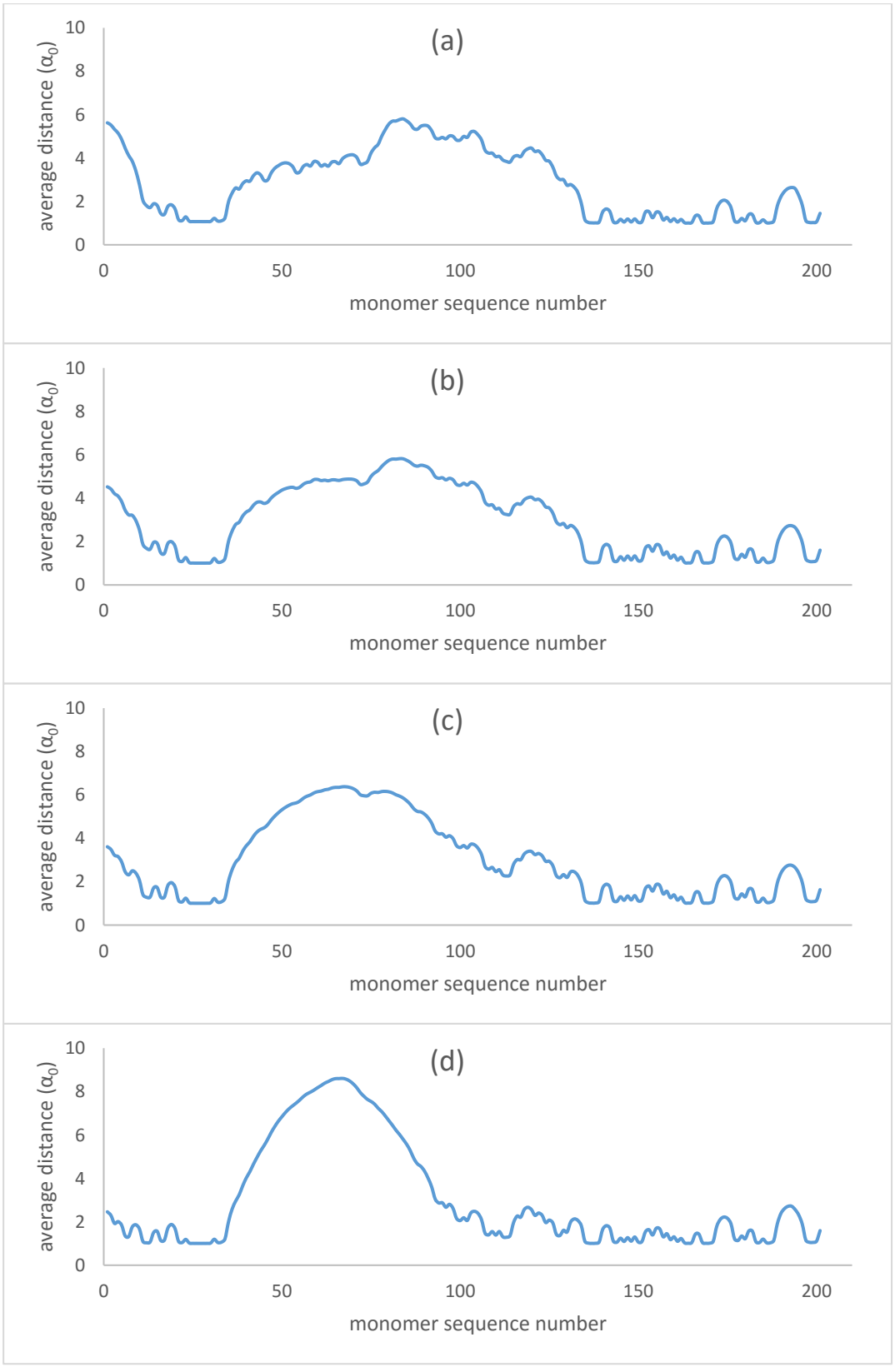

Figure 4.3 Average distance of each monomer from surface for the intact adsorbed α_{s1}-casein at pH=3 (a), pH=4.5 (b), pH=5 (c), and pH=7 (d). The sequence numbering starts from the N-terminus side of the protein.

Figure 4.3 gives an approximate idea about the overlapping distance of α_{s1}-caseins calculated at different pH values since it shows the average distance at which each monomer of α_{s1}-casein resides and not the farthest. According to the graphs, the overlap of interfacial protein layers will start at a longer separation distance at pH=7.0, as compared to other pH values. Therefore, α_{s1}-casein was expected to mediate longer ranged steric repulsion at this pH, when the two surfaces are approaching each other.

The steric repulsion occurring at large surface separations has a key role in overcoming the van der Waals attraction forces and prevent close approach of the droplets, as these latter forces are much bigger at closer separation distances. As seen from Eq.1.1 and Figure 1.1, the van der Waals interaction (V_{vw}) between two droplets, is relatively small at large separation distances, but can be more significant at close distances.

Colloidal stability and instability arise from interplay of repulsive and attractive interactions between the surfaces, mediated by polymers, solvent and free ions in the solution. In order to understand the mechanism of the stability or instability, these interactions must be considered and investigated. Van der Waals attractions and the steric and electrostatic repulsions are the major known interactions between the emulsion droplets. Alongside of these, there are two other aspects to be examined for a better understanding of the colloidal behaviour. These are the depletion and bridging effects. The depletion effect is negligible in this study since we assume beforehand that the concentration of the remaining protein in the solution is small, which is also the case for practical cases of interest.

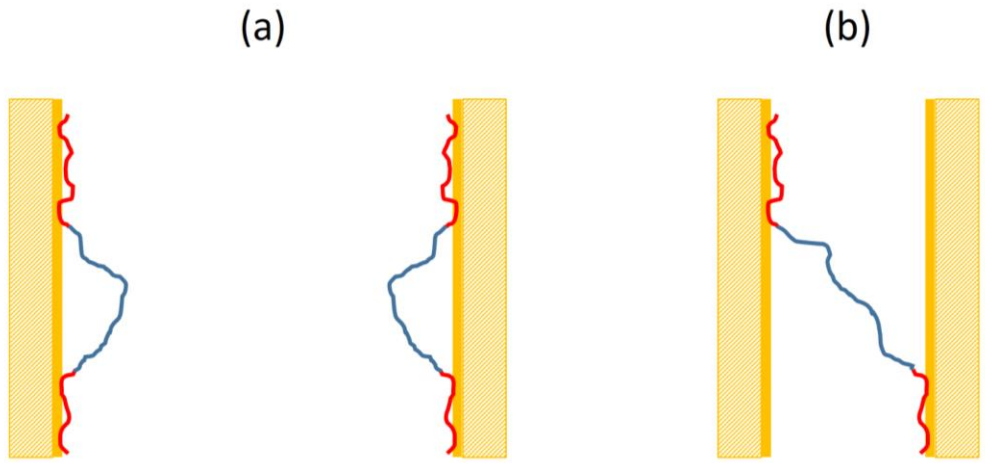

Figure 4.4 Demonstration of train-loop-train configuration of a tri-block type polymer at large separation distances (a) and the bridging conformation of the same type of polymer at short separation distance (b).

The bridging attraction can start when the adsorbed polymer layers on the surfaces just begin to overlap. At such a distance, inadequate strength of the steric repulsion and the van der Waals and bridging interactions contribute to a net overall attraction between the droplets. The surfaces then continue to approach each other by such attractions until the steric repulsions become strong enough and balance the attractive forces at some point where the adsorbed chains are fairly overlapped and entangled. The two surfaces will keep their distance from each other at a balance point between the bridging attraction and the steric repulsion unless an external force is applied (Milner and Witten, 1992, Ettelaie et al., 2003). The separation distance at which this occurs will be seen of course as a minimum in the overall interaction potential.

The tri-block type structure of α_{s1}-casein is prone to causing the bridging flocculation having two hydrophobic regions at two ends and one hydrophilic region in the middle. This type of structure can either create train-loop-train

configurations (Figure 4.4a) or bridging conformations extending from one surface to another (Figure 4.4b). The former is likely to be dominant at large separations whereas the latter is likely to only occur at sufficiently short separation distances.

Electrostatic interactions are crucial to avoid bridging flocculation for above tri-block or multi-block type structures. They prevent the two surfaces from approaching too closely to within the overlapping distance. At low salt concentrations and at pH values far from the isoelectric point of the protein, the electrostatic interactions can provide adequate repulsive force to avoid bridging flocculation. This can be seen in the interaction potentials between the oil droplets of diameter size 1 μm, calculated by this model, presented in Figure 4.5. It shows the interactions induced by the adsorbed intact α_{s1}-casein surface layers at various pH values, including the van der Waals attraction which is independent of the presence of polymers. Figure 4.6 shows the same interactions without the van der Waals attractions. As negative contributors to the mediated interactions, it is clear that the bridging effect has far more significance than the van der Waals attractions on the colloidal state of these systems. The deepest energy minimum was observed at pH 4.5 which was close the isoelectric point of α_{s1}-casein. As discussed above, the lack of the electrostatic potential led to the dominance of bridging effect at the overlapping distance. Combined with the inadequate layer thickness, and the lack of sufficient electrostatic repulsions, the oil droplets were affected stronger by the van der Waals attractions (~10 k_BT) at the shorter separation distance (4.2 nm) compared to the other systems at higher or lower pH values. With such a deep energy minimum (~180 k_BT), the oil droplets will

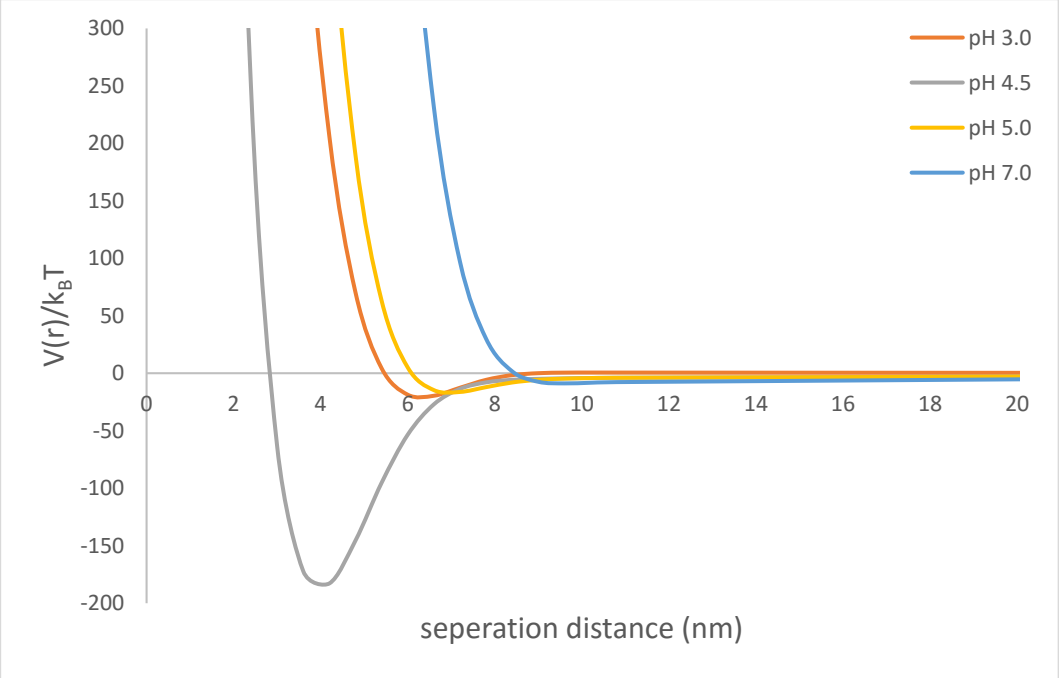

Figure 4.5 The interaction potentials *V*(*r*), between the oil droplets, plotted against the separation distance at pH 3.0, pH 4.5, pH 5.0, and pH 7.0 induced by the intact α_{s1}-casein.

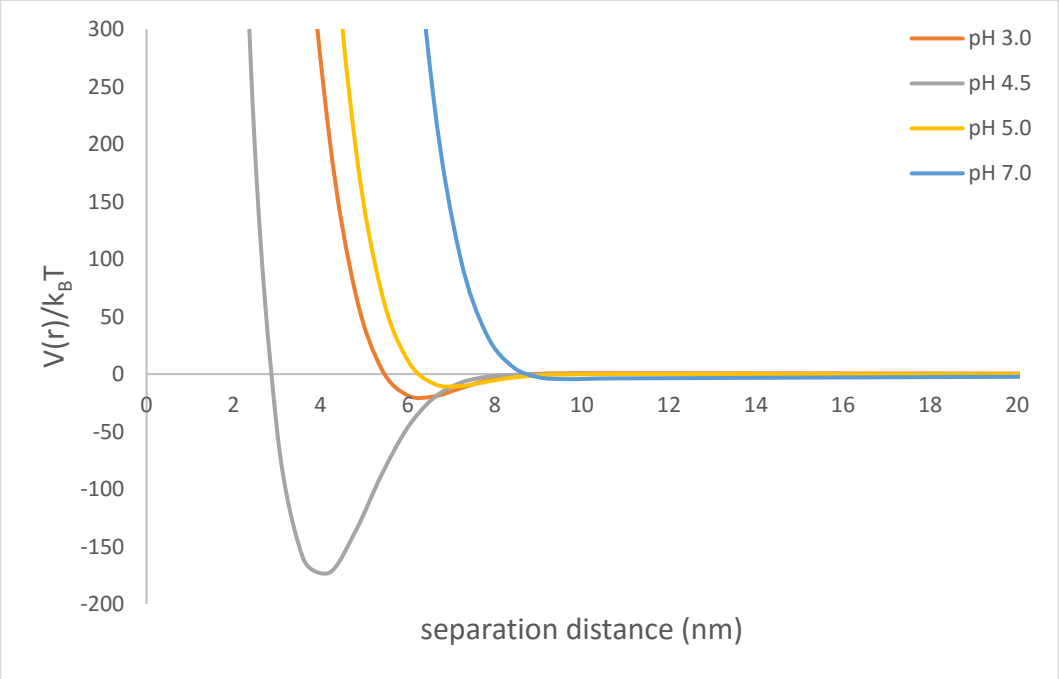

Figure 4.6 The same interaction potentials *V*(*r*) as those in Figure 4.5, but without the van der Waals attraction. Comparison with Figure 4.5 shows that van der Waals interactions are not particularly important compared to interactions induced by the polymer layers.

aggregate strongly and subsequently coalesce which will result in the breakdown of the emulsion. Increasing the pH of the solution to 5.0 or decreasing it to 3.0 changed the total net charge of the interfacial adsorbed protein layer and induced some degree of electrostatic repulsion. As a result of the pH change, the depth of the energy minimum is seen to be lower to 16 k_BT at 7.2 nm for pH 5.0 and 26 k_BT at 6.6 nm for pH 3.0 (Figure 4.5). This showed the significance of the electrostatic interactions on reducing the bridging effect for α_{s1}-casein stabilised emulsions, as well as many other proteins. Nevertheless, these energy minimums were still large enough to destabilise the emulsion. The van der Waals interaction potentials at 7.2 nm and 6.6 nm were 5.8 k_BT and 6.3 k_BT respectively which shows that the bridging effect is still more important contributor to the instability of emulsion and the resulting flocculation of oil droplets at these pH values.

At pH 7.0, the depth of the energy minimum was observed to be only a few k_BT and the improvement was provided by the combination of the increased total net charge of the protein and the further extension of the loop to the solution as seen in Figure 4.3d. The strong electrostatic repulsions and the longer ranged steric repulsion keep the surfaces apart and dramatically decrease the tendency for bridging as well as easily overcoming the van der Waals forces. The Brownian motion of the oil droplets can then easily overcome an energy of minimum of a few k_BT, and the emulsion system remains stable at this pH value.

4.2.3 Surface Adsorption Properties of Protein Fragments Resulting from Selective Single Bond Hydrolysis

In the previous section, the colloidal behaviour of intact α_{s1}-casein was discussed. The most obvious outcome was that α_{s1}-casein is not an ideal colloidal stabiliser which is already known and highlighted in the literature (Dickinson et al., 1997a, Dickinson et al., 1997b). This feature of the protein arises from the triblock-like structure responsible for the bridging effect. The same is of course also true in the case of most other proteins. However, this undesirable effect does not appear in the emulsion systems stabilised by β-casein, which has a diblock-like structure. Therefore, it is thought that the breakdown of α_{s1}-casein can improve emulsion stability by producing diblock peptide fragments by hydrolysing a single selected peptide bond. In this section, the colloidal stabilising properties of the diblock peptides will be examined and compared with each other and with the intact α_{s1}-casein. There are 20 susceptible peptide bonds that the trypsin can attack on the backbone of α_{s1}-casein. Therefore, breaking only one bond out of the 20 is not at present easily achievable practically. However, the aim is to examine the different parts of the protein for a superior stability. Thus, the experimental difficulty of designing such a system remains a separate issue that will not be addressed here.

α_{s1}-casein has a hydrophobic-hydrophilic-hydrophobic structure. The hydrophobic parts prefer to be at the interfacial layer (e.g. in contact with oil) whereas the hydrophilic part protrudes towards the solution as seen in Figure 4.3. The largest diblock peptides can be created by breaking a peptide bond from either end of the hydrophilic middle section. Breaking the bond from anywhere other than the

two ends of the middle part gives smaller diblock peptides which are expected to have a lower stabilising ability. According to the Figure 4.1, the hydrophilic middle part is composed of the N35-N106 amino acid residues, counting from the N-terminus side of the polymer. Therefore, the protein was broken from either the 35th or the 106th residue. It should be noted that only one single peptide bond will be broken in each system for now. It is also known that the trypsin enzyme breaks the bond at the C-terminus side of the Arg or Lys amino acids. Upon the breakage, there will be a diblock type peptide and a relatively more hydrophobic peptide left in the system.

4.2.3.1 Breaking the Peptide Bond Between the 35th and 36th Amino Acid Residues of α_{s1}-casein

The protein α_{s1}-casein was assumed to be split into two fragments by hydrolysing the peptide bond between the 35th (Lys) and 36th (Glu) residues. The N1-N35 and N36-N201 were obtained and are both present in the solution. Figure 4.6 shows the interaction potentials, V(r), predicted by our SCF calculations, between two droplets of size 1μm in a solution of such fragmented α_{s1}-casein. The most obvious result was that the energy minima was reduced to only a few k_BT at all pH values. For instance, the depth of the energy well at pH 4.5 was significantly lower at 3.5 k_BT compared to that observed at 180 k_BT for the intact protein. The difference between the systems involving hydrolysed (Figure 4.7) and non-hydrolysed protein (Figure 4.6) was also considerable at pH 3.0 and pH 5.0 which indicates that the stability was also achieved at these pH values. As a result, the emulsions stabilised by such fragments were predicted to remain stable even

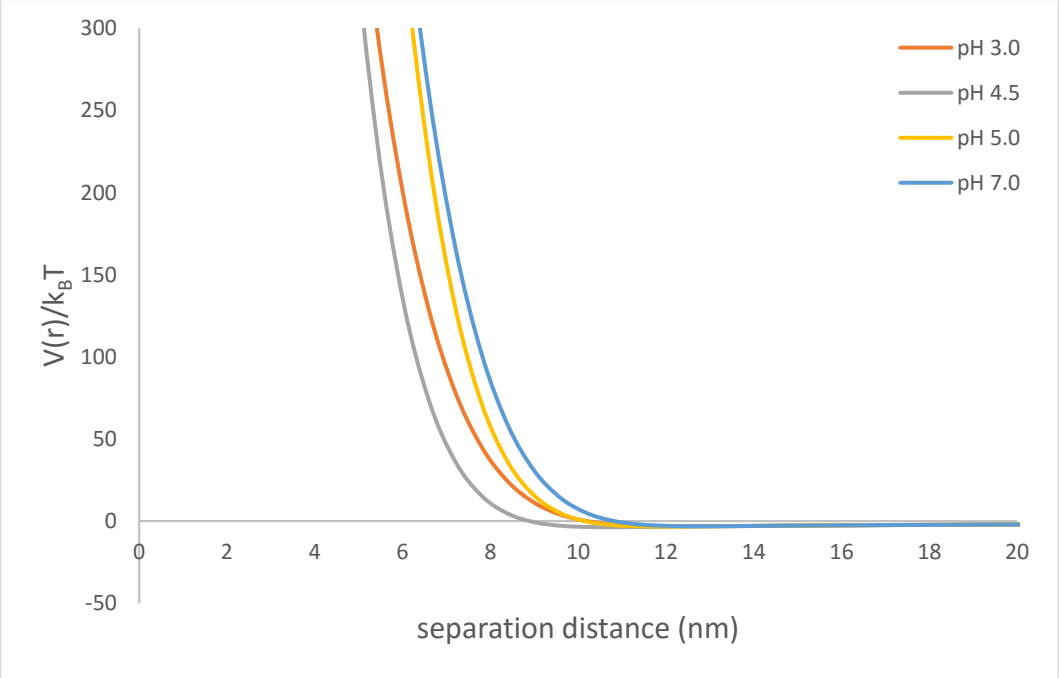

Figure 4.7 The same results as those in Figure 4.5, but now involving two fragments (N1-N35 and N36-N201 residues) of α_{s1}-casein together in the system, as opposed to the intact protein.

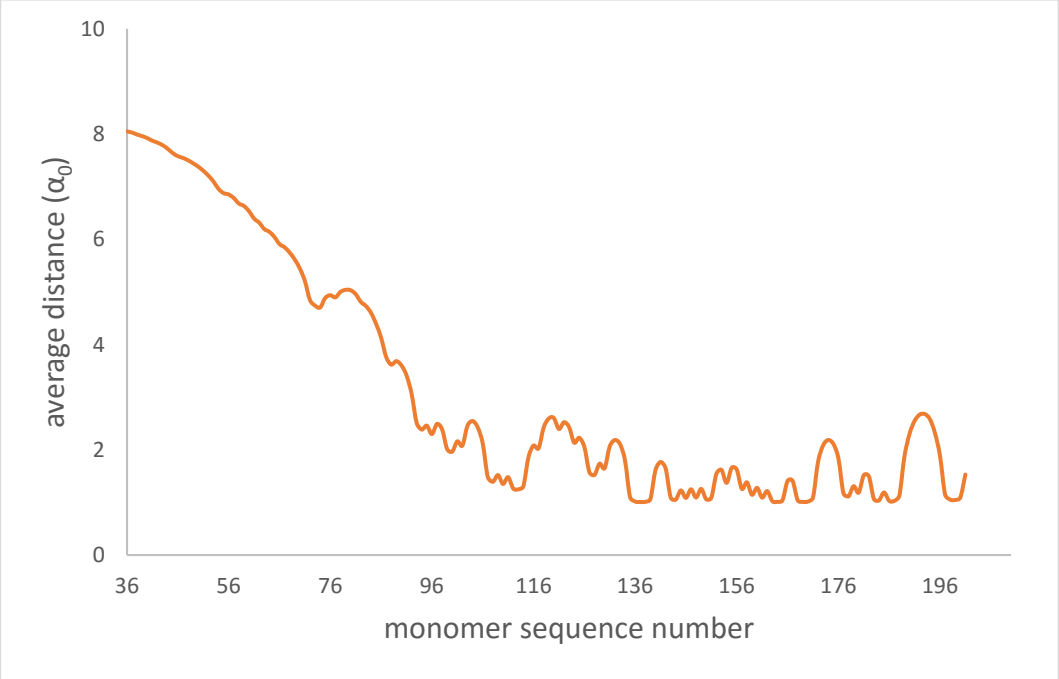

Figure 4.8 Average distance of each monomer on the C-terminal segment (N36-N201 residues) away from a flat surface at pH=4.5.

near the isoelectric point of α_{s1}-casein, and that they provided better stability than the intact α_{s1}-casein at all pH values.

Figure 4.8 explains the improvement in the stability of emulsion at pH=4.5 close to isoelectric point of α_{s1}-casein. It shows the average distance of each monomer on the C-terminal side fragment (i.e. N36-N201 residues) away from a flat surface. The system considered was the same one as that studied in Figure 4.7, and can be compared with the system involving only the intact α_{s1}-casein in Figure 4.3b. Unlike the intact protein, a diblock-type fragment was formed, which reduces the bridging effect. It is seen that one side of the polypeptide fragment is adsorbed and resides closely to the surface, whereas the other side extends away from the interface. In addition to that, the dangling end of the fragment extended towards the solution up to 8 nm whereas the loop of the intact protein extended only up to 5 nm. Therefore, a thicker interfacial layer can be formed by utilising fragments to obtain steric repulsion at longer separation distances between the surfaces.

4.2.3.2 Breaking the Peptide Bond Between the 106th and 107th Amino Acid Residues of α_{s1}-casein

Breaking the protein at the other end of the loop should also give a similar type of behaviour one may initially expect. The peptide bond between the 106th (Lys) and 107th (Val) residues was taken to be broken to examine such behaviour for two different parts of the α_{s1}-casein. This time around the more hydrophobic C-terminus side of the protein was one of the fragments, with the rest of the protein, which is a diblock-like fragment, becoming the other fragment. Apart from this

difference in the location of broken bond, all the other system properties were the same as before.

The interaction potentials, V(r), induced by these two fragments at different pH values were plotted against the separation distance, as shown in Figure 4.9. At pH values of 3.0, 5.0, and 7.0, a reasonable degree of stability was provided by the fragments according to the calculated results. However, at pH=4.5 where the electrostatic interactions are barely present in the system, the colloidal behaviour of the fragments is clearly different compared to those obtained for the bond breakage occurring at 35-36th residues. A deep energy minimum (318 k_BT) was obtained at a short separation distance (1.2 nm).

Although the N-terminal segment shows a similar diblock type behaviour and extends up to 8 nm away from the surface into the solution (Figure 4.10), it seems that it nonetheless does not provide sufficient amount of stability. The main reason for this turns out to be the inadequate adsorption of this diblock-like fragment. The N107-N201 seems to be more competitive and thermodynamically more favourable for the adsorption, compared to the more desirable di-block fragment, N1-N106. This is due to the more hydrophobic structure of the N107-N201, as seen in Figure 4.1, causes this unrequired fragment to displace the di-block one from the interface.

The volume fractions of the two fragments adsorbed on the surface at pH=4.5 are plotted against the distance away from the surface in Figure 4.11. The inset graph shows the very small volume fraction of N-terminal segment (i.e. the desirable di-block one) that could not be observed on the main graph.

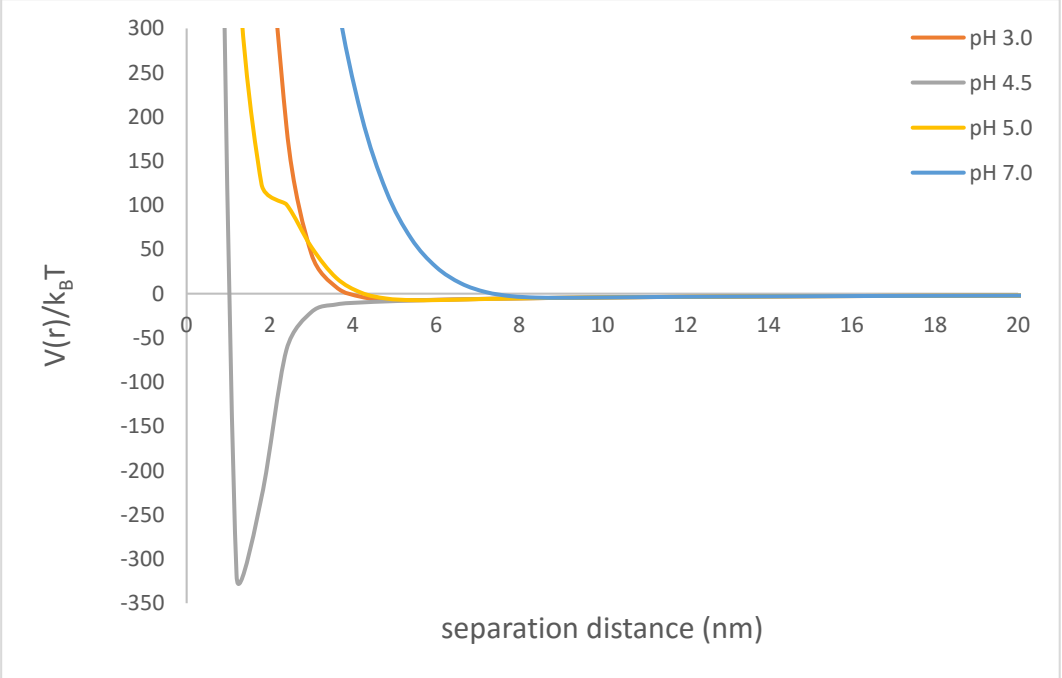

Figure 4.9 The same results as those in Figure 4.5, but now involving two fragments (N1-N106 and N107-N201 residues) of α_{s1}-casein both simultaneously present in the system.

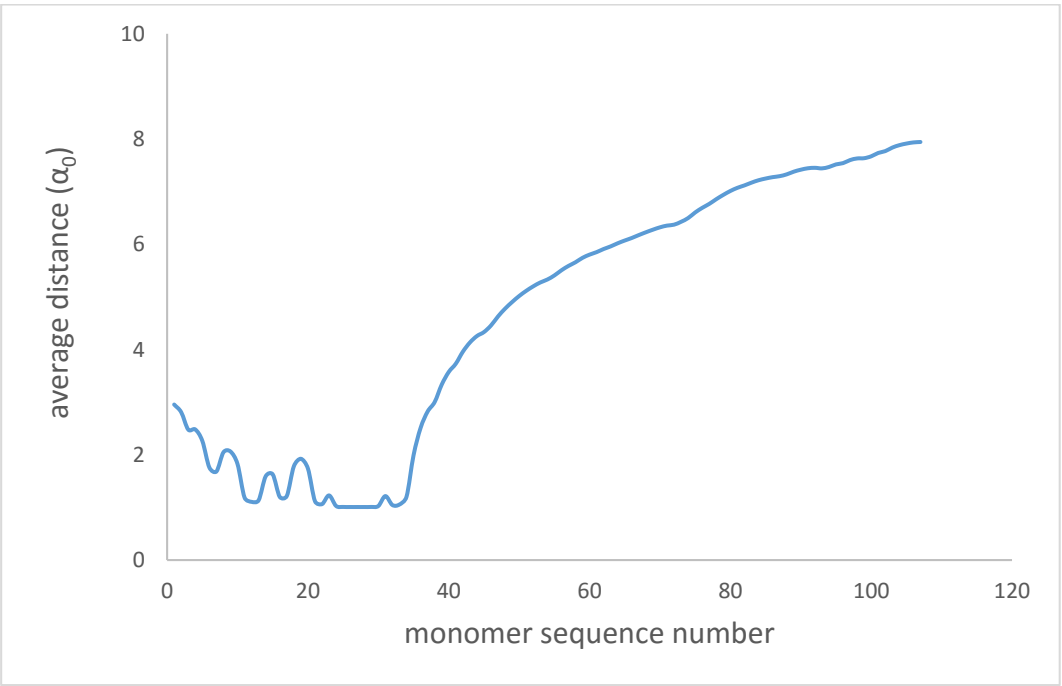

Figure 4.10 Average distance of each monomer on the N-terminal segment (N1-N106 residues) away from a flat surface at pH=4.5.

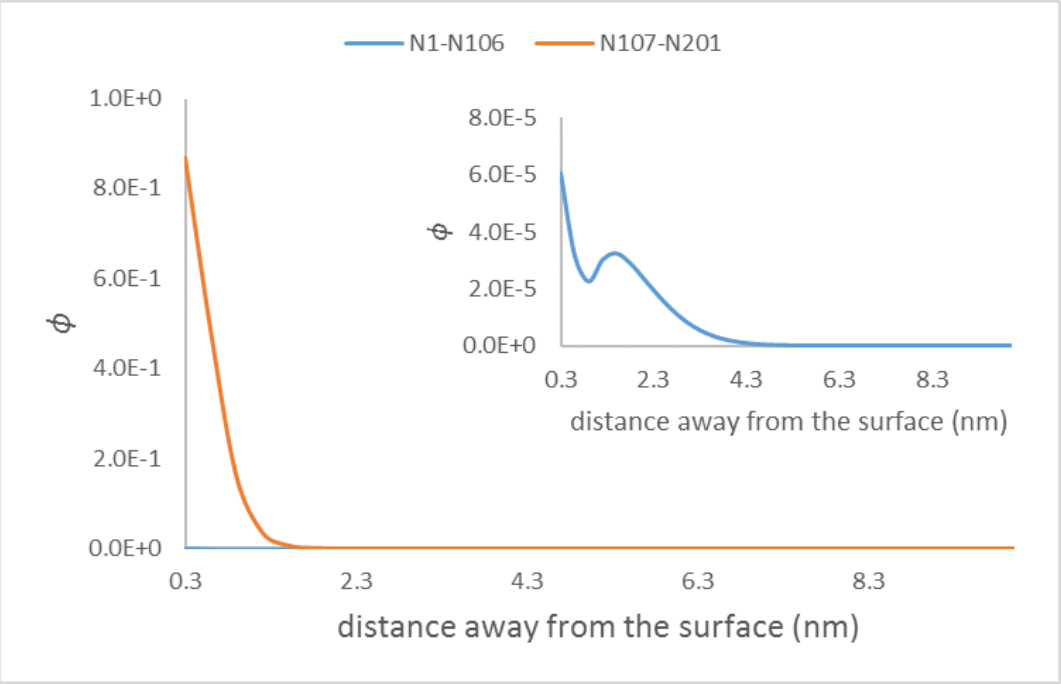

Figure 4.11 Volume fractions (ϕ) of adsorbed fragments (the N1-N106 and N107-N201) plotted against the distance away from the surface (nm) at pH=4.5. The small volume fraction of the N1-N106 fragment can only be observed in the magnified inset graph, due to very small degree of adsorption of this fragment.

The graphs show that the surface was dominantly covered by the more hydrophobic C-terminus segment (i.e. the N107-N201), with a very little amount of the N-terminal di-block like fragment (i.e. the N1-N106) present on the interface. Therefore, the steric repulsion from the N1-N106 and the electrostatic repulsion from the two fragments at this pH were not adequate to keep the droplets far apart. Further approach of two surfaces to shorter separation distances leads to a strong bridging where the dominant N107-N201 on two opposite surfaces start to overlap.

At pH 5.0 where the net charge of the protein was slightly positive, the depth of the energy well was decreased to a few k_BT, which the Brownian motion of the

droplets can easily overcome. One of the reasons behind such significant improvement was the noticeable increase in the amount of the adsorbed N1-N106 on the surface, where the volume fraction of the more hydrophobic fragments (N107-N201) was markedly decreased (Figure 4.12). The raise in the volume fraction of the N1-N106 provides a stronger and a longer-range steric repulsion. The result also shows that this fragment was more competitive at adsorption at pH=5.0 when compared to pH=4.5. This is because its net charge decreased at pH=5.0 while the net charge of its competitor fragment (i.e. the N107-N201) increases. This means that the adsorption of N107-N201 made the surface charged higher at pH=5.0 compared to pH=4.5. Higher charge on surface leads to stronger coulombic repulsion achieved for the same fragments in the solution. The total adsorbed amount of N107-N201 decreased by 8.5% and this amount was replaced with the di-block like N1-N106 fragment.

The first part of the energy barrier obtained between the separation distances of around 3-5 nm (Figure 4.9 at pH=5.0) was due to the combination of the electrostatic and the steric repulsion. The steric repulsion at such distances seems to be provided by the N1-N106. At a closer distance (2-3 nm), some bridging connections is likely to take place where the N107-N201 started to overlap. Once the two droplets get even closer, the steric repulsion induced by the adsorbed N107-N201 becomes a strong contribution to the overall mediated interactions between the droplets.

The competitive adsorption led to surface coverage with the undesirable C-terminal hydrophobic fragment at pH=4.5. One way of improving the colloidal stability of this system is to remove this undesirable fragment by some kind of

filtration. Another solution can be the full hydrolysis of the undesirable fragment with the trypsin enzyme thus chopping this to many smaller pieces. However, trypsin breaks the Arg-C and Lys-C bonds indiscriminately and it will be difficult to prevented from doing so in order to only produce the required diblock fragment. The practical difficulties of targeting such bonds only on C-terminus fragment but not the N-terminus one will not be addressed here. Rather, the aim is to monitor the competitive adsorption and the colloidal stability under these conditions.

There are 5 susceptible peptide bonds on the undesirable C-terminal fragment (i.e. the N107-N201) that trypsin can attack for the full hydrolysis of this fragment to even smaller polypeptide pieces. These are the 120th,125th, 133rd, 152^{nt}, and 194th peptide bonds.

This part of the research could not be carried out without our extended SCF model because the maximum number of breakages is limited to 2 in the usual SCF model. The interaction potentials induced by the two systems (i.e. two solutions) mentioned above are plotted against the separation distance in Figure 4.13. Both suggested strategies for the removal of the energy minima worked well as seen on the graphs. The depths of the energy wells were only a few k_BT which can easily be overcome by the Brownian motion of the droplets. In the case of the filtration or the full hydrolysis of the undesirable C-terminal fragment, the systems were predicted to be reasonably stable even at pH=4.5 (isoelectric point of intact α_{s1}-casein).

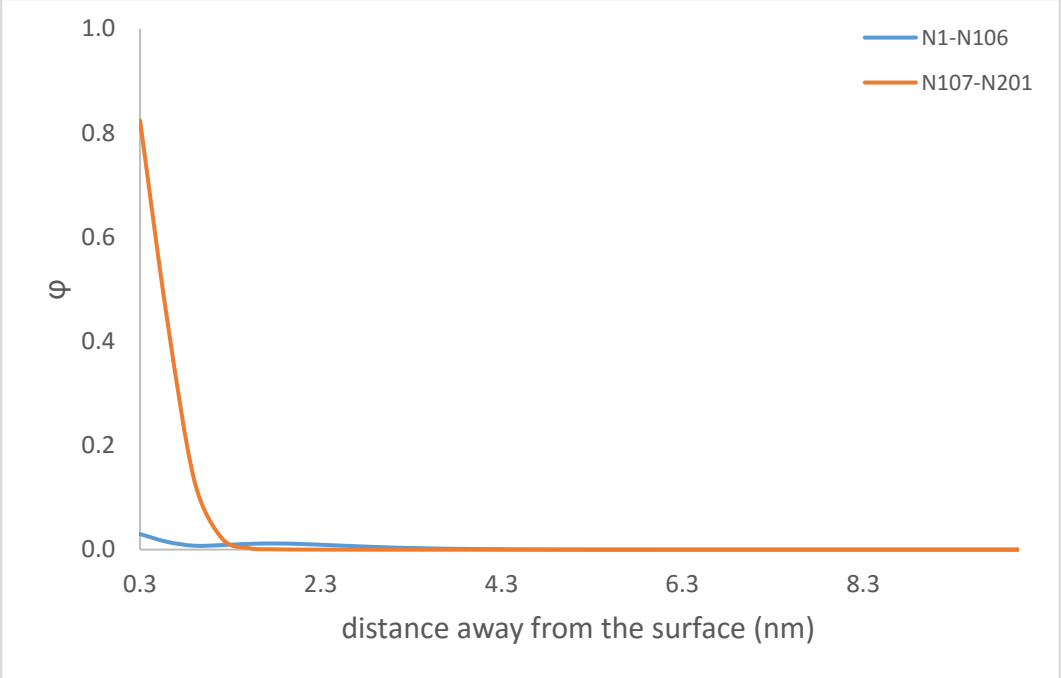

Figure 4.12 Volume fractions of adsorbed fragments (N1-N106 and N107-N201) plotted against the distance away from the surface (nm) at pH=5.0.

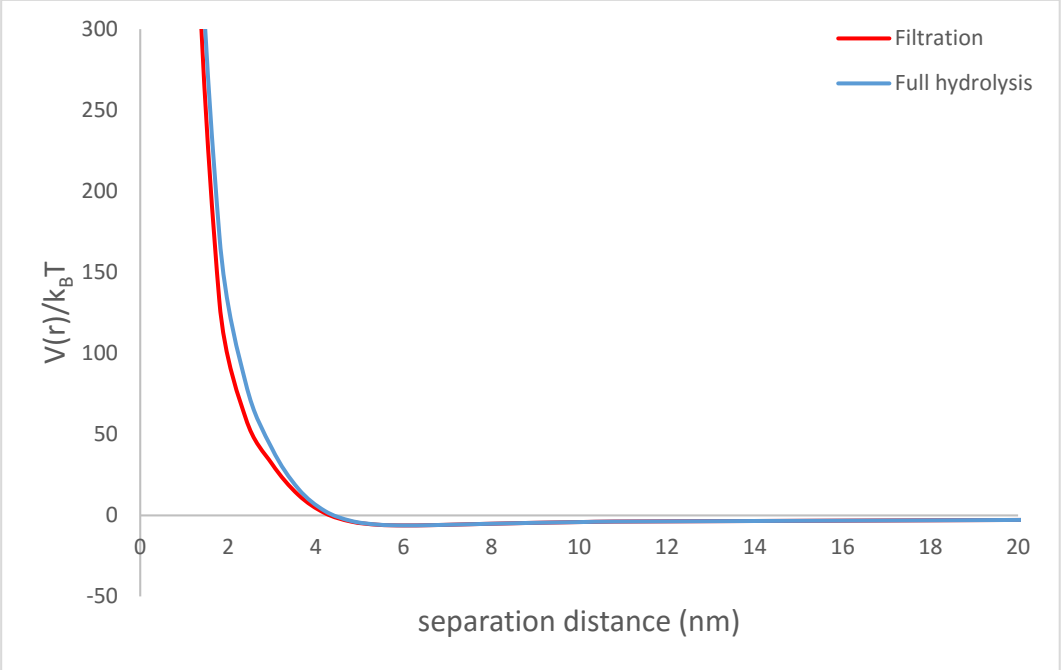

Figure 4.13 The interaction potentials V(r), between the droplets of size 1μm, induced by the N-terminal diblock fragment (the N1-106) (red) on its own and together with fully hydrolysed and highly broken up C-terminal fragment (blue), plotted against the separation distance (nm) at pH=4.5. These graphs are to be compared with the graph in Figure 4.9 for the same pH value.

4.3 Conclusions

α_{s1}-casein was fragmented into two polypeptides by the tryptic hydrolysis of a single peptide bond each time chosen from the one or other end of its hydrophilic middle section. The cleavage points were chosen to obtain diblock-like fragments which were thought to have better emulsion stabilising properties than the intact triblock-like protein. The amino acids on the protein backbone were divided into six categories and their interactions with each other and with the surface, solvent and free ions were specified by the Flory-Huggins interaction parameters.

The interactions between the droplets induced by the intact protein confirms that at high salt concentrations and pH values near the isoelectric point of the protein, the limited extension of the middle hydrophilic part of the protein into the solution led to the formation of a thin adsorbed layer. The lack of electrostatic interactions (near the isoelectric point of the intact α_{s1}-casein) together with the thin adsorbed layer made bridging connections possible, which induced attractive interactions between the droplets. It was shown that better emulsion stability, compared to the intact α_{s1}-casein particularly near its isoelectric point, can be achieved by the diblock-like fragments. However, hydrolysing the protein from the right place to obtain the right structure does not always guarantee better stability. It is also essential to ensure that the right structure is adequately adsorbed and not displaced by the other fragment, which is also of course present in the solution as a result of hydrolysis. This effect was also shown in our calculations of the emulsion system where the hydrophilic middle part of the protein was broken from the C-terminal side. It was demonstrated that filtering out the undesirable

fragment or fully hydrolysing it are the two possible solutions to increase the adsorption of the diblock-like peptide.

The calculations in this study were performed for α_{s1}-casein to obtain the polypeptides that have superior emulsion stabilising properties. Exploring such fragments in cheap protein sources such as vegetable proteins would be of the greatest commercial interest to the food industry.

Trypsin was assumed to hydrolyse only particular bonds among all of its potential targets in this study, which is not feasible in reality at present. However the desired part of the proteins can be obtained by using chemical means (Nilsson et al., 2005). The chemical means are not suitable for large scale food production but they can be used in experimental studies to verify these theoretical predictions. In the next chapter, the protein will be hydrolysed from all the targeted bonds by Trypsin, which is more feasible at present, and our SCF calculations will be extended to cover proteins in the emulsion systems involving multiple breakages and a large variety of fragments.

Chapter 5 Colloidal Behaviour of Hydrolysed α_{s1}-casein: Non-Selective Multiple Bond Breakage

In the previous chapter, the colloidal stabilising properties of α_{s1}-casein fragments produced by breaking of only one selective peptide bond, were investigated. In this chapter, simultaneous breakage of 20 peptide bonds on the backbone of α_{s1}-casein susceptible to hydrolysis by trypsin enzyme, were considered at 20%, 40%, 60%, 80%, and 100% degree of hydrolysis (DH). Apart from the number of hydrolysed peptide bonds, all the other system properties were the same as the previous chapter. The colloidal stabilising behaviour of the resulting fragments together with the remaining unbroken protein, was investigated at pH values of 3.0, 4.5, 5.0, and 7.0. This part of the research could only be carried out with the SCF_N approach presented in section 2.3 of this study. This is due to the limitations in the maximum number of breakages that the usual SCF computational methodology can handle. The breakage probabilities (p) for the 20 bonds were set to a number between 0 and 1 to achieve the various DH. All the trypsin targeted bonds were assumed to have the same probability of breakage though in practice perhaps some of these are more accessible to the enzyme than others. For instance, to achieve a DH of 50%, the value of p for all the 20 bonds was taken as 0.5.

5.1 pH 3.0

In this section, the colloidal stabilising behaviours of the polymers were monitored at pH=3.0 where the electrostatic stabilisation is expected to be an important factor for the colloidal stability of the emulsion systems. This is because this pH value is far from the isoelectric point of the intact α_{s1}-casein where the electrostatic interactions are present. These interactions are critical to keep the surfaces far from each other in the emulsion systems stabilised by triblock-like polymers since this type of polymers are prone to make bridging connections between two surfaces at close separation distances (see Figure 4.4). Figure 5.1 shows the interaction potentials between the two droplets against the separation distance and Figure 5.2 shows the same interactions but without the inclusion of van der Waals attractions. When the two figures are compared, it is clear that the van der Waals attraction does not make a major contribution to the overall interactions at low DH values. However, the presence of van der Waals (attractive) interaction becomes relatively more significant at DH 60%, 80% and 100% due to the thinner adsorbed layer obtained for these DH values, as shown in Figure 5.3. This figure shows the total volume fractions of the hydrolysed α_{s1}-casein at various DH values plotted against the distance away from the surface, as calculated by our SCF programs. Droplet surfaces with thinner adsorbed layers can approach each other more closely where the van der Waals attractions between the droplets are stronger. The range of the repulsive interactions induced by the fragments at high DH will be short because of the higher adsorption of smaller fragments. Thus, the effect of the van der Waals

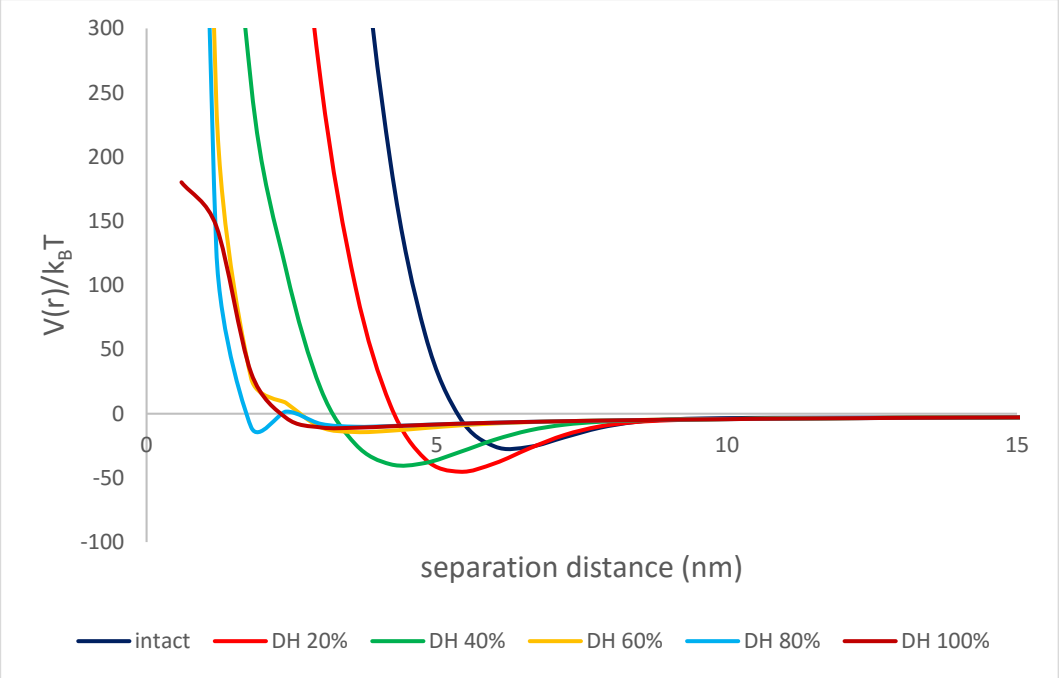

Figure 5.1 The interaction potentials *V*(*r*), between the droplets of size 1μm, induced by the hydrolysed α_{s1}-casein with various DH values at pH=3.0, plotted against the separation distance between the droplets (nm).

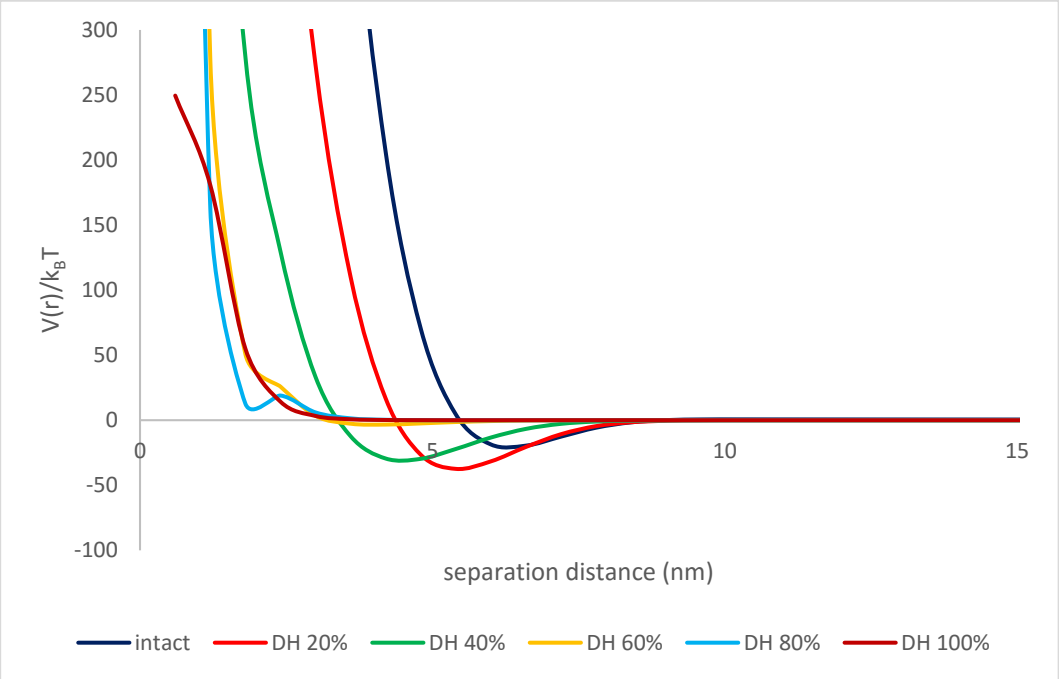

Figure 5.2 The same interaction potentials *V*(*r*), as those in Figure 5.1, but without the inclusion of van der Waals attraction component.

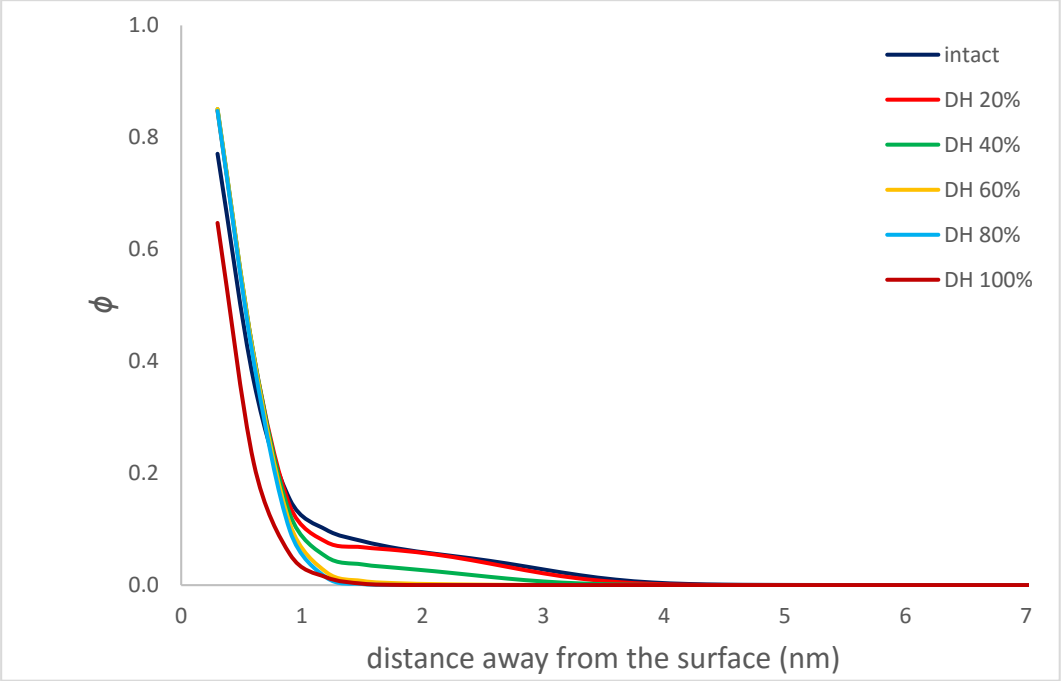

Figure 5.3 The total volume fractions of the hydrolysed α_{s1}-casein at various DH values at pH=3.0, plotted against the distance away from the surface (nm).

attractions will indeed be more significant for emulsion systems stabilised by highly fragmented proteins.

The first observation from Figure 5.1 is that the stabilising ability of the fragments decreased with the increased degree of hydrolysis up to DH 40%. However further hydrolysis of the protein improved the stability of the emulsion system with the energy well in the interaction potential becoming shallower. In order to understand this behaviour and to interpret the details of Figure 5.1, the electrostatic potentials (Figure 5.4), and the excess volume fractions of the more commonly adsorbed polymer sizes at various DH (Figure 5.5) were presented. Figure 5.4a shows the actual electrostatic

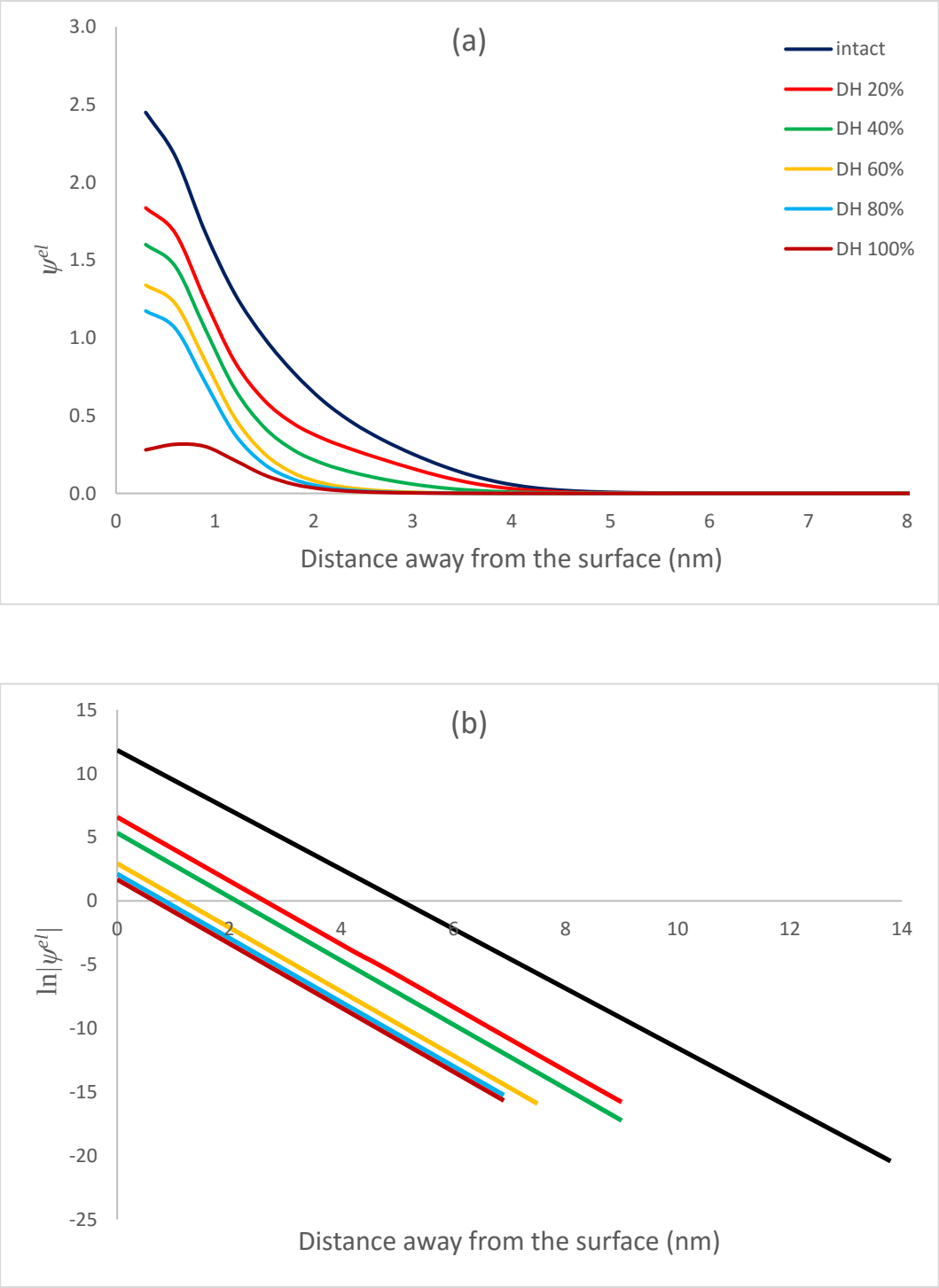

Figure 5.4 The electrostatic potentials $\psi^{el}(k_BT/e)$ (a), $\ln(|e\psi^{el}/k_BT|)$ (b), obtained at various DH values at pH=3.0, plotted against the distance away from the surface (nm). The DH values are the same as corresponding ones in Figure 5.4a.

potentials against the distance away from the surfaces whereas Figure 5.4b shows the logarithm of the absolute values of the effective surface potentials. The effective surface potentials were calculated to compare the long ranged interactions (the electrostatic component of the interaction potentials) observed at various DH and pH values. The details of this novel way of estimating effective surface potential is given in section 2.4.

The effective surface potentials obtained in this way (Figure 5.4b) were found to be very large for the intact protein. This is because the tails of the intact protein reach to the far distances (~12nm) away from the surface which create an electrostatic potential at such far distances. The Debye-Hückle approximation (Eq. 2.57) can be used to describe the variation of these low electrostatic potentials in the outer parts of the adsorbed layer in this model. Thus the electrostatic potentials (Figure 5.4a) obtained at very far distances away from the surface (>13nm) were extrapolated back to the actual interface to calculate the effective surface potentials. This leads to very large values near the surfaces since the potential in the Debye-Hückle approximation increases exponentially as one approaches the surface plane.

The electrostatic potentials fall continuously as DH increases (Figure 5.4). The lower electrostatic repulsions provided by the adsorbed layers of the protein fragments will let the droplets approach each other more closely and enable the fragments to simultaneously adsorb on two droplets (more bridges between the droplet surfaces). For the emulsion system stabilised by the intact protein, the energy well was calculated as 25 k_BT, as seen in Figure 5.1. Introducing a DH of 20%, increases the depth of the energy well to 45 k_BT. This is because, the lower

electrostatic potentials at DH 20% led to more bridging conformations of the adsorbed fragments, which induces attractive forces between the droplets.

At DH 20%, the size of the fragments that were predominantly adsorbed at the surface were mainly 68, 95, 178, and 193 in monomer units, as seen in Figure 5.5a. Table 5.1 shows more details of the adsorbed fragments. The table lists the main fragment sizes (m) that are adsorbed on the surface (column 1), as well as their excess volume fractions ($\phi_{ex}(m)$ is calculated by subtracting actual volume fraction from the bulk volume fraction, see Eq.2.56) in the interfacial region and percentages as a fraction of total adsorbed amount (column 2). For each fragment size, the table lists the possible sections of α_{s1}-casein that could contribute to that size (column 3). In addition, the table also shows the bulk volume fractions (Φ) of the possible sections of α_{s1}-casein that are in column 3 (column 4). For instance, 37.66% (ϕ_{ex}=1.34) of the total adsorbed polymer at the surface layer had a size of 68 at DH 20%, and there were 4 possible fragments with this size. These were fragments made from monomer residues N134-N201, N85-N152, N36-N103, and N24-N91. The proportions of these 4 equally sized but different fragments as a percentage fraction of all adsorbed chains of this size can be seen in the third column. According to the table, the proportion of the fragment N134-N201 was almost 100%. This was the result of the preferential adsorption of a more hydrophobic fragment (N134-N201), compared to all the other 3 chains of this size. The adsorption of such fragment by the hydrophobic surface was clearly much more favourable. Another reason for the high adsorption of N134-N201 was its higher availability in the system at DH 20%, compared to the other 3 fragments (Table 5.1 column 4) following fragmentation.

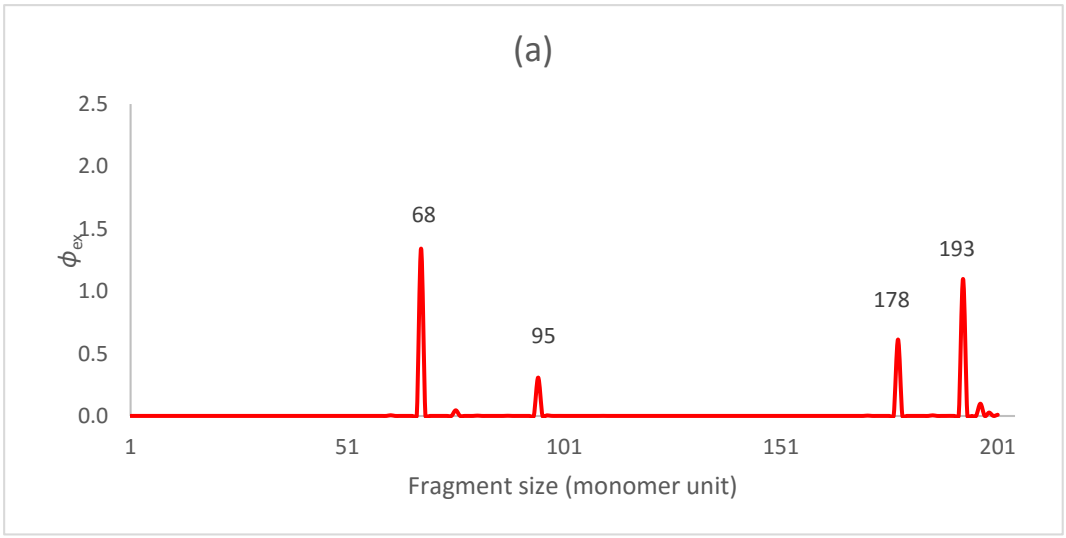
(a)
2.5
2.0
1.5
1.0
0.5
0.0
ϕ_{ex}
68
95
178
193
1
51
101
151
201
Fragment size (monomer unit)

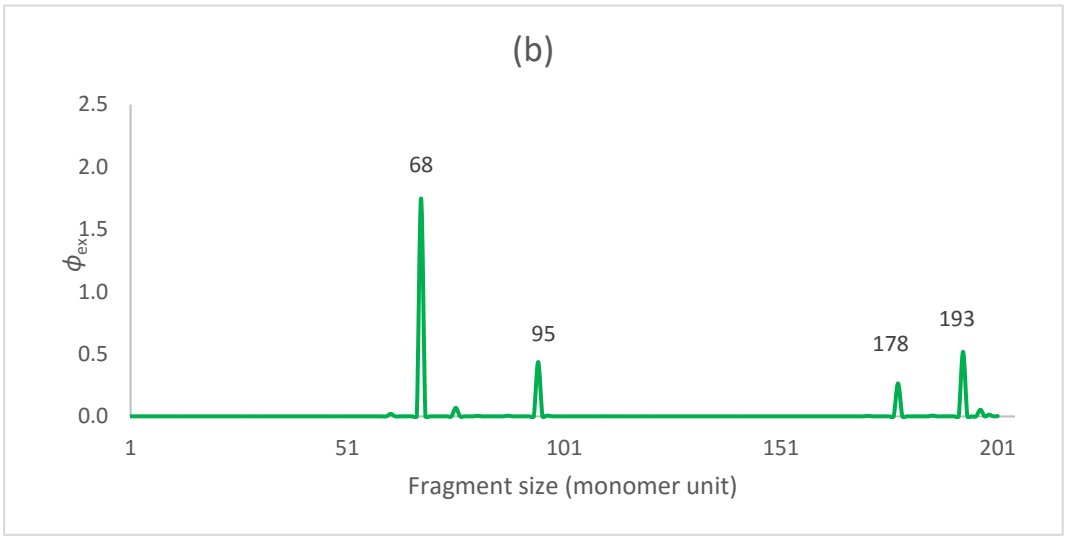
(b)
2.5
2.0
1.5
1.0
0.5
0.0
ϕ_{ex}
68
95
178
193
1
51
101
151
201
Fragment size (monomer unit)

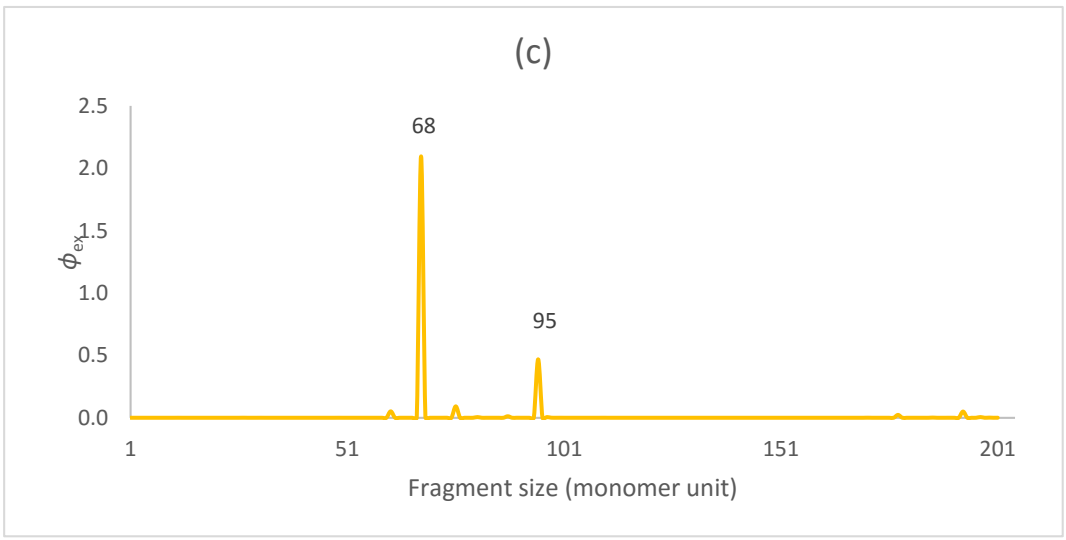
(c)
2.5
2.0
1.5
1.0
0.5
0.0
ϕ_{ex}
68
95
1
51
101
151
201
Fragment size (monomer unit)

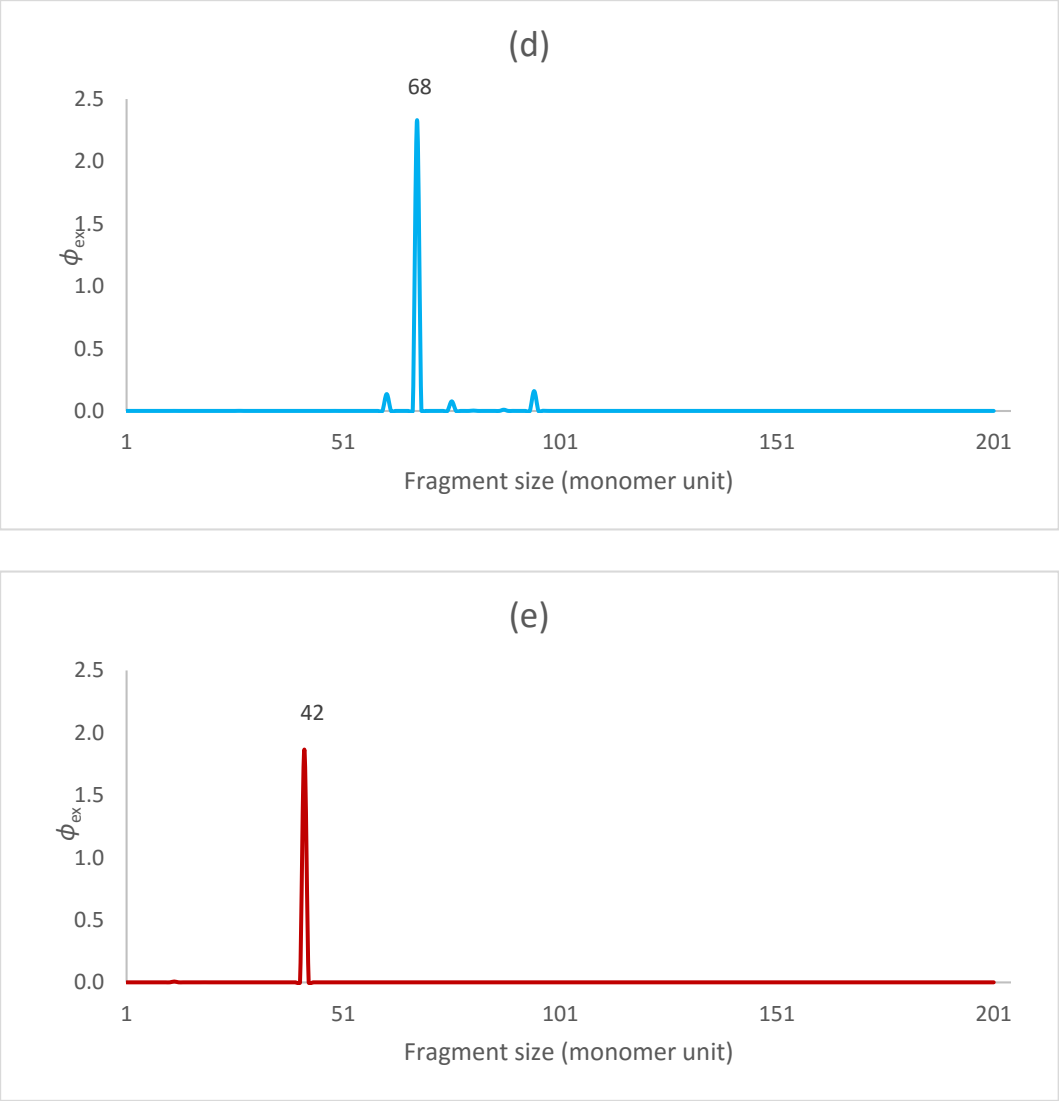

Figure 5.5 The excess volume fractions ($\phi_{ex}(m)$) at the interface for various fragment sizes (m). Only the main adsorbed fragments obtained by the hydrolysis of the α_{s1}-casein are shown. Results are for DH values of 20% (a), 40% (b), 60% (c), 80% (d), and 100% (e), all at pH=3.0.

This was likely due to the fact that other fragments had bonds in this backbone prone to cleavage which then caused a large number of these to be broken to even smaller sizes. N134-N201 was also the most adsorbed fragment among all the other fragment sizes at all DH values, except 100%. The main reason for this was again its more hydrophobic structure. The main adsorbed fragment sizes shown in Table 5.1 at DH 20% were the same for the other DH values except at 100% breakage.

m	$\phi_{ex}(m)$, %	jk, %	Φ
DH 20%			
68	1.34, 37.66%	134-201, ~100% 85-152, ~0% 36-103, ~0% 24-91, ~0%	4.33E-13 2.27E-14 3.74E-14 3.55E-14
95	0.31, 8.64%	107-201, ~100% 9-103, ~0%	3.10E-13 2.54E-14
178	0.61, 17.20%	24-201, 100%	4.98E-14
193	1.10, 30.83%	9-201, 100%	4.32E-14
DH 40%			
68	1.75, 55.50%	134-201, ~100% 85-152, ~0% 36-103, ~0% 24-91, ~0%	4.87E-13 9.11E-15 1.52E-14 2.52E-14
95	0.44, 13.84%	107-201, ~100% 9-103, ~0%	1.47E-13 7.62E-15
178	0.26, 8.40%	24-201, 100%	9.99E-16
193	0.52, 16.44%	9-201, 100%	6.50E-16
DH 60%			
68	2.01, 74.44%	134-201, ~100% 85-152, ~0% 36-103, ~0% 24-91, ~0%	3.25E-13 7.96E-16 1.99E-15 4.99E-15
95	0.47, 16.64%	107-201, ~100% 9-103, ~0%	2.91E-14 4.47E-16
DH 80%			
68	2.33, 85.65%	134-201, ~100% 85-152, ~0% 36-103, ~0% 24-91, ~0%	1.08E-13 5.54E-18 2.77E-17 1.39E-16
DH 100%			
42	1.87, 99.64%	153-194, 100%	2.09E-12

Table 5.1 The size of the main adsorbed fragments, m (column 1), their excess volume fractions ($\phi_{ex}(m)$) at interfacial region and percentages as a fraction of total excess amount (column 2) attributed to all chains of this size, the parts of α_{s1}-casein that belong to the fragments (jk) corresponding to that size group and their contributions to the adsorbed amount in column 2 is given in column 3 as a percentage function, and the bulk volume fractions (Φ) of the fragments in column 3 (column 4), obtained at DH 20%, 40%, 60%, 80%, and 100%, at pH=3.0.

The majority of the main adsorbed fragments were found to have tri-block type structures up to a degree of hydrolysis DH=60%, at pH=3.0. The main adsorbed fragments in this range of hydrolysis are N9-N201 (size 193), N24-N201 (size 178), N107-N201 (size 95) and N134-201 (size 68) (Table 5.1). It can be seen from Figure 4.1 of previous chapter that the first three fragments have tri-block type structures which are prone to make bridging conformations at the separation distances that correspond to overlap of two layers on approaching droplets.

Going back to the interaction potentials in Figure 5.1, the depth of the energy well did not change much at DH 40% compared to DH 20%, despite the fact that the effective electrostatic surface potential and with it the electrostatic component of the interaction had decreased (Figure 5.4). The bridging conformation of adsorbed fragments was expected to increase while the electrostatic interaction part decreased. However, it seems that this did not occurred. The reason for this could be the reduced availability of the large adsorbed fragments on the droplet surfaces at the value of higher DH (40%). The larger adsorbed polymers could initiate the bridging attraction at larger separation distances, when the two droplets are approaching. The sum of the ϕ_{ex} of the adsorbed large tri-block type fragments (size 178 and 193) was reduced from 1.71 to 0.78 at DH 40% (Table 5.1). This reduction can keep the droplets with fewer bridges until they approach much closer than otherwise is the case at DH=20%. It seems that this reduction in possible bridging attraction component was partially balanced with the loss in the degree of electrostatic repulsion, so that the overall interaction was not changed much (Figure 5.1).

At DH 60%, the ϕ_{ex} of the large tri-block type fragments became significantly lower and barely visible in Figure 5.5c. Therefore, the bridging effect possibly decreased and consequently a considerable reduction in the depth of the energy well was observed (Figure 5.1). Further hydrolysis of α_{s1}-casein at a higher DH (80%) brought further reduction in the depth of the energy well in the same manner. Although the electrostatic repulsion was also lower at the high DH values, the positive contribution to the overall interactions by prevention of the bridging effect was more significant and decreased the depth of the energy wells. However, increasing DH to 100% did not make the same effect. The lowest energy minimum (~10 k_BT) was obtained at DH 80%, and not at DH 100%. The reason for this seems to be that the electrostatic repulsive component of potential was higher at DH 80% (Figure 5.4) and the surface was covered by the larger hydrophobic (mainly size 68 and 95) fragments (Figure 5.5) compared to DH 100%. However, this energy minimum (~10 k_BT) could still initiate the flocculation of the droplets and make the emulsion system unstable. Also at DH 100%, a change was observed in the slope of the steep steric repulsive interaction from around r=1.2 nm to r=0.3 nm in Figure 5.1. It seems that this is due to the bridging interaction of small size fragments (i.e. size 42) which are the most commonly adsorbed fragments at this degree of hydrolysis (Table 5.1).

In the case of hydrolysis of homopolymers and copolymers, the higher molecular weight fragments are thermodynamically more favourable to be adsorbed. This of course also depends on their availability in the system as discussed in the chapter 3 following cleavage of bonds. Larger fragment size in homopolymers and copolymers means the higher number of monomers that have affinity for the surface sites which leads to the preferential adsorption of such fragments.

However, this does not always hold true for the proteins. The varied amino acid sequence of resulting fragments is more significant rather than just the fragment size itself. The more hydrophobic fragments will have more affinity for the adsorption and prefer to reside on the surface whereas the fragments with larger portion of hydrophilic amino acid residues will have a higher tendency to reside in the solution. Fragments that have hydrophobic and hydrophilic blocks can also compete for the surface sites. The hydrophobic blocks of course prefer to be adsorbed on the surface and the hydrophilic blocks will tend to protrude towards the solution. Table 5.1 also shows the competitive adsorption of the remaining intact α_{s1}-casein and its fragments at various DH. At this pH (3.0), the dominantly adsorbed fragments were of size 42, 68, 95, 178, and 193. At low DH values, the larger fragments (size 178 and 193) were commonly found in the bulk solution. Therefore, their percentage on the surface was quite high at DH 20% and 40%. However, at DH 60% and higher hydrolysis, the larger fragments were barely present, both in the bulk solution or adsorbed on the surface. Once their availability is reduced to critically low values in the bulk solution, they could not compete anymore for the adsorption and disappeared from the graphs in Figure 5.5. It is clear that these two large fragments adsorbed more competitively than the intact protein. It seems that the removal of the hydrophilic fragments from the N-terminus side of α_{s1}-casein made these fragments more favourable to be adsorbed. In addition to that, the availability of these large fragments in the bulk solution is more than the intact protein itself at these low levels of hydrolysis. Therefore, the intact protein did not preferentially adsorb in preference to these large fragments, which dominated the interfacial region at these values of DH.

In the 68 and 95 size groups, there were 4 possible fragments in the former and 2 in the latter. The more hydrophobic fragments were adsorbed more favourably among the fragments of the same size and showed a higher surface affinity. Thus, the N134-N201 and N107-N201 were the dominantly adsorbed fragments in the 68 and 95 size groups, respectively.

The net charge of the protein fragments is also an important factor in their preferential adsorption. The adsorption of the charged fragments will make the surface electrically charged and thus the surface will start to repel the other like-charged non-adsorbed fragments. The repulsion will become stronger as more like-charged fragments are adsorbed. It can be seen for instance in Table 5.1 that N134-N201 (size 68) was adsorbed more than N107-N201 (size 95). Firstly, N134-N201 was more available compared to N107-N201 within the bulk solution at all DH values. Secondly, the net charge of N134-201 was less positive than N107-N201, so the positively charged surface (by adsorption of positively charged fragments) remains less repulsive to N134-N201 throughout the adsorption, compared to N107-N201. Another example for the like-charge effect can be the higher adsorption of lesser charged N9-N201 (size 193) and N24-N201 (size 178) as compared to the intact protein. The higher amount of net positive charge of the intact protein along with its lower availability in the bulk solution and its relatively more hydrophilic structure, also negatively affected its preferential adsorption compared to these large fragments (with sizes 178 and 193). At pH=3.0, the number of positively charged residues was a key parameter in determining the net charge of the fragment and consequently the character of the interaction between such fragment and the surface.

At complete hydrolysis (DH 100%), a total of 99.64% of the adsorbed fragments are N153-N194 (size 42). This fragment is the largest hydrophobic fragment remaining available in the system at this DH. Therefore, it is highly dominant on the surface.

5.2 pH 4.5

In the previous section, the colloidal stabilising ability of α_{s1}-casein fragments was investigated in a colloidal system where the total net charge of the intact protein was positive. In this section, the same investigation was carried out at pH=4.5 which is very near the isoelectric point of α_{s1}-casein where the intact protein carries no net charge. Of course, the isoelectric point of the α_{s1}-casein fragments can be different from the intact protein depending on their amino acid sequences. Thus, the surface net charge will be dependent on the number of adsorbed fragments and their charged amino acid composition.

The interaction potentials with and without the van der Waals attractions, and the electrostatic potentials were plotted against the separation distance in Figure 5.6, Figure 5.7 and Figure 5.8, respectively. When the interaction potentials obtained at pH values 3.0 (Figure 5.1) and 4.5 (Figure 5.6) are compared, it can be seen that the depth of the energy wells observed at pH=4.5 are generally higher than those at pH=3.0, which characterise a more unstable emulsion system. A lower electrostatic repulsive component of the interaction potential obtained at pH=4.5 is expected to cause such deeper energy wells. The electrostatic potentials vary at different DH values and also alter sign at intermediate DH values within the adsorbed interfacial layers consisting of fragments, as seen in Figure 5.8a. This is because the volume fraction of the charged residues varies throughout the

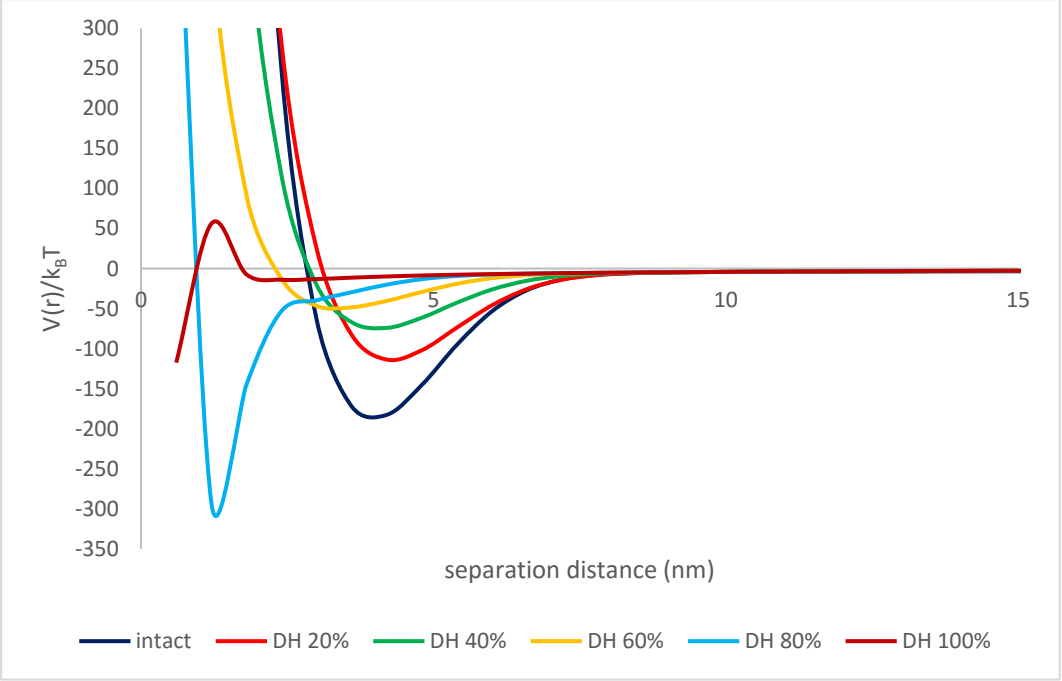

Figure 5.6 The interaction potentials *V*(*r*), between two droplets of size 1μm, induced by the hydrolysed α_{s1}-casein, at various DH values at pH=4.5, plotted against the separation distance between droplets (nm).

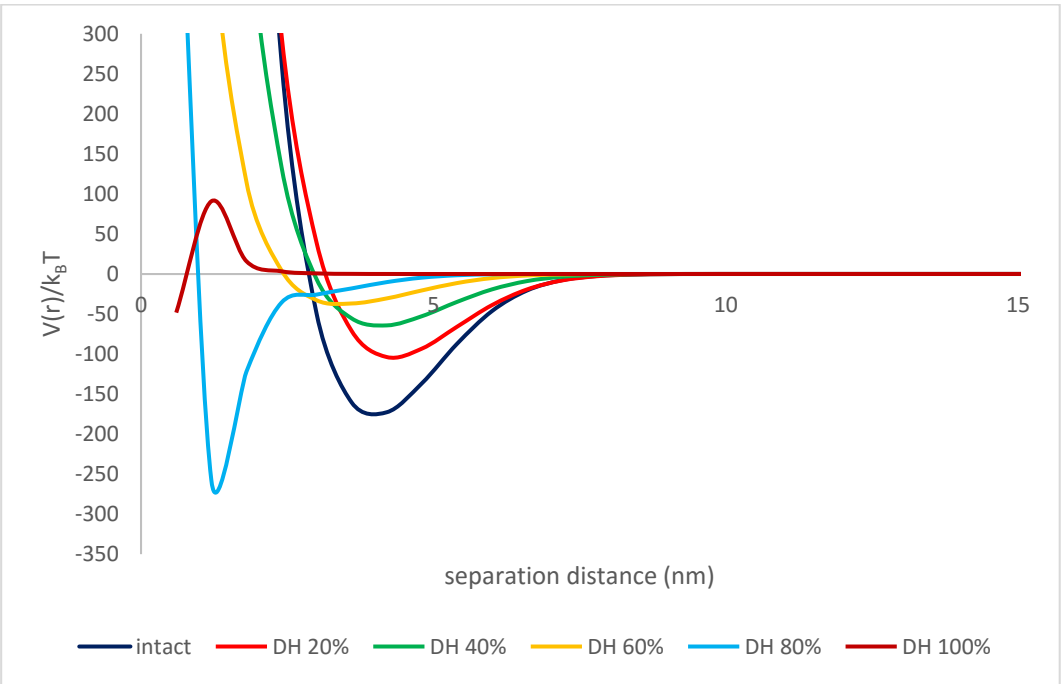

Figure 5.7 The same interaction potentials *V*(*r*) as those in Figure 5.6, but now without the inclusion of van der Waals attraction component.

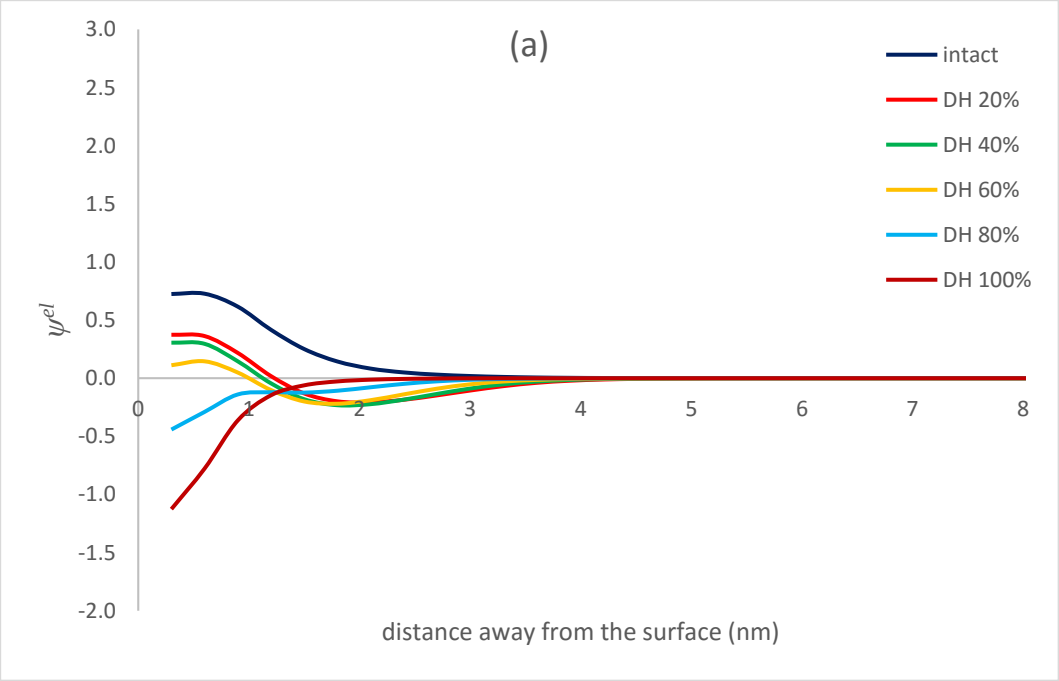

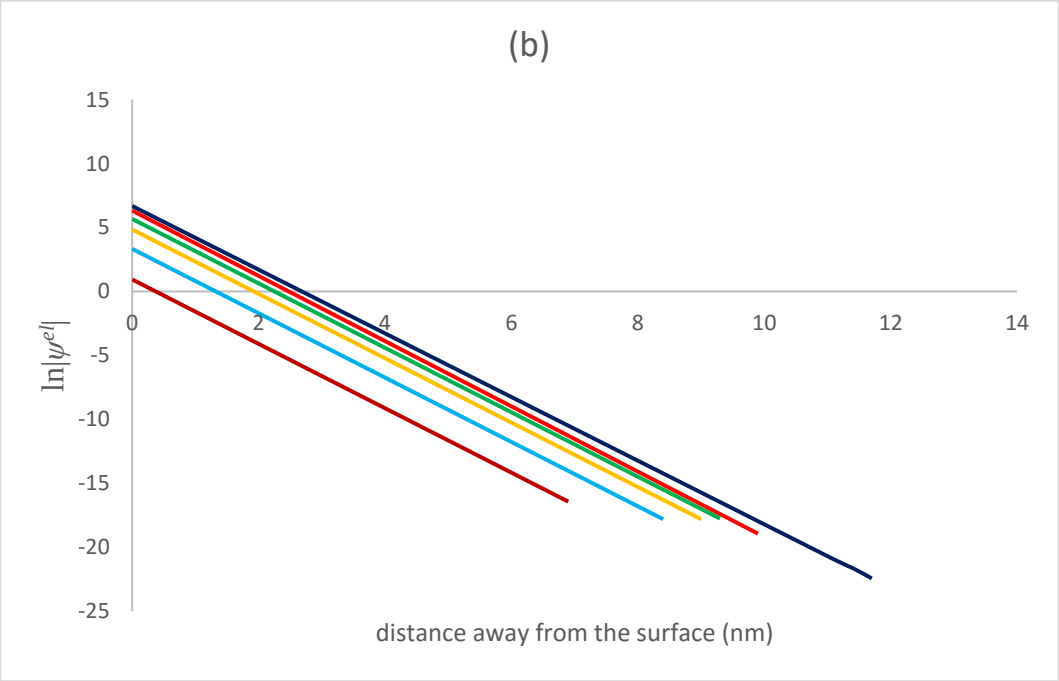

Figure 5.8 The electrostatic potentials $\psi^{el}(k_BT/e)$ (a), $\ln(|e\psi^{el}/k_BT|)$ (b), obtained at various DH values at pH=4.5, plotted against the distance away from the surface (nm). The DH values are the same as corresponding ones in Figure 5.8a.

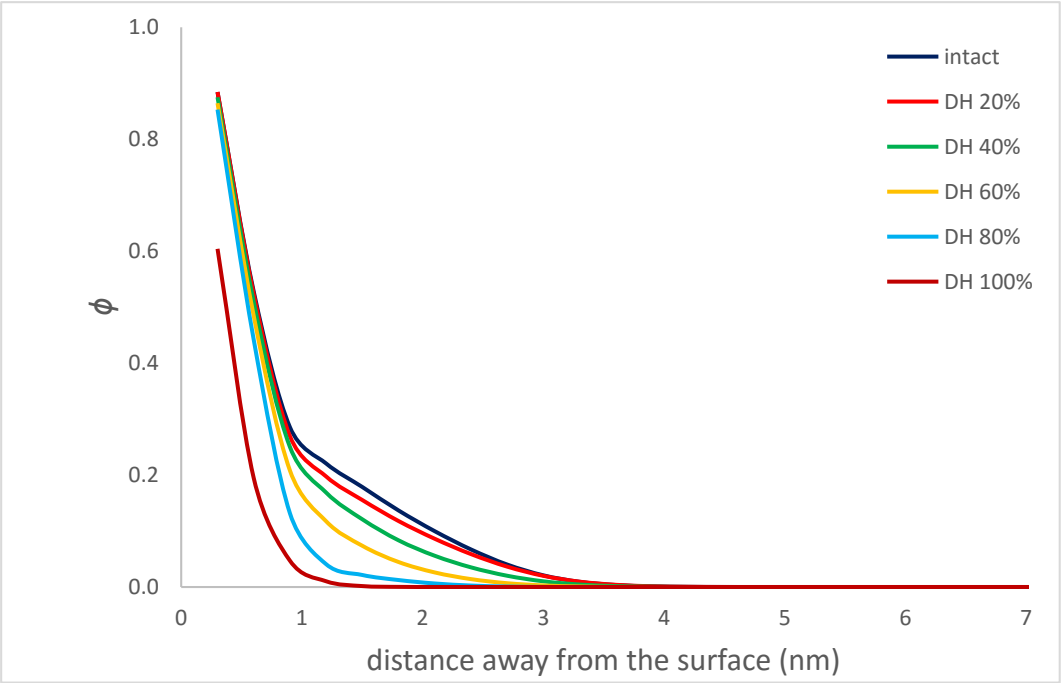

Figure 5.9 The total volume fractions of the hydrolysed α_{s1}-casein at various DH values at pH=4.5, plotted against the distance away from the surface (nm).

layer as one moves away from the surface. Figure 5.8b shows the effective surface potentials now plotted in a way that makes easier to compare between various degrees of hydrolysis.

The electrostatic potentials of the intact α_{s1}-casein are positive throughout interfacial area (Figure 5.8a). The potentials in the positively charged sections of the interfacial layers decrease, while DH increases and it turns completely negative at a DH value of 80%. This indicates that the charged amino acid composition in this region changes significantly with degree of hydrolysis. This could occur both by the adsorption of different fragments and by the different configuration of the same fragments near the surface. At DH 80%, not only the positive electrostatic potentials near the surface (0.3-1.5 nm) has turned

negative, but also the decreasing trend in the depth of the energy wells with increasing DH ceases and instead a deep energy well was obtained at such DH, as seen in Figure 5.6. This shows that the characteristic of the adsorbed fragments was significantly changed between a DH=60% and DH=80%.

An explanation for the above results is provided by Figure 5.10 and Table 5.2 showing the nature of the adsorbed fragments at different levels of hydrolysis. According to the graphs in Figure 5.10, the large tri-block type polypeptides (size 178, 193, 197, 199, and 201) were dominantly adsorbed at DH 20%, 40%, and 60%. However, at DH 80%, the intermediate size fragments (size 68, 95) started to become the dominant chains and possibly this turned the electrostatic potentials near the surface (0.3-1.5 nm) from a positive to a negative value. Therefore, the net charge of the intermediate size fragments may be expected to be negative. Table 5.2 provides further details of those fragments that are not available in Figure 5.10. It can be obtained from the table that the total percentage of the large fragments were 98.58%, 93.83%, 72.9%, and 21.76% at DH values 20%, 40%, 60%, and 80%, respectively. The table also shows that N134-N201 and N107-N201 were the main adsorbed fragments amongst the polypeptides of size 68 and 95, respectively. The net charges of these two fragments at pH=4.5 were found to be -2.5 and -0.48 (i.e. both negative). These results show that the large fragments were no longer dominant at DH 80% and were replaced with the more negatively charged intermediate size fragments, and in particular with these two polypeptides.

The depth of the energy wells decreases with the increased DH up to 60% in Figure 5.6. This could be the evidence of the reduction in bridging attraction

m	$\phi_{ex}(m)$, %	jk,%	Φ
DH 20%			
178	0.38, 8.07%	24-201, 100%	4.98E-14
193	1.63, 34.52%	9-201, 100%	4.32E-14
197	1.15, 25.12%	5-201, 100%	3.53E-14
199	0.82, 17.31%	3-201, 100%	2.85E-14
201	0.68, 14.44%	1-201, 100%	1.15E-13
DH 40%			
68	0.05, 1.08%	134-201, ~100% 85-152, ~0% 36-103, ~0% 24-91, ~0%	4.87E-13 9.11E-15 1.52E-14 2.52E-14
95	0.13, 2.94%	107-201, ~100% 9-103, ~0%	1.47E-13 7.62E-15
178	0.31, 7.29%	24-201, 100%	9.99E-16
193	1.68, 39.42%	9-201, 100%	6.50E-16
197	1.12, 26.27%	5-201, 100%	3.98E-16
199	0.67, 15.69%	3-201, 100%	2.41E-16
201	0.22, 5.16%	1-201, 100%	3.66E-16
DH 60%			
68	0.23, 6.15%	134-201, ~100% 85-152, ~0% 36-103, ~0% 24-91, ~0%	3.25E-13 7.96E-16 1.99E-15 4.99E-15
95	0.57, 15.38%	107-201, ~100% 9-103, ~0%	2.91E-14 4.47E-16
178	0.16, 4.41%	24-201, 100%	2.28E-18
193	1.22, 32.97%	9-201, 100%	9.90E-19

DH 60% cont.			
197	0.84, 22.74%	5-201, 100%	4.04E-19
199	0.41, 11.18%	3-201, 100%	1.63E-19
201	0.06, 1.60%	1-201, 100%	1.10E-19
DH 80%			
68	0.57, 18.70%	134-201, ~100% 85-152, ~0% 36-103, ~0% 24-91, ~0%	1.08E-13 5.54E-18 2.77E-17 1.39E-16
95	1.29, 42.54%	107-201, ~100% 9-103, ~0%	1.21E-15 1.55E-18
178	0.02, 0.67%	24-201, 100%	4.65E-23
193	0.25, 8.38%	9-201, 100%	1.01E-23
197	0.26, 8.72%	5-201, 100%	2.05E-24
199	0.11, 3.74%	3-201, 100%	4.16E-25
201	0.01, 0.25%	1-201, 100%	1.05E-25
DH 100%			
42	1.69, 98.31%	153-194, 100%	2.09E-12

Table 5.2 The size of the main adsorbed fragments, m (column 1), their excess volume fractions ($\phi_{ex}(m)$) at interfacial region and percentages as a fraction of total excess amount (column 2) attributed to all chains of this size, the parts of α_{s1}-casein that belong to the fragments (jk) corresponding to that size group and their contributions to the adsorbed amount in column 2 is given in column 3 as a percentage function, and the bulk volume fractions (Φ) of the fragments in column 3 (column 4), obtained at DH 20%, 40%, 60%, 80%, and 100%, at pH=4.5.

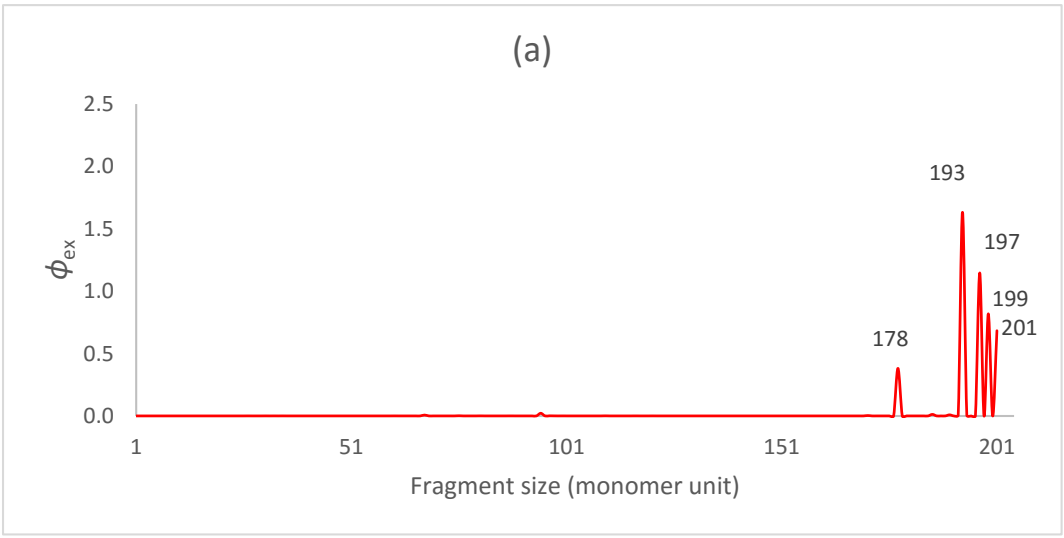
(a)
2.5
2.0
1.5
1.0
0.5
0.0
ϕ_{ex}
193
197
199
201
178
1
51
101
151
201
Fragment size (monomer unit)

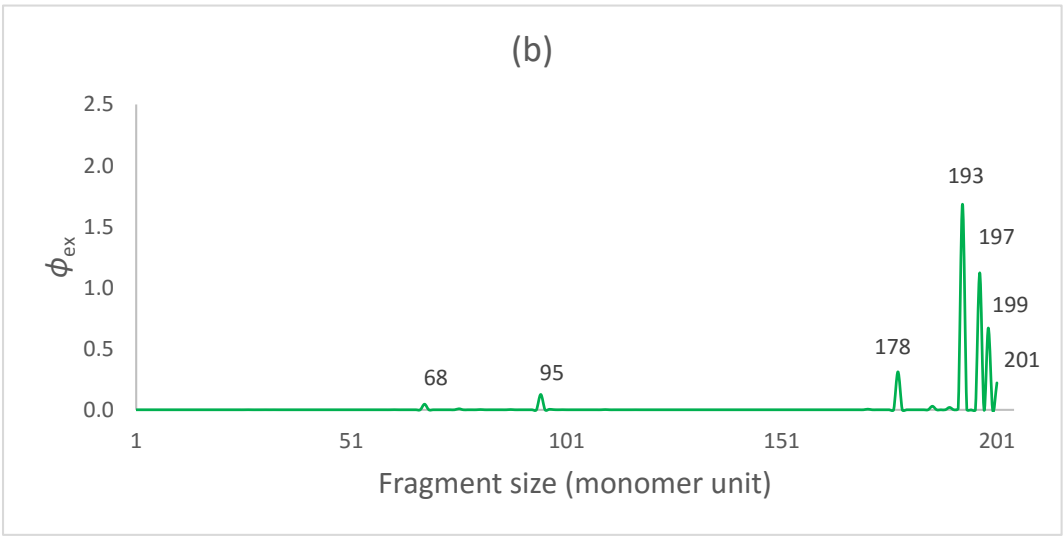
(b)
2.5
2.0
1.5
1.0
0.5
0.0
ϕ_{ex}
193
197
199
201
178
68
95
1
51
101
151
201
Fragment size (monomer unit)

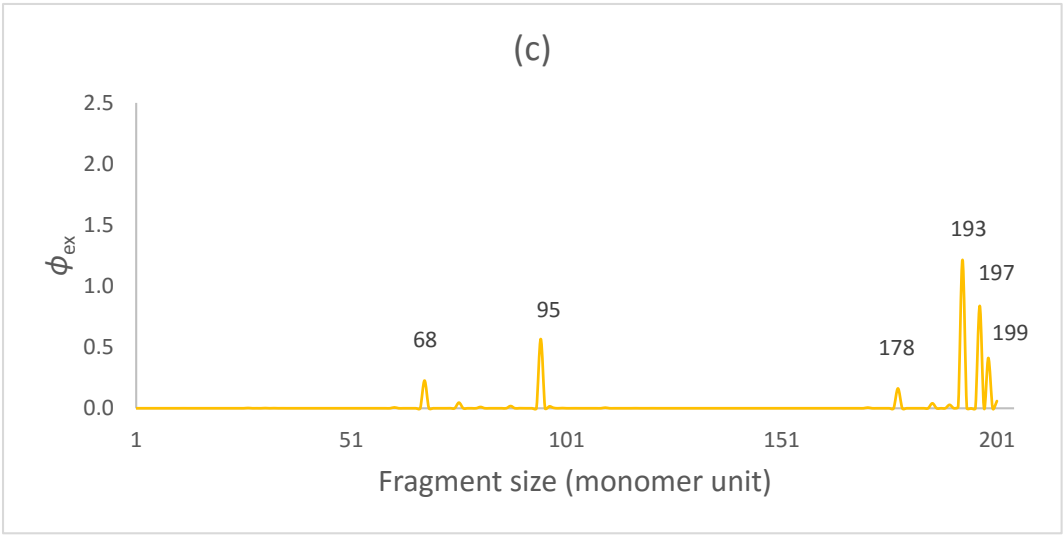
(c)
2.5
2.0
1.5
1.0
0.5
0.0
ϕ_{ex}
193
197
199
178
68
95
1
51
101
151
201
Fragment size (monomer unit)

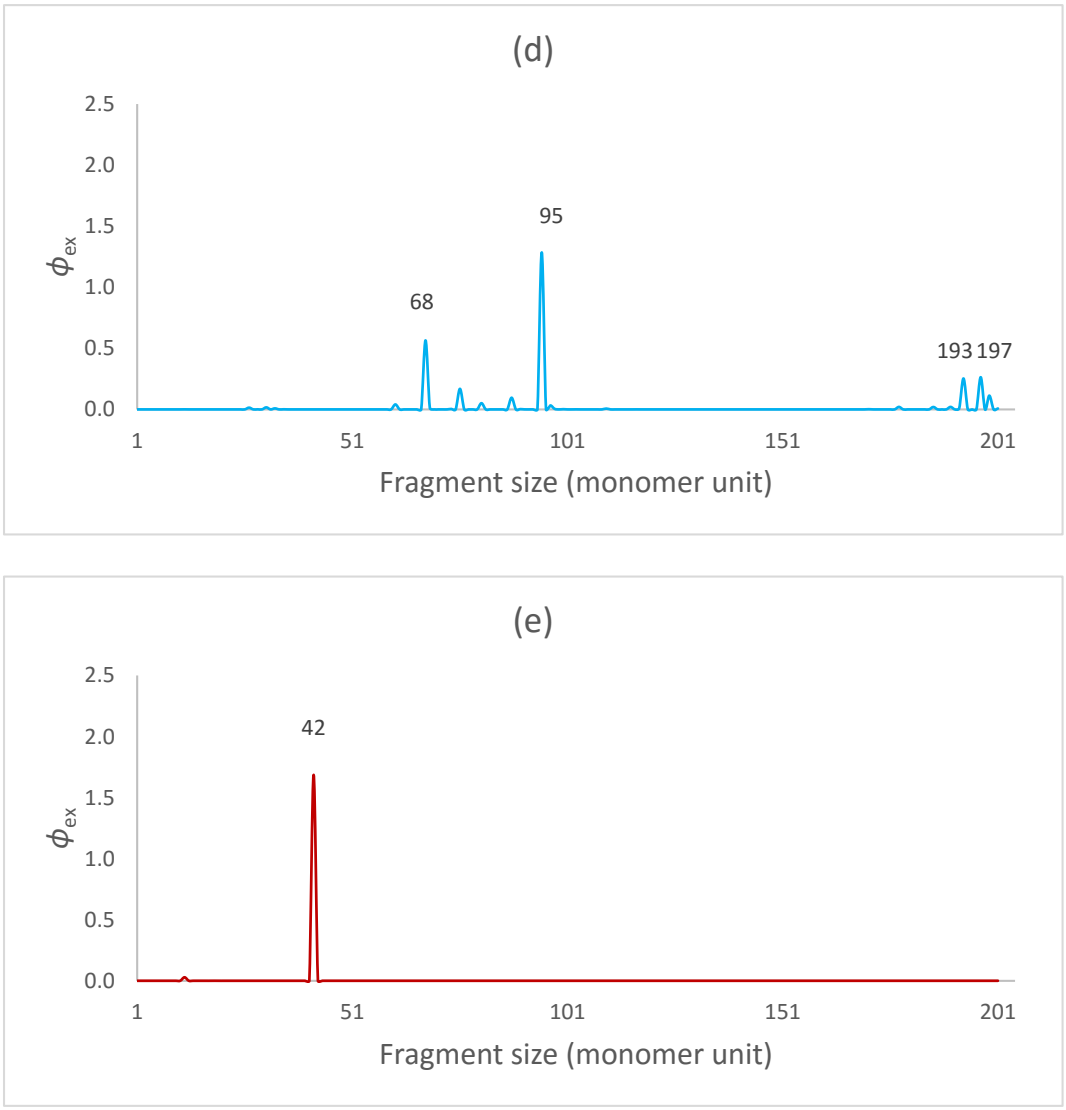

Figure 5.10 The excess volume fractions ($\phi_{ex}(m)$) plotted against the size of the main adsorbed fragments, obtained by the hydrolysis of the α_{s1}-casein at DH 20% (a), 40% (b), 60% (c), 80% (d), and 100% (e), at pH=4.5.

induced by the large fragments as these fragments become increasingly less likely at higher levels of hydrolysis.

The smaller abundance of these larger fragments, leads to lower adsorption of these and results in less bridging attraction. Although the large fragments make bridges and induce attraction between the two opposite surfaces, it seems that they also prevent such surfaces from further approach even closer at

separations. This can be seen in Figure 5.6 as energy barriers obtained at separation distances where interfacial layers formed by these large fragments become strongly overlapped. The prevention of the very closer approach of the surfaces was provided sufficiently up to a DH value of 60%, where the adsorbed amount of the large fragments was still enough to produce the required steric repulsion for this to occur. At DH 80%, there were two different slopes in the energy well (Figure 5.6). This indicates that the bridging was first induced by the large fragments and then further, and more strongly, bridging attraction was mediated by the intermediate size fragments as surfaces got even closer to each other. At this DH, the volume fraction of the adsorbed large fragments seems to be not enough to keep the surfaces sufficiently away from each other for preventing the excessive bridging of the intermediate size fragments at around 1.2 nm separation distance. However, the bridging attraction turns into steric repulsion eventually at closer separations. A steep energy barrier is obtained by the steric effect of highly overlapped intermediate and large fragments.

Comparing the graphs in Figure 5.6 and Figure 5.7, it can be seen that the relative importance of the van der Waals effect was considerable at DH 100%, because of the thin adsorbed layer (Figure 5.9) obtained at this DH. The minimum in the interaction potential was found at 2.4 nm as ~14 k_BT (Figure 5.6) at this level of hydrolysis, which is enough to enable the formation of the flocs. At closer separation distances there was an energy barrier evident in the corresponding graph of Figure 5.6. The barrier is substantial with a value of ~50 k_BT. Once this barrier was passed with an external force, the droplet surfaces will be stuck to each other because of the high bridging attraction as well as van der Waals forces. At this DH value of 100%, around 98% of the adsorbed fragments

were found to be N153-N194 (Table 5.2). This fragment is short and highly hydrophobic as seen in Figure 4.1 and does not possess the structure that can lead to large loops and long tails at the surface. The thickness of the adsorbed layer at DH 100% is therefore much smaller than the ones obtained at the other DH values (Figure 5.9). That is why the energy barrier was observed at a very close separation distance in Figure 5.6, as was the overall interaction potential being much shorter ranged. The net charge of this fragment was found to be -1.5e, which produces some degree of negative electrostatic potential as seen on Figure 5.8a. The energy barrier is the result of the interplay between the steric and electrostatic repulsions on one hand and bridging and van der Waals attractions on the other, with the first three of these arising by adsorption of fragment N153-194. The energy minimum at longer separations is not as deep as that for a DH=80%. The first reason behind this could be the non-existence of the large polymers in the system at such high levels of hydrolysis, and consequently the absence of long ranged bridging attraction. The second reason could be the stronger adsorption of the more hydrophobic fragments to the surface compared to DH 80% case, which disabled the formation of tails and loops and ultimately the formation of the bridges, as such hydrophobic chains will lie more or less in a flat conformation on the surface.

The main adsorbed polymers at pH=4.5 at various different stages of hydrolysis were of sizes 42, 68, 95, 178, 193, 197, 199, and 201, as seen in Figure 5.10. Comparing the two systems at pH values 3.0 and 4.5, the large polymers as oppose to the intermediate size ones, were more competitive and dominant on the surfaces at pH=4.5. The total net charge of the intact protein was 20.05e and

1.69e at pH values 3.0 and 4.5, respectively. The low net charge of the intact protein at pH=4.5 means that the charge of the large polymers was also low at such pH value. The repulsive electrostatic force provided between the surfaces by the like-charged fragments becomes less at pH=4.5 compared to pH=3.0, when large fragments are involved. The other difference in the profile of the adsorbed fragments between the two systems (pH=3.0 and 4.5) was that N107-N201 (size 95) adsorbed more strongly than N134-N201 (size 68) at pH=4.5, which is the reverse of what happens at pH=3.0. The net charges of N134-N201 and N107-N201 were 1.72e and 6.1e at pH=3.0. However, these values become -2.5e and -0.48e at pH=4.5. This shows that the less favourable N107-N201 at pH=3.0 becomes the more favourable at pH=4.5, compared to N134-N201, due to the less net charge of former. As we have discussed previously, all else being the same a lower charged fragment will have a high tendency for adsorption. This is because chain strands at surface will not repel each other as strongly.

The competitive adsorption between the same size fragments at pH=4.5 had the same behaviour (the more hydrophobic fragments is more adsorbed) as it was at pH=3.0. Therefore, N134-N201 was the dominant adsorbed fragment among the all fragments with a size of 68 residues and the N107-N201 among the size 95 ones as is shown in Table 5.2.

5.3 pH 5.0

In this section, the colloidal stabilising ability of α_{s1}-casein fragments obtained at various degrees of hydrolysis was investigated at pH=5.0. The electrostatic interactions are expected to be considerably more significant, though the pH is only slightly away from the isoelectric point of the protein. This time, unlike the two previous sections, the pH will be on the other side of the isoelectric point of the protein where the net charge of the intact protein has a negative sign.

Figure 5.11 and Figure 5.12 show the interaction potentials were plotted against the separation distance between two droplets of size 1μm, at various DH values, with and without the van der Waals interactions, respectively. The depth of the energy wells at all DH were only a few k_BT in Figure 5.12. The Brownian motion of the droplets can easily overcome this to prevent aggregation of the droplets. Once the van der Waals interactions are included in the interaction potentials, as shown in Figure 5.11, the magnitudes of the energy wells decreased to below -10 k_BT, which now begins to be sufficient to lead the flocculation of the droplets. The volume fraction of the α_{s1}-casein fragments in the interfacial area was significantly lower at DH 80% and 100% as compared to the low levels of hydrolysis, as shown in Figure 5.13. It means that the adsorption layer will be rather thinner at such DH values, so the layers of fragments will only begin to overlap at closer separations between the droplets. At such separation distances, the van der Waals attractions are quite strong as it can be seen by the comparison of the Figure 5.11 and Figure 5.12 and according to Eq. 1.1 in chapter 1. The adsorption layer was thicker at low level of hydrolysis, but

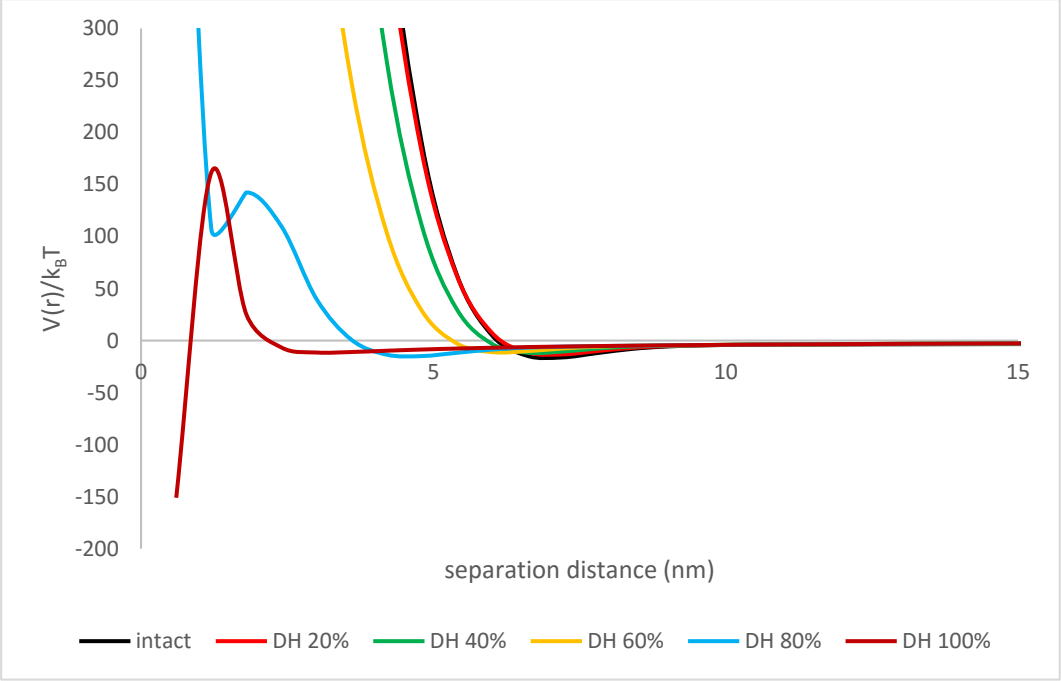

Figure 5.11 The interaction potentials *V*(*r*), between the droplets of size 1μm, induced by the hydrolysed α_{s1}-casein at various levels of hydrolysis and at a pH=5.0, plotted against the separation distance between the drops (nm).

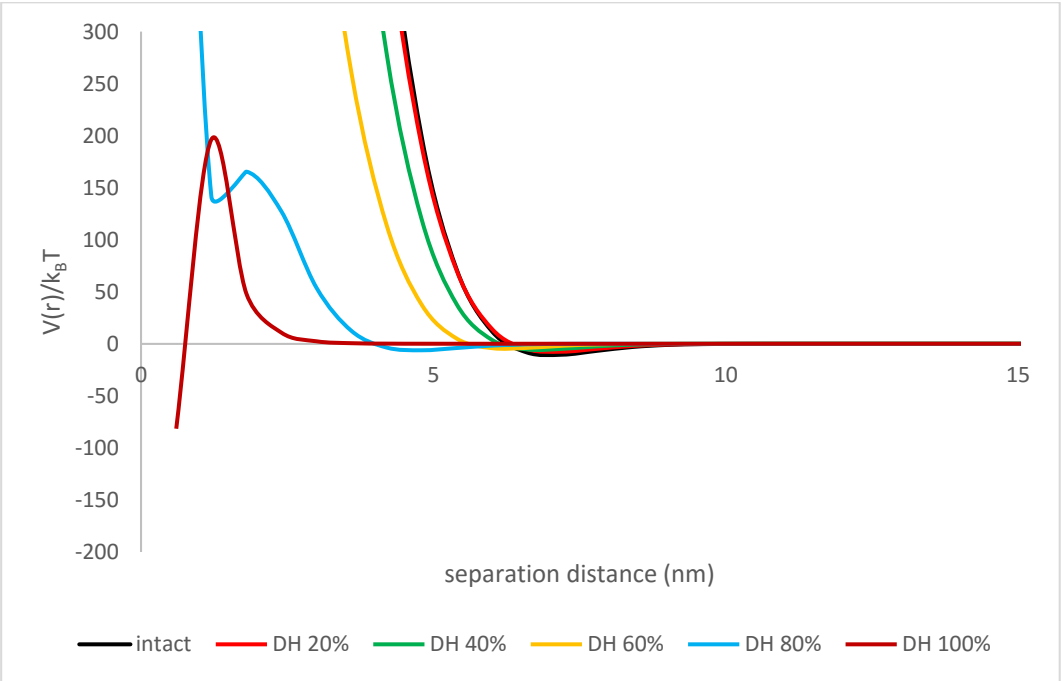

Figure 5.12 The same interaction potentials *V*(*r*) as those in Figure 5.11, but now without inclusion of the van der Waals attraction.

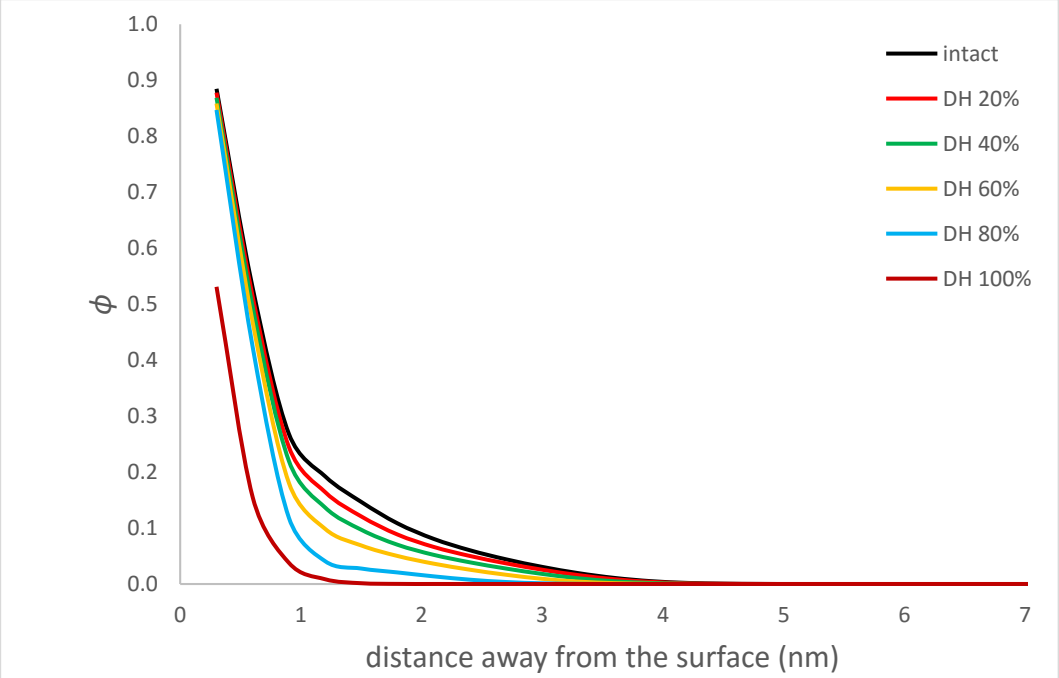

Figure 5.13 The total volume fractions of the hydrolysed α_{s1}-casein at various degrees of hydrolysis at pH=5.0, plotted against the distance away from the surface (nm) for an isolated interface.

nevertheless, the van der Waals attractions are still sufficient to make the emulsion systems unstable. Figure 5.11 shows that the bridging effect was considerably suppressed by the higher electrostatic interactions compared to what was found at pH=4.5 (comparing Figure 5.14b and Figure 5.8b). However, the bridging effect induced by the adsorbed large tri-block type polypeptides seems to be still present to some extent and leads to the energy minima of around -10 k_BT at these low DH values. The electrostatic potentials decreased with the increasing level of hydrolysis as displayed in Figure 5.14b. Conversely, the depth of the energy minima also decreases slightly while the electrostatic potentials were reduced with the increased DH. This could be an evidence that the higher DH values reduced the adsorption of the larger molecular weight fragments which reduces the number of chains forming bridges between the two

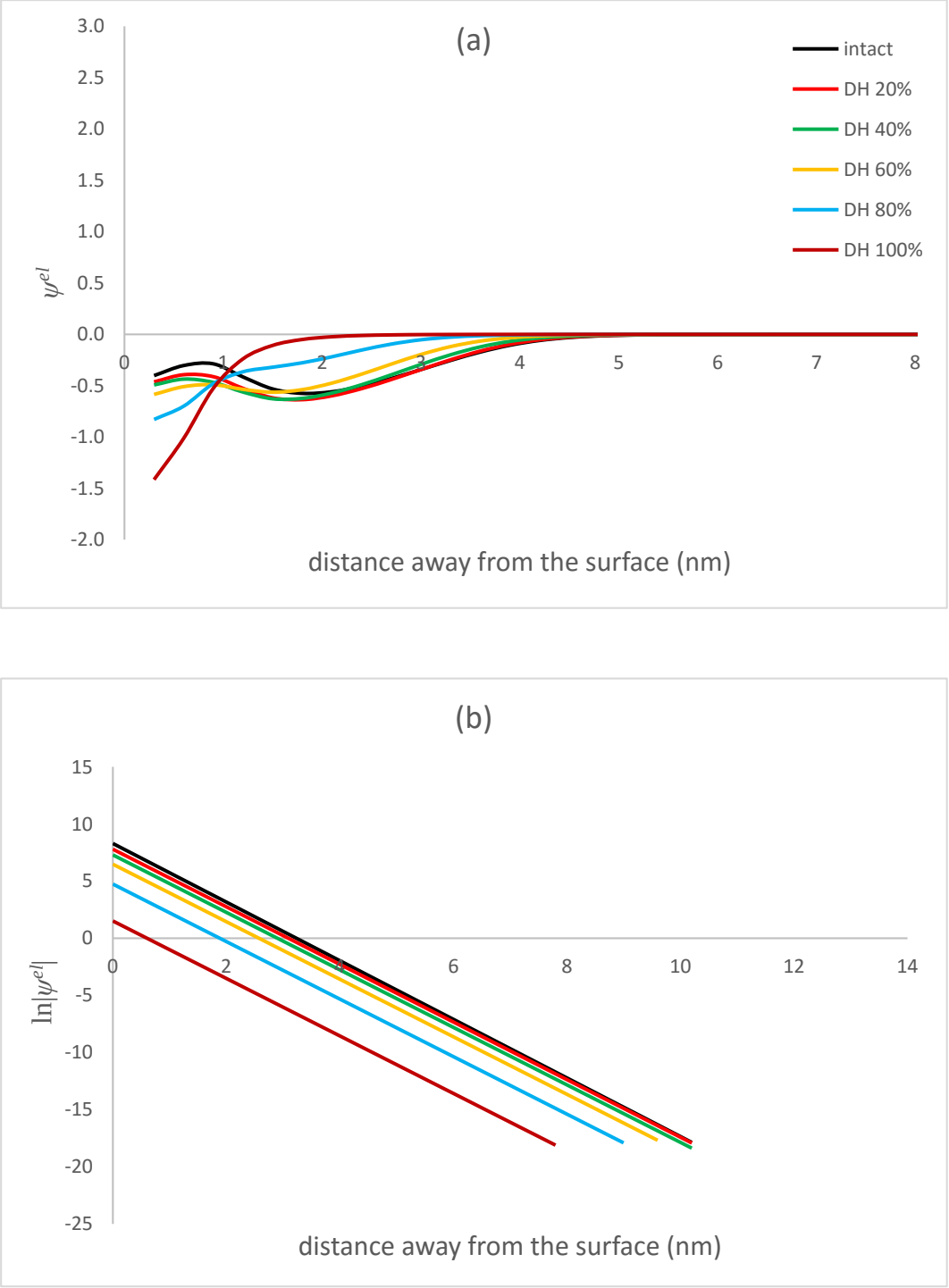

Figure 5.14 The electrostatic potentials $\psi^{el}(k_BT/e)$ (a), $\ln(|e\psi^{el}/k_BT|)$ (b), obtained at various DH values at pH=5.0, plotted against the distance away from the surface (nm). The DH values are the same as corresponding ones in Figure 5.14a.

opposite surfaces, at longer separation distances. This has a positive contribution to the overall interactions between the two approaching surfaces in terms of stability of emulsion. This contribution seems to be more than enough to compensate the loss in the electrostatic surface potential and resulting electrostatic repulsion. Therefore, the net contribution remained positive in keeping droplets apart.

The fragments make bridging connections when the opposing layers on two approaching surfaces start to touch. This induces attraction for reasons we mentioned in the introductory chapter (section 1.2.4). However, once they approach even more closely and layers become fairly overlapped, the steric repulsion rapidly increases. The combination of these two effects leads to an energy potential graph with an energy minimum which also has a steep repulsive energy barrier as the two surfaces approach each other (see Figure 5.11).

Figure 5.15 shows the sizes of the most significantly adsorbed fragments at various DH values and Table 5.3 gives their exact volume fractions at interfacial region and percentages as a fraction of total excess amount. Also the possible parts of the α_{s1}-casein for each size group is provided in column 3. According to the table, the sum of the percentages of the 4 commonly adsorbed large fragments (193, 197, 199, 201) constitutes 97.64%, 92.32%, 73.97%, and 28.52% of the total amount of adsorbed protein at the interface at DH values of 20%, 40%, 60%, and 80%, respectively. Up to 60% hydrolysis, these 4 large fragments were dominating the interface. The interaction potentials in this range of hydrolysis (0-60%) showed a similar trend (an energy minimum of around -10 k_BT at longer separation and a steep energy barrier at shorter separation).

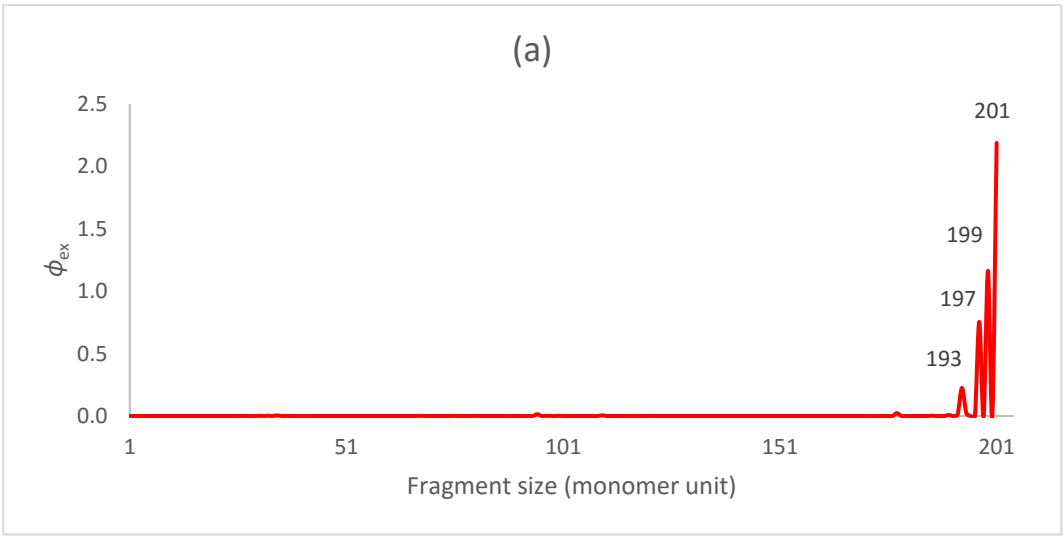
(a)
2.5
2.0
1.5
1.0
0.5
0.0
ϕ_{ex}
201
199
197
193
1
51
101
151
201
Fragment size (monomer unit)

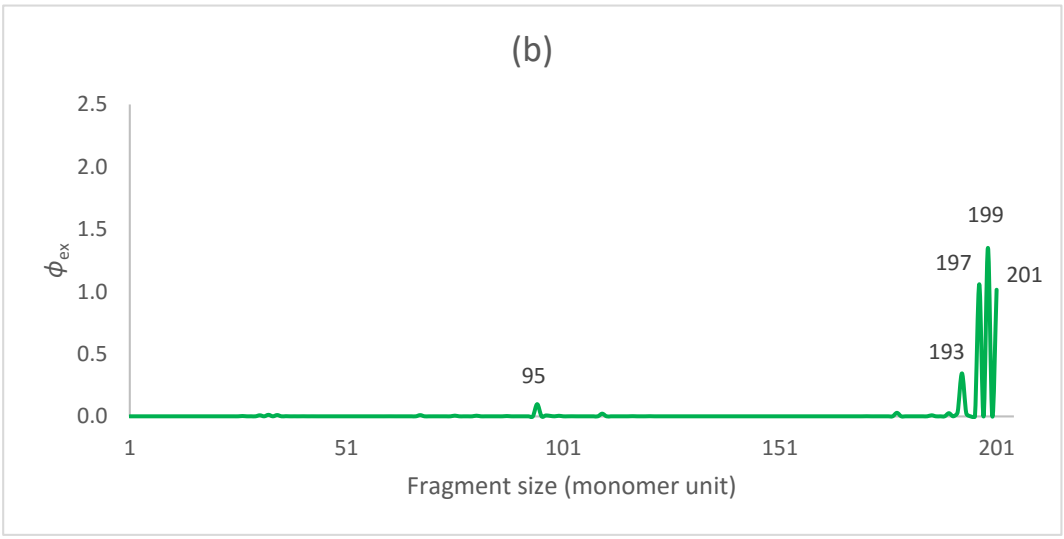
(b)
2.5
2.0
1.5
1.0
0.5
0.0
ϕ_{ex}
199
197
201
193
95
1
51
101
151
201
Fragment size (monomer unit)

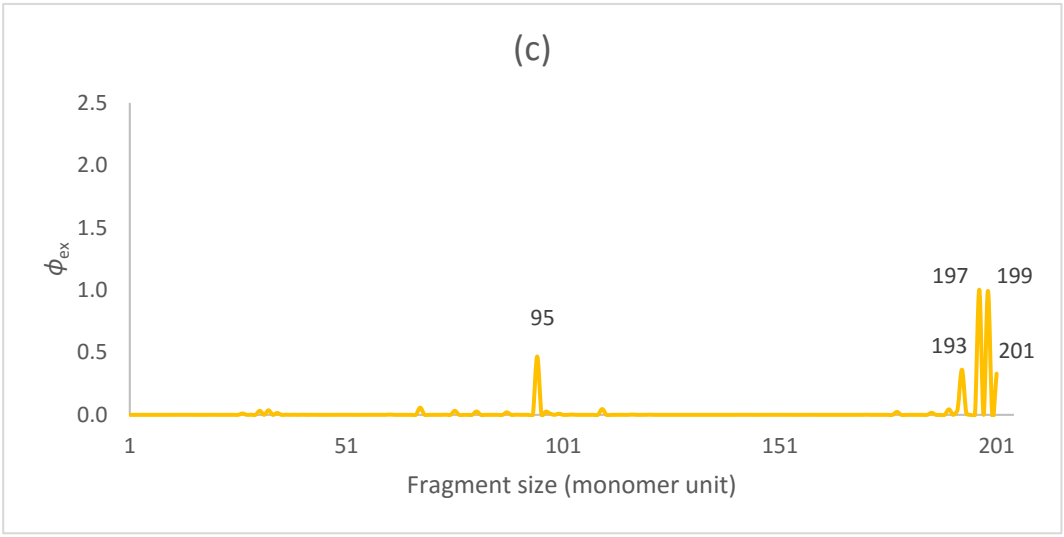
(c)
2.5
2.0
1.5
1.0
0.5
0.0
ϕ_{ex}
197
199
95
193
201
1
51
101
151
201
Fragment size (monomer unit)

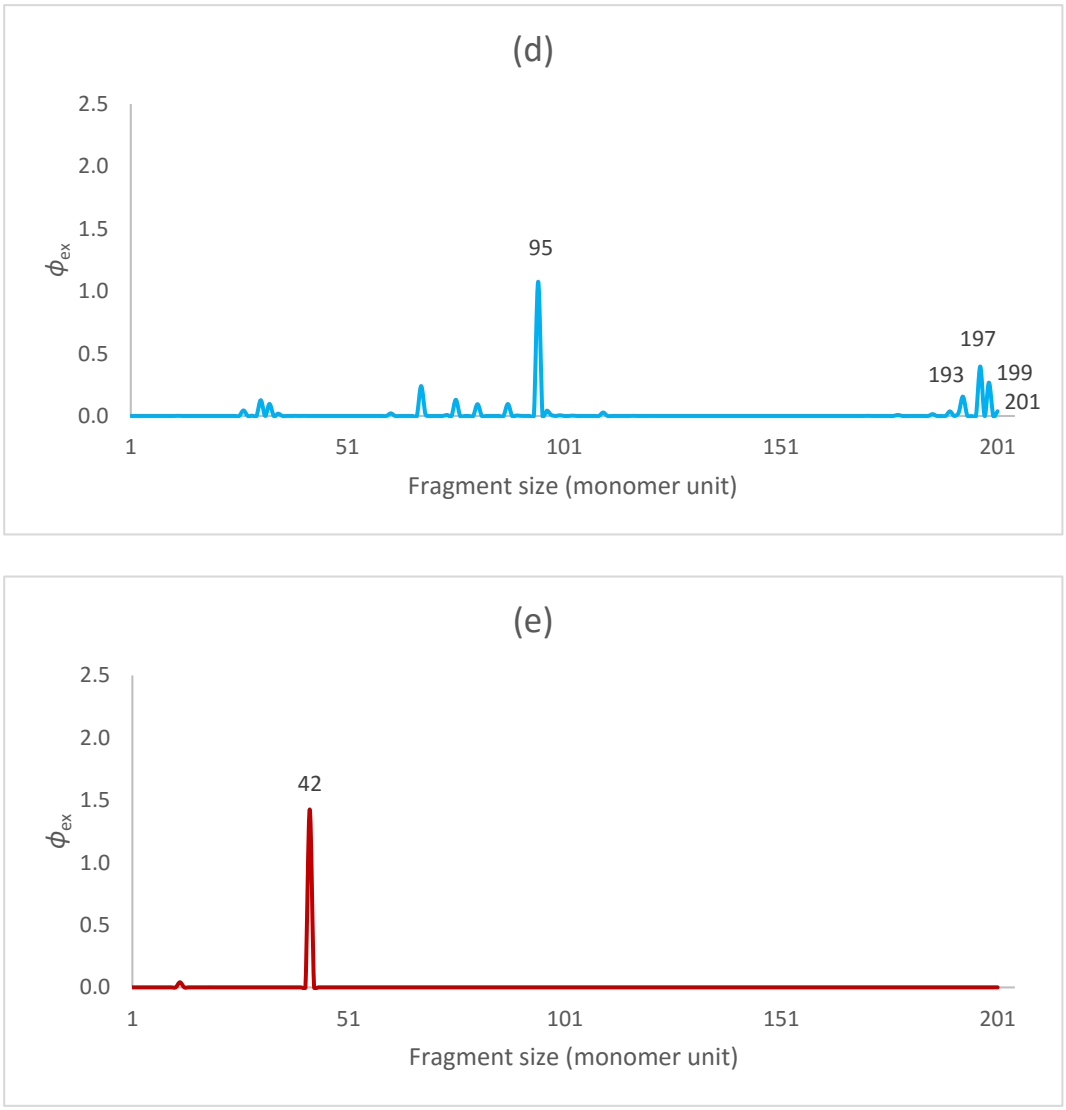

Figure 5.15 The excess volume fractions ($\phi_{ex}(m)$) plotted against the size of the main adsorbed fragment sizes (m) adsorbed at the interfacial region, resulting from the hydrolysis of the α_{s1}-casein at DH 20% (a), 40% (b), 60% (c), 80% (d), and 100% (e), at pH=5.0.

However, at DH 80%, an intermediate size fragment (i.e. size 95) became the more dominant fragment on the surface. That is why we see a different interaction potential graph (Figure 5.11) at DH 80% that has two energy barriers caused firstly by the steric repulsion of the larger fragments at around a separation distance of 4nm and secondly by the intermediate size fragments at a

distance of around 2nm. The larger adsorbed fragments seem to overlap strongly at a separation distance of around 4nm and the droplets start to repel each other due to the steric effect induced by these overlapped fragments. This can be seen in Figure 5.11 as a positive increase in the interaction potential starting at around a distance of 4nm. If the surfaces come closer (to ~2nm) by unlikely thermal fluctuations (Brownian motion), the intermediate fragments start to make bridges which provide an attractive contribution to the mediated interactions (Figure 5.11). This causes the lowering of interaction potential and a minimum at these separation distances. At further approach, even these intermediate fragments will be highly overlapped and eventually they will all provide steric repulsion. At this DH (80%), the energy well was slightly deeper than the one at DH 60% at longer separations. One reason for this is the higher van der Waals attractions at the closer separation distance at DH 80%. From Figure 5.14 it is evident that the thickness of the interfacial adsorbed layer is less at DH=80% compared to DH=60%. Therefore, all the polymer mediated interactions, whether bridging attraction or steric repulsion occur at smaller separation distances, where the van der Walls forces are more significant.

The depth of the energy well was slightly reduced at DH 100% compared to DH 80% because of the lower adsorption of the larger fragments (Table 5.3) and thus their lower bridging effect at DH 100%. The energy well at this DH was formed by the van der Waals attraction which can be seen by comparing Figure 5.11 and Figure 5.12 where in absence of van der Waals forces no detectable energy well is observed. The energy barrier at closer approach was obtained by a combination of the electrostatic and steric repulsive interactions provided by N153-N194 fragment.

m	$\phi_{ex}(m)$, %	jk, %	Φ
DH 20%			
193	0.22, 5.07%	9-201, 100%	4.32E-14
197	0.75, 17.01%	5-201, 100%	3.53E-14
199	1.16, 26.22%	3-201, 100%	2.85E-14
201	2.19, 49.34%	1-201, 100%	1.15E-13
DH 40%			
95	0.10, 2.39%	107-201, ~100% 9-103, ~0%	1.47E-13 7.62E-15
193	0.34, 8.44%	9-201, 100%	6.50E-16
197	1.06, 25.94%	5-201, 100%	3.98E-16
199	1.35, 33.08%	3-201, 100%	2.41E-16
201	1.01, 24.86%	1-201, 100%	3.66E-16
DH 60%			
95	0.47, 12.87%	107-201, ~100% 9-103, ~0%	2.91E-14 4.47E-16
193	0.36, 9.96%	9-201, 100%	9.90E-19
197	1.00, 27.61%	5-201, 100%	4.04E-19
199	0.99, 27.32%	3-201, 100%	1.63E-19
201	0.33, 9.08%	1-201, 100%	1.10E-19
DH 80%			
95	1.08, 35.79%	107-201, ~100% 9-103, ~0%	1.21E-15 1.55E-18
193	0.16, 5.17%	9-201, 100%	1.01E-23
197	0.40, 13.19%	5-201, 100%	2.05E-24
199	0.27, 8.91%	3-201, 100%	4.16E-25
201	0.04, 1.25%	1-201, 100%	1.05E-25
DH 100%			
42	1.43, 97.22%	153-194, 100%	2.09E-12

Table 5.3 The size of the main adsorbed fragments, m (column 1), their excess volume fractions ($\phi_{ex}(m)$) at interfacial region and percentages as a fraction of total excess amount (column 2) attributed to all chains of this size, the parts of α_{s1}-casein that belong to the fragments (jk) corresponding to that size group and their contributions to the adsorbed amount in column 2 is given in column 3 as a percentage function, and the bulk volume fractions (Φ) of the fragments in column 3 (column 4), obtained at DH 20%, 40%, 60%, 80%, and 100%, at pH=5.0.

When the interaction potentials at pH=4.5 (Figure 5.6) and pH=5.0 (Figure 5.11) are compared, it can be seen that the colloidal stabilising ability of the adsorbed α_{s1}-casein fragments seems to be better at pH=5.0. It is obvious that the electrostatic stabilisation contributes more to the stability of emulsion at pH=5.0 compared to pH=4.5 by reducing the bridging effect, as well as providing more direct electrostatic repulsion.

The colloidal stabilising ability of the adsorbed intact α_{s1}-casein at pH=5.0 and 3.0 were found to be similar (Figure 4.5). The depth of the energy wells obtained at both pH values were approximately the same. However, introducing hydrolysing the protein by of 20% provides negative contribution to the energy well at pH=3.0, while it provides a positive contribution at pH=5.0. Figure 5.4b shows that the magnitude of the effective surface potential at pH=3.0 was rapidly reduced at the first level of hydrolysis (DH 20%) whereas the same level of drop was not obtained at pH=5.0 (see Figure 5.14b). The possible reason for this is that the different fragments of the protein were adsorbed at these two pH values. The adsorbed fragments at this pH values can be seen in Figure 5.5 and can be compared to those at pH=5.0 in Figure 5.15. At pH=5.0, the dominant fragments at the surface were the large polymers. However, at pH=3.0, the intermediate size fragments were adsorbed in larger amounts, even at low DH values. The net charges of the intermediate fragments significantly less than the net charge of the intact protein or that of the large fragments. Therefore, the preferential adsorption of the intermediate size fragments at pH=3.0 provided lower electrostatic surface potentials.

The main adsorbed fragments at various DH values were of the size 42, 95, 193, 197, 199, and 201 monomers at pH=5.0, as shown in Figure 5.15. Size 42 was the only fragment size at DH 100%, due to its more hydrophobic nature and larger size among other available fragments. This fragment was the only dominating fragment at DH 100% across all pH values. The total excess volume fraction of this fragment varied depending on the pH-related changes in the net charge.

There were two possible fragments of size 95, namely N107-N201 and N9-N103. N107-N201 was preferentially adsorbed because of its more hydrophobic structure containing more hydrophobic amino acid residues. This fragment became preferentially adsorbed compared to fragments of α_{s1}-casein with larger sizes at DH 80%, where the availability of the larger fragments was significantly reduced in the bulk solution, due to more extensive level of hydrolysis.

Unlike at pH=3.0, the larger fragments at pH=5.0 dominated the surface up to a much high level of hydrolysis, DH 80%. For instance, at DH 20%, the total percentage of the intermediate size fragments (i.e. size 68, 95) was nearly 50% at pH=3.0. However, at pH=5.0, they do not even appear in the graph in Figure 5.15a for the same value of DH. This is because at pH=3.0, the intact and large fragments in the solution were highly charged which as we have mentioned before reduces their ability for adsorption and therefore allows more room at the surface for the adsorption of intermediate size fragments. In contrast, the net charge of the large fragments was quite low at pH=5.0 and the same effect hindering their adsorption was no longer present. Thus, they were preferentially

adsorbed until their abundance become critically low, at higher levels of hydrolysis.

5.4 pH 7.0

In the previous section, the investigation of colloidal stabilising properties of hydrolysed α_{s1}-casein was carried out at pH=5.0, which is slightly away from the isoelectric point of the intact protein. In this section, the same investigation is carried out at an even higher pH=7.0, which is quite far from the isoelectric point. The electrostatic contribution to the stabilisation of emulsion droplets is therefore expected to be stronger than in the previous system.

The interaction potentials between two approaching surfaces both with and without the van der Waals attractions were plotted against the separation distance in Figure 5.16 and Figure 5.17, respectively. The electrostatic interactions (Figure 5.18) and the total volume fractions of α_{s1}-casein fragments (Figure 5.19) were plotted against the distance away from the surface for an isolated interface.

At pH=7.0, the emulsion systems involving α_{s1}-casein fragments obtained at DH values up to 60% were predicted to be stable since the energy wells at this range of hydrolysis were all found to be a few k_BT and therefore can be overcome by Brownian motion of the droplets (Figure 5.16). However, at DH values 80% and 100%, the energy wells were found to be around 10 k_BT. The kinetic energy of the Brownian motion would not be sufficient to break such bonds between the droplets. When Figure 5.16 and Figure 5.17 are compared, it can be seen that the van der Waals attraction pulls down the interaction potentials to around

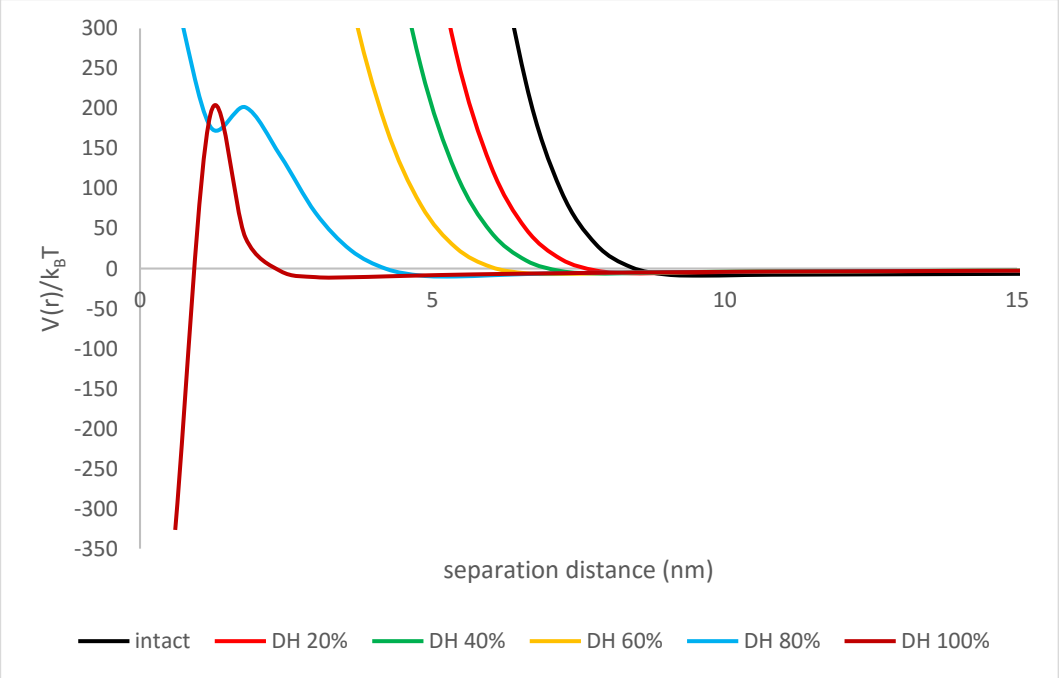

Figure 5.16 The interaction potentials *V*(*r*), between the droplets of size 1μm, induced by the hydrolysed α_{s1}-casein at various DH values at pH=7.0, plotted against the separation distance between the droplets (nm).

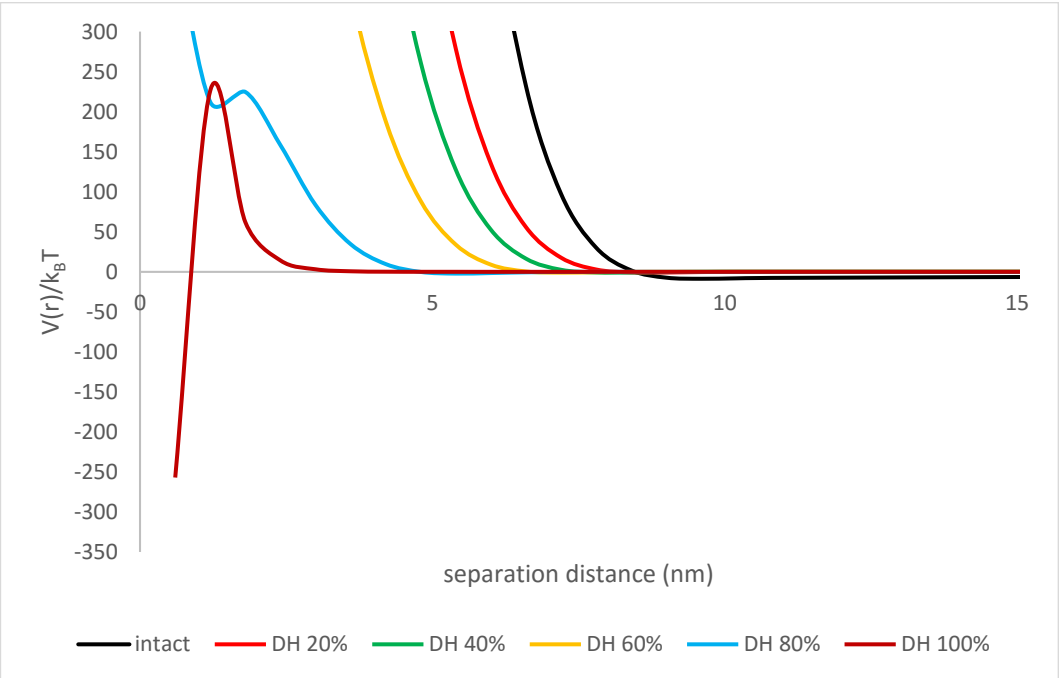

Figure 5.17 The same interaction potentials *V*(*r*) as those in Figure 5.16, but now without the inclusion of the van der Waals attraction.

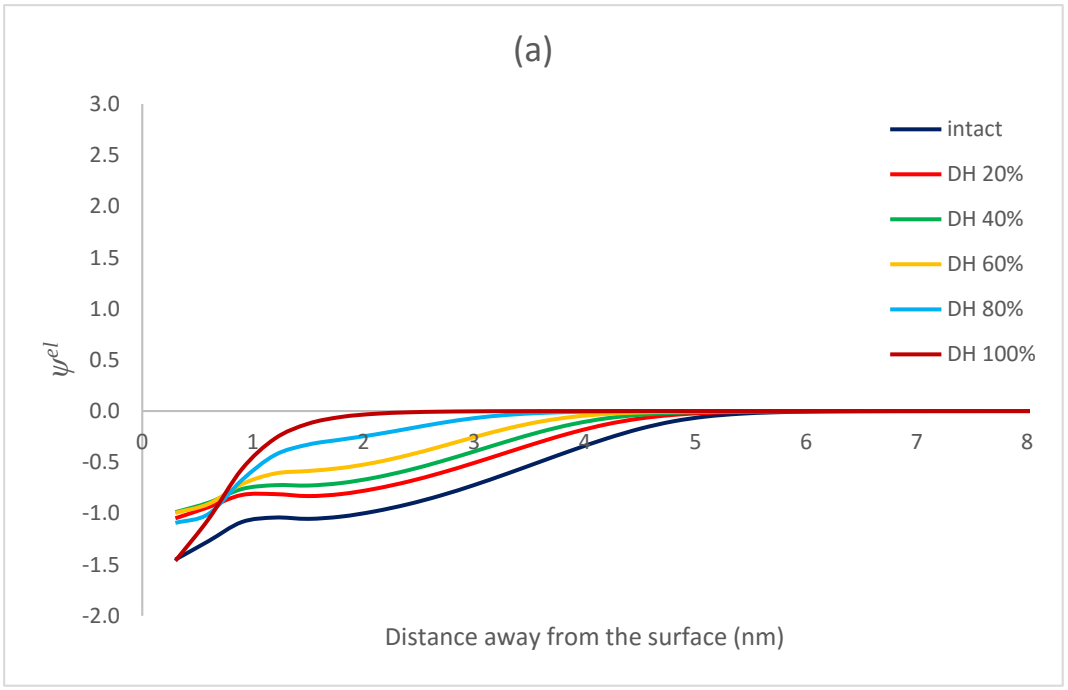

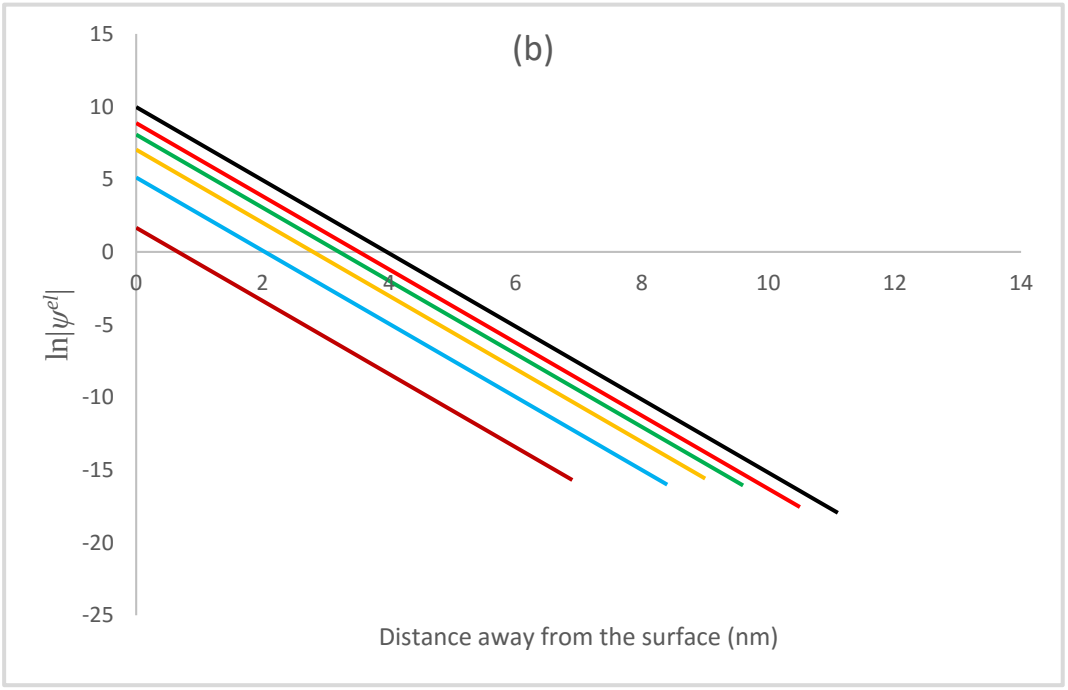

Figure 5.18 The electrostatic potentials $\psi^{el}(k_BT/e)$ (a), $\ln(|e\psi^{el}/k_BT|)$ (b), obtained at various DH values at pH=7.0, plotted against the distance away from the surface (nm). The DH values are the same as corresponding ones in Figure 5.18a.

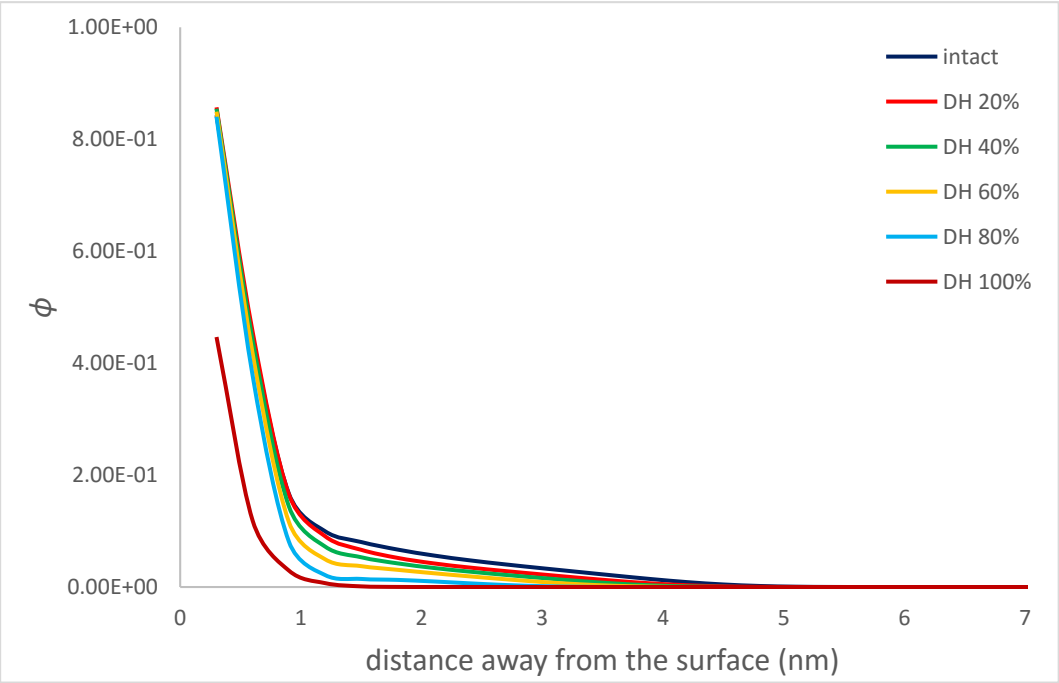

Figure 5.19 The volume fractions of the hydrolysed α_{s1}-casein at various DH values at pH=7.0, plotted against the distance away from an isolated single surface (nm).

-10 k_BT at DH 80% and 100%. This was due to the short ranged nature of steric repulsion and low electrostatic interactions obtained at high DH values. At the lower DH values, the van der Waals effect was not significant, as seen in Figure 5.16 and Figure 5.17. The interaction potential graphs were found to be broadly similar to the ones obtained at pH=5.0. The energy minima at all DH values were less at pH=7.0, compared to pH=5.0. This is expected due to the higher electrostatic interactions at pH=7.0, this being further than the isoelectric point for α_{s1}-casein. The higher electrostatic interaction supresses the formation of bridges and provides a positive repulsive contribution to the overall interactions between two opposite surfaces. The interaction potentials at DH 0%, 20%, 40% and 60% followed the same trend (an energy minimum of a few k_BT at longer separation

and a steep energy barrier at shorter separation) and the energy barriers shifted to closer separation distances with increasing DH (Figure 5.16). The separation distances at which the energy barriers were obtained show where the two adsorbed fragment layers start to overlapped and steric repulsion takes place. In other words, it shows the range of the steric repulsion at each corresponding DH value. Higher levels of hydrolysis reduced the availability of the larger fragments. Therefore, the polymer concentration at longer distances away from the surface, decreases more rapidly at high DH values, as seen in Figure 5.19. The overlapping of the polymers therefore occurs at increasingly closer distances to the surface. That is why the range of steric repulsion was also shifted to smaller distances, as the protein was hydrolysed to a higher degree.

At DH 80%, the availability of the larger fragments in the bulk solution was even lower, as well as the number of adsorbed large chains when compared to low levels of hydrolysis. This can be seen in Figure 5.20 and from Table 5.4, which show the details of the adsorbed polymers. The total percentages of the adsorbed large fragments (of sizes 197, 199, and 201) on the surface at DH 20%, 40%, 60%, and 80% were 78.09% (ϕ_{ex}=2.90), 62.91% (ϕ_{ex}=2.17), 42.82% (ϕ_{ex}=1.35), and 14.39% (ϕ_{ex}=0.39), respectively. These results confirmed that the adsorbed amount of the large fragments is significantly reduced at DH 80%. That is why the steric repulsion at this DH starts to operate at a shorter separation distance (~4nm) when compared to the lower DH values (Figure 5.16). If the surfaces approach each other even more closely and reach a separation of around 1.8nm, then the adsorbed intermediate size fragments on the two surfaces can also start to overlap. As before, initially this causes bridging attraction, but this is followed by a strong steric repulsion as droplets move even

closer to each other. The bridging leads to a sharp reduction in the interaction potentials at that separation distance, clearly seen in Figure 5.16. Whereas the steric repulsion upon closer approach of the surfaces (~1.2nm) leads to a sharper energy barrier when comparable to the one obtained at ~4nm separation distance caused by larger fragments at the same DH (80%) (Figure 5.16).

At DH 100%, 96.96% of the adsorbed fragments consisted of the one made from residues N153-N194, which is the largest fragment in the emulsion system at this DH value. The combination of the electrostatic and steric repulsions created an energy barrier as shown in Figure 5.16. Once this barrier is passed, the small fragments will make small bridges between the two surfaces at very close separation distances. At this point the droplet surfaces will stick to each other with the highly hydrophobic fragments. This manifest itself as sharp decrease in the interaction potentials between the opposite surfaces at separation distances less than 1.2 nm at full level of hydrolysis, i.e. 100% (Figure 5.16). The sharp decrease at the very close separation distances at this DH is not observed for instance at pH=3.0 (Figure 5.1). The droplets do not stick but repel each other due to 44.4% higher volume fraction of polymers in the first layer (the layer adjacent to the surface) and 55.8% more adsorbed fragments in the interfacial area at pH=3.0 (data not presented here). The former reduces the number of bridges that could occur between two approaching surfaces and the latter increases the steric repulsion at such a close separation distance. Both these effects make a positive repulsive contribution to the mediated interactions between the two droplets.

The polymers on the surface were more diverse at this pH value as displayed in Figure 5.20. The intermediate and small size fragments seemed to be more competitive for adsorption at pH=7 compared to pH=5.0. This is because at pH=7.0 there is a higher net charge caused by large polymers. As we mentioned previously higher repulsion between individual polypeptide chains serves to limit the number adsorbed on the interface. Nevertheless, the large polymers are still dominating the surface up to 60% level of hydrolysis.

The intact protein was adsorbed in different amounts at DH of 20% depending on the pH of the system. At this level of hydrolysis there are still a small number of chains that remain intact in the system i.e. have none of their bonds broken by chance. At pH=3.0, no such intact chains adsorb on surface appeared in Figure 5.5a. The intact α_{s1}-casein chains were most competitive at pH=7.0 and pH=5.0 compared to the other pH values. The variations in the adsorbed amounts of the intact protein across different pH values, is related to the net charge of α_{s1}-casein at each pH values. For instance, at pH=3.0, the net charge of the intact protein (~21 e) is much higher than the intermediate size competitor fragments of sizes 68 (~1.7 e) and 95 (~6.1 e) and also relatively high compared to the large size competitor fragments of sizes 178 (~14 e) and 193 (~16 e). This makes the intact protein less favourable for adsorption. However, for instance at pH=5.0, the net charge of the intact protein (~ - 6.4 e) is less than the competitor fragments of sizes 199 (~ - 8.4 e), 197 (~ - 9.4 e), and 193 (~ - 11.4 e) at DH value of 20% (Figure 5.15a). Breaking a few of the positively charged amino acids from the N-terminus end of α_{s1}-casein decreases the net positive charge of the competitor fragments of the intact protein at pH=3.0, but increases the net negative charge of the competitors at pH=5.0. Thus, the adsorption of the intact protein is not

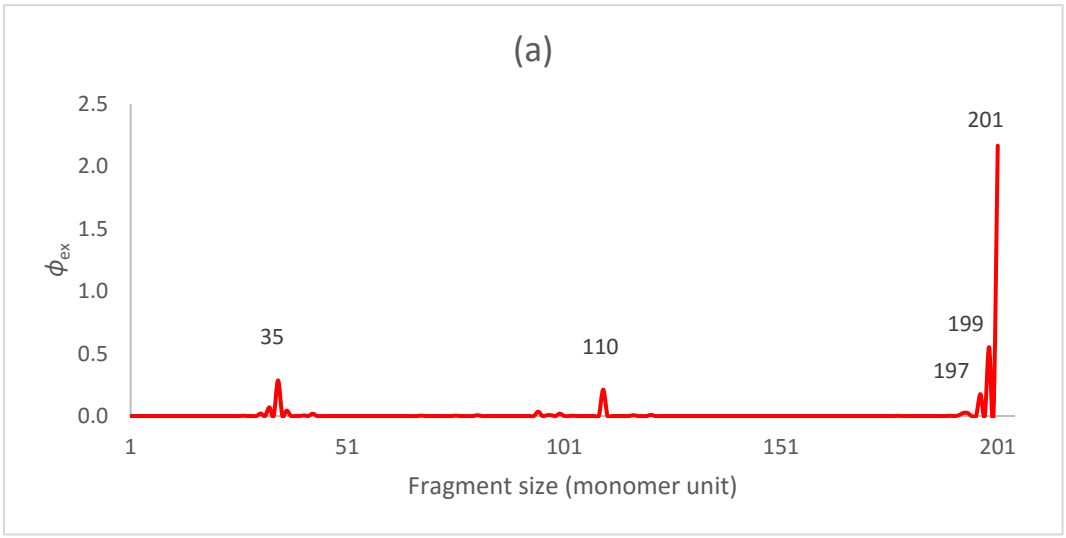
(a)
2.5
2.0
1.5
1.0
0.5
0.0
ϕ_{ex}
35
110
197
199
201
1
51
101
151
201
Fragment size (monomer unit)

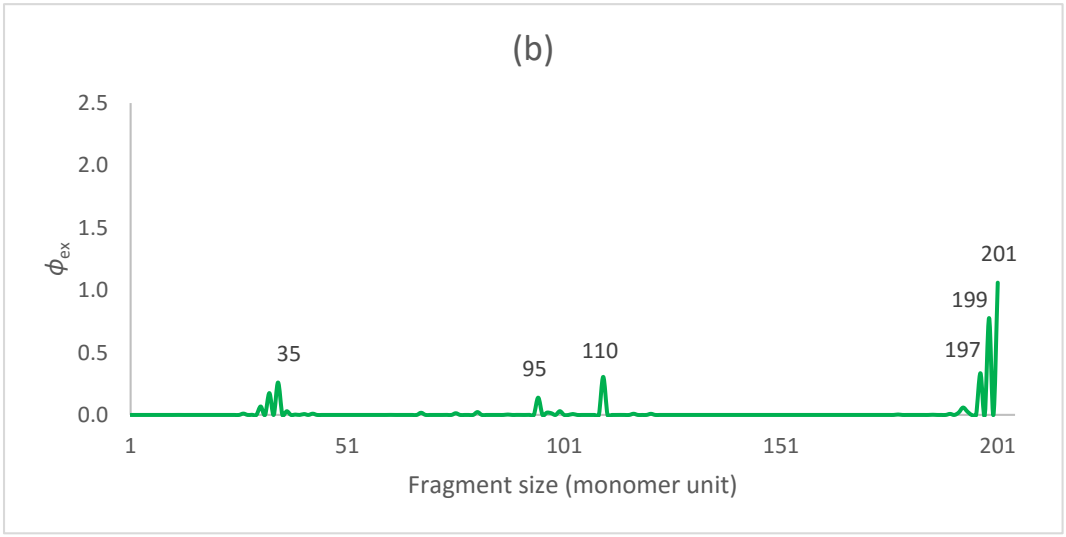
(b)
2.5
2.0
1.5
1.0
0.5
0.0
ϕ_{ex}
35
95
110
197
199
201
1
51
101
151
201
Fragment size (monomer unit)

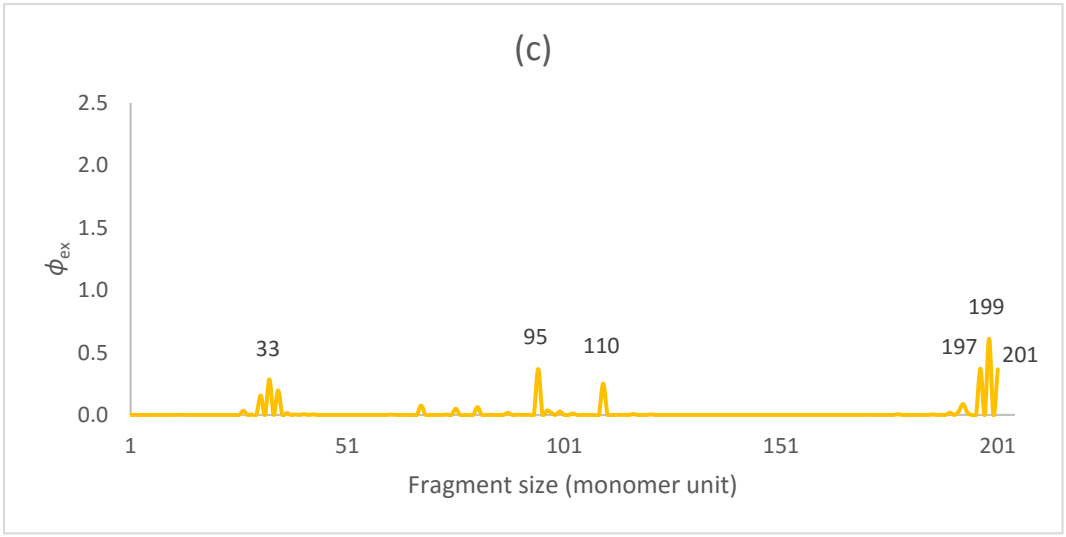
(c)
2.5
2.0
1.5
1.0
0.5
0.0
ϕ_{ex}
33
95
110
197
199
201
1
51
101
151
201
Fragment size (monomer unit)

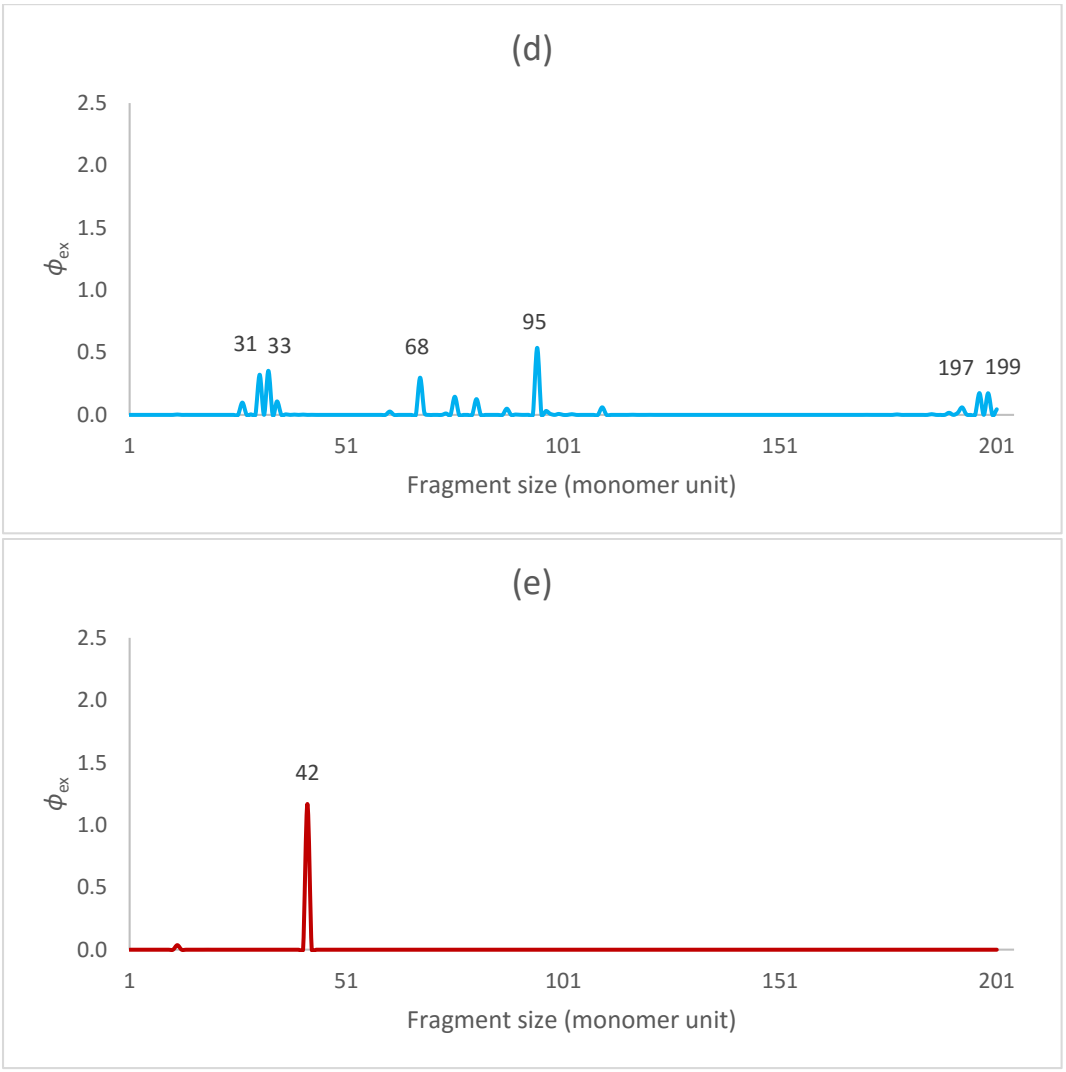

Figure 5.20 The excess volume fractions ($\phi_{ex}(m)$) of fragments of each size (m) at the interfacial region plotted against the size of the adsorbed fragments shown for the dominant fragments on the surface. The fragments are produced during the hydrolysis of the α_{s1}-casein at various levels of hydrolysis, 20% (a), 40% (b), 60% (c), 80% (d), and 100% (e), at pH=7.0.

favourable at pH=3.0 (Figure 5.5a), whereas it was dominantly adsorbed at pH=5.0 (Figure 5.15a).

The fragment with a size of 35 amino acid residues appeared in the charts only at pH=7.0 (at DH values of 20% and 40%). There were 3 possible fragments of size 35 (Table 5.4). The most competitive fragment among fragments of size 35 was

m	$\phi_{ex}(m)$, %	jk, %	Φ
DH 20%			
35	0.29, 7.69%	1-35, 96.21% 3-37, 3.74% 9-43, 0.06%	1.43E-13 2.85E-14 3.57E-14
110	0.21, 5.70%	92-201, 99.96% 85-194, 0.04% 24-133, ~0%	1.47E-13 2.94E-14 1.20E-14
197	0.18, 4.74%	5-201, 100%	3.53E-14
199	0.55, 14.89%	3-201, 100%	2.85E-14
201	2.17, 58.46%	1-201, 100%	1.15E-13
DH 40%			
35	0.26, 7.54%	1-35, 91.69% 3-37, 8.13% 9-43, 0.19%	9.03E-14 3.61E-14 6.02E-14
95	0.14, 4.03%	107-201, ~100% 9-103, ~0%	1.47E-13 7.62E-15
110	0.31, 8.85%	92-201, 99.92% 85-194, 0.08% 24-133, ~0%	2.21E-14 8.82E-15 1.14E-15
197	0.33, 9.70%	5-201, 100%	3.98E-16
199	0.78, 22.50%	3-201, 100%	2.41E-16
201	1.06, 30.71%	1-201, 100%	3.66E-16
DH 60%			
33	0.29, 9.06%	3-35, 95.04% 5-37, 4.96%	3.80E-14 3.80E-14
95	0.37, 11.69%	107-201, ~100% 9-103, ~0%	2.91E-14 4.47E-16

DH 60% cont..			
110	0.25, 7.99%	92-201, 99.88% 85-194, 0.12% 24-133, ~0%	8.61E-16 5.17E-16 1.32E-17
197	0.37, 11.78%	5-201, 100%	4.04E-19
199	0.61, 19.41%	3-201, 100%	1.63E-19
201	0.37, 11.63%	1-201, 100%	1.10E-19
DH 80%			
31	0.32, 11.79%	5-35, 100%	3.94E-14
33	0.35, 12.93%	3-35, 95.51% 5-37, 4.49%	8.42E-15 8.42E-15
68	0.30, 10.92%	134-201, ~100% 85-152, ~0% 36-103, ~0% 24-91, ~0%	1.08E-13 5.54E-18 2.77E-17 1.39E-16
95	0.54, 19.66%	107-201, ~100% 9-103, ~0%	1.21E-15 1.55E-18
197	0.18, 6.39%	5-201, 100%	2.05E-24
199	0.17, 6.36%	3-201, 100%	4.16E-25
201	0.04, 1.64%	1-201, 100%	1.05E-25
DH 100%			
42	1.17, 96.96%	153-194, 100%	2.09E-12

Table 5.4 The size of the main adsorbed fragments, m (column 1), their excess volume fractions ($\phi_{ex}(m)$) at interfacial region and percentages as a fraction of total excess adsorbed amount attributed to all chains of this size (column 2), the set of α_{s1}-casein residues that belong to the fragments (jk) in each corresponding size group and their contributions to the adsorbed amount as a fraction of all chains of that size on the interface (column 3), and the bulk volume fractions (Φ) of each fragments shown in column 3 (column 4). Results are obtained for α_{s1}-casein hydrolysed at DH values 20%, 40%, 60%, 80%, and 100%, at pH=7.0.

N1-N35, which constituted over 90% of the adsorbed amount of protein in this size range at DH values of 20% and 40%. The number of hydrophobic residues are almost the same for the three fragments. However, N1-N35 has a higher net positive charge, compared to the other two fragments. We note that at this pH the charge of the surface is negative. This makes the more positively charged N1-N35 likely to be attracted to the surface more strongly than the other two fragments of the same size of 35.

The SCF model developed in this study provides the advanced details on the adsorbed fragments as have been discussed throughout the chapter. These details go some way in helping to understand and explain the colloidal stabilising and the surface adsorption properties of the polypeptide fragments. Figure 5.21 shows some extra features of a specific fragment which were not presented in any figure or table in the previous sections. The purpose of the figure is simply to present another aspect of our model, which though not studied in detail here can provide additional useful information on behaviour of fragments adsorbed at interfaces. This feature of the model aims to focus on a specific fragment and its conformation at the surface. For this, N107-N201 was chosen as an example, since this fragment always was present at interface at a DH of 60%, at all pH values.

Figure 5.21a provides the volume fractions of the chosen fragment plotted against the distance away from the surface. On the other hand, Figure 5.21b gives the average distance at which each monomer on this fragment residue away from the flat surface at several different pH values. The colour representation of the residues is given in Figure 5.21c, with each colour

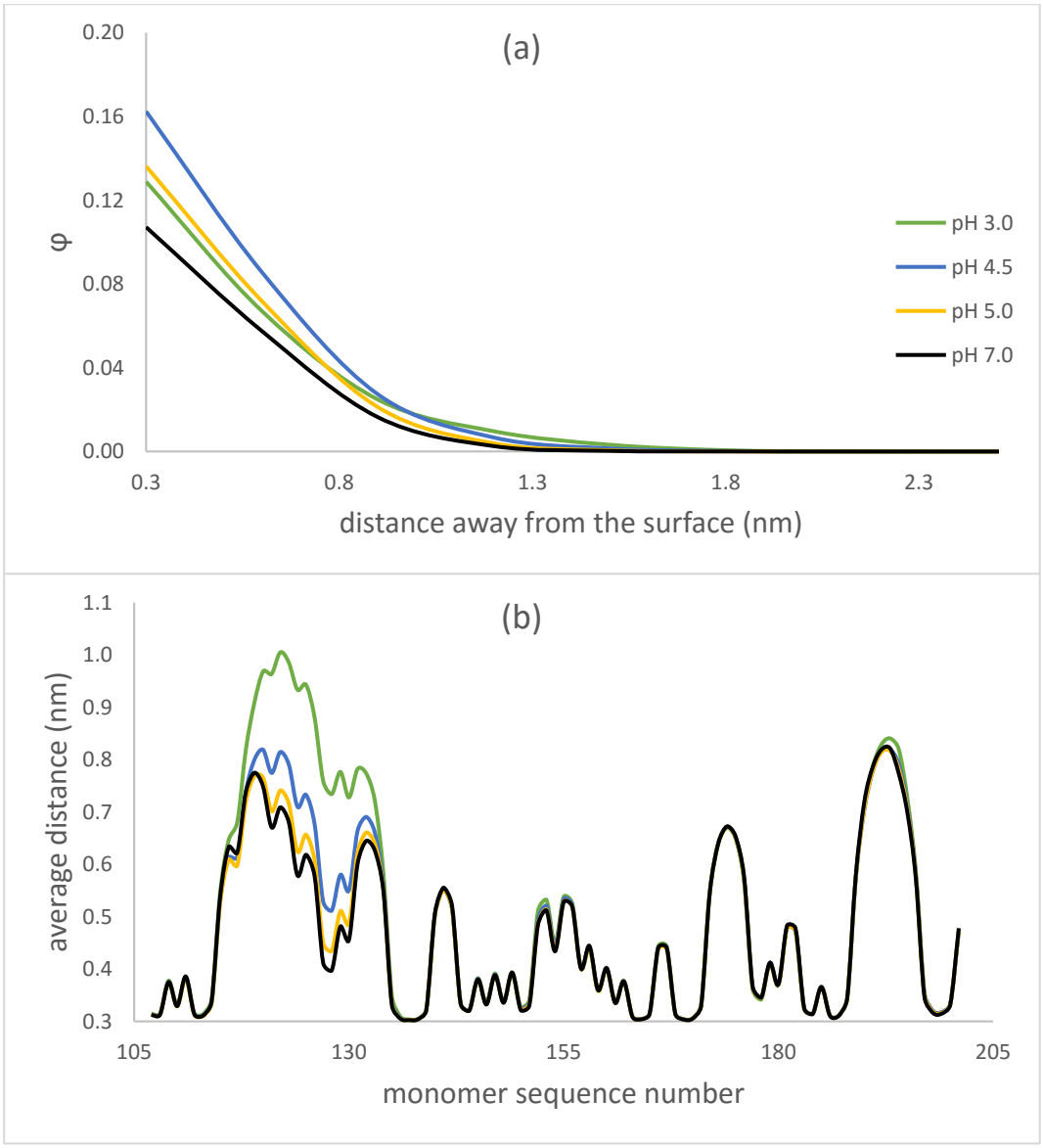

Figure 5.21 (a) The total volume fraction of N107-N201 fragment in the interfacial region, produced by 60% hydrolysis of the intact α_{s1}-casein at various pH values, plotted against the distance away from the surface (nm).(b) Average distance of each monomer of the N107-N201 fragment away from a flat surface (nm) on which the fragment is adsorbed, (c) Representation of N107-N201 primary structure based on the type of monomers as given in Figure 4.1.

representing a monomer type the details of which can be found in Figure 4.1. At pH=3.0, this fragment (N107-N201) protrudes further into the solvent because the net charge of the loop section is at its highest at pH=3.0. The positively charged surface (due to the positive net charge of the most of the adsorbed fragments) at pH=3.0, is less favourable for the loop section of the N107-N201, which also carries a high positive charge at the same pH value. The volume fraction of this fragment in the interfacial area is related to the other available fragments in the system due to the competitive adsorption which was discussed in previous sections.

5.5 Conclusions

Hydrolysed fragments of α_{s1}-casein obtained by the action of enzyme trypsin were considered at DH values of 20%, 40%, 60%, 80%, and 100%. Twenty possible peptide bonds susceptible to attack by this enzyme were broken to obtain a polydisperse system containing polypeptides of different molecular weights and primary amino acid sequence structures. The colloidal stabilising and surface adsorption properties of the resulting polypeptides, as well as the intact protein, were investigated and compared at pH values 3.0, 4.5, 5.0, and 7.0.

At pH 3.0, the hydrolysed protein layers induce shallower energy wells, particularly at high DH (60% and above) compared to the intact protein itself. Nevertheless, this was not enough to maintain the stability of the emulsion. The adsorbed large triblock-like polypeptides destabilise the emulsion at low DH (i.e. up to 40%) where such large fragments are more abundant. This is caused the bridging attraction between the two opposite droplet surfaces. At DH 60%, a

highly hydrophobic fragment (N134-N201) and a triblock-like fragment (N107-N201) were found to be the main adsorbed fragments on the surface. Similarly, hydrophobic fragments N134-N201 and N153-N194 dominated the surface at DH 80% and 100%. The non-ideal structures (i.e. monoblock-like and triblock-like) of the most commonly adsorbed polypeptides, the lower electrostatic interactions, and the ever present van der Waals attractions were the reasons for the instability of the emulsions at DH 60%, 80%, and 100%.

At pH 4.5, hydrolysing α_{s1}-casein up to 60% gradually improves the emulsion stabilising ability of the fragmented protein. However, it was demonstrated that the improvement was not adequate for having a stable emulsion. It was predicted that this improvement was due to the hydrolysis of the large triblock-like polypeptides which are prone to make the bridging repeated connections between two approaching droplets. The large polypeptides were preferentially adsorbed and dominant up to a DH value of 60%. However, at DH of 80%, the majority of the surface was covered with a thin layer of the intermediate size fragments N134-N201 and N107-N201, which are found to be unable to provide sufficient steric stability. Conversely, they also induced bridging attraction, though at smaller separation distances, and cause the aggregation and eventually breakdown of the emulsion.

The fragmentation of α_{s1}-casein at pH=5.0 could not change the colloidal state of the emulsion which was already unstable even with the intact protein. The large polypeptides continued to be dominant on the surface up to a level of hydrolysis of 60%. It was again found that N107-N201 is the major adsorbed fragment on the surface at DH of 80%. Because of its low net charge at this pH value and its

triblock-like structure similar to that of the intact protein, the bridging attraction was unavoidable. On the other hand, the effect of the van der Waals attractions at such a high level of hydrolysis was significant, since thinner adsorbed layers mean that protein mediated forces only became apparent at short separation distances.

At DH values up to 60%, the emulsions involving adsorbed layers of fragmented α_{s1}-casein at pH=7.0 were found to be stable. Although the large triblock-like polypeptides were dominant on the surfaces up to DH 60%, the presence of strong electrostatic interactions at this pH reduced the possible influence of bridging attraction induced by polypeptides. However, at high DH values (80% and 100%), the electrostatic repulsive interactions decreases and consequently the bridging and the van der Waals attractions pull down the energy wells to around -10 $k_B T$, where the Brownian motion of the droplets is no longer able to overcome bonds formed between droplets. At pH=7.0, the adsorbed fragments at various DH values were found to be more diverse compared to the other pH values.

The diblock-like fragments, which are considered the best stabiliser structure, could not be adsorbed adequately due to the preferential adsorption of the triblock-like or highly hydrophobic monoblock-like fragments from the C-terminal side of the α_{s1}-casein. One reason for their preferential adsorption could be their higher surface affinities since the C-terminal side of the protein is highly hydrophobic. Another reason for their preferential adsorption could be their higher availability in the bulk solution. This is because the number of Arg and Lys amino acids are lower on the C-terminus side of the protein which means that this part

of the protein is less likely to be broken. Trypsin breaks the peptide bonds next to these amino acids and in such distribution of Arg and Lys residues, trypsin will create fragments at high level of hydrolysis which do not have large blocks of hydrophobic and hydrophilic residues one may require for good emulsion stabilisers. At low DH values, the large triblock-like peptides (similar to intact α_{s1}-casein itself) are preferentially adsorbed due to their higher availability in the bulk solution and their larger number of hydrophobic residues that have the affinity for the surface.

A better colloidal stability compared to the one provided by the intact α_{s1}-casein could not be achieved by the non-specific breakage of peptide bonds that are targeted by trypsin on the backbone of α_{s1}-casein. This situation is in contrast with that involving very specific breakage of particular bond(s), which was discussed in chapter 4.

Chapter 6 Conclusions

The colloidal stabilising and surface adsorption properties of the hydrolysed macromolecules have been theoretically investigated. The usual Self-Consistent Field (SCF) approach was found not to be capable of modelling such a polydisperse system involving simultaneous presence of a large number of different fragmented polypeptides obtained by the hydrolysis. The failure of the usual approach arises from its high computer memory requirement amongst other limitations to perform the SCF calculations. The memory requirement is high because all the different chains in the system are considered separately and have to be dealt with one by one in the normal approach. Therefore, the usual approach can only model a hydrolysis where the original polymer is broken from say a maximum of about two places. In order to reduce the high memory requirement and make SCF calculations applicable to such highly fragmented chains, we had to introduce composite segment weight functions to replace the usual segment weight functions. The composite segment weight functions consider all the fragments containing a monomer of the original polymer. A new composition law and free energy equation have also been derived based on the new composite segment weight functions as necessary. We also obtain the new set of recursive relations necessary in order to compute these composite segment density functions. A much more efficient computer program was implemented for the SCF calculations based on this new approach and was validated against the more usual approach, for few cases involving a small

number of bond breakages. The separate consideration of different fragments in the usual approach also requires individual data input for the different fragments which becomes unfeasible when the system involves many different fragments. The new computer program does not require such an elaborate and time consuming input data process, as the data input is only required for the intact original polymer. In this study, we also introduced a novel way of calculating the “effective” electrostatic surface potentials. These potentials were calculated to compare the long ranged interactions (the electrostatic component of the interaction potentials between two approaching surfaces) observed at various degrees of hydrolysis and at different pH values.

The SCF_N approach and the novel way of calculating effective surface potentials are the significant methodological contributions of this study, which can be used in the future theoretical investigations of the fragmented macromolecules more generally. In this study, we have also presented the first use of our newly developed methods in the modelling of the colloidal systems involving hydrolysed homopolymers and more importantly proteins.

6.1 Homopolymers

In the homopolymer case, we have investigated the preferential adsorption of hydrolysed homopolymers. The effect of the solution concentration, degree of hydrolysis (DH), the intact size of the original homopolymer (N) and the strength of the affinity (χ) of monomers to the surface on the preferential adsorption of large polymers were explored.

Key findings of this part of the work can be summarised as follows. When the probability of breakage is smaller than 0.5 (p<0.5), the concentration of the remaining intact polymers in the bulk solution upon hydrolysis becomes higher than the large fragments of similar sizes. Although the difference is very small, the effect on the adsorbent profile of the surface is huge, particularly at low p and N values. In such situation, the adsorption of the intact homopolymers is strongly favoured by their slightly greater availability in the solution, compared to the similar size large fragments.

The surface adsorption behaviours of the polymers were found to be dependent on the solution concentration. The level of adsorption of large polymers was higher at low solution concentrations. The polymer size became less significant in the denser solutions, which was explained by the scaling theory of De Gennes (1979) and the fact that the adsorption behaviour is governed by the mesh size, ξ, rather than the radius of gyration of polymers if the latter is larger than the former (De Gennes, 1979).

The adsorption of large polymers was found to be favoured by a higher strength of affinity between the surface and monomers that make up the chains. This was related to the total strength of affinity of chains which becomes even more prominent for longer chains as the affinity for surface per a monomer reside becomes stronger. The effect was found to be very strong and can make larger chains dominate the adsorption despite their very small concentrations in the bulk solution.

The availability of large fragments was significantly reduced in the bulk solution even at relatively low levels of hydrolysis. Their adsorption was found

to be dependent on the balance of their size and their availability. The largest polymer whose availability had not dropped to a critically low level, following hydrolysis, was the most commonly adsorbed fragment on the surface.

6.2 Proteins

The SCF_N approach has also been used to model hydrolysed proteins in this study. For this, α_{s1}-casein was hydrolysed by the enzyme trypsin. The protein was hydrolysed in two different ways, highly selective single particular bond and a more non-selective multiple bond hydrolysis.

6.2.1 Selective Single Bond Hydrolysis

In this type of hydrolysis, one peptide bond was chosen among 20 potential targets of the enzyme for cleavage. In this, we focused on bonds aimed at obtaining a large diblock-like fragment from a triblock-like protein, by breaking such a peptide bond. Two bonds (the 35^{th} and 106^{th} peptide bonds along the α_{s1}-casein backbone) were identified for this purpose.

The key findings of this section of the project were as follows. It was confirmed that the intact α_{s1}-casein displays poor colloidal stabilising properties at high salt concentrations and at pH values near its isoelectric point due to the screening of the electrostatic repulsion or its absence resulting from the loss of surface charge.

Hydrolysing the protein from its 35^{th} peptide bond resulted in a significant improvement in the stability of the emulsion. The improvement was found to be provided by the adsorption of the diblock-like fragment N36-N201 (“N” indicates

monomers are counted from the N-terminus end of the protein) and related to the formation of thicker adsorbed layers around the droplets and a significant reduction in bridging effect, in contrast to that observed for the intact protein case.

Hydrolysing the protein from its 106th peptide bond did not make a similar effect on the stability despite formation of a suitable diblock-like fragment. This was related to the inadequate adsorption of the diblock-like fragment N1-N106. The other fragment produces from the breakage of the bond, N107-N201, also present in the system, was found to be dominantly adsorbed at the surfaces and induced high bridging attraction between the approaching surfaces at the pH value (4.5) close to the isoelectric point of the intact protein.

These results show that hydrolysing the protein from the right place to obtain the right structure is not always sufficient to guarantee better stability. It is also essential to ensure that the right structure is adequately adsorbed and it is not displaced from surface by the less desirable fragment that also result during the hydrolysis process.

6.2.2 Non-Selective Multiple Bond Hydrolysis

In this type of hydrolysis, all the 20 potential peptide bonds suitable to breakage by trypsin were targeted by the enzyme with an equal probability of breakage. The influence of the degree of hydrolysis on the colloidal stabilising properties of the hydrolysate at various pH values was investigated by performing the SCF calculations at DH values 20%, 40%, 60%, 80% and 100%.

The more significant conclusions of this study are summarized below. At pH 3.0, hydrolysing α_{s1}-casein up to 60% gradually decreased the emulsion stabilising ability of the fragmented protein due to the decline in the electrostatic potentials, in line with the result of many reported experiments. However, a better emulsion stabilising ability was observed for the protein hydrolysates obtained by higher levels of hydrolysis compared to the intact protein which so far has not been reported by experiments in the literature. This may well be due to the fact that the improvement was not enough to maintain the stability of the emulsion and for practical purpose any difference in stability would most likely not be detectable. The improvement was attributed to the reduced bridging effect of the large triblock-like fragments. At high levels of hydrolysis, the availability of these fragments in the bulk solution is critically low which does not favour their adsorption.

At a higher pH of 4.5, hydrolysing α_{s1}-casein up to 60% gradually increased the emulsion stabilising ability of the fragmented proteins in contrast to pH 3.0. However, this improvement was insufficient to keep the emulsions stable and once again predicted not to be sufficient to be observed in practical experiments. The improvement was once again related to the decreasing adsorption of large triblock-like fragments which are prone to forming the bridging connections between two approaching surfaces. At higher levels of hydrolysis, the intermediate size fragments were the most commonly adsorbed polypeptides. The intermediate size fragments were also unable to provide a sufficient stability.

At pH 5.0, hydrolysing α_{s1}-casein up to 60% slightly improved the stabilising ability of the protein hydrolysates but did not change the colloidal state of the

emulsion which was already unstable with the intact protein. The higher levels of hydrolysis changed the most commonly adsorbed fragments from the large sized fragments to the intermediate ones. This replacement did not make a considerable difference in the stability of emulsions.

At pH 7.0, the emulsions were already stable with the adsorbed layers of the intact protein. Hydrolysing α_{s1}-casein up to 60% did not change the colloidal state of the emulsions. However, the composition of the adsorbed layers significantly changed at higher levels of hydrolysis and this led to the loss of stability.

At all pH values, the adsorption of the desired diblock-like polypeptides were not favourable. Generally, up to 60% degree of hydrolysis, the intact proteins and the large fragments which have a similar amino acid structures to the intact protein were the dominant polypeptides in the interfacial region. At higher levels of hydrolysis, the availability of these dominant polypeptides in the bulk solution becomes critically low. This makes their adsorption unfavourable. At this point, the desired diblock-like fragments could in principle be adsorbed at the surfaces. However, this did not occur, since the “triblock-like” or the highly hydrophobic “monoblock-like” intermediate size fragments from the C-terminal half of the protein were the ones dominating the surface adsorption. The reason for this could be a combination of their higher surface affinity and greater availability in the bulk solution. The former is governed by a higher number of hydrophobic residues on the backbone of polypeptide fragment, and the latter is related to the smaller number of Arg and Lys residues (i.e. smaller number of peptide bonds to be broken by the action of the enzyme trypsin) on the C-terminal half of the protein.

The non-selective peptide bond hydrolysis in the case of α_{s1}-casein did not provide a practically better colloidal stability compared to the intact α_{s1}-casein at all pH values. However, it was shown that a better colloidal stability can be achieved by a careful selective peptide bond hydrolysis.

6.3 Future Work

We have developed a new SCF approach (SCF_N) for the investigation of colloidal stabilising and surface adsorption properties of polydisperse colloidal systems obtained by hydrolysis of a macromolecule. We have presented the first use of the new approach for 1) homopolymers and 2) proteins. In the case of proteins, α_{s1}-casein was assumed to be hydrolysed with trypsin and the resulting fragments were modelled. The new approach can be used in modelling of many different protein-enzyme combinations. For instance, investigation of the emulsion stabilising properties of vegetable protein fragments would be of the greater commercial interest to the food industry, as vegetable proteins are cheaper protein sources. The appropriate protein-enzyme combination is a key factor to achieve superior emulsion stabilising properties. For this, the resulting fragments, upon hydrolysis of a protein, should have large hydrophobic and hydrophilic blocks. On the other hand, these ideal fragments should be adequately adsorbed to the surfaces in preference to other fragments also generated during hydrolysis. This depends on the competitiveness of the other non-ideal fragments present in the system. It is of course easier to obtain such ideal fragments that are sufficiently adsorbed at the interfaces by very selective cleavage of particular peptide bonds, compared to the non-selective hydrolysis. However, the former is not practically feasible at present without chemical

means, as we mentioned in chapter 4. The latter method requires one to choose very precisely the correct protein-enzyme combination.

It is difficult to manually evaluate a protein-enzyme combination to see the possibility of achieving the desired fragments. A simple computer software would be very helpful for this purpose as a first line of screening the most potentially useful cases. The software can look for the patterns (i.e. amino acid sequence) of a substrate on the amino acid sequence of a protein and it can list the breakage points (required for the SCF calculations) as well as the possible fragments with a coloured representation showing the hydrophobic and hydrophilic blocks. The software can also provide the relative availability (i.e. volume fractions) of the fragments in the bulk solution according to the provided degree of hydrolysis which is important for their preferential adsorption. Then one can easily evaluate such protein-enzyme combination to choose it for a detailed theoretical investigation by our SCF calculations, as described in this work.

The SCF_N approach developed in this study allows one to model a polydisperse system obtained by hydrolysis of a single macromolecule. The new approach can be developed further to handle situations involving multiple intact polymers at the start of hydrolysis. Polydisperse systems can then be obtained by the hydrolysis of all or some of these polymers. In addition, one can form a polydisperse system by defining a number of different polymers which are not subject to hydrolysis. For instance, a polydisperse system involving a hydrolysed protein and a non-hydrolysed polysaccharide can be modelled once the new approach is extended.

Finally we mention that breakage of bonds also occurs during high shear treatment of polymer solutions (Nilsson et al., 2006). This non-energetic cleavage

of bonds can also produce a solution consisting of intact polymers and their various fragments. The work here should also be of significant in studying of surface adsorption properties of such shear-threated polymer solutions.

Appendix I

7.1 Proof by Induction for the Second Term of Eq. 2.51

$$\sum_{j=1}^{k} \frac{p(j-1)p(k)}{1-p(k)} \prod_{l=j}^{k} 1-p(l) = p(k) \tag{7.1}$$

Assume the above equation is true for k. Here is the proof that it is also true for k+1.

$$\sum_{j=1}^{k+1} \frac{p(j-1)p(k+1)}{1-p(k+1)} \prod_{l=j}^{k+1} 1-p(l)$$

$$= \sum_{j=k+1}^{k+1} \frac{p(j-1)p(k+1)}{1-p(k+1)} \prod_{l=j}^{k+1} 1-p(l) + \sum_{j=1}^{k} \frac{p(j-1)p(k+1)}{1-p(k+1)} \prod_{l=j}^{k+1} 1-p(l)$$

$$= \frac{p(k+1)}{1-p(k+1)} \left\{ p(k) \prod_{l=k+1}^{k+1} 1-p(l) + \sum_{j=1}^{k} p(j-1) \prod_{l=j}^{k+1} 1-p(l) \right\}$$

$$= p(k)p(k+1) + \frac{p(k+1)}{1-p(k+1)} \frac{1-p(k)}{p(k)} \sum_{j=1}^{k} \frac{p(k)p(j-1)}{1-p(k)} \prod_{l=j}^{k} [1-p(l)]\,[1-p(k+1)]$$

$$= p(k)p(k+1) + \frac{p(k+1)[1-p(k)]}{p(k)} p(k)$$

$$= p(k)p(k+1) + [1-p(k)]p(k+1)$$

$$= p(k+1)$$

7.2

We have assumed that Eq. 7.1 is true. This can be proved for k=1 as follows:

$$\sum_{j=1}^{1} \frac{p(0)p(1)}{1-p(1)} \prod_{l=j}^{1} 1-p(l) = \frac{p(0)p(1)}{1-p(1)}[1-p(1)] = p(0)p(1)$$

7.3

The probability of breakage for bond 0 is equal to 1 ($p(0) = 1$) since it is already broken for intact chain. So

$$p(0)p(1) = p(1)$$

7.4

List of References

ADLER-NISSEN, J. 1984. Control of the proteolytic reaction and of the level of bitterness in protein hydrolysis processes. *Journal of Chemical Technology and Biotechnology. Biotechnology,* 34**,** 215-222.

ADLER-NISSEN, J. & OLSEN, H. S. 1979. The influence of peptide chain length on taste and functional properties of enzymatically modified soy protein. *Functionality and protein structure.* American Chemical Society.

AKHTAR, M. & DICKINSON, E. 2007. Whey protein–maltodextrin conjugates as emulsifying agents: An alternative to gum arabic. *Food Hydrocolloids,* 21**,** 607-616.

AKINSHINA, A., ETTELAIE, R., DICKINSON, E. & SMYTH, G. 2008. Interactions between adsorbed layers of αs1-casein with covalently bound side chains: A self-consistent field study. *Biomacromolecules,* 9**,** 3188-3200.

ARAI, S., NOGUCHI, M., KUROSAWA, S., KATO, H. & FUJIMAKI, M. 1970. Applying proteolytic enzymes on soybean. 6. Deodorization effect of aspergillopeptidase A and debittering effect of aspergillus acid carboxypeptidase. *Journal of Food Science,* 35**,** 392-395.

ATKINS, P. 2002. *Physical chemistry,* Oxford, Oxford University Press.

ATKINSON, P. J., DICKINSON, E., HORNE, D. S. & RICHARDSON, R. M. 1995. Neutron reflectivity of adsorbed protein films. *Proteins at Interfaces II,* 602**,** 311-320.

BERGMANN, M., FRUTON, J. S. & POLLOK, H. 1939. The specificity of trypsin. *Journal of Biological Chemistry,* 127**,** 643-648.

BOUCHIER, P. J., FITZGERALD, R. J. & O'CUINN, G. 1999. Hydrolysis of αs1- and β-casein-derived peptides with a broad specificity aminopeptidase and proline specific aminopeptidases from Lactococcus lactis subsp. cremoris AM2. *FEBS Letters,* 445**,** 321-324.

BRODERICK, E., LYONS, H., PEMBROKE, T., BYRNE, H., MURRAY, B. & HALL, M. 2006. The characterisation of a novel, covalently modified, amphiphilic alginate derivative, which retains gelling and non-toxic properties. *Journal of Colloid and Interface Science,* 298**,** 154-161.

CAESSENS, P. W. J. R., GRUPPEN, H., SLANGEN, C. J., VISSER, S. & VORAGEN, A. G. J. 1999. Functionality of β-casein peptides: Importance

of amphipathicity for emulsion-stabilizing properties. *Journal of Agricultural and Food Chemistry,* 47**,** 1856-1862.

CHALAMAIAH, M., RAO, G. N., RAO, D. G. & JYOTHIRMAYI, T. 2010. Protein hydrolysates from meriga (Cirrhinus mrigala) egg and evaluation of their functional properties. *Food Chemistry,* 120**,** 652-657.

CHOBERT, J. M., BRIAND, L., GUÉGUEN, J., POPINEAU, Y., LARRÉ, C. & HAERTLÉ, T. 1996. Recent advances in enzymatic modifications of food proteins for improving their functional properties. *Food / Nahrung,* 40**,** 177-182.

COSGROVE, T. 2010. *Colloid science: principles, methods and applications*, John Wiley & Sons.

DAVIS, J. P., DOUCET, D. & FOEGEDING, E. A. 2005. Foaming and interfacial properties of hydrolyzed β-lactoglobulin. *Journal of Colloid and Interface Science,* 288**,** 412-422.

DE GENNES, P. G. 1979. *Scaling concepts in polymer physics*, Cornell university press.

DELEU, M., RAZAFINDRALAMBO, H., POPINEAU, Y., JACQUES, P., THONART, P. & PAQUOT, M. 1999. Interfacial and emulsifying properties of lipopeptides from Bacillus subtilis. *Colloids and Surfaces A: Physicochemical and Engineering Aspects,* 152**,** 3-10.

DICKINSON, E. 1992. *An introduction to food colloids*, Oxford University Press.

DICKINSON, E. 2005. *Food colloids: Interactions, microstructure and processing*, Royal Society of Chemistry.

DICKINSON, E. 2008. Interfacial structure and stability of food emulsions as affected by protein-polysaccharide interactions. *Soft Matter,* 4**,** 932-942.

DICKINSON, E. 2015. Colloids in food: Ingredients, structure, and stability. *Annual Review of Food Science and Technology,* 6**,** 211-233.

DICKINSON, E. & GALAZKA, V. B. 1991. Emulsion stabilization by ionic and covalent complexes of β-lactoglobulin with polysaccharides. *Food Hydrocolloids,* 5**,** 281-296.

DICKINSON, E., HORNE, D. S., PHIPPS, J. S. & RICHARDSON, R. M. 1993. A neutron reflectivity study of the adsorption of .beta.-casein at fluid interfaces. *Langmuir,* 9**,** 242-248.

DICKINSON, E., HORNE, D. S., PINFIELD, V. J. & LEERMAKERS, F. A. M. 1997a. Self-consistent-field modelling of casein adsorption - Comparison of results for alpha(s1)-casein and beta-casein. *Journal of the Chemical Society-Faraday Transactions,* 93**,** 425-432.

DICKINSON, E., J. PINFIELD, V., S. HORNE, D. & A. M. LEERMAKERS, F. 1997b. Self-consistent-field modelling of adsorbed casein Interaction between two protein-coated surfaces. *Journal of the Chemical Society, Faraday Transactions,* 93**,** 1785-1790.

DICKINSON, E. & SEMENOVA, M. G. 1992. Emulsifying properties of covalent protein—dextran hybrids. *Colloids and Surfaces,* 64**,** 299-310.

DICKINSON, E. & STAINSBY, G. 1982. *Colloids in food*, Applied Science Publishers.

DOLAN, A. K. & EDWARDS, S. F. 1975. The effect of excluded volume on polymer dispersant action. *Proceedings of the Royal Society of London A: Mathematical, Physical and Engineering Sciences,* 343**,** 427-442.

DREWNOWSKI, A. 1997. Taste preferences and food intake. *Annual review of nutrition,* 17**,** 237-253.

DREWNOWSKI, A. 2001. The science and complexity of bitter taste. *Nutrition Reviews,* 59**,** 163-169.

ETTELAIE, R. & AKINSHINA, A. 2014a. Colloidal interactions induced by overlap of mixed protein + polysaccharide interfacial layers. *Food Hydrocolloids,* 42, Part 1**,** 106-117.

ETTELAIE, R. & AKINSHINA, A. 2014b. Colloidal interactions induced by overlap of mixed protein plus polysaccharide interfacial layers. *Food Hydrocolloids,* 42**,** 106-117.

ETTELAIE, R., AKINSHINA, A. & DICKINSON, E. 2008a. Mixed protein-polysaccharide interfacial layers: a self consistent field calculation study. *Faraday Discussions,* 139**,** 161-178.

ETTELAIE, R., AKINSHINA, A. & DICKINSON, E. 2008b. Mixed protein–polysaccharide interfacial layers: a self consistent field calculation study. *Faraday Discussions,* 139**,** 161-178.

ETTELAIE, R., AKINSHINA, A. & MAURER, S. 2012. Mixed protein-polysaccharide interfacial layers: effect of polysaccharide charge distribution. *Soft Matter,* 8**,** 7582-7597.

ETTELAIE, R., DICKINSON, E. & MURRAY, B. S. 2005. Self-consistent-field studies of mediated steric interactions in mixed protein plus polysaccharide solutions. *In:* DICKINSON, E. (ed.) *Food Colloids: Interactions, Microstructure and Processing.*

ETTELAIE, R., KHANDELWAL, N. & WILKINSON, R. 2014a. Interactions between casein layers adsorbed on hydrophobic surfaces from self consistent field theory: κ-casein versus para-κ-casein. *Food Hydrocolloids,* 34**,** 236-246.

ETTELAIE, R. & LISHCHUK, S. V. 2015. Detachment force of particles from fluid droplets. *Soft matter,* 11**,** 4251-4265.

ETTELAIE, R., MURRAY, B. S. & JAMES, E. L. 2003. Steric interactions mediated by multiblock polymers and biopolymers: role of block size and addition of hydrophilic side chains. *Colloids and Surfaces B: Biointerfaces,* 31**,** 195-206.

ETTELAIE, R., ZENGIN, A. & LEE, H. 2014b. Fragmented proteins as food emulsion stabilisers: A theoretical study. *Biopolymers***,** n/a-n/a.

EUSTON, S. R. 2014. Molecular simulation of adsorption of hydrophobin HFBI to the air–water, DPPC–water and decane–water interfaces. *Food Hydrocolloids,* 42, Part 1**,** 66-74.

EVERS, O. A., SCHEUTJENS, J. M. H. M. & FLEER, G. J. 1990a. Statistical thermodynamics of block copolymer adsorption. 1. Formulation of the model and results for the adsorbed layer structure. *Macromolecules,* 23**,** 5221-5233.

EVERS, O. A., SCHEUTJENS, J. M. H. M. & FLEER, G. J. 1990b. Statistical thermodynamics of block copolymer adsorption. 2. Effect of chain composition on the adsorbed amount and layer thickness. *Journal of the Chemical Society, Faraday Transactions,* 86**,** 1333-1340.

EVERS, O. A., SCHEUTJENS, J. M. H. M. & FLEER, G. J. 1991. Statistical thermodynamics of block copolymer adsorption. 3. Interaction between adsorbed layers of block copolymers. *Macromolecules,* 24**,** 5558-5566.

FANG, Y. & DALGLEISH, D. G. 1993. Dimensions of the adsorbed layers in oil-in-water emulsions stabilized by caseins. *Journal of Colloid and Interface Science,* 156**,** 329-334.

FANUN, M. 2010. *Colloids in biotechnology*, CRC Press.

FELTER, R. E., MOYER, E. S. & RAY, L. N. 1969. Gel permeation chromatography applied to polymer adsorption studies. *Journal of Polymer Science Part B: Polymer Letters,* 7**,** 529-533.

FELTER, R. E. & RAY JR, L. N. 1970. Polymer adsorption studies at the solid-liquid interface using gel permeation chromatography: I. Molecular weight distribution along the adsorption isotherm. *Journal of Colloid and Interface Science,* 32**,** 349-360.

FLEER, G. J., COHEN STUART, M. A., SCHEUTJENS, J. M. H. M., COSGROVE, T. & VINCENT, B. 1993. *Polymers at interfaces,* London, Chapman & Hall.

FLORY, P. J. 1953. *Principles of polymer chemistry*, Cornell University Press.

FURUSAWA, K. & YAMAMOTO, K. 1983. Adsorption of monodisperse polystyrene onto porous glass. *Journal of Colloid and Interface Science,* 96**,** 268-274.

FURUSAWA, K., YAMASHITA, K. & KONNO, K. 1982. Adsorption of monodisperse polystyrene onto porous glass. I. preference adsorption and displacement of high-molecular-weight species. *Journal of Colloid and Interface Science,* 86**,** 35-42.

GENIN, G. 1958. Casein as a stabilizer for latex paint. *Lait,* 38**,** 276-283.

GILL, I., LOPEZFANDINO, R., JORBA, X. & VULFSON, E. N. 1996. Biologically active peptides and enzymatic approaches to their production. *Enzyme and Microbial Technology,* 18**,** 162-183.

GRIGOROVICH, N. V., MOISEENKO, D. V., ANTIPOVA, A. S., ANOKHINA, M. S., BELYAKOVA, L. E., POLIKARPOV, Y. N., KORICA, N., SEMENOVA, M. G. & BARANOV, B. A. 2012. Structural and thermodynamic features of covalent conjugates of sodium caseinate with maltodextrins underlying their functionality. *Food & Function,* 3**,** 283-289.

GROSBERG, A. & KHOKHLOV, A. 1994. *Statistical physics of macromolecules*, AIP Press; New York.

GUZEY, D. & MCCLEMENTS, D. J. 2006. Formation, stability and properties of multilayer emulsions for application in the food industry. *Advances in Colloid and Interface Science,* 128–130**,** 227-248.

GUZEY, D. & MCCLEMENTS, D. J. 2007. Impact of electrostatic interactions on formation and stability of emulsions containing oil droplets coated by β-lactoglobulin−pectin complexes. *Journal of Agricultural and Food Chemistry,* 55**,** 475-485.

HARNSILAWAT, T., PONGSAWATMANIT, R. & MCCLEMENTS, D. J. 2006a. Characterization of β-lactoglobulin–sodium alginate interactions in aqueous solutions: A calorimetry, light scattering, electrophoretic mobility and solubility study. *Food Hydrocolloids,* 20**,** 577-585.

HARNSILAWAT, T., PONGSAWATMANIT, R. & MCCLEMENTS, D. J. 2006b. Influence of pH and ionic strength on formation and stability of emulsions containing oil droplets coated by β-lactoglobulin−alginate interfaces. *Biomacromolecules,* 7**,** 2052-2058.

HEINIO, R. L., NORDLUND, E., POUTANEN, K. & BUCHERT, J. 2012. Use of enzymes to elucidate the factors contributing to bitterness in rye flavour. *Food Research International,* 45**,** 31-38.

HEMAR, Y., CHENG, L., OLIVER, C., SANGUANSRI, L. & AUGUSTIN, M. 2010. Encapsulation of resveratrol using water-in-oil-in-water double emulsions. *Food Biophysics,* 5**,** 120-127.

HIRAI, H. & YAKURA, N. 2001. Protecting polymers in suspension of metal nanoparticles. *Polymers for Advanced Technologies,* 12**,** 724-733.

HLADY, V., LYKLEMA, J. & FLEER, G. J. 1982. Effect of polydispersity on the adsorption of dextran on silver iodide. *Journal of Colloid and Interface Science,* 87**,** 395-406.

HOFMANN, K. & BERGMANN, M. 1939. The specificity of trypsin II. *Journal of Biological Chemistry,* 130**,** 81-86.

HOWARD, G. J. & WOODS, S. J. 1972. Adsorption of polymers at the solution-solid interface. VIII. Competitive effects in the adsorption of polystyrenes on silica. *Journal of Polymer Science Part A-2: Polymer Physics,* 10**,** 1023-1028.

HUANG, X., KAKUDA, Y. & CUI, W. 2001. Hydrocolloids in emulsions: particle size distribution and interfacial activity. *Food Hydrocolloids,* 15**,** 533-542.

HUNTER, R. J. 2001. *Foundations of colloid science*, Oxford University Press.

INAGAMI, T. & MITSUDA, H. 1964. The mechanism of the specificity of trypsin catalysis. *Journal of Biological Chemistry,* 239**,** 1388-1394.

ISHIBASHI, N., ONO, I., KATO, K., SHIGENAGA, T., SHINODA, I., OKAI, H. & FUKUI, S. 1988. Role of the hydrophobic amino acid residue in the bitterness of peptides (Food & Nutrition). *Agricultural and Biological Chemistry,* 52**,** 91-94.

JANARDHAN, R., GEDAM, P. H. & SAMPATHKUMARAN, P. S. 1990. The effect of polymer molecular weight in the adsorption process. *Journal of Colloid and Interface Science,* 140**,** 391-400.

JOST, R., MONTI, J., C., BAECHLER, R. & FUMEAUX, D. 1982. Emulgateurs peptidiques obtenus par l'hydrolyse enzymatique partielle de la protéine sérique du lait. *Lait,* 62**,** 521-530.

JUVEKAR, V. A., ANOOP, C. V., PATTANAYEK, S. K. & NAIK, V. M. 1999. A continuum model for polymer adsorption at the solid−liquid interface. *Macromolecules,* 32**,** 863-873.

KATO, A., SASAKI, Y., FURUTA, R. & KOBAYASHI, K. 1990. Functional protein–polysaccharide conjugate prepared by controlled dry-heating of ovalbumin–dextran mixtures. *Agricultural and Biological Chemistry,* 54**,** 107-112.

KODERA, T., ASANO, M. & NIO, N. 2006. Characteristic property of low bitterness in protein hydrolysates by a novel soybean protease D3. *Journal of Food Science,* 71**,** S609-S614.

LEE, S. W., SHIMIZU, M., KAMINOGAWA, S. & YAMAUCHI, K. 1987. Emulsifying properties of peptides obtained from the hydrolyzates of β-

casein (Food & Nutrition). *Agricultural and Biological Chemistry,* 51**,** 161-166.

LEERMAKERS, F. A. M., ATKINSON, P. J., DICKINSON, E. & HORNE, D. S. 1996. Self-consistent-field modeling of adsorbed beta-casein: Effects of pH and ionic strength on surface coverage and density profile. *Journal of Colloid and Interface Science,* 178**,** 681-693.

LEERMAKERS, F. A. M., SCHEUTJENS, J. M. H. M. & LYKLLEMA, J. 1983. On the statistical thermodynamics of membrane formation. *Biophysical Chemistry,* 18**,** 353-360.

LEMIEUX, L. & SIMARD, R. E. 1991. Bitter flavour in dairy products .1. A review of the factors likely to influence its development, mainly in cheese manifacture. *Lait,* 71**,** 599-636.

LIFSHITZ, I., GROSBERG, A. Y. & KHOKHLOV, A. 1978. Some problems of the statistical physics of polymer chains with volume interaction. *Reviews of Modern Physics,* 50**,** 683.

LIM, J. K., MAJETICH, S. A. & TILTON, R. D. 2009. Stabilization of superparamagnetic iron oxide core− gold shell nanoparticles in high ionic strength media. *Langmuir,* 25**,** 13384-13393.

LINDEN, C. V. & LEEMPUT, R. V. 1978. Adsorption studies of polystyrene on silica I. Polydisperse adsorbate. *Journal of Colloid and Interface Science,* 67**,** 63-69.

LINDEN, C. V. & VAN LEEMPUT, R. 1978. Adsorption studies of polystyrene on silica I. Monodisperse adsorbate. *Journal of Colloid and Interface Science,* 67**,** 48-62.

MATOBA, T. & HATA, T. 1972. Relationship between bitterness of peptides and their chemical structures. *Agricultural and Biological Chemistry,* 36**,** 1423-1431.

MCCLEMENTS, D. J. 2006. Non-covalent interactions between proteins and polysaccharides. *Biotechnology Advances,* 24**,** 621-625.

MCCLEMENTS, D. J. 2010. Design of nano-laminated coatings to control bioavailability of lipophilic food components. *Journal of Food Science,* 75**,** R30-R42.

MILNER, S. T. & WITTEN, T. A. 1992. Bridging attraction by telechelic polymers. *Macromolecules,* 25**,** 5495-5503.

MOORE, D. S. 1985. Amino acid and peptide net charges: A simple calculational procedure. *Biochemical Education,* 13**,** 10-11.

MORÉ, J. J., SORENSEN, D. C., HILLSTROM, K. E. & GARBOW, B. S. 1984. The minpack project. *Sources and Development of Mathematical Software***,** 88-111.

MURRAY, B. S., DURGA, K., DE GROOT, P. W. N., KAKOULLI, A. & STOYANOV, S. D. 2011. Preparation and characterization of the foam-stabilizing properties of cellulose–ethyl cellulose complexes for use in foods. *Journal of Agricultural and Food Chemistry,* 59**,** 13277-13288.

NADEN, B. J., KESSELL, L. M., LUCKHAM, P. F. & TADROS, T. F. 2015. Adsorption of poly(hydroxystearic acid) to TiO2 nanoparticles, studied using gel permeation chromatography. *Colloids and Surfaces A: Physicochemical and Engineering Aspects,* 478**,** 36-44.

NAPPER, D. H. 1983. *Polymeric stabilization of colloidal dispersions*, Academic Pr.

NILSSON, B. L., SOELLNER, M. B. & RAINES, R. T. 2005. Chemical synthesis of proteins. *Annu Rev Biophys Biomol Struct,* 34**,** 91-118.

NILSSON, L., LEEMAN, M., WAHLUND, K.-G. & BERGENSTÅHL, B. 2006. Mechanical degradation and changes in conformation of hydrophobically modified starch. *Biomacromolecules,* 7**,** 2671-2679.

NORTON, J. E. & NORTON, I. T. 2010. Designer colloids-towards healthy everyday foods? *Soft Matter,* 6**,** 3735-3742.

OGAWA, S., DECKER, E. A. & MCCLEMENTS, D. J. 2003. Production and characterization of O/W emulsions containing cationic droplets stabilized by lecithin−chitosan membranes. *Journal of Agricultural and Food Chemistry,* 51**,** 2806-2812.

OH, J. K., DRUMRIGHT, R., SIEGWART, D. J. & MATYJASZEWSKI, K. 2008. The development of microgels/nanogels for drug delivery applications. *Progress in Polymer Science,* 33**,** 448-477.

OLSEN, J. V., ONG, S.-E. & MANN, M. 2004. Trypsin cleaves exclusively C-terminal to arginine and lysine residues. *Molecular & Cellular Proteomics,* 3**,** 608-614.

PARKINSON, E. L., ETTELAIE, R. & DICKINSON, E. 2005. Using self-consistent-field theory to understand enhanced steric stabilization by casein-like copolymers at low surface coverage in mixed protein layers. *Biomacromolecules,* 6**,** 3018-3029.

PATTANAYEK, S. K. & JUVEKAR, V. A. 2003. Adsorption of polymer from solution to solid surface: effect of polydispersity. *Macromolecules,* 36**,** 956-960.

PERONA, J. J., HEDSTROM, L., RUTTER, W. J. & FLETTERICK, R. J. 1995. Structural origins of substrate discrimination in trypsin and chymotrypsin. *Biochemistry,* 34**,** 1489-1499.

POLTICELLI, F., HONIG, B., ASCENZI, P. & BOLOGNESI, M. 1999. Structural determinants of trypsin affinity and specificity for cationic inhibitors. *Protein Science,* 8**,** 2621-2629.

POWELL, M. J. D. 1964. An efficient method for finding the minimum of a function of several variables without calculating derivatives. *The Computer Journal,* 7**,** 155-162.

QI, M., HETTIARACHCHY, N. S. & KALAPATHY, U. 1997. Solubility and emulsifying properties of soy protein isolates modified by pancreatin. *Journal of Food Science,* 62**,** 1110-1115.

RAKSAKULTHAI, R. & HAARD, N. F. 2003. Exopeptidases and their application to reduce bitterness in food: A review. *Critical Reviews in Food Science and Nutrition,* 43**,** 401-445.

RAMMILE, E., ANNA, A. & ERIC, D. 2009. A theoretical self-consistent field study of mixed interfacial biopolymer films. *Micro/Nanoencapsulation of Active Food Ingredients.* American Chemical Society.

RHYU, M. R. & KIM, E. Y. 2011. Umami taste characteristics of water extract of Doenjang, a Korean soybean paste: Low-molecular acidic peptides may be a possible clue to the taste. *Food Chemistry,* 127**,** 1210-1215.

ROE, R. J. 1980. Selective adsorption of polymers from solution. *In:* LEE, L.-H. (ed.) *Adhesion and Adsorption of Polymers.*

ROEFS, S. P. F. M., SCHEUTJENS, J. M. H. M. & LEERMAKERS, F. A. M. 1994. Adsorption theory for polydisperse polymers. *Macromolecules,* 27**,** 4810-4816.

ROUDOT-ALGARON, F. 1996. The taste of amino acids, peptides and proteins: Examples of tasty peptides in casein hydrolysates. *Lait,* 76**,** 313-348.

SAHA, B. C. & HAYASHI, K. 2001. Debittering of protein hydrolyzates. *Biotechnology Advances,* 19**,** 355-370.

SÁNCHEZ-VIOQUE, R., BAGGER, C. L., LARRÉ, C. & GUÉGUEN, J. 2004. Emulsifying properties of acylated rapeseed (Brassica napus L.) peptides. *Journal of Colloid and Interface Science,* 271**,** 220-226.

SÁNCHEZ-VIOQUE, R., BAGGER, C. L., RABILLER, C. & GUÉGUEN, J. 2001. Foaming properties of acylated rapeseed (Brassica napus L.) hydrolysates. *Journal of Colloid and Interface Science,* 244**,** 386-393.

SCHEUTJENS, J., FLEER, G. & TADROS, T. F. 1982. The effect of polymers on dispersion properties. Academic Press, London.

SCHEUTJENS, J. M. H. M. & FLEER, G. J. 1979. Statistical theory of the adsorption of interacting chain molecules. 1. Partition function, segment density distribution, and adsorption isotherms. *The Journal of Physical Chemistry,* 83**,** 1619-1635.

SEMENOVA, M. G., BELYAKOVA, L. E., POLIKARPOV, Y. N., ANTIPOVA, A. S. & DICKINSON, E. 2009. Light scattering study of sodium caseinate +

dextran sulfate in aqueous solution: Relationship to emulsion stability. *Food Hydrocolloids,* 23**,** 629-639.

SHIMIZU, M., LEE, S. W., KAMINOGAWA, S. & YAMAUCHI, K. 1986. Functional properties of a peptide of 23 residues purified from the peptic hydrolyzate of as1-casein: Changes in the emulsifying activity during purification of the peptide. *Journal of Food Science,* 51**,** 1248-1252.

SIKORA, E., KALICKA, D., OGONOWSKI, J. & GREGA, T. 2007. Ocena możliwoci zastosowania serwatki z mleka krowiego jako surowca w recepturowaniu szamponów do włosów. *Towaroznawcze Problemy Jakości***,** 54-63.

SMITH, S., CHEN, J. & DUGAS, A. 2001. Water-based bottle labeling adhesive. Google Patents.

SOLMS, J. 1969. Taste of amino acids, peptides, and proteins. *Journal of Agricultural and Food Chemistry,* 17**,** 686-688.

STUART, M. A. C., SCHEUTJENS, J. M. H. M. & FLEER, G. J. 1980. Polydispersity effects and the interpretation of polymer adsorption isotherms. *Journal of Polymer Science: Polymer Physics Edition,* 18**,** 559-573.

SUN, X. D. 2011. Enzymatic hydrolysis of soy proteins and the hydrolysates utilisation. *International Journal of Food Science and Technology,* 46**,** 2447-2459.

SWAISGOOD, H. 1992. Chemistry of the caseins. *Advanced dairy chemistry-1: Proteins.***,** 63-110.

TADROS, T. 2013. Flory-Huggins interaction parameter. *In:* TADROS, T. (ed.) *Encyclopedia of Colloid and Interface Science.* Berlin, Heidelberg: Springer Berlin Heidelberg.

TIMOTHY, M. O. & PETER, C. G. 1999. Polymer adsorption: Fundamentals. *Principles of polymer science and technology in cosmetics and personal care.* CRC Press.

TURGEON, S. L., GAUTHIER, S. F., MOLLE, D. & LEONIL, J. 1992. Interfacial properties of tryptic peptides of .beta.-lactoglobulin. *Journal of Agricultural and Food Chemistry,* 40**,** 669-675.

TURGEON, S. L., GAUTHIER, S. F. & PAQUIN, P. 1991. Interfacial and emulsifying properties of whey peptide fractions obtained with a two-step ultrafiltration process. *Journal of Agricultural and Food Chemistry,* 39**,** 673-676.

UMETSU, H. & ICHISHIMA, E. 1988. Mechanism of digestion of bitter peptides from soybean protein by wheat carboxypeptidase. *Journal of the Japanese Society for Food Science and Technology,* 35.

YUSOFF, A. & MURRAY, B. S. 2011. Modified starch granules as particle-stabilizers of oil-in-water emulsions. *Food Hydrocolloids,* 25**,** 42-55.

Source Codes for the Programs

```
c The main FORTRAN program that runs the SCF calculations
c  written by Adem Zengin

      PROGRAM MAIN
      CHARACTER str
      integer neq,maxeq
      parameter(maxeq=3000)
      INTEGER J,MAXFEV,ML,MU,MODE,NPRINT,INFO,NFEV,LDFJAC,LR,NWRITE
      DOUBLE PRECISION XTOL,EPSFCN,FACTOR,FNORM

      DOUBLE PRECISION X(maxeq),FVEC(maxeq),DIAG(maxeq),
     * FJAC(maxeq,maxeq),R(maxeq*(maxeq+1)/2),QTF(maxeq),
     * WA1(maxeq),WA2(maxeq),WA3(maxeq),WA4(maxeq)
      DOUBLE PRECISION ENORM,DPMPAR
      double precision X1,X2,X3,crossT,totPolBulk
      parameter (X1=1.0d0/6.0d0,X2=4.0d0/6.0d0,X3=1.0d0/6.0d0)

      INTEGER L,Z,Nmax,typee,nn,ii,i,t,tt,k,s,h
      INTEGER MaxType,numMol,MaxMol,nBreak,rL
      parameter (Nmax=1000,MaxType=10,Lmax=500,MaxMol=20)
      INTEGER mapp(Nmax+1),N(MaxMol),totN,breP(0:Nmax)
      double precision QpM(MaxMol),nTypeBulk(0:MaxType+1)
      double precision pb(0:Nmax+2),Esurf(Lmax+1,0:MaxType+1)
      double precision E(Lmax+1,0:MaxType+1),q(0:MaxType+1)
      double precision ExtEp(0:MaxType+1,0:MaxType+1),total6
      double precision kesitP(Nmax+1,Nmax+1),Qf(Nmax+1, 0:Lmax+2)
      double precision QpType(-1:Lmax+5,0:MaxType+1),total5
      double precision ExcessP(0:MaxMol),ExcessS,ExcessI
      double precision totalAB,totalHC,total1,total2,total3
      double precision eN,kB,Temp,LatS,eps,eps0,ElecFac,elF,elL
      double precision Qelec(Lmax+1),molBulks(0:MaxMol+1)
      double precision total4,total,freeE,F2,totalExc
      double precision Qmol(Lmax,0:MaxMol+1),tot1,tot2
      double precision Qrp(Nmax+2,Lmax+2),averDist(Nmax+2)
      double precision bela0,bela1,bela,arabela,bela2
      double precision vProb,Cons(MaxMol,Lmax),pH,iElec
      EXTERNAL FCN

      common /GroupA/ Qrp,ExtEp,kesitP,Esurf,Qf,QpType,Qmol,
     &                nTypeBulk,molBulks,QpM,pb,q,totalHC,
     &                ElecFac,elF,elL,mapp,numMol,totN,N,Z,typee


      eN                = -1.6d-19

      kB                = 1.38d-23

      Temp              = 298.0

c      beta             = 1/(kB*Temp)

      LatS              = 3.0d-10

      eps               = 78.5
```

```
      eps0              = 8.85d-12

      ElecFac           = eN**2/(kB*Temp*eps*eps0*LatS)
c Opening files
c      open (8,file="Qt.txt")
      open (9,file="input.txt")
      open (10,file="map.txt")
      open (16,file='map.out')
      open (19,file='free.out')

c      open (11,file="Qrs.txt")
c      rewind (8)
      rewind (9)
      rewind (10)
c Input parameters
      read(9,*)typee
      read(9,*)numMol
      read(9,*)rL
      read(9,*)L
      read(9,*)elF
      read(9,*)elL
      read(9,*)nBreak
      read(9,*)bela1
      close(9)

c RRR Read the structure of all the polymers/arms and ions
      h=0
      do k=1,numMol
       N(k)=0
       read (10,*) nn,t

        do while (nn.gt.0)

           do s=N(k)+1,N(k)+nn
             h=h+1
             mapp(h)=t
             write(16,*)mapp(h)
           end do
           N(k)=N(k)+nn
           read (10,*) nn,t
         end do
      end do
      close(16)
      Print *, "N:",N(1)
      Print *, "No of Breaks:",nBreak

c Read the molecule Bulks
      totPolBulk=0.0d0
      totN=h
      open (15,file='molBulks.in')
      do t=1,numMol
         read(15,*)molBulks(t)
         QpM(t)=molBulks(t)/N(t)
         totPolBulk=totPolBulk+molBulks(t)
      end do
      close(15)
c     for Solvent
      molBulks(0)=1.0d0-totPolBulk

c     Bulk Volume Frations of Monomers of type t
      nTypeBulk(0)=molBulks(0)
```

```
      k=0
      do t=1,numMol
        do nn=1,N(t)
           k=k+1
           nTypeBulk(mapp(k))=nTypeBulk(mapp(k))+QpM(t)
        end do
      end do

c Read the ExtEp
      open (12,file='ExtEp.in')
         ExtEp(0,0)=0.0d0
      do t=1,typee-1
         ExtEp(t,t)=0.0d0
         do tt=0,t-1
            read(12,*)ExtEp(t,tt)
            ExtEp(tt,t)=ExtEp(t,tt)
c            Print *,t,",",tt," ",ExtEp(t,tt),"-",0.3d0
         end do
      end do
      close(12)
c Read the charges
      open (14,file='charge.in')
      do t=0,typee
         if(t.eq.0)then
            read(14,*)pH
            print *,"pH:",pH
         else
            read(14,*)q(t-1)
         end if
      end do
      close(14)

c assigning probabilities

      pb(0)=1.0d0
      pb(N(1))=1.0d0

      do nn=1,N(1)-1
        pb(nn)=0.0d0
      end do

c      pb(158)=1.0d0
c Read the charges
      if(nBreak.gt.0)then
        open (17,file='prob.in')
        do t=1,nBreak
           read(17,*)breP(t),vProb
           pb(breP(t))=vProb
           PRINT *, "p",breP(t),":",pb(breP(t))
        end do
        close(17)
      end if

c   Total probability for every number of monomers

         do nn=1,N(1)
            kesitP(nn,1)=pb(nn-1)
         end do

         do nn=1,N(1)
            if (pb(nn-1).eq.0.0d0)then
```

```
                do ii=2,N(1)
                   kesitP(nn,ii)=0.0d0
                end do
             end if
             h=0

             if (pb(nn-1).ne.0.0d0)then
                do h=2,N(1)
                   if ((h+1).le.(N(1)+1))then
c                       h+nn olmali. us2f.java ya bak.
                      kesitP(nn,h)=kesitP(nn,h-1)*(1-pb(nn+h-2))
                   end if
                end do
             end if
          end do
       DATA NWRITE /6/
       INFO=1
c       bela=0.000001d0

       arabela=bela1
       bela2=1.0d0
       Z=rL
       do while ((INFO.eq.1).AND.(Z.lt.L))
 22          if(z.eq.68)then
               z=118
             end if
          Z=Z+2
          do nn=1, typee*Z/2
c            X(nn)=-dlog(bela)
             X(nn)=bela0
          end do
          bela0=1.0d0
          arabela=1.0d0
          bela2=50.0d0

          print *,"================Z",Z,"=================="

c Read the Esurf

       open (11,file='Esurf.in')
       do t=0,typee-1
          read(11,*)Esurf(1,t),Esurf(Z,t)
          do i=2,Z-1
             Esurf(i,t)=0.0d0
          end do
       end do
       close(11)
       go to 99

 33    if(bela2.lt.1.0d-15)then
          arabela=arabela*700.0d0
          bela2=arabela
       end if

       bela2=bela2/10.0d0
       bela=-dlog(bela2)
       do nn=1, typee*Z/2
          X(nn)=bela
       end do
       go to 99
 55    bela0=bela0/10.0d0
```

```
            if(bela.lt.1.0d-30)then
               print *,"===============Z",Z,"X================"
               go to 22
            end if
          do nn=1, typee*Z/2
              X(nn)=bela0
          end do
          go to 99

   99     neq=(typee+1)*Z/2

          DO 10 J = Z/2, neq, Z/2

   10       CONTINUE

          LDFJAC = neq
          LR = neq*(neq+1)/2
C
C     SET XTOL TO THE SQUARE ROOT OF THE MACHINE PRECISION.
C     UNLESS HIGH PRECISION SOLUTIONS ARE REQUIRED,
C     THIS IS THE RECOMMENDED SETTING.
C
c      XTOL = DSQRT(DPMPAR(1))
       XTOL = 1.0d-7
C
          MAXFEV = 15000
          ML = neq-1
          MU = neq-1
          EPSFCN = 0.0D0
          MODE = 2
          DO 20 J = 1, neq
             DIAG(J) = 0.01d0
   20        CONTINUE
c       FACTOR = 1.D2
          FACTOR = 0.1d0
          NPRINT = 10
          CALL FCN(neq,X,FVEC,0)

           CALL HYBRD(FCN,neq,X,FVEC,XTOL,MAXFEV,ML,MU,EPSFCN,DIAG,
     *           MODE,FACTOR,NPRINT,INFO,NFEV,FJAC,LDFJAC,
     *           R,LR,QTF,WA1,WA2,WA3,WA4)

          if (INFO.ne.1)then
              print *,"INFO:",INFO
              if (arabela.gt.700.0d10)then
c                 print *,"gecis",bela0
                 go to 55
              end if
              go to 33
          end if

c ////////////Free Energy/////////////

c Write the E
          tt=0
          do t=0,typee
             ii=Z
             do i=1,Z/2
                tt=tt+1
                E(i,t)=X(tt)
                E(ii,t)=X(tt)
```

```
            ii=ii-1
         end do
       end do

c    Calculation of extTotal
       totalAB=0.0d0
       do ii=1,Z
         do t=0,typee-1
            do tt=0,typee-1
               totalAB=
     &         (QpType(ii,t)*(X1*QpType(ii-1,tt)+X2*QpType(ii,tt)
     &         +X3*QpType(ii+1,tt)))
               totalAB=totalAB-nTypeBulk(t)*nTypeBulk(tt)
               crossT=crossT+0.5d0*ExtEp(t,tt)*totalAB
            end do
         end do

       end do

       total=0.0d0

       do k=0,numMol
         ExcessP(k)=0.0d0
       end do

       do i=1,Z
         do k=1,N(1)
            total=total+((pb(k)*Qf(k,i))-pb(k-1))
         end do

         do t=2,numMol
           ExcessP(t)=ExcessP(t)+Qmol(i,t)-molBulks(t)
         end do
         ExcessP(0)=ExcessP(0)+Qmol(i,0)-molBulks(0)
       end do


       ExcessP(1)=QpM(1)*total

       totalExc=0.0d0
       do t=0,numMol
         totalExc=totalExc+ExcessP(t)
       end do


       total1=0.0d0
       do t=0,typee-1
          do i=1,Z
             total1=total1+(E(i,t)*QpType(i,t))
          end do
       end do

       total4=0.0d0
       do t=0,typee-1
             QpType(0,t)=0.0d0
             QpType(Z+1,t)=0.0d0
             QpType(-1,t)=0.0d0
             QpType(Z+2,t)=0.0d0

            do tt=0,typee-1
               total4=total4+(nTypeBulk(t)*nTypeBulk(tt)*ExtEp(t,tt))
```

```
            end do

          end do

          total2=0.0d0
          total3=0.0d0
          do ii=0,Z+1
            do t=0,typee-1
               do tt=0,typee-1
                  total2=
     &            (QpType(ii,t)-nTypeBulk(t))*((X1*QpType(ii-1,tt)
     &            +X2*QpType(ii,tt)+X3*QpType(ii+1,tt))-nTypeBulk(tt))
                  total3=total3+0.5d0*total2*ExtEp(t,tt)
               end do
            end do

          end do
          total5=0.0d0
          do t=0,typee-1

             total5=total5+Esurf(1,t)*(QpType(1,t)+QpType(Z,t))

          end do

          total6=0.0d0
          do ii =1,Z
           Qelec(ii) = 0.0d0
          enddo

          do ii=1,Z
            do tt=0,typee-1
               Qelec(ii)=Qelec(ii)+q(tt)*QpType(ii,tt)

            end do

          end do

          do ii=1,Z
             iElec=0.5d0*E(ii,typee)*Qelec(ii)
             total6=total6+iElec
          end do

          F2=0.0d0
          F2=-totalExc-total1+total3-total4+total5+total6
          write (19,*)Z,"    ",F2
           end do
           close(19)

           WRITE (NWRITE,1000) NFEV,INFO

          Print *,"============================================================"

     1000 FORMAT (5X,31H NUMBER OF FUNCTION EVALUATIONS,I10 //
     *         5X,15H EXIT PARAMETER,16X,I10 //
     *         5X,27H FINAL APPROXIMATE SOLUTION // (5X,3D15.7))

    c Write the E
          tt=0
          open (21,file='E.out')
          write(21,*)"==============",Z,"================"
          do t=0,typee
```

```
            do i=1,Z
               write(21,*)E(i,t)
            end do
         end do
         close(21)

c Writing the electrostatics
         open (20,file='iElec.out')
         write(20,*)"==============",Z,"================"

         do ii=1,Z
            write (20,*)E(ii,typee)
         end do
         close(20)
c Write average distance of n
           tot1=0.0d0
           tot2=0.0d0
         open (13,file='averDist.out')
         do nn=N(1),1,-1
           averDist(nn)=0.0d0
           do i=1,Z/2
              tot1=tot1+(i*Qrp(nn,i))
              tot2=tot2+Qrp(nn,i)
           end do
           averDist(nn)=tot1/tot2
           tot1=0.0d0
           tot2=0.0d0
           Write(13,*)averDist(nn)
         end do
         close(13)

         open (18,file='Cons.out')
c        Solvent
         write(18,*)"==============",Z,"================"

         Write(18,*)"============Solvent============="
         do i=1,Z
            Write(18,*)QpType(i,0)
         end do
c        Polymer
         Write(18,*)"============Polymer============="
         do i=1,Z
            Write(18,*)Qmol(i,1)
         end do
c        Fragments
         breP(0)=0
         breP(nBreak+1)=N(1)
         if (nBreak.gt.0)then
         do tt=1,nBreak+1
         Write(18,*)"============Frag",tt,"==========="
            do i=1,Z
               do nn=breP(tt-1)+1,breP(tt)
                  Cons(tt,i)=Cons(tt,i)+Qrp(nn,i)
               end do
               Write(18,*)Cons(tt,i)
            end do
         end do
         end if
c        Ions
         if (numMol.gt.1)then
         t=nBreak+1
```

```
      do tt=2,numMol
      Write(18,*)"===========Ion",tt-1,"==========="
         t=t+1
         do i=1,Z
               Cons(t,i)=Qmol(i,tt)
               Write(18,*)Cons(t,i)
         end do
      end do
      end if
c     Adsorbed
      Write(18,*)"===========Adsorbed==========="
      do nn=N(1),1,-1
               Write(18,*)Qrp(nn,1)
      end do

      close(18)


      PRINT *, "========================================="
      write(*,11)"Monomer Depletion  :",-ExcessP(0)
      write(*,11)"Polymer            :",-ExcessP(1)
      do k=2,numMol
        write(*,12)"ION ",k-1,"             :",-ExcessP(k)/N(k)
      end do
      write(*,11)"TotalEh            :",(2*totalHC)
      write(*,11)"Internal Energy    :",crossT
      write(*,11)"Electrostatic      :",total6
      write(*,*)""
      write(*,11)"Free Energy        :",F2
      PRINT *, "========================================="
      if(nBreak.gt.0)then
        do t=1,nBreak
           PRINT *, "p",breP(t),":",pb(breP(t))
        end do
      end if
   11 format(A,e17.10)
   12 format(A,i2,A,e17.10)

      END

c The FORTRAN subroutine program that is cycled by the main FORTRAN
progmram
c  written by Adem Zengin

      SUBROUTINE FCN (neq,X,FVEC,IFLAG)
      INTEGER neq,IFLAG,nq
      DOUBLE PRECISION X(neq),FVEC(neq)


      INTEGER Z,Nmax,typee,nn,ii,tt,t,i,k,s,m,h
      INTEGER MaxType,MaxMol,numMol,totN
      parameter (Nmax=1000,MaxType=10,Lmax=500,MaxMol=20)
      INTEGER mapp(Nmax+1),N(MaxMol)
      double precision QpBulk,QsBulk,QnTypeBulk,total
      double precision pb(0:Nmax+2),Esurf(Lmax+1,0:MaxType+1)
      double precision ExtEp(0:MaxType+1,0:MaxType+1)
      double precision E(Lmax+1,0:MaxType+1),elF,elL
      double precision Eh(Lmax+1,0:MaxType+1),nTypeBulk(0:MaxType+1)
      double precision X1,X2,X3,precisionn,ads,p,QpM(MaxMol)
      parameter (X1=1.0d0/6.0d0,X2=4.0d0/6.0d0,X3=1.0d0/6.0d0)
      double precision Gp(Nmax+1,0:Lmax+2),Kp(Nmax+1,Lmax+2)
```

```
      double precision Qf(Nmax+1, 0:Lmax+2),Qb(Nmax+1,0:Lmax+2)
      double precision reGp(Nmax+1,0:Lmax+2),reKp(Nmax+1,Lmax+2)
      double precision Gs(Lmax+2),Qt(Lmax+2),Gother(MaxMol,Lmax+2)
      double precision Qrp(Nmax+2,Lmax+2)
      double precision mProbability,m1Probability,QnTotal(Nmax+1)
      double precision kesitP(Nmax+1,Nmax+1)
      double precision QpType(-1:Lmax+5,0:MaxType+1),Qelec(Lmax+1)

      double precision Elec(-1:Lmax+5,0:MaxType+1)
      double precision extTotal(Nmax,0:MaxType),molBulks(0:MaxMol+1)
      double precision totalHC,q(0:MaxType+1),ElecFac
      double precision sumGType(Lmax,0:MaxMol,0:MaxType+1)
      double precision sumGMol(Lmax,0:MaxMol+1),sumTot
      double precision Qmol(Lmax,0:MaxMol+1)

      common /GroupA/ Qrp,ExtEp,kesitP,Esurf,Qf,QpType,Qmol,
     &                nTypeBulk,molBulks,QpM,pb,q,totalHC,
     &                ElecFac,elF,elL,mapp,numMol,totN,N,Z,typee


c        assigning E(ii,tt) values
         tt=0
c                not typee-1 because of electrostatic field x
      do t=0,typee
         ii=Z
         do i=1,Z/2
            tt=tt+1
            E(i,t)=X(tt)
            E(ii,t)=X(tt)
            ii=ii-1
         end do
      end do

c !!! Calculations for out of lattice (zero)
      do nn=1,N(1)
        Qf(nn,Z+1)=0.0d0
        Qb(nn,Z+1)=0.0d0
        Qf(nn,0)=0.0d0
        Qb(nn,0)=0.0d0
      end do

      do tt=0, typee-1
        QpType(0,tt)=0.0d0

      end do
      do ii=1, Z
         do k=0, numMol
            sumGMol(ii,k)=0.0d0
            do tt=0, typee-1
               sumGType(ii,k,tt)=0.0d0
            end do
         end do
      end do


c Starting iteration

         do ii=1,Z

c Calculation for the first segment Gp
```

```
              do nn=1,N(1)
                  Kp(nn,ii)=exp(-E(ii,mapp(nn)))
              end do

              do nn=N(1),1,-1
                  reKp(nn,ii)=exp(-E(ii,mapp(nn)))
              end do

              Qf(1,ii)=exp(-E(ii,mapp(1)))
              Qb(N(1),ii)=exp(-E(ii,mapp(N(1))))

c Calculation for the first segment Gs

              Gs(ii)=exp(-E(ii,0))
              do k=2,numMol
                do t=1,N(k)
                   Gother(k,ii)=exp(-E(ii,mapp(N(1)+k-1)))
                end do
              end do


          end do


c Calculation for the rest

          do nn=1,N(1)-1

              do ii=1,Z
                  Qf(nn+1,ii)=Kp(nn+1,ii)*((1.0d0-pb(nn))
     &            *((Qf(nn,ii-1)*X1)+(Qf(nn,ii)*X2)
     &            +(Qf(nn,ii+1)*X3))+pb(nn))
              end do

          end do

          do nn=N(1),2,-1

              do ii=1,Z
                  Qb(nn-1,ii)=reKp(nn-1,ii)*((1.0d0-pb(nn-1))
     &            *((Qb(nn,ii-1)*X1)+(Qb(nn,ii)*X2)
     &            +(Qb(nn,ii+1)*X3))+pb(nn-1))
              end do

          end do

c Calculation of total concentration in i layer

c   Initialisation of QpType and Qt
          do ii=1,Z
              Qt(ii)=0.0d0
              do t=0,typee-1
                  QpType(ii,t)=0.0d0

              end do
              do k=0,numMol
                  Qmol(ii,k)=0.0d0
              end do
          end do

c   Calculation of QpType and Qt
```

```
          sumTot=0.0d0
          do ii=1,Z

             do nn=1,N(1)
                sumTot=(Qf(nn,ii)*Qb(nn,ii)/Kp(nn,ii))
                Qrp(nn,ii)=Qpm(1)*sumTot

                sumGType(ii,1,mapp(nn))=sumGType(ii,1,mapp(nn))+sumTot
                sumGMol(ii,1)=sumGMol(ii,1)+ sumTot
             end do
c    ...for other molecules (ions)
             do k=2,numMol
               do t=1,N(k)
                 sumGType(ii,k,mapp(N(1)+k-1))=
     &           sumGType(ii,k,mapp(N(1)+k-1))+Gother(k,ii)
                 sumGMol(ii,k)=sumGMol(ii,k)+ Gother(k,ii)
               end do
             end do

             do tt =1,numMol
                 Qmol(ii,tt)=molBulks(tt)*sumGMol(ii,tt)/N(tt)
             enddo
c    ...for solvent
             Qmol(ii,0)=molBulks(0)*Gs(ii)
             QpType(ii,0)=molBulks(0)*Gs(ii)

          end do

        do ii=1,Z
           do k =0,numMol
              Qt(ii)=Qt(ii)+Qmol(ii,k)
           enddo
          QpType(ii,0)=QpType(ii,0)/Qt(ii)
        end do

        do ii=1,Z
          QpType(ii,0)=QpType(ii,0)/Qt(ii)
        end do

          do tt=1,typee-1
              do ii=1,Z

           QpType(ii,tt)= QpType(ii,tt)+molBulks(1)*sumGType(ii,1,tt)/
     &                N(1)/Qt(ii)
              enddo
          end do

        do k=2,numMol
c          do t=1,N(k)
             do ii=1,Z

              QpType(ii,mapp(N(1)+k-1))= QpType(ii,mapp(N(1)+k-1))
     &        +molBulks(k)*sumGType(ii,k,mapp(N(1)+k-1))/N(k)/Qt(ii)
             enddo
c          end do
        end do

c ////////////////////////////////////
c       Electrostatic Section
```

```
      do ii =1,Z

         Qelec(ii) = 0.0d0

      enddo


      do ii=1,Z
        do tt=0,typee-1
           Elec(ii,tt)=q(tt)*E(ii,typee)

           Qelec(ii)=Qelec(ii)+q(tt)*QpType(ii,tt)
        end do
      end do

c ////////////////////////////////////

c   Calculation of extTotal
        do ii=1,Z
          do t=0,typee-1
c   Initialisation of extTotal
             extTotal(ii,t)=0.0d0
             do tt=0,typee-1
                extTotal(ii,t)=extTotal(ii,t)
     &          +(ExtEp(t,tt)*(X1*QpType(ii-1,tt)+X2*QpType(ii,tt)
     &          +X3*QpType(ii+1,tt)-nTypeBulk(tt)))
             end do
             extTotal(ii,t)=extTotal(ii,t)+Esurf(ii,t)+Elec(ii,t)
          end do

      end do


c ////////////////////////////////////
         totalHC=0.0d0
c       nq=0
      do ii=1,Z/2
c          write(33,*)"Qt",ii,"",Qt(ii)
         FVEC(ii)=dlog(Qt(ii))

         totalHC=totalHC+X(ii)-extTotal(ii,0)
      end do
c       close(33)


      do t=1,typee-1
         do ii=1,Z/2
            FVEC(ii+(Z/2)*t)=X(ii+(Z/2)*t)-extTotal(ii,t)
     &                      -(X(ii)-extTotal(ii,0))
         end do
      end do
c     Electrostatic zero equations for first, middle and last layers
       if (Z.gt.2) then


        FVEC(1+(Z/2)*typee)= -1.0d0*X(1+(Z/2)*typee)
     &                      +X(2+(Z/2)*typee)+ElecFac*Qelec(1)

        do ii=2,(Z/2)-1
           FVEC(ii+(Z/2)*typee)=-2.0d0*X(ii+(Z/2)*typee)
```

```
     &      +X(ii+1+(Z/2)*typee)+X(ii-1+(Z/2)*typee)
     &      +ElecFac*Qelec(ii)

         end do


         FVEC((Z/2)+(Z/2)*typee)=-1.0d0*X((Z/2)+(Z/2)*typee)
     &   +X((Z/2)-1+(Z/2)*typee)+ElecFac*Qelec(Z/2)

       elseif (Z.eq.2) then
         FVEC(1+(Z/2)*typee)=Qelec(1)
       else
         print *,"Z has to be greater than 2"
       endif
c           ////////////////////////////////////////

       RETURN


999    stop
       END
```

```
/* A program to calculate the volume fraction of a specific fragment
(jk) at a position (r)
 * written by Adem ZENGIN
 */

import static java.lang.System.out;
import java.io.*;
import java.util.*;
public class us2f {

    public static void main(String[] args) {

        int N=201;
        int [] map= new int [N+2];
        int type=9;

         int Lmax=180;
         int L=0;
         double dL=0.0;
         int nBreak=2;
         int kir[]=new int [N+2];
         int kk=0;
         boolean okkay=false;

         double averdist[]=new double [N+2];
         double tot1=0.0;
         double tot2=0.0;

         Scanner keyboard=new Scanner(System.in);
         String[] iAndP={"0","2.0"};
         String filePath="./E_files/ph3.0_test";
         double QpBulk=0.0001;
         double Qions=0.02;      // Concentration of polymer in bulk
solution (needed to be given) //
         double QpM=QpBulk/N;  // Bulk concentration of one monomer of
the given type //

         double pb[] = new double [N+2];
```

```
          pb[0]=1.0;
          pb[N]=1.0;
          int gg=0;

          for (int i=1; i<=N-1; i++){
              pb[i]=0.0;
         }


          PrintWriter output=null;
          PrintWriter outType=null;
          PrintWriter outAver=null;

          try{
                  output = new PrintWriter(new
FileOutputStream("zzz.txt",false));//written file//
                  outType = new PrintWriter(new
FileOutputStream("ads_in.txt",false));//written file//
                  outAver = new PrintWriter(new
FileOutputStream("Javerdist.txt",false));//written file//

                  BufferedReader input=new BufferedReader(new
FileReader("map.out"));//Read file//
                  BufferedReader inputProb=new BufferedReader(new
FileReader("prob.in"));//Read file//
                  String line=null;

                  for (int n=1; n<=N; n++){
                      line= input.readLine();
                      map[n]=Integer.parseInt(line.trim());
                  }
                  input.close();


          //-------------------------------------------------------------
----------------------

              String fileName="/E0.0.out";
              if(nBreak>0){
                  for (int i=1; i<=nBreak; i++){
                  //assigning probabilities
                  line=inputProb.readLine();
                  iAndP=line.split(" ");

pb[Integer.parseInt(iAndP[0])]=Double.parseDouble(iAndP[1]);
                  System.out.println(pb[Integer.parseInt(iAndP[0])]);
                  //pb[i]=0.0;
                  }

                  fileName="/E"+iAndP[1]+".out";
              }

                  BufferedReader inputField=new BufferedReader(new
FileReader(filePath+fileName));//Read file//
                  BufferedReader inputField2=new BufferedReader(new
FileReader(filePath+fileName));//Read file//


            //-----------------------------------------------------------
------------------------------
```

```
                    double[][]E=new double [Lmax+1][type+1];//Arrays
starting 0, ending n-1//
                    double [][]Qptype=new double
[Lmax+1][type+1];//Volume Fractions of every type in every layer
                    int n=0;
                    int i=0;


                   while((line=inputField.readLine())!=null)
                   {
                       dL=dL+1;
                   }
                   inputField.close();

                   dL=dL/(type+1);
                   System.out.println("dL:"+dL);
                   L=(int)dL;
                   System.out.println("L:"+L);

                   if(dL!=L){
                       System.out.println("Check the white space in the
E file!");
                       System.exit(0);
                   }

                   for(n=0; n<=type; n++){
                               for (i=1; i<=L; i++)
                               {
                                   line= inputField2.readLine();
                                   E[i][n]=Double.parseDouble(line);
                               }
                   }

                   double Qkk[][][]=new double [10][N+2][L+2];
                   double Qk[]=new double [L+2];

                    //X_1,X0,X1,TT are dimension factors depending on
geometry of lattice model//
                    double X1=1.0/6.0;
                    double X2=4.0/6.0;
                    double X3=1.0/6.0;


                   // Creating Gp(n,r) variable (Segment weighting
factor) //
                       double [][] Gp = new double [N+2][L+2];
                       double [][] Kp = new double [N+2][L+2];

                   // Creating Gp(n,r) variable (Segment weighting
factor) //
                       double [][] reGp = new double [N+2][L+2];
                       double [][] reKp = new double [N+2][L+2];

                   // Creating Gs(n,r) variable (Segment weighting
factor) //
                       double []Gs = new double [L+2];

                       // Calculations for out of lattice (zero) //
                        for (n=1; n<=N; n++)
                        {
```

```
                        Gp[n][0]=0.0;
                        reGp[n][0]=0.0;
                        Gp[n][L+1]=0.0;
                        reGp[n][L+1]=0.0;
                        Kp[n][0]=0.0;
                        reKp[n][0]=0.0;
                        Kp[n][L+1]=0.0;
                        reKp[n][L+1]=0.0;
                        }

                       // Calculations for out of lattice (zero) //

                        Gs[0]=0;
                        Gs[L+1]=0;


                           double Qrp [][]= new double [N+2][L+2];
//Total concentration of polymer in r layer //
                           double Qrs []= new double [L+2]; //Total
concentration of solvent in r layer //

                           double ExcessP=0.0;
                           double [][]Excessp=new double [N+1][L+1];
                           double Qnbulk=0.0;
                           double [] QnTotal=new double [N+1];
                           double total=0.0;
                           double []Qp= new double [L+1];

                           double mProbability;
                           double m1probability;

                           //Total probability for every number of
monomers

                           double kesitP[][]=new double[N+1][N+1];
                           int h=0;
                           for (i=1; i<=N; i++){
                               kesitP[i][1]=pb[i-1];
                           }

                           for (i=1; i<=N; i++){
                               if (pb[i-1]==0.0){
                                   for (n=2; n<=N; n++){
                                       kesitP[i][n]=0.0;
                                   }
                               }
                               h=0;
                               if (pb[i-1]!=0.0){
                                   for (h=2; h<=N; h++){
                                       if((h+i)<=N+1){
                                           kesitP[i][h]=kesitP[i][h-
1]*(1-pb[i+h-2]);

                                       }

                                   }
                               }
                           }


                           //Second G
```

```
                                for (i=1; i<=L; i++){


                                    for (n=1; n<=N; n++){
                                        Kp[n][i]=Math.pow(Math.E, -
E[i][map[n]]);
                                    }
                                    for (n=N; n>=1; n--){
                                        reKp[n][i]=Math.pow(Math.E, -
E[i][map[n]]);
                                    }


                                    Gp[1][i]=Math.pow(Math.E, -
E[i][map[1]]);
                                    reGp[N][i]=Math.pow(Math.E, -
E[i][map[N]]);
                                    Gs[i]=Math.pow(Math.E, -E[i][0]);


                                }

                                //calculations for m=1

                                for (n=1; n<=N; n++){

m1probability=kesitP[n][1]*pb[n];//pb[n+1];//Probability of size 1 at
position n

                                    for(i=1; i<=L; i++){

                                            Qrs [i]=(1.0-QpBulk-
Qions)*Gs[i];


                                            Qnbulk=m1probability*QpM;

                                            total=Qnbulk*(Kp[n][i]);
                                            Qrp[1][i]+=total;
                                            Qptype[i][map[n]]+=total;
                                            Excessp[1][i]+=total-Qnbulk;
                                            Qnbulk=0.0;
                                            total=0.0;
                                    }
                                    QnTotal[1]+=m1probability;
                                    m1probability=0.0;

                                }

                                 // Calculation for the rest //

                                for (int m=2; m<=N; m++){
                                    for (n=1; n<=N-m+1; n++){
                                        if(n+m<=N+1){

                                            for (i=1; i<=L; i++){//
Gp[first] and reGp[last] calculation

                                                Gp[n][i]=Kp[n][i];
```

```
                                                    reGp[m+n-1][i]=reKp[m+n-
1][i];

                                                }

                                                for (int s=1; s<=m-1; s++){

                                                    for (i=1; i<=L; i++){

Gp[n+s][i]=Kp[n+s][i]*((Gp[n+s-1][i-1]*X1)+(Gp[n+s-1][i]*X2)+(Gp[n+s-
1][i+1]*X3));
                                                    }
                                                }

                                                for (int s=m-1; s>=1; s--){

                                                    for (i=1; i<=L; i++){

                                                        reGp[n+s-1][i]=
reKp[n+s-1][i]*((reGp[n+s][i-
1]*X1)+(reGp[n+s][i]*X2)+(reGp[n+s][i+1]*X3));
                                                    }
                                                }


mProbability=kesitP[n][m]*pb[n+m-1];//pb[n+m];//Probability of size m at
position n
                                                Qnbulk=mProbability*QpM;
                                                if(m==201){
                                                    if(mProbability>0){

output.println("========="+(N-n-m+2)+"-"+(N-
n+1)+"==========QnBulk:"+Qnbulk*m+"==========");
                                                    kk=kk+1;
                                                    kir[kk]=N-n-m+2;
                                                    System.out.println(n);
                                                    okkay=true;
                                                    }
                                                }
                                                for(i=1; i<=L; i++){

                                                    for (int k=1; k<=m;
k++){


total=Qnbulk*(Gp[n+k-1][i]*reGp[n+k-1][i]/Kp[n+k-1][i]);

                                                    if(okkay){

Qkk[kk][k][i]=total;

Qk[i]+=total-Qnbulk;//Excess

                                                    }

                                                    Qrp[m][i]+=total;
                                                    Qptype[i][map[n+k-
1]]+=total;
```

```
Excessp[m][i]+=total-Qnbulk;

                                                    total=0.0;
                                                }

                                                if(okkay){

output.println(Qk[i]);
                                                    Qk[i]=0.0;
                                                }

                                             }
                                            QnTotal[m]+=mProbability;
                                            Qnbulk=0.0;
                                            mProbability=0.0;
                                            okkay=false;

                                        }
                                    }
                                }

                                 for (i=1; i<=L; i++){

                                    for (int m=1; m<=N; m++){
                                         Qp[i]+=Qrp[m][i];

ExcessP+=Excessp[m][i]/m;//Weight Average//Number Average
                                        }

                                 }

                                //total adsorbed(m)
                                double []adM1=new double [N+1];
                                for (int m=1; m<=N; m++){

                                     for (i=1; i<=L; i++){
                                    adM1[m]+=Excessp[m][i];//m;//Weight
Average//Number Average
                                     }
                                 }


                                        for (i=1; i<=L; i++){

//outType.println(Qptype[i][t]);

System.out.println(i+":"+Qp[i]);
                                        }


                                 //in solution(m)
                                   double []inSolution=new double [N+1];
                                 for (int m=1; m<=N; m++){


inSolution[m]=QnTotal[m]*QpBulk*m/N;

                                }
```

```
                                    //print total polymer(m), total
adsorbed(m), in solution(m)
                                    for (int m=1; m<=N; m++){
                                        outType.println(adM1[m]+"
"+inSolution[m]+"    "+Qrp[m][1]);
                                    }

                                   for (int sss=1; sss<=kk; sss++){

outAver.println("======="+kir[sss]+"-"+(kir[sss]+201-1)+"=======");

                                       for (int k=201; k>=1; k--){

                                           averdist[k]=0.0;

                                           for(i=1; i<=L/2; i++){

tot1=tot1+(i*Qkk[sss][k][i]);
                                               tot2=tot2+Qkk[sss][k][i];

                                           }

                                           averdist[k]=tot1/tot2;
                                           outAver.println((kir[sss]+201-
k)+"  "+averdist[k]);

                                           tot1=0.0;
                                           tot2=0.0;

                                       }

                                   }


              //-------------------------------------------------------------
-------------------------------------------------


          output.close();
          outAver.close();
          inputField2.close();
          outType.close();
          }
          catch (IOException e) {
             e.printStackTrace();
         }

          System.out.println("2nd Done...");


    }

}
```